The
Philosophical Magazine

FIRST PUBLISHED IN 1798

A Journal of Theoretical Experimental and Applied Physics

Vol. 4 April 1959 No. 40
Eighth Series

UNIVERSITY OF HAWAII LIBRARY
MAY 19 '59

£1 5s. 0d., plus postage
Annual Subscription £13 10s. 0d., payable in advance

ALERE FLAMMAM

Printed and Published by
TAYLOR & FRANCIS LTD
RED LION COURT, FLEET STREET, LONDON, E.C.4

THE PHILOSOPHICAL MAGAZINE

Editor

Professor N. F. Mott, M.A., D.Sc., F.R.S.

Editorial Board

Sir Lawrence Bragg, O.B.E., M.C., M.A., D.Sc., F.R.S.
Sir George Thomson, M.A., D.Sc., F.R.S.
Professor A. M. Tyndall, C.B.E., D.Sc., F.R.S.

Authors wishing to submit papers for publication in the Journal should send manuscripts directly to the Publishers.

Manuscripts should be typed in *double* spacing on one side of quarto (8 × 10 in.) paper, and authors are urged to aim at absolute clarity of meaning and an attractive presentation of their texts.

References should be listed at the end in alphabetical order of authors and should be cited in the text in terms of author's name and date. Diagrams should normally be in Indian ink on white card, with lettering in soft pencil, the captions being typed on a separate sheet.

A leaflet giving detailed instructions to authors on the preparation of papers is available on request from the Publishers.

Authors are entitled to receive 25 offprints of a paper in the Journal free of charge, and additional offprints can be obtained from the Publishers.

The *Philosophical Magazine* and its companion journal, *Advances in Physics*, will accept papers for publication in experimental and theoretical physics. The *Philosophical Magazine* publishes contributions describing new results, letters to the editor and book reviews. *Advances in Physics* publishes articles surveying the present state of knowledge in any branch of the science in which recent progress has been made. The editors welcome contributions from overseas as well as from the United Kingdom, and papers may be published in English, French and German.

INTERNATIONAL JOURNAL OF

RADIATION BIOLOGY

and related studies in Physics, Chemistry and Medicine

Editor
W. M. DALE, M.D., D.SC.
Dept. of Biochemistry, Christie Hospital & Holt Radium Institute, Withington, Manchester, 20

Assistant Editor
JOHN WAKEFIELD, B.A., F.Z.S.

Editorial Board
Charlotte Auerbach, *U.K.;* J. H. Baxendale, *U.K.;* D. W. van Bekkum, *Holland;* E. H. Betz, *Belgium;* H. A. S. van den Brenk, *Australia;* A. A. Buzzatti-Traverso, *Italy;* J. Coursaget, *France;* F. Devik, *Norway;* † J. Firket, *Belgium;* M. Haissinsky, *France;* A. Hollaender, *U.S.A.;* B. F. Kaufmann, *U.S.A.;* G. Klein, *Sweden;* H. Langendorff, *Germany;* M. Magat, *France;* † N. Miller, *U.K.;* M. Nakaidzumi, *Japan;* E. Paterson, *U.K.;* H. Ulrich, *Switzerland;* M. Westergaard, *Denmark.*

Contents of January, 1959

The Mechanism of Radiation Protection by Histamine and other Biological Amines. By C. van der Meer and D. W. van Bekkum, Medical Biological Laboratory of the National Defence Research Council T.N.O., Lange Kleiweg 139 Rijswijk (Z.H.), The Netherlands

5-Hydroxytryptamine as a Radiation Protective Substance in Animals. By H. Langendorff, H.-J. Melching and H.-A. Ladner, Radiology Institute, University of Freiburg, Baden, Germany

The DNA Content of the Small Intestine as a Quantitative Measure of Damage and Recovery after Whole Body Irradiation. By R. H. Mole and Diana M. Temple, M.R.C. Radiobiological Research Unit, A.E.R.E., Harwell, Berks.

DNA Synthesis in the Thoracic-Duct Lymphocytes of Rats during Recovery from Sub-Lethal Irradiation. By E. H. Cooper, The Department of Biochemistry, The University of Oxford

Hexokinase, Aldolase and ATP-Creatine Transphosphorylase in X-Irradiated Rats. By M. B. Sahasrabudhe, M. K. Nerurkar and A. J. Baxi, Biology Division, Atomic Energy Establishment, Trombay Indian Cancer Research Centre, Parel, Bombay, India and D. K. Mahajan, Human Variation Unit, Indian Cancer Research Centre, Parel, Bombay, India

On the Relative Role of Mutation and Recombination in Responses to Selection for Polygenic Traits in Irradiated Populations of D. Melanogaster. By R. E. Scossiroli and S. Scossiroli, Istituto di Genetica, Universitá, Pavia, Italy

An Attempt to Assess the Activity of Tumour Cells by the Study of Nucleolar Morphology, Mitotic Index and Phosphorus with ^{32}P. By S. Mitra, P. De, R. Chatterjee, K. Bhattacharya, A. Bose and H. Dutta, Departments of Cell Research and Biophysics, Chittaranjan National Cancer Research Centre, Calcutta

The Inactivation of SH Enzymes by X-Rays. By Rolf Lange, Alexander Pihl and Lorentz Eldjarn, Norsk Hydro's Institute for Cancer Research, The Norwegian Radium Hospital, Oslo, Norway

X-Ray-Induced Abnormal Differentiation of the Epithelium of the Small Intestine in the Mouse. By Richard A. McGrath and C. C. Congdon, Biology Division, Oak Ridge National Laboratory, Oak Ridge, Tennessee

Price per part £1 0s. 0d. plus postage
Subscription per volume (4 issues) £3 15s. 0d. post free, payable in advance

Printed and Published by
TAYLOR & FRANCIS LTD
RED LION COURT, FLEET STREET, LONDON, E.C.4

Orders originating in U.S.A. and Canada should be sent to the
Academic Press Inc., 111 Fifth Avenue, New York 3, N.Y., U.S.A.

A new International Journal

Molecular Physics

Editor: **H. C. LONGUET-HIGGINS, F.R.S.**
Associate Editor: **J. H. VAN DER WAALS**

Editorial Board:

J. Bjerrum, *Copenhagen*; G. Careri, *Padua*; C. A. Coulson, *Oxford*; F. H. C. Crick, *Cambridge;* P. J. W. Debye, *Cornell*; D. Hadži, *Ljubljana*; O. Hassel, *Oslo*; W. Heitler, *Zürich*; J. O. Hirschfelder, *Wisconsin*; D. F. Hornig, *Princeton*; J. A. A. Ketelaar, *Amsterdam*; J. G. Kirkwood, *Yale*; R. Kronig, *Delft*; J. W. Linnett, *Oxford*; A. Liquori, *Rome*; Dame Kathleen Lonsdale, *London*; P-O. Löwdin, *Uppsala*; M. Magat, *Paris*; R. S. Mulliken, *Chicago;* A. Münster, *Frankfurt*; L. J. Oosterhoff, *Leiden*; L. E. Orgel, *Cambridge*; J. A. Pople, *Teddington*; I. Prigogine, *Brussels*; R. E. Richards, *Oxford*; J. S. Rowlinson, *Manchester*; G. S. Rushbrooke, *Newcastle upon Tyne*; L. E. Sutton, *Oxford*; H. W. Thompson, *Oxford*; B. Vodar, *Bellevue, Paris.*

Contents of January, 1959

Zur Theorie der generalisierten Gesamtheiten. Von A. Münster, Physikalisch-chemisches Institut der Universität Frankfurt/Main

Pressure-dependent Partition Functions. By R. A. Sack, Department of Theoretical Chemistry, University of Cambridge and British Rayon Research Association, Wythenshawe, Manchester

On Mayer's Ionic Solution Theory. By Harold L. Friedman, Faculté des Sciences, Université Libre de Bruxelles

Rotational Effect on the Thermodynamic Properties of Isotopes. By Agnessa Babloyantz, Faculté des Sciences de l'Université Libre de Bruxelles, Belgique

The Structure of Shock Fronts in Various Gases. By W. H. Andersen and D. F. Hornig, Metcalf Research Laboratory, Brown University, Providence, Rhode Island

Relationship between Proton Shielding Constants and Electric Dipole Moments in the Hydrogen Halides. By H. F. Hameka, Department of Chemistry, Carnegie Institute of Technology, Pittsburgh, Pennsylvania

Chemical Shifts of Thallium Resonance Spectra in Solutions of Thallous Salts. By R. Freeman, R. P. H. Gasser, R. E. Richards and D. H. Wheeler, Physical Chemistry Laboratory, South Parks Road, Oxford

Correlations between the Electronic Spectra of Alternant Hydrocarbon Molecules and their Mono- and Di-valent Ions. I. Benzene, Coronene and Triphenylene. By G. J. Hoijtink, Chemical Laboratory of the Free University, Amsterdam

Absorption Spectra of Actinide Compounds. By Chr. Klixbüll Jørgensen, Chemistry Department A, Technical University of Denmark, Copenhagen, Denmark

Price per part £1 5s. 0d. plus postage
Subscription per volume (4 issues) £4 15s. 0d. post free, payable in advance

Printed and Published by
TAYLOR & FRANCIS LTD
RED LION COURT, FLEET STREET, LONDON, E.C.4

Orders originating in U.S.A. and Canada should be sent to the
Academic Press Inc., 111 Fifth Avenue, New York, 3, N.Y., U.S.A.

Journal of Electronics and Control

A Philosophical Magazine Associated Journal

Editor:
J. Thomson, M.A., D.Sc., M.I.E.E., F.Inst.P.
Consultant Editor:
Professor N. F. Mott, F.R.S.
Editorial Board:
Professor P. Aigrain (France)
Professor H. B. G. Casimir (Holland)
J. F. Coales (U.K.)
Professor K. G. Emeleus (U.K.)
D. W. Fry (U.K.)
Dr. W. Klein (Germany)
Dr. R. Kompfner (U.S.A.)

Contents of February, 1959

Electronics Section

Field Effect at High Frequency. By F. Berz, Mullard Research Laboratories, Salfords, Nr. Redhill, Surrey

An Experimental C.W. Power Travelling-wave Tube. By M. O. Bryant, J. F. Gittins and F. Wray, Services Electronics Research Laboratory Extension, Admiralty, Harlow, Essex

Breakdown in Silicon pn Junctions. By J. Shields, Research Laboratory, British Thomson-Houston Co. Ltd., Rugby

Evaporation of Barium from Cathodes Impregnated with Barium–Calcium–Aluminate. By I. Brodie, R. O. Jenkins and W. G. Trodden, Communication from the Staff of the Research Laboratories of The General Electric Co. Ltd., Wembley, England

A Method of Studying the Electrical Recovery of a Gas after a Pulse Discharge. By R. J. Armstrong, Royal Radar Establishment, Malvern, Worcestershire

Control Section

The Optimization of Logical Goal-seeking Procedures. By A. Porter, College of Engineering, University of Saskatchewan, Canada and P. K. T. Vaswani, Imperial College of Science and Technology, London

On the Iterative Solution of the Equations of a Single-loop System with One Non-linearity. By Olavi Hellman, Department of Mathematics, University of California at Los Angeles

---

Price per part £1 5s. plus postage
Price per volume £7 post free, payable in advance
6 monthly issues per volume

Printed and Published by

TAYLOR & FRANCIS LTD
RED LION COURT, FLEET STREET, LONDON, E.C.4

Orders originating in U.S.A. and Canada should be sent to the
Academic Press Inc., 111 Fifth Avenue, New York, 3, N.Y., U.S.A.

Physics in Medicine and Biology

A Taylor & Francis Journal published in association with The Hospital Physicists' Association

Editor: **J. E. Roberts, D.Sc.**
Consultant Editor: Professor N. F. Mott, F.R.S.

Editorial Board

R. Bonet-Maury, *Paris*; J. Dainty, *Edinburgh*; H. E. Johns, *Toronto*; W. A. Langmead. *London*; D. A. McDonald, *London*; J. S. Mitchell, *Cambridge*; G. J. Neary, *Harwell*; B. Rajewsky, *Frankfurt*; J. Rotblat, *London*; S. Rowlands, *London*; H. P. Schwan, *Philadelphia*; R. Sievert, *Stockholm*; F. W. Spiers, *Leeds*; J. F. Tait, *Massachusetts*; A. J. H. Vendrik, *Nijmegen.*

Contents of January, 1959

The Measurement of Exposure Dose for High Energy Radiation with Cavity Ionization Chambers. By T. E. Burlin, B.Sc., Physics Department, Hammersmith Hospital, London, W.12

The Energy Response of a Victoreen Condenser Ionization Chamber. By A. J. D. Szilvasi, Ph.D. and G. N. Whyte, Ph.D., National Research Council, Ottawa, Canada

An Analysis of Clasp Design in Partial Dentures. By J. A. Warr, M.A.(Cantab.), B.Sc. (London), B.D.S.(London), L.D.S.R.C.S.Eng., Department of Prosthetics, The London Hospital Medical College, Turner Street, London, E.1

A Study of the External Gamma-ray Field Arising from a Radioactive Source Situated in Air and in a Scattering Medium. By H. A. B. Simons, M.A., Ph.D. and S. Chomet, M.Sc., Physics Department, The Royal Free Hospital School of Medicine, 8 Hunter Street, London, W.C.1

A Wide Range Direct Reading X-Ray Dosemeter. By S. Stuart, Electronic Instruments Ltd., Richmond, Surrey and S. B. Osborn, B.Sc., A.Inst. P., University College Hospital, London, W.C.1

Pulmonary Diffusion of Oxygen. By B. F. Visser, Ph.D. and A. H. J. Maas, M.Sc., Pulmonary Function Laboratory, State University Hospital, Utrecht, Netherlands

The Influence of the Anomalous Viscosity of Blood upon its Oscillatory Flow. By M. G. Taylor, M.D., Physiology Department, Medical College of St. Bartholomew's Hospital, London

Subscription price per volume £3 10s. post free, payable in advance
4 parts per volume—£1 per part plus postage

Printed and Published by

TAYLOR & FRANCIS, LTD

RED LION COURT, FLEET STREET, LONDON, E.C.4
Orders originating in U.S.A. and Canada should be sent to the
Academic Press Inc., 111 Fifth Avenue, New York, 3, N.Y., U.S.A.

A new International Journal

ERGONOMICS

HUMAN FACTORS IN WORK, MACHINE CONTROL AND EQUIPMENT DESIGN

General Editor
A. T. WELFORD
University of Cambridge, Psychological Laboratory, Downing Place, Cambridge

Associate Editor (Anatomy and Physiology)
W. F. FLOYD

Assistant Editor
Miss H. M. CLAY

Editorial Board

H. Bastenier, *Belgium*; R. B. Bromiley, *Canada* ; R. Bonnardel, Bernard Metz, *France*; E. A. Müller, *Germany*; M. G. Bennett, W. E. Hick, Sir Charles Lovatt Evans, L. G. Norman, *Great Britain*; F. H. Bonjer, *Netherlands*; S. P. M. Forssman, *Sweden*; E. Grandjean, *Switzerland*; H. S. Belding, P. M. Fitts, *U.S.A.*

Contents of February, 1959

Symposium on Training

Introductory Address. By P. H. St. J. Wilson, C.B., C.B.E., Chief Industrial Commissioner, Ministry of Labour and National Service
Physiological Bases of Training. By Albert Hemingway, Department of Physiology, School of Medicine, University of Leeds
Training Operatives in Industry. By W. Douglas Seymour, Clent, Worcestershire
The Training of Shoe-Machinists. By W. T. Singleton, The British Boot, Shoe and Allied Trades Research Association, Kettering
A Theory of the Acquisition of Speed-Skill. By E. R. F. W. Crossman, Department of Psychology, Reading University, England
Practice and Knack : Some Comments on Learning and Training in Industry. By Isabel Blain, National Institute of Industrial Psychology
The Operator as a Self-Regulating System: A Factory Experiment. By S. David M. King, Organization & Training (Consultants) Limited, 19 Bolton Street, London, W.1
Note on Current Trends in Literature on Training. By Ezra V. Saul, Institute for Applied Experimental Psychology, Tufts University, Medford, Massachusetts
Circuit Training. By G. T. Adamson, Department of Physical Education, The University, Leeds
The Limitations of a ' Procrustean ' Approach to the Optimization of Man–Machine Systems. By F. V. Taylor and W. D. Garvey, U.S. Naval Research Laboratory, Washington, D.C.
Physical Training in Relation to the Energy Expenditure of Walking and to Factors Controlling Respiration During Exercise. By J. E. Cotes and F. Meade, Medical Research Council, Pheumoconiosis Research Unit, Llandough Hospital, Penarth, Glamorgan, Wales
Problems of Training of the Cardiovascular System. By M. J. Karvonen, Institute of Occupational Health, Helsinki, Finland
Training Muscle Strength. By E. A. Müller, Max-Planck-Institut für Arbeitsphysiologie, Dortmund, Germany
Abstracts of other Papers Delivered at the Symposium

Price £1 5s. 0d. per part plus postage
Subscription price per volume £4 15s. 0d. post free, payable in advance

Printed and Published by
TAYLOR & FRANCIS LTD
RED LION COURT, FLEET STREET, LONDON, E.C.4

Orders originating in U.S.A. and Canada should be sent to the Academic Press Inc., 111 Fifth Avenue, New York, 3, N.Y., U.S.A.

Advances in Physics

A Quarterly Supplement of the Philosophical Magazine

Editor:
PROFESSOR N. F. MOTT, M.A., D.Sc., F.R.S.

Editorial Board:
SIR LAWRENCE BRAGG, O.B.E., M.C., M.A., D.Sc., F.R.S.
SIR GEORGE THOMSON, M.A., D.Sc., F.R.S.
PROFESSOR A. M. TYNDALL, C.B.E., D.Sc., F.R.S.

Contents of January, 1959

The Theory of Superconductivity. By C. G. Kuper, Department of Natural Philosophy, St. Salvator's College, St. Andrews

The Modern Theory of Superconductivity. By I. M. Khalatnikov and A. A. Abrikosov, Institute of Physical Problems, Kaluzhskove Shosse, 32 Moscow, U.S.S.R.

Price per part £1 plus postage

Price per annum £3 15s. post free

Printed and Published by

TAYLOR & FRANCIS LTD

RED LION COURT, FLEET STREET, LONDON, E.C.4

INTERNATIONAL JOURNAL

OPTICA ACTA

European Journal of Optics **Journal Européen d'Optique** **Europäische Zeitschrift für Optik**

English Editor: C. G. Wynne, 13 Elwill Way, Beckenham, Kent, U.K.

Rédacteur Français: A. Maréchal, 3 Boulevard Pasteur, Paris, France

Deutscher Herausgeber: G. Franke, Laufdorfer Weg 2, Wetzlar, Germany

Editorial Board

J. M. Otero y Navascues, *Madrid;* R. W. Ditchburn, *Reading;* A. Arnulf, *Paris;* A. Biot, *Gand;* J. Cabannes, *Paris;* P. Fleury, *Paris;* F. Gabler, *Vienna;* G. Hansen, *Oberkochen;* E. Ingelstam, *Stockholm;* H. Korte, *Braunschweig;* W. S. Stiles, *London;* G. Toraldo di Francia, *Florence;* A. C. S. van Heel, *Delft.*

Contents of January, 1959

N.P.L. Colour-Matching Investigation: Final Report (1958). By W. S. Stiles and J. M. Burch, National Physical Laboratory, Teddington, Middlesex

Optical Constants of Evaporated Films of Zinc Sulphide and Germanium in the Infra-Red. By Lennart Huldt and Torsten Staflin, Institute of Optical Research, Royal Institute of Technology, Stockholm

Das Moiré-Gitter als vielseitiges Testobjekt: Photoelektrische Aberrationsmessung. Von A. Lohmann, z.Zt. Institutet för optisk forskning, Stockholm 70

Matrix Formalism in the Theory of Diffusion of Light. By I. Kuščer, Institute of Physics, University of Ljubljana and M. Ribarič, J. Stefan Institute, Ljubljana, Yugoslavia

Lage und Sichtbarkeit von Keilinterferenzen bei Instrumenteller Beobachtung (Beitrag zur Kohärenztheorie eines Unsymmetrischen Interferenzfalles). Von Rudolf Landwehr, Menden/Sauerland, Deutschland

Essai de Détermination des Très Faibles Diamètres Apparents en Radioastronomie. Par J. Arsac, Observatoire de Meudon

Price per part £1 (1375 fr.), (DM 11.75), ($2.80), plus postage

Subscription price per volume (4 parts) £3 15s. (5155 fr.), (DM 44), ($10.50), post free, payable in advance

Printed and Published by

TAYLOR & FRANCIS LTD

RED LION COURT, FLEET STREET, LONDON, E.C.4

A HISTORY OF MATHEMATICS

from antiquity to the early nineteenth century

by J. F. SCOTT, B.A., D.Sc., Ph.D.
Vice-Principal of St. Mary's College,
Strawberry Hill, Twickenham,
Middlesex

Author of *The Scientific Work of René Descartes* (1596–1650), *Mathematical Work of John Wallis, D.D., F.R.S.* (1616–1703), and other works.

CONTENTS : Mathematics in Antiquity—Greek Mathematics—The Invention of Trigonometry—Decline of Alexandrian Science and the Revival in Europe—Mathematics in the Orient—Progress of Mathematics during the Renaissance—New Methods in Geometry—The Rise of Mechanics—the Invention of Decimal Fractions and of Logarithms—Newton and the Calculus—Taylor and Maclaurin, the Bernoullis and Euler, Related Advances—The Calculus of Variations, Probability, Projective Geometry, Non-Euclidean Geometry—Theory of Numbers—Lagrange, Legendre, Laplace, Gauss.

This volume is intended primarily to help students who desire to have a knowledge of the development of the subject but who have too little leisure to consult original works and documents. The author has availed himself of the facilities afforded by the Royal Society and other learned Societies to reproduce extracts from manuscripts and many scarce works.

$9\frac{3}{4} \times 6\frac{3}{4}$ Price 3 guineas

Printed and Published by
TAYLOR & FRANCIS LTD.
Red Lion Court, Fleet Street,
London, E.C.4

THE SCIENTIFIC WORK OF RENÉ DESCARTES 1596-1650

BY

J. F. SCOTT, B.A., M.SC., PH.D.

With a Foreword by

H. W. Turnbull, M.A., F.R.S.

This book puts the chief mathematical and physical discoveries of Descartes in an accessible form and fills an outstanding gap upon the shelf devoted to the history of philosophy and science. There is to be found in this volume the considerable contribution that Descartes made to the physical sciences, which involved much accurate work in geometrical optics and its bearing upon the practical problem of fashioning lenses, as also the deeper problems of light and sight and colour. The careful treatment that Dr. Scott has accorded to the work of Descartes is very welcome. The book is well worth reading and will be an asset to all libraries. This publication is recommended and approved by the Publication Fund Committee of the University of London.

212 *pp.* 7 × 10 *amply illustrated*

PRICE £1–0–0 NET

Printed and Published by
TAYLOR & FRANCIS LTD.
Red Lion Court, Fleet Street,
London, E.C.4

Thermally Activated Glide in Face-Centred Cubic Metals and its application to the Theory of Strain Hardening†

By Z. S. Basinski
Division of Pure Physics, National Research Council, Ottawa, Canada

[Received August 16, 1958]

Abstract

The influence of temperature and strain rate on the flow stress of polycrystalline aluminium, and single crystals of aluminium, copper and silver was studied. Tensile tests were carried out at various temperatures down to 1·7°K. The results indicate that the reversible change of flow stress (after correction for variation in elastic modulus in experiments involving temperature change) results from the thermally activated surmounting of barriers by glide dislocations. The main barriers are believed to be forest dislocations cutting the glide plane. The variation of the force between a dislocation and an obstacle with their separation was derived for the three metals ; the values agreed well with the expected forms. The maximum force can be computed if the distance at which the force rises steeply is assumed to be equal to the Burgers vector ; the values are, for aluminium, $3{\cdot}5\times10^{-5}$ dynes, and for copper, $6{\cdot}3\times10^{-5}$ dynes.

It has been shown that the internal stress varying over distances larger than the separation between successive dislocations emitted from the same source will not contribute appreciably to the hardening, and that the most important source of hardening is the dislocation forest. This is borne out by the fact that the flow stress ratio is approximately the same for polycrystalline and single crystal specimens of aluminium deformed both in tension and torsion, and also for commercially pure aluminium.

The rate of strain hardening in the linear region has been calculated using the above assumptions, and agrees well with experimental data.

§ 1. Introduction

The detailed mechanism of the increase in strength of metals resulting from plastic deformation remains one of the most important problems in the dislocation theory awaiting satisfactory solution. It is generally agreed that the finite stress needed to cause plastic flow is due to obstacles impeding the motion of dislocations through a crystal. The relative importance of various types of obstacles in determining the flow stress of strain hardened metals, however, is still a subject of speculation. It is convenient to divide obstacles into two groups according to the distance over which they interact with the glide dislocations. The obstacles exerting short range forces, such as forest dislocations (Cottrell

---

† Communicated by the Author. This work was first presented at the annual metal physics conference, Kingston, Ontario, September 1957 ; and also at the Ottawa Symposium on Melting, Diffusion and related topics, October 1957 (Basinski 1958).

1952) or jogs (Mott 1951, Seitz 1952) can be overcome at finite temperatures with the help of thermal fluctuations, even though the force on the glide dislocations is smaller than the force exerted by the obstacles. This type of interaction will lead to temperature and strain rate dependent flow stress. On the other hand, the activation energies involved when the dislocation moves under adverse stress over a large distance would be outside the range of thermal fluctuations at ordinary temperatures. We must therefore expect that the flow stress originating from long-range elastic interactions between dislocations should be independent of the strain rate, and depend on temperature only through elastic moduli. Experiments on the temperature and strain rate variation of the flow stress should therefore provide a means of distinguishing between long- and short-range obstacles. We must remember, however, that any obstacle interacting with the glide dislocations over distances larger than 5–10 interatomic spacings will behave as a long-range obstacle in this type of experiment, and that some additional justification will be needed to identify it with the long-range elastic stress field of other dislocations whose wavelength will be comparable to, or larger than the average distance between the dislocations.

Cottrell and Stokes (1955) pointed out that the difference in flow stress when a specimen is deformed to the same strain at two different temperatures arises from two distinct contributions; i.e. the difference arising from the variation of the dislocation configuration with temperature and the 'reversible' difference due to the help from thermal fluctuations in overcoming the obstacles. Here, we shall be concerned only with the 'reversible' contribution.

The reversible change of flow stress was measured down to liquid nitrogen temperature by Cottrell and Stokes (1955) and Adams and Cottrell (1955) in single crystals of aluminium and copper. Their results indicate that the ratio of flow stresses at two given temperatures settles down to a constant value after the initial few per cent of deformation, this value being independent of the thermal and mechanical history of the specimen. Essentially the same result was reported more recently by Seeger *et al.* (1957) for single crystals of copper. The increase of the temperature and strain rate dependent flow stress with the total stress can also be deduced from the work of Wyatt (1953) on creep of polycrystalline copper. In this case, however, the experimental scatter is too large to enable an unambiguous conclusion on the constancy of the flow stress ratio to be reached.

In most of the existing theories the major part of strain hardening is ascribed to the long-range elastic interactions between parallel dislocations accumulating in the lattice during the deformation. According to Mott (1953) the back stress radiating from a group of dislocations piled up behind Cottrell–Lomer barriers can stop the generation of further dislocations by the source until the applied stress is increased. Quantitative development of the theory leads to a parabolic stress–strain relation.

Friedel's theory (1955) of linear hardening observed in face-centred cubic metals at low temperatures, assumes that each source forms a complete Cottrell–Lomer barrier around itself in the early stages of deformation. Here again, the back stress from the piled-up loops is responsible for the increase in strength during the deformation. Seeger *et al.* (1957) identify the main obstacles with the internal stress field in the crystal produced by groups of about 25 piled-up dislocations, although the mechanism responsible for arranging the dislocations in such groups is not specified.

These theories all suffer from a common drawback. It is difficult to explain with their help the almost total irreversibility of plastic deformation. The mechanisms relying on Cottrell–Lomer barriers are also incapable of being extended to body-centred cubic and hexagonal close-packed metals, since no dislocation reaction leading to a strong sessile is known for these lattices. Also, recent calculations by Stroh (1956) suggest that these barriers are not as strong as formerly thought, and that it is unlikely that they will be able to support a large number of dislocations piled up behind them.

Several explanations have been advanced to account for the remarkable constancy of the flow stress ratio, which implies proportionality between long and short-range forces exerted by the obstacles at all stages of hardening. Adams and Cottrell (1955) suggest that the pattern of dislocations remains constant during the deformation and only the scale changes. According to the theory of Seeger *et al.* (1957), the amplitude of the internal stress increases as the square root of the dislocation density; since the flow stress arising from the interaction with the forest should also depend in this way on the dislocation density, the theory requires proportionality of the hardening from the two sources.

Finally, it was suggested by Mott (see Cottrell and Stokes 1955) that "the important elastic forces on a glide dislocation are those from its immediate neighbours rather than the long-range stresses from piled up groups, for then the elastic forces and the forest forces acting on the dislocation can both be ascribed to the same thing, the presence of nearby dislocations". This idea is attractive. However, if it is to explain the constancy of the flow stress ratio, the important elastic forces must be restricted to those dislocations which can act as short-range obstacles, i.e. the dislocations threading the glide plane.

In the present work an attempt has been made to identify the obstacles by the distance over which they interact, and to form a consistent picture of the hardening process. The temperature dependence of the flow stress was measured both for polycrystalline and single crystal samples of high purity aluminium, and for single crystals of copper and silver, down to temperatures approaching absolute zero. To obtain additional information on the nature of the retarding forces created by obstacles, and to eliminate the possibility of stress change resulting from effects other than the thermal activation of the dislocations over obstacles, the strain rate dependence of the flow stress of single crystals was measured over the whole temperature range. The results were used to determine the form of the relation between the distance over which the dislocation has to move to overcome the obstacle, and the retarding force on it. An approximate value of the maximum force was obtained. Some experiments were designed to try to upset the proportionality between long- and short-range forces.

It will be shown that the internal stresses whose wavelengths are large in comparison with the mean separation of the dislocations could not be effective in retarding the glide, and that the forces between individual dislocations are mainly responsible for strain hardening.

The model proposed accounts for most observations on deformation. The values of the rate of hardening, and the magnitude of the Bauschinger effect derived from it, agree well with experimental data. The difficulties associated with the interpretation of hardening in body-centred cubic metals are also removed.

§ 2. MATERIALS AND TECHNIQUES

Polycrystalline aluminium specimens were prepared from the high purity metal presented by Aluminum Company of America. The analysis supplied was,

Cu, 0·002%; Fe, 0·001%; Si, 0·002%; Mg, 0·001%.

Specimens having a gauge length of 5 cm and a diameter of 3 mm were machined from rod drawn down to 4·8 mm diameter. Fillets of radius 3 mm were left at each end of the specimen. A grain size of about 120 grains per mm^2 was produced by annealing at 325°C for one hour. The specimens were electropolished in a sulphuric-phosphoric acid mixture. Single crystal specimens of high purity aluminium were made from Johnson-Matthey spectroscopically pure metal containing,

Cu, 0·0005%; Fe, 0·0005%; Si, 0·0005%; Mg, 0·005%.

The rods provided were drawn into wires of 2·2 mm diameter and cut into 60 cm lengths. These, after being carefully cleaned in sodium hydroxide solution, were packed with high purity alumina into silica tubes and passed through a horizontal furnace at 720°C at a rate of 3 mm per minute. In all cases the whole length of the wire was converted into a single crystal. Subsequent spectrographic analysis disclosed no detectable contamination. Crystals 6·5 cm in length were cut with specially sharpened cutters. Only those specimens which showed no noticeable bending were used for testing. Any adhering alumina powder was removed by etching in sodium hydroxide solution. The crystals were then electropolished.

Copper and silver single crystals of 1·6 mm diameter were made from Johnson-Matthey spectroscopic standard metals of analysis:

Silver: Fe, 0·0002%; Cu and Pb, 0·0001%; Ca, Mg, Si, Na, 0·0001%.

Copper: Ag, 0·0005%; Ni, $<$0·0003%; Pb, $<$0·0004%.

The method of production of the specimens was similar to that used for pure aluminium, but to prevent oxidation, high purity graphite was used to pack the wires in the silica tubes. The specimens cut from long single crystals were designated by letters a, b, etc., starting from the end first to solidify.

The orientations of the axes of tension of the specimens were determined by the rotating crystal method (Schmid and Boas 1950). The orientations are shown in fig. 1.

Fig. 1

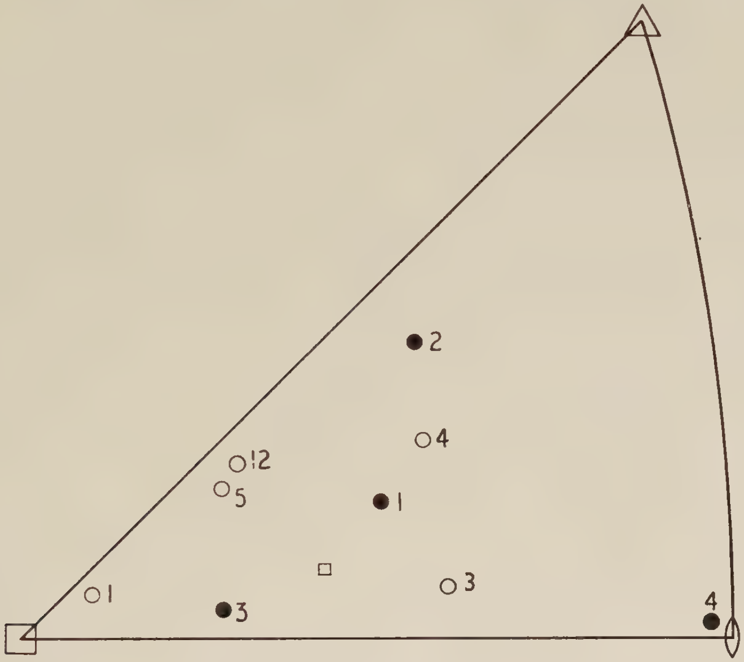

Orientations of crystals tested.
● Aluminium.
○ Copper.
□ Silver.

Polycrystalline specimens were deformed in a screw-driven resistance strain gauge tensile testing machine described previously (Basinski 1957). Experiments on single crystal specimens were carried out using an improved version of this machine†. The stress was measured by means of a cell consisting of four resistance strain gauges in a Wheatstone bridge mounted on a cantilever beam of 24S alloy; the cell was calibrated to 50 kg against dead weights, and was found to be reproducible and linear to better than 0·1%. The output, after amplification, was applied to a Speedomax recorder, producing the load elongation curve directly. Since the changes of stress involved were very small an auxiliary circuit was incorporated allowing the zero to be suppressed in ten steps, thus obtaining high sensitivity, a deflection of 2·54 mm corresponding frequently to about 0·1% of the maximum stress. A sliding O-ring seal between the two crossheads prevented condensation of air in the specimen chamber at very low temperatures without introducing friction on the load transmitting member of the machine. The crosshead was driven from a synchronous motor by two gear boxes in series, one giving a range of strain rate from 10^{-3} to $10^{-6}\,\text{sec}^{-1}$, the other enabling the rate of deformation to be changed instantaneously by a factor of 10. Both the crosshead and the recorder chart were driven from the same shaft.

---

† The author is grateful to Dr. J. W. Christian for collaboration in building this machine.

With the older machine the temperatures were measured with a copper–constantan thermocouple previously calibrated against a gas thermometer. Below 78°K and at 125°K a gas flow cryostat (Swenson and Stahl 1954) was employed; other points were obtained using constant temperature baths. The baths and the respective temperatures which they maintained were: liquid nitrogen, b.p. 78°K; isopropyl chloride, m.p. 144°K; solid acetone, m.p. 179°K; acetone–carbon dioxide, 200°K; ice–calcium chloride, 225°K; ice point, 273°K; boiling water, 373°K; and stanalax, controlled at 483°K. In all cases the baths were stirred gently with a mechanical stirrer and all were reproducible to within 1°K, with the exception of the acetone–carbon dioxide point; in this case it was difficult to keep the temperature within ± 5°K. In the experiments with aluminium, the solid acetone point was 163°K, which probably resulted from pre-cooling with solid carbon dioxide.

In the work with single crystals a cryostat standard in this laboratory (White 1958) was used for points not obtainable by the use of standard baths. Here, the temperature was electronically controlled to within 0·01°K and measured directly with a constant volume gas thermometer.

The single crystals were held in split grips with a threaded circular hole of diameter slightly smaller than that of the specimen, leaving a 5 cm exposed length. No slipping in the grips was detected, and since in many cases easy glide up to about 30% was observed, this method of mounting was considered not to introduce serious deformation in the exposed test section. For the experiments in which the specimens were intermittently twisted during stretching, the lower grip was mounted on a ball race, and had a handle by means of which the grip was easily turned through any angle.

§ 3. Some Theoretical Relations

Since the reversible change of flow stress with temperature increases with the amount of deformation, some obstacles exerting short-range forces on dislocations must be formed during the glide process. Two kinds of obstacle have been considered by previous workers; those arising from the cutting of the dislocation forest by glide dislocations, proposed by Cottrell (1952) and developed theoretically by Seeger (1954); and also the short-range retarding influence of jogs in screw dislocations (Seeger 1955 a). It has been pointed out by Mott (1956 a) that since these jogs can undergo conservative motion, they will be ineffective as obstacles. In the following treatment, we shall therefore consider only the mechanism of overcoming the dislocation forest.

In Seeger's theory it was assumed that the forest is distributed uniformly, and that the activation energy decreases linearly with increasing applied stress over the whole process of intersection of dislocations. The activation energy arises from the work done by the dislocation against the net retarding force in overcoming an obstacle, and the assumption of linear dependence implies that the retarding force exerted by the obstacle is constant, independent of the dislocation position. This assumption, as applied to cases in which dislocations are split into partials, seems questionable, since complete intersection comprises two distinct processes, i.e. the formation of constrictions, and subsequent formation of jogs in the constricted dislocations. These processes might overlap to some extent in metals with low stacking fault energy. There is, however, no justification in assuming that the retarding force from an obstacle will be constant and the same for both processes.

Here, we shall *not* assume *à priori* the form of the variation of activation energy with stress, but rather *derive* relations by which it can be obtained from experimentally observable quantities. Also, we shall not use the restriction of the uniform distribution of the dislocation forest.

Consider a dislocation line pressing against a row of identical forest dislocations whose spacing along the line is not necessarily uniform. We shall assume that the retarding force $\mathrm{F}(x)$, on each segment of a glide dislocation held up by an obstacle will vary in some manner with its distance (x) from the obstacle. The force F pressing the segment forward will depend on its length and on the applied stress. Obviously the obstacle will be overcome when the retarding force is the greater only if sufficient activation energy, U, can be acquired from thermal fluctuations. The value of this energy will be given by,

$$U = -\int_{x_{\mathrm{eq}}}^{0} (\mathrm{F}(x) - F)\,dx$$

where x_{eq} is defined by $\mathrm{F}(x_{\mathrm{eq}}) = F$.

Integrating by parts, we have:

$$U = \int_{F}^{F_{\max}} x\,d\mathrm{F}(x)$$

where F is the force on the dislocation segment from the applied stress, $F_{\max}$ is the maximum retarding force exerted by the obstacle, and x is the distance which the segment must move under adverse force, i.e. the activation distance. The non-uniformity of the forest distribution will result in a corresponding spread in the values of U. To deal with it, following Cottrell (1952), we shall identify an array of segments of glide dislocations held up by obstacles with the 'soft spots' of Wyatt's theory of creep (1953), and we shall derive the rate of thermally activated glide using this formal model. It seems improbable that the passage of one dislocation over an obstacle will appreciably increase the activation energy required by the next dislocation. We shall therefore assume throughout this work that each 'soft spot' can be used n times before being removed. With this modification, Wyatt's equation gives for the strain rate,

$$\dot{\epsilon}=nNAb\,dU/dt \qquad \ldots\ldots\ldots \quad (1)$$

where N, assumed here to be independent of U (Cottrell 1953), is the number of 'soft spots' per cubic centimetre having activation energy between U and $(U+dU)$, A is the area swept by a dislocation after overcoming an obstacle, and b is the Burgers vector; dU/dt is the "rate of advance of the thermal front". As shown by Wyatt the shape of the thermal front remains unchanged during deformation, and its rate of advance is given by

$$\frac{dU}{dt}=\frac{kT}{t}.$$

Since we are not dealing here with creep experiments, the time t is an inconvenient parameter. However, it may be eliminated and the rate of advance of the thermal front expressed in terms of the activation energy, say U_m†, corresponding to the position of steepest slope. Let us now do this. Wyatt's expression for the distribution of activation energy in yet unremoved soft spots modified by assuming that each soft spot may be triggered n times before being removed is

$$N(U,t)=N\exp\left\{-\frac{\nu t}{n}\exp(-U_m/kT)\right\}$$

where ν is the frequency of vibration of a dislocation against the obstacle, k is Boltzmann's constant, and T is absolute temperature.

Differentiating this equation twice with respect to U to yield maximum slope and setting the result equal to zero we find:

$$\frac{1}{t}=\frac{\nu}{n}\exp(-U_m/kT),$$

thus, substituting in the previous equation for dU/dt, we have:

$$\frac{dU}{dt}=\frac{kT\nu}{n}\exp(-U_m/kT)$$

where, we repeat, U_m is the activation energy of soft spots lying on the steepest part of the thermal front.

Combining the last equation with eqn. (1) we get:

$$\dot{\epsilon}=NkTAb\nu\exp(-U_m/kT) \qquad \ldots\ldots \quad (2)$$

which differs from the corresponding formula given by Seeger (1955 a) for uniformly distributed obstacles only in that the number of effective 'soft spots' depends on temperature. The strain rate obtained is thus the same as that produced from NkT 'soft spots' having activation energy U_m. We shall now drop the subscript m, and write the energy simply as U.

---

† The choice of U_m as reference energy is somewhat arbitrary, but since the thermal front is very steep the particular choice of an energy to characterize the front is not very important.

Equation (2) can now be written,

$$U = kT \ln (NkTAb\nu)/\dot{\epsilon}. \qquad (3)$$

The variation of $Ab\nu$ with temperature is small and will be neglected. Differentiating with respect to temperature at constant strain rate, and with respect to $\ln \dot{\epsilon}$ at constant temperature,

$$\left(\frac{\partial U}{\partial T}\right)_{\dot{\epsilon}} = k[\ln NkTAb\nu/\dot{\epsilon} + 1] \qquad (4)$$

and

$$\left(\frac{\partial U}{\partial \ln \dot{\epsilon}}\right)_T = -kT. \qquad (5)$$

The retarding force acting on a segment of dislocation will vary with temperature. The forces acting over a distance larger than a few interatomic spacings will result mainly from the interaction of the elastic stress fields of dislocations, and therefore should be proportional to the elastic modulus, μ. It is more difficult to decide the way in which the forces resulting from the intersection process will depend on temperature. For want of data, and for simplicity, we shall assume here that all retarding forces are proportional to the elastic modulus. Since the variation of lattice parameter with temperature is small in comparison with the variation of elastic modulus, it will be neglected.

The temperature dependence of the activation energy is now,

$$\left(\frac{\partial U}{\partial T}\right)_{\dot{\epsilon}} = \left(\frac{\partial U}{\partial T}\right)_{F/F_{\max}} + \left(\frac{\partial U}{\partial F/F_{\max}}\right)_{\mu T} \left(\frac{\partial F/F_{\max}}{\partial T}\right)_{\dot{\epsilon}} \qquad (6)$$

and since the forces are proportional to μ

$$\left(\frac{\partial U}{\partial T}\right)_{F/F_{\max}} = U \frac{\partial \ln \mu}{\partial T} \qquad (7)$$

also,

$$\left(\frac{\partial U}{\partial \ln \dot{\epsilon}}\right)_T = \left(\frac{\partial U}{\partial F/F_{\max}}\right)_{\mu T} \left(\frac{\partial F/F_{\max}}{\partial \ln \dot{\epsilon}}\right)_T. \qquad (8)$$

From (5), (6), (7) and (8) we get

$$\left(\frac{\partial U}{\partial T}\right)_{\dot{\epsilon}} \bigg/ \left(\frac{\partial U}{\partial \ln \dot{\epsilon}}\right)_T = -\frac{U}{kT}\frac{\partial \ln \mu}{\partial T} + \left(\frac{\partial F/F_{\max}}{\partial T}\right)_{\dot{\epsilon}} \bigg/ \left(\frac{\partial F/F_{\max}}{\partial \ln \dot{\epsilon}}\right)_T \qquad (9)$$

but from (4) and (5)

$$\left(\frac{\partial U}{\partial T}\right)_{\dot{\epsilon}} \bigg/ \left(\frac{\partial U}{\partial \ln \dot{\epsilon}}\right)_T = -\frac{1}{T}[\ln (NkTAb\nu/\dot{\epsilon}) + 1] \qquad (10)$$

combining (3), (9) and (10),

$$\ln (NkTAb\nu/\dot{\epsilon}) = -\left(1 + \frac{(\partial(F/F_{\max})/\partial T)_{\dot{\epsilon}}}{(1/T)(\partial(F/F_{\max})/\partial \ln \dot{\epsilon})_T}\right) \bigg/ \left(1 - \frac{T\,\partial \ln \mu}{\partial T}\right). \qquad (11)$$

At any given dislocation configuration,

$$\frac{F}{F_{\max}}=\frac{\sigma/\mu}{\sigma_0/\mu_0}$$

where σ is the flow stress, and subscript 0 indicates the value at absolute zero.

Equation (11) then becomes,

$$\ln(NkTAb\nu/\dot{\epsilon})=-\left[1+\frac{\left(\partial\frac{\sigma/\mu}{\sigma_0/\mu_0}\Big/\partial T\right)_{\dot{\epsilon}}}{\frac{\sigma/\mu}{\sigma_0/\mu_0}\frac{1}{T}\left(\frac{\partial\ln\sigma}{\partial\ln\dot{\epsilon}}\right)_T}\right]\Bigg/\left(1-\frac{T\,\partial\ln\mu}{\partial T}\right). \qquad (12)$$

The value of the activation energy can be obtained from (3) and (12). Thus the measurement of the change of flow stress with both temperature and strain rate should enable us to obtain the values of $\ln NkTAb\nu/\dot{\epsilon}$ and the activation energy for overcoming obstacles.

The variation of the activation distance with the force on the dislocation segment should be of interest, since the form of this curve may yield some information about the obstacle. The form of the curve connecting the force and activation distance can be obtained in the following manner.

The variation of the activation energy with the applied force on a dislocation segment will be given by,

$$\left(\frac{\partial U}{\partial F}\right)_\mu=-x \quad . \quad . \quad . \quad . \quad . \quad . \quad . \quad . \quad (13)$$

or,

$$\left(\frac{\partial U}{\partial F/F_{0\max}}\right)_\mu=-xF_{0\max} \quad . \quad . \quad . \quad . \quad . \quad . \quad . \quad (14)$$

where $F_{0\max}$ is the maximum retarding force exerted by an obstacle under conditions corresponding to absolute zero. Using an equation corresponding to (5) and (8) where $F_{\max}$ is replaced by $F_{0\max}$, we obtain,

$$\left(\frac{\partial U}{\partial F/F_{0\max}}\right)_\mu\left(\frac{\partial F/F_{0\max}}{\partial\ln\dot{\epsilon}}\right)_T=-kT, \quad . \quad . \quad . \quad . \quad (15)$$

therefore

$$xF_{0\max}=kT\Big/\frac{F}{F_{0\max}}\left(\frac{\partial\ln F}{\partial\ln\dot{\epsilon}}\right)_T. \quad . \quad . \quad . \quad . \quad (16)$$

Since all the changes are taken at a given dislocation configuration, we can write,

$$xF_{0\max}=kT\Big/\frac{\sigma}{\sigma_0}\left(\frac{\partial\ln\sigma}{\partial\ln\dot{\epsilon}}\right)_T. \quad . \quad . \quad . \quad . \quad . \quad (17)$$

The values of $F_0/F_{0\max}$, the ordinates of the force–distance curve, are most easily obtained from the temperature variation of the flow stress by using the expression,

$$\frac{F_0}{F_{0\max}}=\frac{\sigma/\mu}{\sigma_0/\mu_0} \quad . \quad . \quad . \quad . \quad . \quad . \quad . \quad . \quad (18)$$

where F_0 is the force corresponding to the absolute zero value of the modulus.

The above calculation gives only the form of the required curve. A method of obtaining absolute values of the forces involved will be considered later.

§ 4. TEMPERATURE AND STRAIN RATE DEPENDENCE OF THE FLOW STRESS

The reversible changes of the flow stress with temperature and strain rate were measured by deforming the specimens alternately at two different temperatures at a tensile strain rate of $1 \cdot 1 \times 10^{-4}\,\mathrm{sec}^{-1}$ for aluminium polycrystals, and $10^{-4}\,\mathrm{sec}^{-1}$ for all single crystal samples. The rate of deformation of single crystals was taken to $10^{-5}\,\mathrm{sec}^{-1}$ and back several times at each temperature; in some experiments the strain rate was also taken to $10^{-3}\,\mathrm{sec}^{-1}$ and back to check the linearity of the flow stress change with $\ln \dot{\epsilon}$.

To limit the deformation by creep during the period when the temperatures were being altered, the load had to be relaxed. It was, however, found that this unloading introduced a small yield point on retesting at the same temperature. Similar behaviour was also observed by Haasen and Kelly (1957) in nickel, and more recently in copper by Makin (1958 a). A compromise solution was therefore adopted, the load on the specimens being kept to a minimum of 85% of the flow stress while the temperature was being changed. At temperatures below about 50°K, decreasing thermal expansion, specific heat and creep rate, enabled the maximum unloading to be limited to about 2%. Since the change in strain rate was accomplished instantaneously, no complications due to unloading were introduced here.

Copper and silver single crystals usually showed large regions of easy glide deformation, in some cases extending to strains as high as 30%. In the easy glide region, the stress–strain curve was usually serrated, smoothing out only when rapid hardening began. Some typical portions of the load elongation curves of copper single crystals are shown in fig. 2.

At temperatures below about 100°K in the early stages of deformation, the load followed an almost stepwise path when either the temperature or strain rate was changed. At higher strains, for both strain rate and temperature alteration, a region of decreased or even negative strain hardening followed the increase in load, giving the appearance of a small yield point. Conversely a dip in the curve was always associated with decreasing strain rate, and a gradual transition between elastic and plastic deformation was typical of reloading at higher temperatures. At temperatures and strain rates corresponding to stage III of hardening, the increase in strain rate produced a sharp change of stress followed by an increase in the slope of the curve, before the normal rate of hardening was resumed. Decreasing the strain rate resulted in a sharp drop in load which then slowly decreased before resuming the normal rate of strain hardening. The flow stress changes of aluminium and silver single crystals followed a similar form on changing either the strain rate or temperature. The stress–strain curves obtained from polycrystalline samples of aluminium followed essentially the same pattern as the single crystal curves. In general, however, the transitions between elastic and plastic deformation were less well defined.

The similarity in form of the curves following increase in strain rate and decrease in temperature, and vice versa, is striking.

We are interested in the difference in the flow stress corresponding to the same dislocation configuration at two temperatures or strain rates. To avoid the difficulty of defining the transition between elastic and plastic flow, and the complications introduced by work softening, only the changes resulting from the increase in stress were used for determination of the reversible temperature and strain rate dependence of the flow stress. For this purpose, it must be decided which value of the flow stress after the change, corresponds to the original dislocation configuration. Since no extraneous effects are introduced by altering the strain rate, immediately adjacent values (A and B, fig. 2) are taken.

Fig. 2

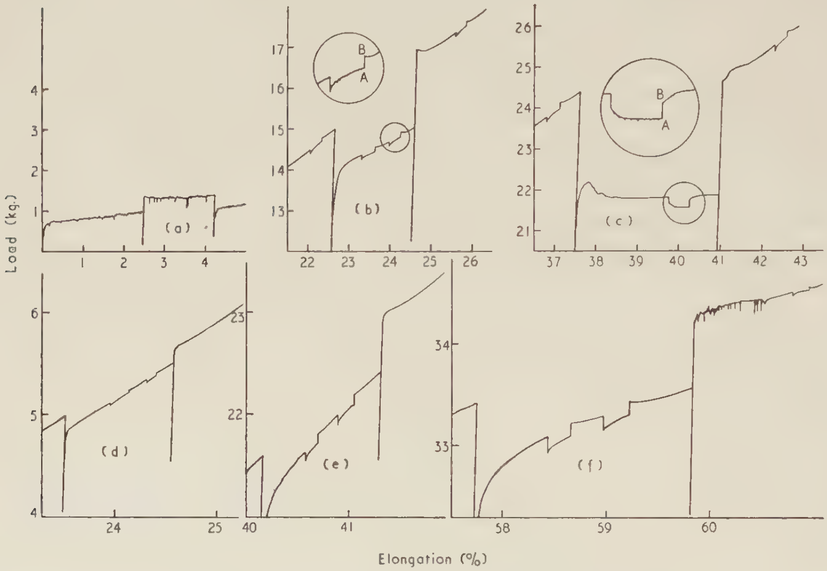

Portions of the load–elongation curves of copper crystals. (*a*), (*b*) and (*c*), specimen 4c, temperatures shown 295 and 78°K. (*d*), (*e*) and (*f*), specimen 4d, temperatures shown 4·2 and 25·9°K. The serrations after the change of temperature to 4·2°K in (*f*) probably represent unstable adiabatic slip resulting from the decreased rate of strain hardening.

Because of the similarity of the forms of the curves, it was expected that the same mechanism was responsible for the appearance of a hump in the curve on lowering the temperature, and immediately adjacent values were also used in this case. It might be argued that in this way a small increase in stress resulting from the inloading would be included. However, this was always kept to a minimum and the error introduced by such a procedure should not be large.

It should be noticed that the yield points are produced always when the stress is suddenly increased, independent of whether it is due to increase in the strain rate, decrease in temperature, or previous unloading. On the other hand, a decrease in stress results in a sharp dip in the curve. This type of behaviour may be explained as a certain amount of cooperation between the glide dislocations in overcoming obstacles. When the effective strength of the obstacles is suddenly increased, the dislocations will redistribute themselves during subsequent glide. The average number of dislocations which can be held behind a row of obstacles will increase, resulting in a lower observed flow stress. Conversely, a decrease in the effective obstacle strength will cause a redistribution leading to an increase in the flow stress on subsequent deformation.

Makin (1958 a) interpreted the appearance of yield points on reloading in terms of the formation of Cottrell–Lomer sessiles during unloading. The additional stress needed to dissociate them subsequently, accounted for the yield point. On this basis Makin (1958 b) decided that the curve should be extrapolated back through the yield point to obtain a value of the flow stress corresponding to the previous dislocation configuration. Makin's theory, however, cannot explain the appearance of the yield point with increasing strain rate, nor the dip following decrease in strain rate.

Similar yield points were observed after unloading also in polycrystalline iron specimens (Basinski and Christian 1959) where no possible sessiles of this type are known to form. We therefore believe that the unextrapolated values are still preferable.

The flow stress ratios for temperature change were found to be substantially constant, independent of the value of total stress both in stage II and stage III of the deformation, after a few per cent deformation in the linear portion of the curve. This is in agreement with the work of Cottrell and Stokes (1955) on aluminium and Adams and Cottrell (1955) on copper. Constancy of the ratios was also observed in the strain rate experiments. Deviations from proportionality were found early in the deformation, especially at stage I, at temperatures above 80°K (cf. Seeger *et al.* 1957). At low temperatures (below 35–40°K) the ratios were constant over the entire range of deformation.

Figure 3 shows the flow stress ratios for strain rate changes from $10^{-5}\,\mathrm{sec}^{-1}$ to $10^{-4}\,\mathrm{sec}^{-1}$ plotted against the stress at $10^{-5}\,\mathrm{sec}^{-1}$ for aluminium at 17·2°K and 78°K and copper at 25·9°K and 78°K. The ratio in the early stages of deformation varies from specimen to specimen, whereas it is approximately the same for all work hardened specimens at each temperature.

Seeger *et al.* (1957) interpreted the larger fractional changes of the stress in the easy glide region as indicating that the short-range forces arising from dislocation interactions are unrelated to the long-range interactions. In view of the results described above it seems more reasonable to conclude that the interactions between the dislocations give rise to a constant flow stress ratio, and that the deviations are due to some other mechanism, such as the effect of impurity atoms, a small Peierls–Nabarro force, etc. A small stress depending on temperature and strain rate, but not on strain would predominate when the stress due to the interaction of dislocations is small, but at higher strains, when the dislocations are more dense, it would be masked.

Fig. 3

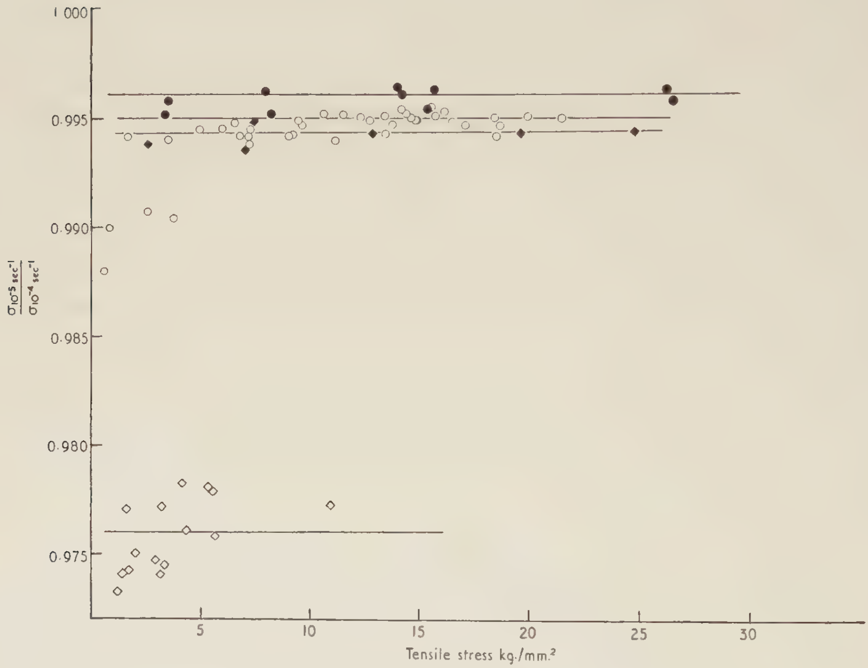

Ratio of the flow stresses at strain rates of 10^{-5} and 10^{-4} sec^{-1}.
◇ Aluminium 78°K ; ◆ Aluminium 17·2°K.
○ Copper 78°K ; ● Copper 25·9°K.

That this assumption is not unreasonable follows from the work of Basinski and Christian (1959) on the temperature and strain rate dependence of the flow stress of iron, where the absolute values of the flow stress changes were independent of the total stress. The data obtained on unhardened specimens should be treated with caution as is indicated by a result on silver during easy glide, which *softened* reversibly when cooled from 78° to 4·2°K. It is interesting to note that the strain rate flow stress dependence had the right sign. In the linear hardening region the temperature dependence became normal again. No explanation is offered here for this curious behaviour, but it is hoped that the question will be investigated further.

The ratio of the flow stress of aluminium at a temperature T to that at 4·2°K is shown as a function of temperature in fig. 4.

The data were taken from the constant ratio region. Two standard temperatures were used, below 78°K specimens were cooled directly to 4·2°; to avoid prohibitive consumption of helium, the transitions from higher temperatures were made to 78°K, and the ratios of the flow stresses at T°K and 4·2°K were obtained from the relation,

Fig. 4

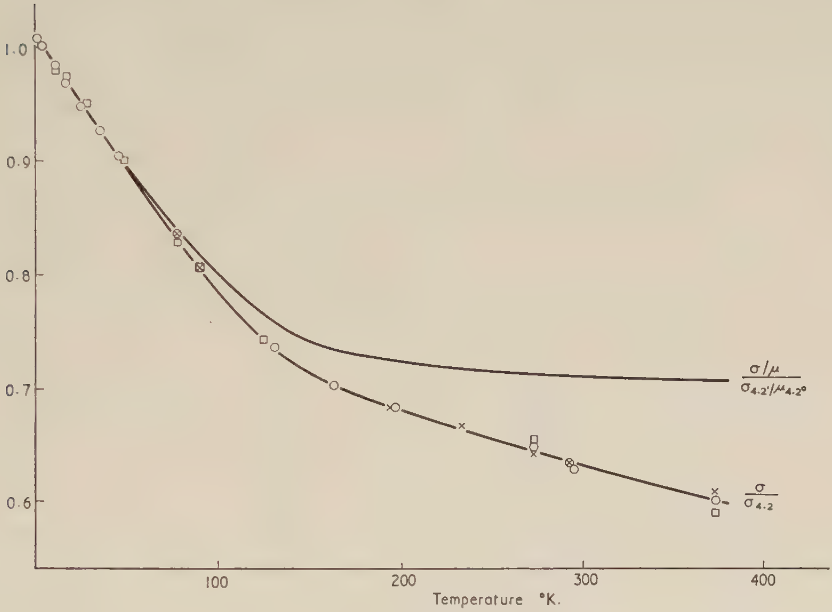

The ratio of the flow stresses at temperature, T, to that at 4·2°K for aluminium.
□ Date from polycrystalline specimens.
○ Data from single crystals.
× Points of Cottrell and Stokes (1955) normalized at 78°K.

$$\frac{\sigma_T}{\sigma_{4\cdot2}} = \frac{\sigma_T}{\sigma_{78}} \cdot \frac{\sigma_{78}}{\sigma_{4\cdot2}}.$$

The validity of this type of relation was clearly demonstrated by Cottrell and Stokes (1955), whose data normalized to 78°K are included in the figure for comparison. The upper curve gives the flow stress corrected for the temperature variation of elastic modulus. It was assumed that the appropriate modulus was that given by Foreman (1955) for a mixed dislocation lying in a $\{111\}$ plane; Sutton's values (1953) for c_{11}, c_{12} and c_{44} were used.

The corrected curve drops almost linearly down to 80°K then bends over and becomes almost horizontal at about 300°K. No discontinuity between the temperature dependent and independent portions of the curve (Seeger 1956) was found. The agreement between the different sets of data is very satisfactory. The absence of any appreciable difference between the ratios obtained on single crystals and polycrystalline samples strongly indicates that the distribution of the dislocations cannot play an important part in determining the values of the flow stress.

The flow stress changes produced by taking the strain rate from $10^{-5}\,\mathrm{sec}^{-1}$ to $10^{-4}\,\mathrm{sec}^{-1}$ and from $10^{-4}\,\mathrm{sec}^{-1}$ to $10^{-3}\,\mathrm{sec}^{-1}$ were essentially the same, indicating that the flow stress varies linearly with $\ln \dot{\epsilon}$ at least over this range of strain rates. The values of $(1/T)(\partial \ln \sigma/\partial \ln \dot{\epsilon})_T$ were therefore obtained from the stress changes between the strain rates of $10^{-5}\,\mathrm{sec}^{-1}$ and $10^{-4}\,\mathrm{sec}^{-1}$, and are shown for aluminium in fig. 5. Numerical values are given in table 1.

Table 1. Strain Rate Sensitivity of Aluminium

Temperature (°K)	$\frac{1}{T}\left(\frac{\partial \ln \sigma}{\partial \ln \dot{\epsilon}}\right)_T \times 10^5$
4·2	28·0
11·5	15·1
17·2	14·1
26·0	15·9
35·5	14·1
45·5	15·3
78·0	13·4
90·0	10·8
131·0	5·4
163·0	2·7
200·0	2·3
295·0	0·6

For stress changes resulting from a thermally activated process, $(1/T)(\partial \ln \sigma/\partial \ln \dot{\epsilon})$ which we shall call the strain rate sensitivity, should be approximately proportional to

$$\left[\frac{\partial(\sigma/\mu)/(\sigma_0/\mu_0)}{\partial T}\right]_{\dot{\epsilon}}$$

(see eqn. (12)) and should thus follow approximately the slope of the flow stress ratio–temperature curve.

Disregarding for the moment the increase in the strain rate sensitivity at 4·2°K, which will be discussed later, comparison of figs. 4 and 5 shows that the qualitative agreement between the strain rate and temperature data is good. At temperatures up to about 80°K the flow stress decreases almost linearly with temperature, and the strain rate sensitivity is almost constant, its drop at higher temperatures coincides with the levelling off of the stress–temperature curve.

Fig. 5

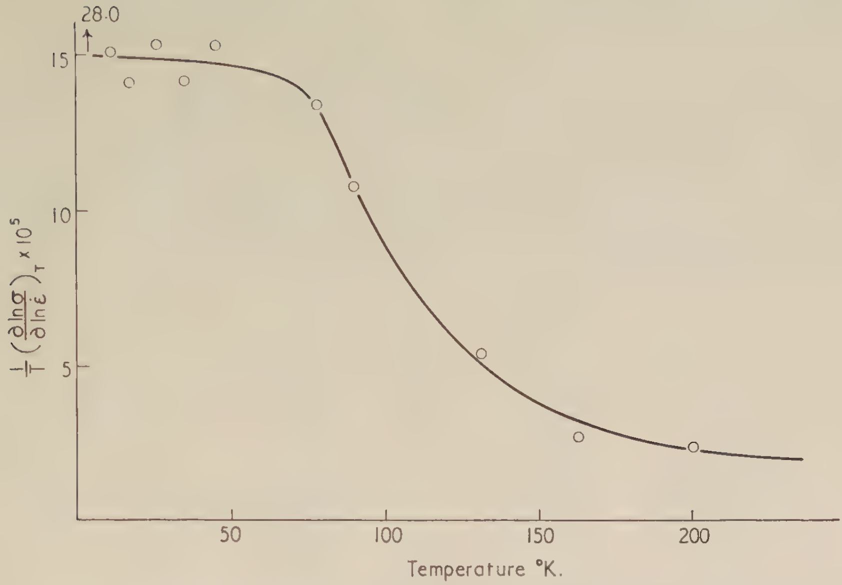

Temperature dependence of the strain rate sensitivity of aluminium.

Fig. 6

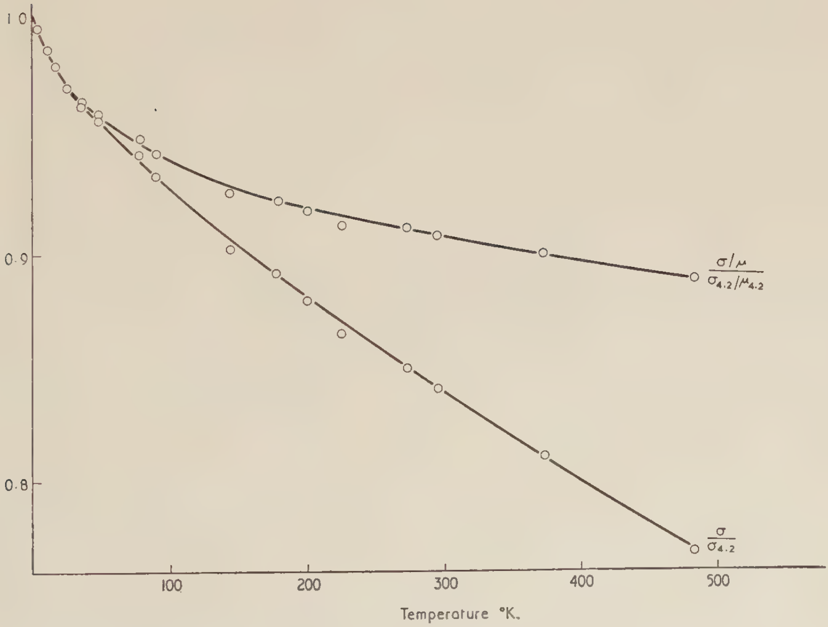

The ratio of the flow stresses at temperature, T, to that at 4·2°K for copper.

The temperature dependence of the flow stress ratio of copper single crystals is shown in fig. 6. Overton and Gaffney's (1955) values of c_{11}, c_{12} and c_{44} were used to calculate the temperature variation of the elastic modulus. The corrected flow stress drops linearly with temperature to about 30°K, the rate of change then decreases slowly with increasing temperature. The curve remains continuous throughout, and no sign of the rapid change near 220°K, reported by Adams and Cottrell (1955) and by Makin (1958 b) was observed. (Although no direct comparison can be made with Makin's results which were obtained by extrapolating across the yield drops.)

Fig. 7

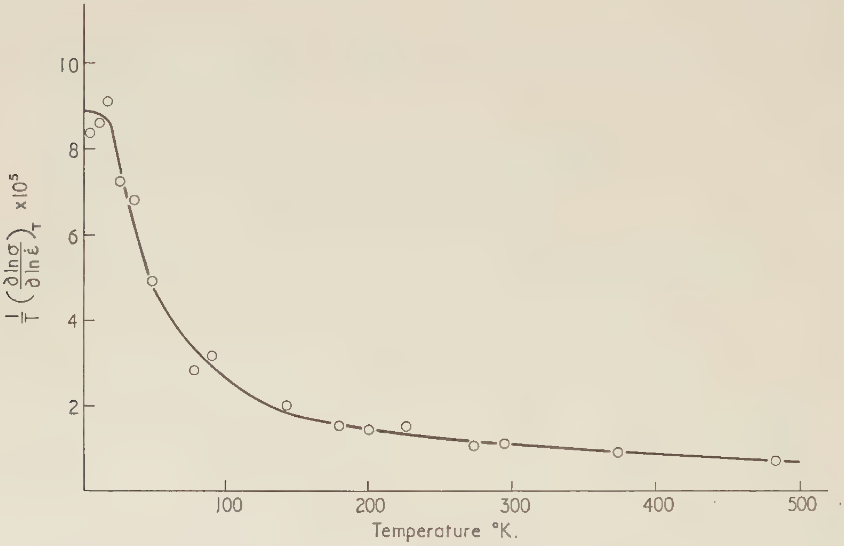

Temperature dependence of the strain rate sensitivity of copper.

The temperature variation of the strain rate sensitivity of copper is shown in fig. 7, and the numerical values are given in table 2.

The agreement between the temperature and strain rate data is also good in this case. No increase in the strain rate sensitivity of the flow stress was found in the region of the step in the temperature dependence reported by the above authors.

The discrepancy between the present data and those of Adams and Cottrell, and Makin is disturbing. In copper, the variation of elastic modulus with temperature is somewhat larger, at any rate above the temperature of liquid nitrogen, than the variation in the corrected flow stress. Also, in the flow stress–temperature experiments, the complicating effects of small possible amounts of recovery and unloading are present. A small step in the stress–temperature curve could thus possibly be masked. None of these sources of error applies to experiments in which the stress changes result from changes in strain rate, and more reliable data can be obtained from these experiments. If the rapid change of stress at the step in the stress–temperature curve were produced by the thermal activation of dislocations during glide (Adams and Cottrell 1955), the strain rate sensitivity would be expected to be several times larger in the corresponding region. No observable change, however, occurred. It thus appears that if such a step is indeed present, it cannot result from any thermally activated process.

Table 2. Strain Rate Sensitivity of Copper

Temperature(°K)	$\frac{1}{T}\left(\frac{\partial \ln \sigma}{\partial \ln \dot{\epsilon}}\right)_T \times 10^5$
4·2	8·3(8)
11·6	8·6(1)
17·2	9·0(9)
25·9	7·2(1)
35·9	6·7(7)
48·5	4·9(2)
78·0	2·8(4)
90·0	3·1(4)
144·0	2·0(2)
179·0	1·5(3)
200·0	1·4(5)
225·0	1·4(8)
273·0	0·9(9)
295	1·0(7)
373	0·9(0)
483	0·6(5)

Table 3. Strain Rate Sensitivity of Silver

Temperature(°K)	$\frac{1}{T}\left(\frac{\partial \ln \sigma}{\partial \ln \dot{\epsilon}}\right)_T \times 10^5$
4·2	—
11·5	6·4(2)
17·2	6·0(6)
26·0	6·1(8)
35·5	5·2(6)
78·0	2·9(5)
90·0	2·7(5)
179·0	2·0(3)
200·0	1·8(9)
295·0	1·3(7)
373·0	0·9(7)

Fig. 8

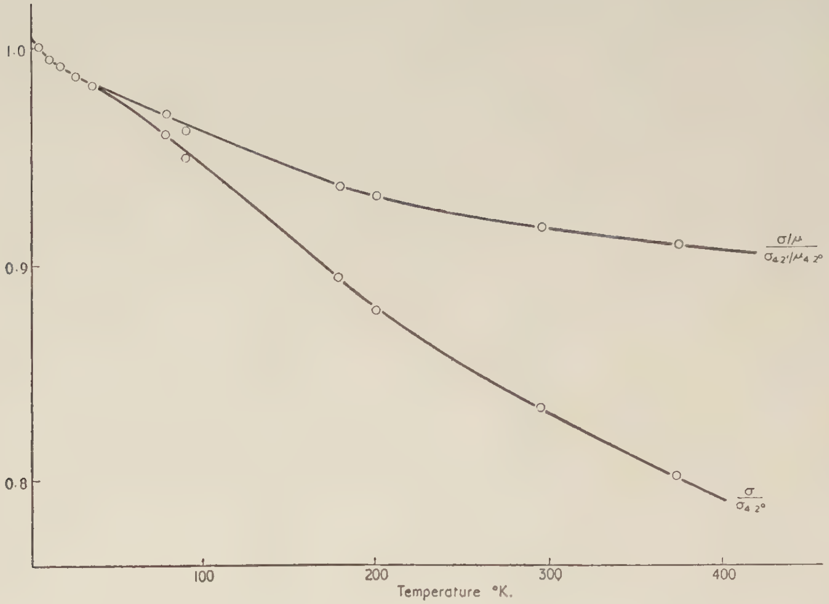

The ratio of the flow stresses at temperature, T, to that at 4·2°K for silver.

Fig. 9

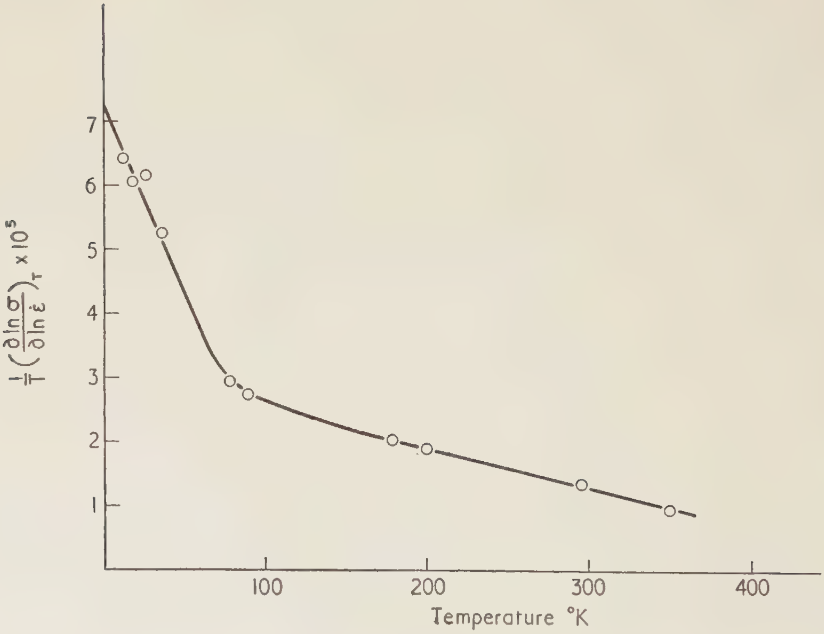

Temperature dependence of the strain rate sensitivity of silver.

To check whether the difference in the behaviour of copper and aluminium arose from their different stacking fault energies, similar experiments were carried out on silver, which was expected to have a lower stacking fault energy than copper (Christian and Spreadborough 1956, Suzuki and Barrett 1958). Figures 8 and 9 and table 3 show the temperature and strain rate sensitivity of silver.

Since no data were available on the temperature variation of the elastic moduli for this metal, an approximate value was derived by multiplying the corresponding data for copper by the ratio of the fractional change of Young's modulus for silver and copper between 78°K and 273°K taken from Köster's data (Köster 1948). The variation of the flow stress with both temperature and strain rate in silver is similar to that already described for copper. Here, however, no linear region in the stress–temperature relation was observed, although some increase in slope is apparent at very low temperatures. The strain rate sensitivity follows the curve expected from the temperature dependence of the flow stress.

By using eqn. (12), the approximate value of $\ln NkTAb\nu/\dot{\epsilon}$ can be obtained from experimental data. At low temperatures, (20–30°K) it was for aluminium $\sim 14{\cdot}7$, for copper $\sim 13{\cdot}4$ and for silver $\sim 13{\cdot}3$; at about 200°K it became $\sim 14{\cdot}2$ for aluminium, $\sim 10{\cdot}5$ for copper and $\sim 13{\cdot}0$ for silver.

Since $NAb\nu$ is approximately independent of temperature, $\ln NkTAb\nu/\dot{\epsilon}$ should be almost temperature independent except at very low temperatures, where its value should decrease sharply. Indication of such a drop has indeed been observed in aluminium, here the flow stress strain rate sensitivity at 4·2°K is larger than that obtained from extrapolating higher temperature values, whereas the temperature dependence of the flow stress remains linear down to 1·7°K. No such increase in strain rate dependence was observed in copper or silver; this, however, may have been due to the inability of the apparatus to record accurately the minute changes of stress involved.

The experimental value of about 13 for $\ln NkTAb\nu/\dot{\epsilon}$ disagrees with the value of 32 derived theoretically by Seeger (1955 a) for the corresponding quantity using the uniform forest model. His calculation assumed that all the intersecting dislocations at any instant contribute to the flow stress, and all 'soft spots' lie within the range of available activation energy. In an actual crystal only a few slip lines are active at any stage of deformation, and therefore only a small number of available dislocations are contributing to the deformation at any instant. Further, presumably only those dislocation–obstacle pairs whose energies of activation lie within a narrow band will affect thermally activated glide. The number of activation sites effective at any instant should thus be only a fraction of the total number of dislocation–obstacle pairs.

In all experiments the behaviour was classical down to the lowest temperatures, and therefore the frequency of vibration of dislocations must be at least two orders of magnitude lower than the atomic frequency. In fact, this frequency is variously estimated as between $\sim 10^9$ and

$\sim 10^{10}\,\mathrm{sec}^{-1}$ (Mott and Nabarro 1948, Friedel 1956). The smaller estimates of the number of activation sites and frequency, as compared to Seeger's value, should result in a much smaller value of $\ln NkTAb\nu/\dot{\epsilon}$, the experimentally observed value is therefore not unreasonable.

The activation energies for creep obtained from eqns. (3) and (12) will be given by $U_0 = 13kT$. As discussed in § 5, the slow increase in flow stress with temperature is believed to correspond to the formation of constrictions in dissociated dislocations, whereas the linear increase with decreasing temperature corresponds to the formation of jogs in the constricted dislocations. For aluminium, extrapolation of the linear portion of the curve to the temperature independent value of the flow stress gives a temperature of ~150°K. The stress becomes temperature independent at ~250–300°K. This gives ~0·073 ev for the energy of formation of jogs in constricted dislocations, and ~0·048–0·073 ev for the formation of constrictions. These values are smaller than usually quoted, however, they lie at the lower limit of energy values given by Seeger (1955 b).

No experimental values for the corresponding energies in copper and silver can be given since the temperature at which the flow stress becomes independent of thermal fluctuations has not been reached for these two metals.

The increase in the strain rate sensitivity observed in aluminium at 4·2°K can be interpreted in two ways. This result would be obtained if the activation distance at stresses approaching that necessary to overcome obstacles without thermal activation decreased somewhat, which, in turn, would lead to faster than linear decrease in activation energy with increasing stress. The failure to observe the corresponding increase in the rate of the variation of flow stress with temperature in this range is easily explained by the decrease of the value of $\ln NkTAb\nu/\dot{\epsilon}$. On the other hand, this behaviour could also result from the 'tunnel' effect of the dislocations through the energy barrier (Glen 1956, Mott 1956 b).

The proportion of creep which would be activated by energy other than thermal energy is here, however, much smaller than that claimed by Glen. At 4·2°K the strain rate sensitivity is only twice as high as that expected from thermally activated glide (assuming, of course, that the linear variation of activation energy with stress is correct).

It can be shown that the constant of logarithmic creep α, can be obtained from the present data by using equation,

$$\alpha = \frac{(\partial \ln \sigma / \partial \ln \dot{\epsilon})_T}{\partial \ln \sigma / \partial \epsilon}$$

$(\partial \ln \sigma / \partial \ln \dot{\epsilon})_{4\cdot 2}$ is obtained from extrapolation of the curves at higher temperatures so that it corresponds to *temperature* activated glide. Taking for $\partial \ln \sigma / \partial \epsilon$ about 3, we get $\alpha_{4\cdot 2} = 13$ for copper, and $\alpha_{4\cdot 2} = 21$ for aluminium, which is of the same order of magnitude as the value obtained by Glen (1956) for creep in cadmium.

More experiments, especially in comparing the rates of creep of metals having relatively high and low zero point energy are needed before the question of zero point energy activated creep can be solved.

§ 5. DISCUSSION OF THE NATURE OF THE OBSTACLES

The constancy of the flow stress ratio, both from temperature and strain rate data, has been established for all face-centred cubic metals tested, both in stage II and stage III of hardening. Significant deviations occur only at very low stresses, and can easily be explained by postulating an additional temperature and strain rate dependent process. It seems significant that the numerical values of this ratio are unaffected by the orientation in the case of single crystals, and are the same also for polycrystalline specimens.

It has hitherto been generally accepted that the total flow stress results from the interactions of dislocations with obstacles exerting both long- and short-range forces. The part of the flow stress which can be affected by temperature or strain rate must be due to obstacles exerting short-range forces, since the activation energy for a dislocation to overcome these must lie within the range of thermal fluctuations. The temperature and strain rate independent part of the flow stress, however, must arise from interactions over distances long enough to render thermal fluctuations ineffective. These long-range forces have been ascribed to elastic interactions between glide dislocations and the internal stress field radiating from piled-up groups of parallel dislocations (Seeger *et al.* 1957, Friedel 1955, Mott 1953). As we have already discussed, there is little alternative to the conclusion that the short-range forces are the result of the intersecting of glide and forest dislocations. The proportionality of the temperature and strain rate dependent flow stress to the total flow stress then requires that the amplitude of the internal elastic stress field be proportional to the magnitude of the forces exerted by forest dislocations.

In the mechanism of hardening due to Seeger *et al.* (1957), dislocations pile up in groups of about 25, the number in a group being independent of strain. They show that under such conditions the amplitude of the internal stress field increases linearly with the square root of the dislocation density. Since the same type of variation of flow stress with the density of forest dislocations is expected (Cottrell 1952) the observed proportionality would seem to be explained.

Adams and Cottrell (1955), on the other hand, suggested that the proportionality may be explained by postulating that the pattern of the dislocation configuration in a cold-worked sample remains similar during deformation, and that only its density changes with strain.

A third possible explanation is that both long- and short-range forces retarding the motion of glide dislocations arise from the same source, namely the interaction between glide and forest dislocations. We should be able to distinguish between these possibilities by altering the dislocation distribution sufficiently. If the two former proposals are correct, this should change the flow stress ratio.

It was pointed out by Cottrell and Stokes (1955) that the dislocation distribution in aluminium deformed at high and low temperatures to the same flow stress, *must* be different, since further deformation at the higher temperature would lead to work softening in the former case and normal hardening in the latter. The flow stress ratio obtained from experiments in which the temperature was changed is the same in the earlier stages of deformation where no work softening occurs and in the later stages, where it is extensive.

The objection might be raised that an appreciable part of the flow stress change is connected with change in the elastic modulus and that this could mask the smaller changes resulting from thermally activated flow. Some experiments were therefore carried out under conditions where this objection could not apply. An aluminium specimen (4a) was deformed at liquid nitrogen temperature and the change in flow stress resulting from the standard change in strain rate was measured immediately before unloading and work softening it at room temperature; after softening it was cooled back to liquid nitrogen temperature, re-strained, and a series of strain rate changes made, the first immediately after the specimen started to deform plastically. This process was repeated several times (see table 4).

Table 4. An example of Stress Change produced by Change of Strain Rate before and after Work Softening

$\left(\frac{\sigma_{10^{-5}}}{\sigma_{10^{-4}}}\right)_{78°}$	Tensile stress (kg/mm²)	Tensile strain (%)
0·9787	11·51	41·3
0·9780†	10·55†	44·1†
0·9778†	11·33†	44·35†
0·9786†	12·23†	45·2†
0·9783†	12·67†	45·7†

Work softened at room temperature.

The flow stress ratio was always the same before and after work softening, and during the rapid hardening observed in the second deformation at low temperature. It is interesting to note that the absolute value of the change of flow stress decreased during work softening, indicating that some forest dislocations must have collapsed during this process. Also, no change in the ratio was found when softening resulted from recovery during anneal at 100°C for 15 min and by recovery with deformation at this temperature.

The distribution of dislocations was also altered by hardening aluminium crystal (1b) in torsion prior to changing the tensile strain rate at 78°K.

The resultant fractional change $\sigma_{10-5}/\sigma_{10-4}=0{\cdot}9752$ agreed very well with the value $\sigma_{10-5}/\sigma_{10-4}=0{\cdot}9759$ from specimens deformed only in tension. Similar results were reported by Seeger *et al.* for flow stress–temperature changes in copper.

These experiments all show that, for several different dislocation distributions in hardened crystals, the ratio of the flow stress is determined only by the original and final temperature or strain rates. This can be so only if both long- and short-range forces arise from the same source. If we now adopt this idea, the first question to be answered is whether the elastic interactions between the forest and glide dislocations (long-range interactions) can be large enough to account for the observed temperature insensitive portion of the flow stress. In aluminium, the only metal for which these temperatures could be reached before recovery effects complicated the observations, the flow stress arising from long-range interactions accounts for about 70% of the total. In copper and silver, unfortunately, no such estimates could be made.

Fig. 10

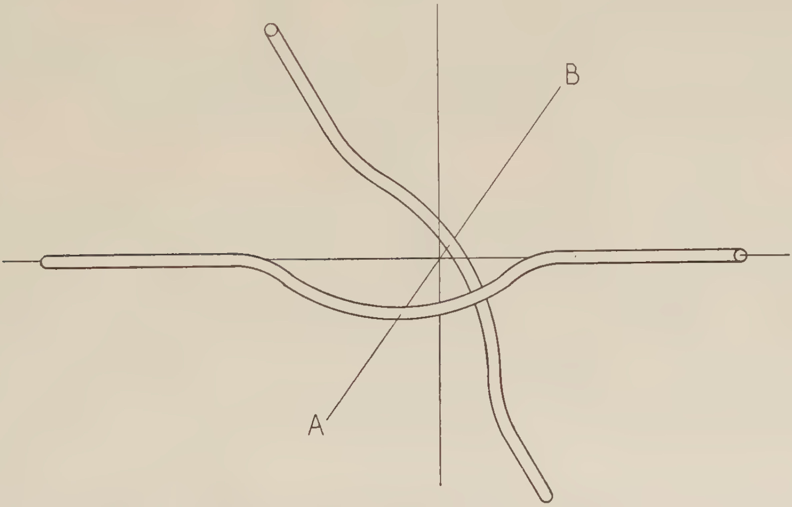

Schematic diagram of two non-parallel dislocations about to intersect. AB is the line of closest approach ; straight portions of the dislocation lines lie in the same plane.

Elastic interactions between perpendicular dislocations in the simple cubic lattice were discussed by Nabarro (1952), who showed that a force exists only between screw dislocations. In the face-centred cubic lattice, it is rather improbable that forest and glide dislocations will be perpendicular. If the angle between the two dislocation lines deviates from 90° they will exert elastic forces upon each other. We may expect therefore that a finite stress will have to be applied before a glide dislocation can approach an obstacle near enough to intersect it with the help of thermal fluctuations.

An exact calculation of the forces between dislocations would be difficult since we would have to determine the equilibrium configuration of the dislocation lines. We can, however, obtain an order of magnitude estimate as follows. Figure 10 shows two dislocations trying to intersect. If they are repelling each other, the lines will be slightly bent, as shown, and therefore the portions at large distances from the line of nearest approach, AB, will lie in the same plane and not contribute to the elastic interaction. On the other hand, the bulging portion of the dislocation lines would be expected to interact. It seems reasonable to assume that the lengths of the dislocation lines contributing to the elastic force will be proportional to their separation, r. To within an order of magnitude this should be equivalent to the force between two parallel dislocations of length r and distance r apart. We can therefore write,

$$F = \beta \mu b^2 / 2\pi \qquad . \quad . \quad . \quad . \quad . \quad . \quad . \quad . \qquad (22)$$

where β is a constant of the order of unity, and the other symbols have their usual meaning. Putting the numerical values for the modulus of copper, and the Burgers vector, we get a value of $4{\cdot}4 \times 10^{-5}$ dynes for the elastic force.

We can now estimate the value of the flow stress resulting from dislocations cutting through the forest from the retarding force of one obstacle, F, and the forest density, ρ, in the following way,

$$\sigma = F \rho^{1/2} / b. \qquad . \quad . \quad . \quad . \quad . \quad . \quad . \quad . \quad . \qquad (23)$$

Taking the value of Blewitt *et al.* (1955) for ρ corresponding to the flow stress of 10^9 dynes/cm^2, we obtain the calculated value of the flow stress 4×10^8 dynes/cm^2, which is of the right order of magnitude.

We can also obtain the value of the force exerted by the obstacles on the glide dislocations from the temperature and strain rate dependence of the flow stress. Force–distance curves obtained from eqns. (17) and (18) for aluminium, copper and silver are shown in fig. 11. To make direct comparison possible, the curves, normalized to the same lattice parameter and elastic modulus are shown in fig. 12. In aluminium, when the separation between the dislocation and obstacle is large, the force between them is almost constant; this force increases with decreasing separation, at first slowly and then more sharply, later rising almost vertically to a maximum value. The constant region is not observed for copper and silver. For copper the very steep rise occurs at a much larger relative force. It is difficult to decide whether it occurs at all for silver. These force–distance curves have the form expected from the process of intersection of dissociated dislocations. Sequence ABCD in fig. 13 shows two dislocations each split into partials cutting across each other. At large distances the force from the elastic interaction between them should change only slowly with their separation corresponding to the first, horizontal, section of the force–distance curve for aluminium; when the two leading partials touch, constrictions start to form, and the force begins

Fig. 11

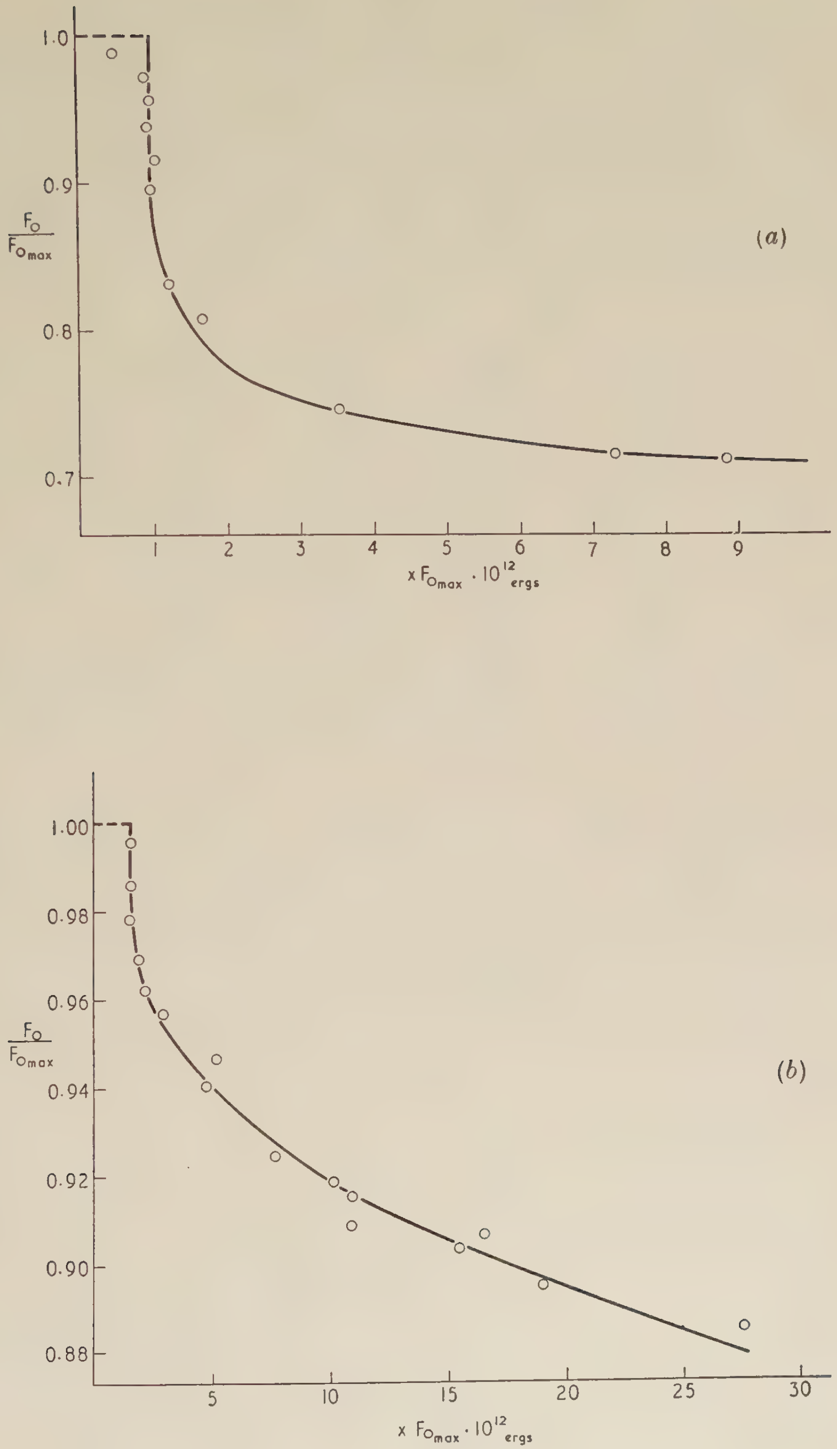
1.0
0.9
0.8
0.7
$\frac{F_0}{F_{0\,max}}$
(a)
1
2
3
4
5
6
7
8
9
$x\,F_{0\,max} \cdot 10^{12}$ ergs
1.00
0.98
0.96
0.94
0.92
0.90
0.88
$\frac{F_0}{F_{0\,max}}$
(b)
5
10
15
20
25
30
$x\,F_{0\,max} \cdot 10^{12}$ ergs

Fig. 11 (*continued*)

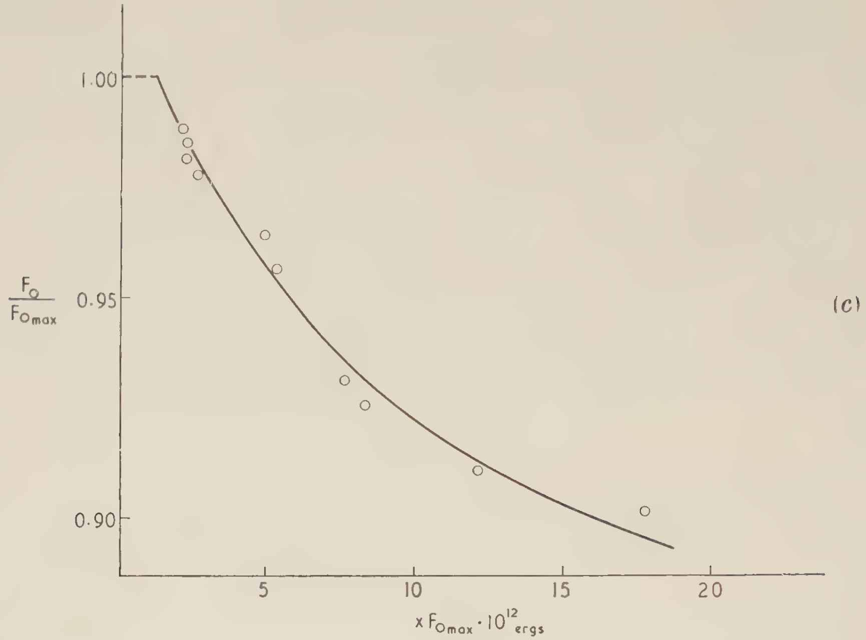

The variation of activation distance with the force pressing a dislocation against an obstacle. (*a*), aluminium ; (*b*), copper ; (*c*), silver.

Fig. 12

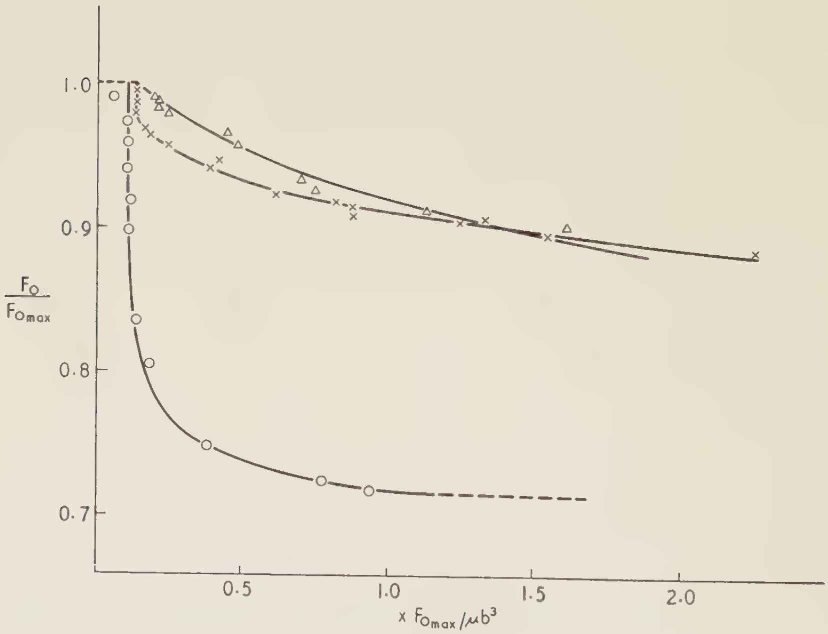

Normalized force–distance curves for aluminium, copper and silver.

to increase more rapidly, as in the sloping portion of the curve. After the constrictions have formed fully and the two partials join at the point of intersection, the dislocations cannot move relative to each other without forming a jog, which requires a larger force, this explains the steeply rising section appearing later in the aluminium curve.

Copper has a relatively low stacking fault energy compared to that of aluminium, here the formation of constrictions starts earlier and the force pressing the two dislocations together when the constrictions are fully formed is relatively larger. Only a small additional force is now necessary to form the jogs. The stacking fault energy of silver may be low enough for the dislocations to cut immediately after forming a full constriction. In this case, the sharp rise in force associated with jog formation would be absent, and the jogs may not be fully constricted, but produce short lengths of stair rod dislocation (Thompson 1953).

Fig. 13

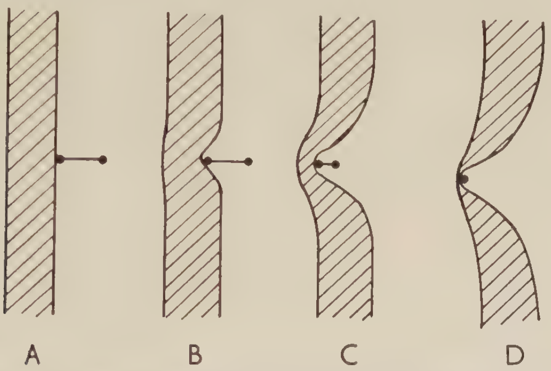

Schematic diagram of the intersection process of dislocations dissociated into partials, showing stages of formation of constrictions.

If we adopt this interpretation of the curves in fig. 11 we can obtain the value of the maximum force exerted by a forest dislocation by assuming that the distance at which the force rises steeply is equal to the interatomic spacing b. The values of $F_{0\,\max}$ are then about $3{\cdot}5\times10^{-5}$ dynes for aluminium, and $6{\cdot}3\times10^{-5}$ dynes for copper. Blewitt *et al.* (1955) have observed that the dislocation density varies as the square of the flow stress in copper single crystals, both in the linear and parabolic hardening region. Obviously such a relation is to be expected for the forest mechanism of hardening. The data of the above authors, and Seeger *et al.* (1957), enable us to calculate the density of dislocations as a function of strain in the linear hardening region. The number of dislocations per square centimetre is found to be $\rho\simeq10^{11}\epsilon^2$. Sosin and Koehler (1956), from measurements of electrical resistivity in deformed aluminium, concluded that the dislocations are distributed isotropically. If we assume this isotropic distribution, the flow stress at absolute zero will be given by

$$\sigma_0=\rho^{1/2}F_{0\,\max}/b \quad . \quad . \quad . \quad . \quad . \quad . \quad . \quad . \quad (24)$$

and the coefficient of strain hardening in stage II by,

$$\frac{d\sigma_0}{d\epsilon} \simeq 3{\cdot}2 \times 10^5 F_{0\,\max}/b \quad \ldots\ldots \quad (25)$$

which gives for copper,

$$\frac{d\sigma_0}{d\epsilon} \simeq 8 \times 10^8 \text{ dynes.}$$

If the same relation between strain and ρ holds for aluminium,

$$\frac{d\sigma_0}{d\epsilon} \simeq 4{\cdot}5 \times 10^8 \text{ dynes.}$$

The experimental value for the coefficient of strain hardening of copper varies between 1·4 and 2×10^9 dynes (Blewitt *et al.* 1955) in reasonably good agreement with the values derived. We can therefore conclude that the forest mechanism is capable of accounting for the observed flow stress.

The calculations presented here deal with the rate of hardening at very low temperatures. Reference to fig. 11 will show that the activation energies involved at higher temperatures are too large for thermal fluctuations to be able to help dislocations to cross the forest to any appreciable extent, thus a large percentage of the flow stress will be temperature and strain rate independent. However, we find no justification in identifying this temperature independent flow stress with much longer range interaction of dislocations with the internal stress field of the lattice.

The arguments so far require that the stresses, long-range in the sense of varying over distances large in comparison with the mean separation of the dislocations, are ineffective in contributing to the observed deformation stress. In the following argument we shall show that this is so. If we imagine a section across the glide plane of a crystal the internal stress field σ_i may be represented by a sinusoidal wave of varying period and amplitude. It is necessary for equilibrium at zero applied stress, σ, that the internal stress, integrated over this, or any plane, will be zero and there will be regions in the glide plane in which the internal stress will aid the applied stress. Frank–Read sources will most probably be distributed randomly over this sinusoidal field.

First, let us consider the special case in which the sinusoidal wave is uniform. Figure 14 (*a*), (*b*) and (*c*), shows the sequence of events when a Frank–Read source, located in a region S, where the aiding internal stress is a maximum, starts generating dislocations. The first dislocation loop will stop at a place where σ_i is zero. The second loop will push the first over into a region where σ_i opposes glide. The process will be repeated until the backward force from dislocations on which a negative internal stress operates, is equal to the positive force on those in the positive stress field. The leading dislocation will now be in a region of maximum negative stress (A and B). This state of affairs is represented in fig. 14 (*a*). Suppose now that a small positive external stress is applied, it will provide a force $b\sigma$ per unit length on all dislocations, causing the loops to expand.

This expansion will be opposed only by those dislocations which have been pushed past the position of maximum negative stress (fig. 14 (*b*)). In equilibrium, therefore, $nb\sigma = -b(\sigma_1 + \sigma_2 + \sigma_3 \ldots)$ where σ_1, σ_2, $\sigma_3 \ldots$ are the negative internal stresses for dislocations at the points 1, 2, 3.... With increasing applied stress, the leading dislocation will be pushed by the next region of positive internal stress to a position C (fig. 14 (*c*)) and its retarding influence on the dislocations behind it will be considerably reduced. The source will start to generate more and more dislocations, and the second negative maximum of internal stress will be overcome in a similar way to the first one. The only difference here is that now we have more dislocations utilizing the applied stress, and the second maximum can be overcome at a smaller applied stress.

Fig. 14

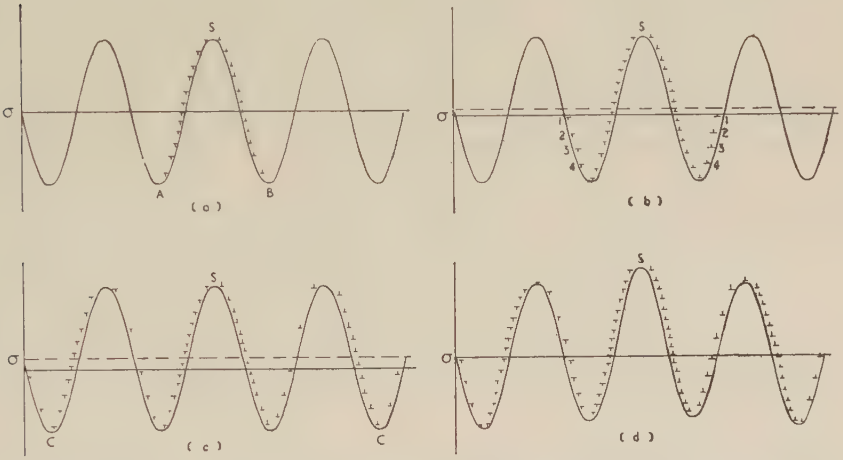

Dislocations from the source, S, overcoming long-range internal stress field. (*a*) Constant wavelength and amplitude stress field, situation at zero applied stress. (*b*) Small applied stress. (*c*) Applied stress sufficient to enable dislocations to overcome the internal stress field. (*d*) Non-uniform internal stress field. Zero applied stress. Favourably located source.

It thus follows that if the wavelength of the internal stress field is sufficiently large for the source to emit a number of dislocations before the first one is stopped by the opposing stress, glide can proceed at an applied stress which is only a fraction of the maximum internal stress.

The amplitude of the internal stress field in a real crystal, however, will vary. If we now consider a Frank–Read source to be located in a region of exceptionally high internal stress the emission of dislocations will not stop at a configuration such as that depicted by fig. 14 (*a*), but will proceed further, and the resulting situation should resemble that of fig. 14 (*d*). Under these circumstances, the stress required to propagate a series of dislocations emanating from the same source through the internal stress field of the lattice, will be reduced to an insignificant value.

The creation of a large number of dislocations by a single source has never been satisfactorily explained. However, here it follows naturally if we take into account the cooperation between the dislocations in overcoming the internal stress field. A small number of dislocations emitted by a source will not be readily visible since they will soon be stopped by the opposing internal stress. Only when a large number is emitted can they spread any appreciable distance through the lattice.

The assumption that only sources in exceptionally favourable positions are utilized during the deformation is not unreasonable, since it is known that at any instant only a relatively small number operate. The internal stress field will change continuously during the deformation, therefore some Frank–Read sources should always be in favourable positions.

Obviously, these arguments do not apply when the wavelength of the internal stress field or the distances between rows of obstacles are comparable to the spacing between individual dislocations. Under such conditions the dislocations will have to overcome the barriers individually —without the help of others in the group. It follows therefore that a dislocation in the forest can still provide an effective obstacle to the movement of glide dislocations, although some cooperation between glide dislocations in overcoming the forest will still undoubtedly be present. Such cooperation would explain the behaviour which is observed when either the temperature or strain rate of a test is changed.

Some objections may be raised on the grounds that the magnitude of the internal stress derived from x-ray data often agrees with the experimental flow stress (Paterson 1954). This, however, is not unexpected, since whatever the mechanism of retarding the glide dislocations, internal stresses larger than the observed flow stress could not exist since they would be relieved by glide.

Two experiments were designed to test the validity of the conclusion that the internal stress field does not contribute appreciably to the flow stress. X-ray investigations of Hall and Williamson (1951) showed that the dislocation densities in high purity and commercial purity aluminium field at room temperature are comparable, but that substantially larger internal stresses were present in the latter. If we assume (with Seeger *et al.*) that the temperature dependent part of the flow stress comes from interaction of glide dislocations with the forest, and the temperature independent part from interaction with the elastic stress field, we would expect that the fractional change in flow stress between room temperature and liquid nitrogen temperature should be appreciably larger in high purity aluminium. The flow stress ratio was measured on very coarsely polycrystalline commercially pure aluminium, and the value observed was, $(\sigma_{295°}/\sigma_{78°})=0{\cdot}762$, showing almost no difference from the corresponding value for high purity aluminium. Furthermore, it is known (Kelly and Roberts 1955) that the long-range stress field produced by deforming high purity aluminium at nitrogen temperatures anneals rapidly at room temperature, and no appreciable softening is known to occur during such an anneal. It has been suggested (Cherian *et al.* 1949) that softening indeed does occur, but is followed by very rapid hardening which quickly restores the original flow stress. Figure 15 shows a portion of the load elongation curve of crystal 4b which has been deformed at 78°K, unloaded, warmed to room temperature, cooled again and re-strained. No plastic flow is detectable here until the flow stress reaches ~80% of the original value and after 0·2% deformation the curve lies 2% below the extrapolated line. Slight decrease in the rate of strain hardening is observed but large-scale softening is definitely absent. These experiments indicate that the internal elastic stresses cannot play an important rôle in determining the flow stress, at least in single crystal samples. In polycrystals the boundary conditions do not impose the restriction of a zero stress field integrated over the glide plane, thus some conclusions reached here may have to be modified. It is possible that in such cases the long-range elastic stress may contribute to some extent to the observed flow stress.

Fig. 15

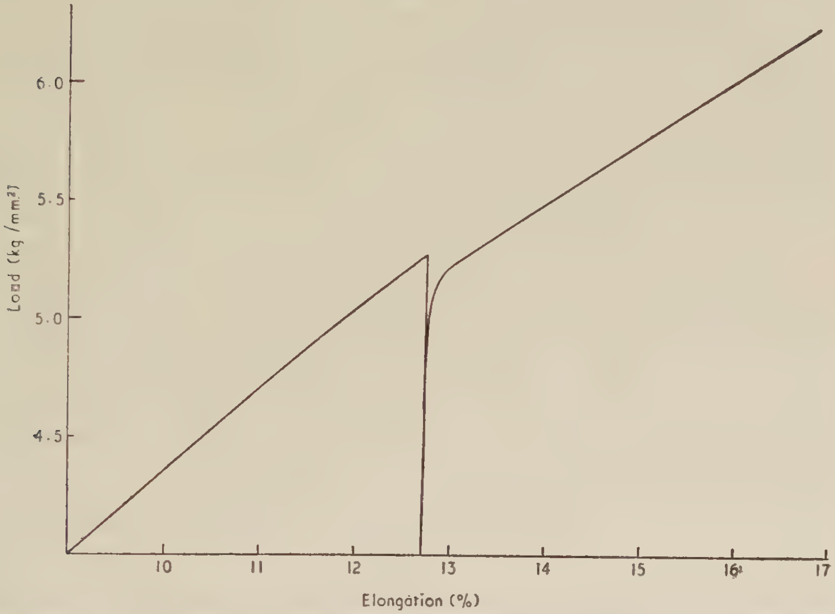

The effect of annealing for 20 minutes at 295°K on the load-elongation curve aluminium specimen 4b.

§ 6. THE WORK-HARDENED STATE

On any elastic interaction theory of strain hardening it is difficult to account for the observed effects when the specimen is unloaded and reloaded in the opposite direction. The unloading is elastic, with a modulus rather close to that expected for a perfect crystal. This requires that all the dislocations be firmly anchored. On reloading in the opposite direction the plastic flow starts at a much lower stress but the original flow stress is regained after only a small amount of deformation—the Bauschinger strain. No visible slip lines are produced during this process, and the value of the Bauschinger strain usually corresponds to the strain which would be produced by all the dislocations moving through a distance corresponding to their separation (Woolley 1953). If the movement of dislocations through the lattice were hindered mainly by the elastic stress field, the unloading would result in most dislocations moving back by a distance of about one-quarter of the wavelength of this field. In the favourable case, where this wavelength corresponds to the mean separation of the dislocations, the shortening of the specimen above that expected from the elastic shortening would be about one-quarter of the Bauschinger strain actually observed. If the important interactions were those between groups of dislocations, the corresponding unloading elastic strain would be larger.

When the direction of stress is reversed, we would expect the dislocations to move by another quarter wavelength before glide in the opposite direction commenced.

The situation would be different however, if the main obstacles to glide were the forest dislocations. In this case, the dislocations should be localized with respect to loading since, in general, they will be interwoven between rows of forest obstacles, i.e. some dislocations will have overcome some dislocations in a row and thus become caught in it. When the direction of stress is reversed, this partially entangled string of dislocations would move back easily over a distance equal to the mean separation of rows. They would then encounter a new row of obstacles and the stress in the reverse direction would therefore rise to the previous value.

The destruction of dislocations already present in a crystal by dislocations produced by the old sources is prevented (Mott 1957) since the sources which will operate are those lying in regions where the internal stress field aids the applied stress. New sources will operate on reversal of the stress, since those which previously operated will be unfavourably situated.

We now have to account for the increase in the density of the forest with deformation, which will lead to a corresponding increase in the flow stress. It is difficult to discuss quantitatively the process of building up the forest, since observations of the slip lines on a deformed specimen—the usual source of information on the dislocation behaviour—provide very little information on slip systems other than the principal one. It may be that the dislocation forest arises from glide on other systems taking place to relieve the internal stress field. If this were so, we would expect that only small groups of dislocations would be activated and these may escape microscopical detection. The density of the forest dislocations could then be quite large without leaving prominent marks on the surface of a deformed specimen. Sosin and Koehler's data (1956) indicate that this density is as large as that of the dislocations in the principal glide system. It is significant that the amount of hardening produced by the deformation is independent of the glide system on which slip takes place. Seeger *et al.* (1957) compared the rate of hardening of identical copper single crystals deformed alternately in tension and torsion and in tension alone. Examination of their data (fig. 2, Seeger *et al.*) shows that if the deformation produced by twisting is *included* in the total deformation, the rate of strain hardening is the same for both types of deformation, indicating that the rate of hardening does not change when some other glide system is brought into operation.

In view of this evidence, we have assumed that the rate of forest formation is the same as the increase in the density of dislocations on the principal glide plane.

It is necessary to find a mechanism by which the distance travelled by dislocations can be limited, thus accounting for the hardening caused by the increase in dislocation density during deformation. It has hitherto been assumed that Cottrell–Lomer sessiles will successfully lock the dislocations, but several arguments may be raised against this mechanism. One of the strongest would seem to be that hardening and accumulation of dislocations occurs during the deformation of body-centred cubic and hexagonal close-packed metals for which no equivalent sessile dislocations have so far been proposed. It has been pointed out by Friedel (1955) and Kelly (1956) that pure screw dislocations cannot form a Cottrell–Lomer barrier with a dislocation belonging to a different glide system; a barrier formed by dislocations from other glide systems can, however, be effective in holding up pure screw dislocations if it lies near enough to the glide plane in which the screw dislocations are moving. It would be expected that effective barriers of this type for screw dislocations would be formed much more rarely than barriers for edge dislocations in the glide plane, and therefore that longer slip lines would be observed on the surface of a specimen where screw dislocations emerge, than on that where edges emerge. This is contrary to observations reported by Kelly (1956) and Seeger *et al.* (1957).

Stroh (1956) has shown that Cottrell–Lomer barriers are weaker than formerly believed. It should be pointed out that the strength of the barriers was invariably considered at a point where the two dislocations forming the sessile were fully joined. It is unlikely that such perfect barriers will occur in a deformed crystal, since both dislocations will most likely contain jogs, giving rise to localized weak regions. A weak spot would also exist at the place where the two dislocations forming the sessile join.

Interactions between individual parallel dislocations might possibly assume the rôle usually ascribed to Cottrell–Lomer sessiles. Dislocations emanating from any source will be stopped if they approach closely enough to a parallel group of arrested dislocations. In order to arrive at some quantitative conclusions, imagine an infinite array of parallel straight dislocations of regular spacing, h, lying in the plane $y=0$, and with their

Burgers vector along the x direction. By using equations developed by Cottrell and Nabarro (Cottrell 1953), it can be shown that the stress from such a group, on a plane parallel to it, will be

$$\sigma_{xy}=\frac{\mu b}{4h(1-\nu)}\left(\frac{\sin 2\pi x/h}{\sin^2 \pi x/h+\sinh^2 \pi y/h}-\pi y\frac{\sin 2\pi x/h \sinh 2\pi y/h}{(\sin^2 \pi x/h+\sinh^2 \pi y/h)^2}\right) \quad (26)$$

if the array comprises only edge dislocations, and,

$$\sigma_{yz}=\frac{\mu b}{4h}\frac{\sin 2\pi x/h}{\sin^2 \pi x/h+\sinh^2 \pi y/h} \quad . \quad . \quad . \quad (27)$$

if it comprises screws. The maximum stress from a group of screw dislocations is given by

$$\sigma_{yz\,\max}=\pm\frac{\mu b}{2h}\frac{1}{\sinh 2\pi y/h}. \quad . \quad . \quad . \quad . \quad . \quad (28)$$

It follows from these expressions that when $y \ll h$ the stress field reduces to that of a single dislocation, and when $y > h$, the stress almost disappears. Figure 16 shows values of $\sigma_{\max}$ as a function of y/h. The rapid decrease in amplitude with increasing separation of the planes is noticeable.

We may thus expect that dislocations emanating from a source will be stopped by a parallel group if the distance between their glide planes is smaller than the distance between individual dislocations in each group. Under these conditions, the first few leading dislocations will be pushed through the adverse stress region until a few overlap those in the arrested group. The dislocations at the extremities of the two parallel groups will thus form pairs, a small number of which should form a strong lock. Both edge and screw dislocations can be locked in this way.

Since the interaction between screw dislocations is greater than that between edges, at small y/h (fig. 16) the screws should travel a shorter distance before becoming locked; this agrees with observations on slip line lengths (Kelly 1956, Seeger *et al.* 1957). Furthermore, according to this model, slip lines formed by groups of piled-up edge dislocations would end in deformation bands, also in agreement with observation (Kelly 1956). Since the number of piled-up groups increases with the deformation, the average distance travelled by the glide dislocations and therefore the length of a newly formed slip line, would decrease.

As long as there is no cross slip, screw dislocations should be stable. However, if the temperature and stress are high enough to allow cross slip, dislocations of opposite sign will annihilate, as pointed out by Mott (1953), thus allowing the sources to emit more dislocations.

In a deformed crystal, in some regions of the glide plane the stress field will be due only to piled-up groups; in regions where the glide plane passes sufficiently near to a piled-up group, there will also be a short-range stress from individual dislocations. We believe that the sources which can operate lie in the former regions, and that glide dislocations have to overcome only the forest. When they become stopped by interaction with other parallel dislocations, they cease to contribute to strain. Thus the idea that the observed flow stress arises from interaction with the forest only, is reconciled with the finite effective interaction between parallel groups of dislocations.

Fig. 16

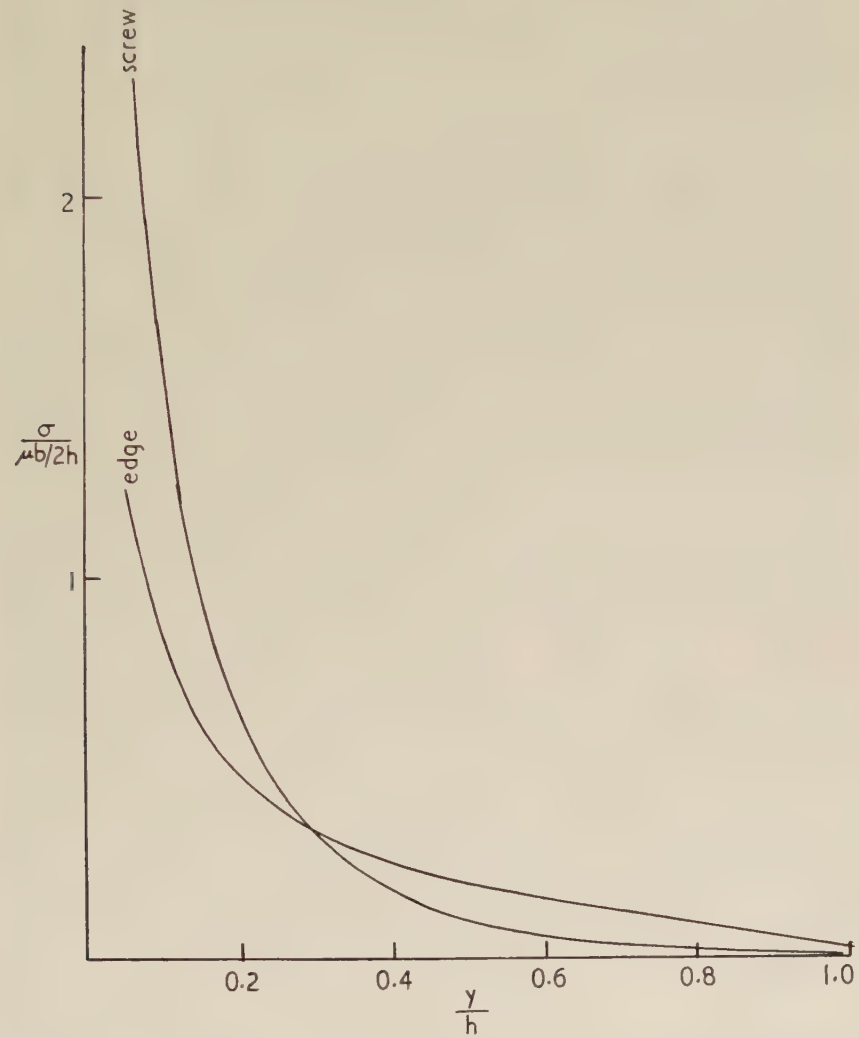

Maximum stress under a row of parallel screw and edge dislocations plotted against y/h. The curve for screw dislocations was calculated from eqn. (28), and points for the curve for edge dislocations were calculated by using eqn. (26). Poisson's ratio was taken as $\frac{1}{3}$.

§ 7. The Three Stages of Hardening

Our picture of the three stages of hardening in face-centred cubic single crystals is rather similar to that described by Seeger *et al.* (1957) except that the effective obstacles to glide are the forest dislocations which accumulate in the lattice at the same rate as those in the main glide system. Also that dislocation travel is limited by the interactions between parallel dislocations on nearby glide planes rather than by Cottrell–Lomer barriers.

In stage I the slip distance is comparable to the dimensions of the specimen, leading to a very small rate of dislocation accumulation. With increasing strain the transition to stage II occurs. Some dislocations are now stopped in the crystal, these produce both the forest and the obstacles to dislocations spreading. In this stage, the slip distance is inversely proportional to strain, resulting in a parabolic increase of the dislocation density, which in turn leads to the linear stage of hardening, stage II. When higher strain levels are reached, the screw dislocations in the main glide system can undergo cross slip under the combined action of stress and thermal fluctuations. This cross slip results in a lower rate of accumulation of dislocations with strain, characterizing stage III.

We have made the implicit assumption that the collapse of dislocations on the main glide system will be accompanied by the collapse of the forest. Such a process is not easily visualized. However, it obviously can happen, since after work softening, the absolute magnitude of the stress change produced by the change of the strain rate decreases, indicating that the density of short-range obstacles decreases during this process.

The controversy regarding the validity of the mechanical equation of state as applied to metals can now be understood. Experiments supporting this relation were carried out on body-centred cubic metals (Hollomon 1947) where cross slip should occur without any help from thermal fluctuations. No piling up of screw dislocations presumably occurred there, and the total density (at temperatures too low for recovery to occur) depended only on the strain. Experiments refuting the mechanical equation of state (Dorn *et al.* 1949) were made on face-centred cubic metals in stage III of the deformation. Here, obviously, the amount of dislocation collapse through cross slip depended on the mechanical and thermal history of the specimen. The situation is different however in stage II in which no cross slip occurs; here again, the work hardened state of the specimen should depend only on the amount of deformation but not on the temperature or strain rate, and the mechanical equation of state should thus be obeyed. This would require that the rate of strain hardening should depend on temperature only through the 'reversible' changes of flow stress, and that no work softening should occur. The experimental observations in stage II fully agree with this conclusion. The arguments do not apply to stage I where most of the glide dislocations leave the specimen. The mechanism of hardening is presumably very different from that in stage II where most of the glide dislocations are retained. The transition from stages I to II depends on the condition of deformation in stage I and is a function of many variables such as specimen size, purity, presence of oxide film etc. Its dependence on temperature does therefore not invalidate the mechanical equation of state within stage II.

ACKNOWLEDGMENTS

Helpful discussions with many colleagues, especially Drs. T. H. K. Barron, J. W. Christian and J. W. Leech, are gratefully acknowledged.

The experiments on polycrystalline aluminium were carried out at the Cryogenic Engineering Laboratory of the Massachusetts Institute of Technology under U.S. Atomic Energy Commission contract number 80(30–1)–1310.

REFERENCES

ADAMS, M. A., and COTTRELL, A. H., 1955, *Phil. Mag.*, **46,** 1187.

BASINSKI, Z. S., 1957. *Proc. roy. Soc.* A, **240,** 229 ; 1958, Report of a Second Symposium on Melting Diffusion and Related Topics. National Research Council of Canada, February 1958, p. 68.

BASINSKI, Z. S., and CHRISTIAN, J. W., 1959, to be published.

BLEWITT, T. H., COLTMAN, R. R., and REDMAN, J. K., 1955, *Defects in Crystalline Solids* (London : Physical Society), p. 369.

CHERIAN, T. V., PIETROKOVSKY, P., and DORN, J. E., 1949, *Trans. Amer. Inst. mech. Engrs*, **185,** 948.

CHRISTIAN, J. W., and SPREADBOROUGH, J., 1956, *Phil. Mag.*, **1,** 1069.

COTTRELL, A. H., 1952, *J. Mech. Phys. Solids*, **1,** 53 ; 1953, *Dislocations and Plastic Flow in Crystals* (Oxford : Clarendon Press), p. 98.

COTTRELL, A. H., and STOKES, R. J., 1955, *Proc. roy. Soc.* A, **233,** 17.

DORN, J. E., GOLDBERG, A., and TIETZ, T. C., 1949, *Trans. Amer. Inst. mech. Engrs*, **180,** 205.

FOREMAN, A. J. E., 1955, *Acta Met.*, **3,** 322.

FRIEDEL, J., 1955, *Phil. Mag.*, **46,** 1169 ; 1956, *Les Dislocations* (Paris : Gauthier-Villars), p. 47.

GLEN, J. W., 1956, *Phil. Mag.*, **1,** 400.

HAASEN, P., and KELLY, A., 1957, *Acta Met.*, **5,** 192.

HALL, W. H., and WILLIAMSON, G. K., 1951, *Proc. phys. Soc. Lond.* B, **64,** 937.

HOLLOMON, J. H., 1947, *Trans. Amer. Inst. mech. Engrs*, **171,** 353.

KELLY, A., and ROBERTS, W. T., 1955, *Acta Met.*, **3,** 96.

KELLY, A., 1956, *Phil. Mag.*, **1,** 835.

KÖSTER, W., 1948, *Z. Metallk.*, **39,** 1.

MAKIN, M. J., 1958 a, *Phil. Mag.*, **3,** 287 ; 1958 b, *Ibid.*, **3,** 309.

MOTT, N. F., 1951, *Proc. phys. Soc. Lond.* B, **64,** 729; 1953, *Phil. Mag.*, **44,** 742; 1956 a, *Deformation and Flow of Solids* (Berlin : Springer-Verlag), p. 53 ; 1956 b, *Phil. Mag.*, **1,** 568 ; 1957, *Dislocations and Mechanical Properties of Crystals* (New York : John Wiley and Sons), p. 458.

MOTT, N. F., and NABARRO, F. R. N., 1948, *Bristol Conference on the Strength of Solids* (London : Physical Society), p. 1.

NABARRO, F. R. N., 1952, *Advanc. Phys.*, **1,** 271.

OVERTON, W. C., and GAFFNEY, J., 1955, *Phys. Rev.*, **98,** 969.

PATERSON, M. S., 1954, *Acta Met.*, **2,** 823.

SCHMID, E., and BOAS, W., 1950, *Plasticity of Crystals* (London : F. A. Hughes), p. 37.

SEEGER, A., 1954, *Z. Naturf.*, **9a,** 870 ; 1955 a, *Phil. Mag.*, **46,** 1194 ; 1955 b, *Defects in Crystalline Solids* (London : Physical Society), p. 331 ; 1956, *Deformation and Flow of Solids* (Berlin : Springer-Verlag), p. 30.

SEEGER, A., DIEHL, J., MADER, S., and REBSTOCK, H., 1957, *Phil. Mag.*, **2,** 323.

SEITZ, F., 1952, *Advanc. Phys.*, **1,** 43.

SOSIN, A., and KOEHLER, J. S., 1956, *Phys. Rev.*, **101,** 972.

Stroh, A. N., 1956, *Phil. Mag.*, **1,** 489.
Sutton, P. M., 1953, *Phys. Rev.*, **91,** 816.
Suzuki, H., and Barrett, C. S., 1958, *Acta Met.*, **6,** 156.
Swenson, C. A., and Stahl, R. H., 1954, *Rev. sci. Instrum.*, **25,** 608.
Thompson, N., 1953, *Proc. phys. Soc. Lond.* B, **67,** 427.
White, G. K., 1958, *Experimental Techniques in Low Temperature Physics* (Oxford : University Press), in press.
Woolley, R. L., 1953, *Phil. Mag.*, **44,** 597.
Wyatt, O. H., 1953, *Proc. phys. Soc. Lond.* B, **66,** 459.

On the Possibility of Thermoelectric Refrigeration at very Low Temperatures†

By D. K. C. MacDonald, E. Mooser, W. B. Pearson,
I. M. Templeton and S. B. Woods
Division of Pure Physics, National Research Council, Ottawa, Canada

[Received November 13, 1958]

§ 1. Introduction

The possible use of thermoelectric cooling (primarily by the Peltier effect) for domestic or industrial refrigeration at ambient temperatures has been considered at various times in the past and probably most exhaustively by Joffé (1957) in his book on the subject. We wish to consider here the problem of thermoelectric refrigeration at very low temperatures, in particular for the attainment of temperatures below 1 °K.

§ 2. Theoretical Considerations

There appear to be four questions involved in a discussion of thermoelectric cooling at low temperatures, namely:

(1) The ideal limit of refrigeration, which one may write $\Delta T_{\max}/T$, in the absence of external heat influx or heat load, say H.

(2) The dependence of $\Delta T/T$ on the heat load and on such factors as the electric current density, $\mathscr{J}$, through the couple.

(3) The rate of refrigeration.

(4) The overall efficiency of refrigeration.

Efficiency of refrigeration is naturally of great importance for industrial refrigeration; on the other hand it can hardly be considered as a serious factor at present in the attainment of very low temperatures. When we use the adiabatic demagnetization of a paramagnetic salt for refrigeration below 1 °K the actual work expended in operating a suitable high-field magnet may be very considerable. For this alone one may easily consume 20 kwh for a single demagnetization cycle which permits us to extract maybe 1/5 calorie at the low temperature; this corresponds to an efficiency of about 10^{-8} (!), but does not deter one from carrying out research at these low temperatures.

We shall see later that the *rate* of refrigeration in thermoelectric cooling would normally be quite rapid and consequently we turn now to consider the ideal limit of refrigeration which could be attained. As our model refrigerator we discuss the circuit of fig. 1. The conductor on the left is of some arbitrary material of electrical conductivity, σ, thermal conductivity,

---

† Communicated by the Authors.

κ, absolute thermoelectric power, S, Peltier heat, Π, and Thomson heat, μ. That on the right is to be a pure superconductor well below its transition temperature so that $\sigma=\infty$, $S=\Pi=\mu=0$. In addition for convenience we shall assume that for this element $\kappa=0$; this of course is not strictly true, but is a reasonable simplification of the problem since the thermal conductivity of a pure superconductor generally falls off rather rapidly below the transition point.

Fig. 1

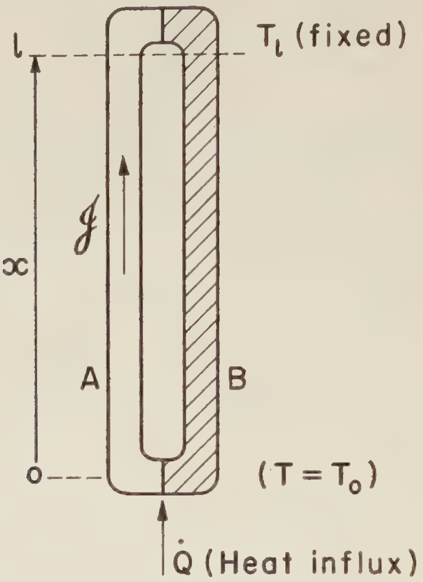

Schematic thermoelectric circuit for refrigeration.

The steady-state equations are then:

$$\kappa\frac{\partial^2 T}{\partial x^2}+\frac{\partial\kappa}{\partial T}\left(\frac{\partial T}{\partial x}\right)^2=\mu\mathscr{J}\frac{\partial T}{\partial x}-\frac{\mathscr{J}^2}{\sigma}, \quad \ldots\ldots \quad (1)$$

$$\left(\frac{\partial T}{\partial x}\right)_{x=0}=\mathscr{J}\frac{\Pi_0}{\kappa_0}-\frac{\dot{Q}}{\kappa_0 A}, \quad \ldots\ldots \quad (2a)$$

$$=\mathscr{J}\frac{T_0 S_0}{\kappa_0}-\frac{\dot{Q}}{\kappa_0 A}, \quad \ldots\ldots \quad (2b)$$

where $\mathscr{J}$ is the electric current density, $\dot{Q}$ is the heat influx per unit time, and A is the cross sectional area of the non-superconducting element.

We shall see that—at present certainly—only a very small cooling is possible at very low temperatures. In that case the Thomson term $[\mu\mathscr{J}(\partial T/\partial x)]$ may be neglected, and we may treat κ and σ as constants. We then have

$$T_l=T_0+\frac{JT_0S_0}{\kappa}-\frac{H}{\kappa}-\frac{J^2}{2\kappa\sigma}, \quad \ldots\ldots \quad (3)$$

where $J=\mathscr{J}l$, and $H=\dot{Q}l/A$.

T_0 is a minimum for a given T_l, when :

$$J = \sigma S_0 T_0 \quad . \quad . \quad . \quad . \quad . \quad . \quad . \quad . \quad . \quad . \quad (4)$$

and we then have

$$T_l = T_0 + \frac{\sigma S_0^2 T_0^2}{2\kappa} - \frac{H}{\kappa}. \quad . \quad . \quad . \quad . \quad . \quad . \quad (5a)$$

In principle we can neglect the effect of a given heat leak, $\dot{Q}$, by diminishing l (or l/A) sufficiently; reducing l means of course from eqn. (4) that the current density $\mathscr{J}$ would have to be *increased* proportionately. We might note that if we assume $\sigma \simeq 10^9$ (ohm cm)$^{-1}$ and that S has a magnitude of about 5×10^{-6} v/°c†, around $T \simeq 1$°K (values appropriate to very pure gold, which we shall discuss below), then from eqn. (4): $J = 5 \times 10^3$ amps/cm. Thus a conductor of 1 sq. mm cross section with $l = 10$ cm would then require a net current of 5 amps for optimum performance. With these dimensions the term H/κ could be neglected in (5a) if $\dot{Q}/A$ did not exceed about 10^{-4} joules/sq. cm sec, i.e. a net heat load of 10^{-6} joules/sec, that is 10 ergs/sec or 600 ergs/min. This would mean in fact a refrigeration efficiency of about 4%, although as mentioned previously this is not a primary consideration.

If then we design our system so that the heat load term in (5a) can be neglected, we see that the *limit* of refrigeration is given by

$$T_l - T_0 = \sigma S_0^2 T_0^2 / 2\kappa \quad . \quad . \quad . \quad . \quad . \quad . \quad . \quad (5b)$$

a result, together with (4), obtained by Joffé (loc. cit.). Alternatively we may write:

$$\Delta T / T_0 = S_0^2 / 2L_0 \quad . \quad . \quad . \quad . \quad . \quad . \quad . \quad (5c)$$

where $L_0 = \kappa/\sigma T_0$, the Lorenz number at the temperature T_0. We shall see from some experimental results below, that we need only concern ourselves with metals as possible refrigerating elements at low temperatures. Now around 1°K even pure metals may generally be expected to have their conductivities limited by chemical impurities and/or physical imperfections, and the Lorenz number then has its limiting value of about $2{\cdot}5 \times 10^{-8}$ (volts/deg)^2 (theoretically $\pi^2 k^2/3e^2$ cf. e.g. Mott and Jones 1936, pp. 306–7, Wilson 1953, pp. 18, 201). Theoretically we should expect metals to show an absolute thermoelectric power, $S \sim c_{el}/e$ where c_{el} is the electronic specific heat (per conduction electron)‡. This would mean $S \sim 10^{-8}$ volts/deg at about 1°K for a typical metal, and we see from (5c) that we should then have $\Delta T/T_0 \simeq 2 \times 10^{-9}$, which would seem sufficiently small to discourage any further investigation. However, recent experiments (MacDonald *et al.* 1958) have shown that certain metals show thermoelectric powers at 1°K and below greatly in excess of theoretical predictions. In particular, pure gold is found to have an absolute thermoelectric power of about $-5{\cdot}5\,\mu$v/deg at 1°K and about $-4{\cdot}1\,\mu$v/deg at 0·5°K. Thus, using pure gold, $\Delta T/T_0$ would be increased to the order of 10^{-3}. Of course this is still too small to be of any practical value, but until and unless adequate theory is forthcoming to show that *even higher* values of thermoelectric power cannot be looked for in some particular pure metal or alloy, it appears well worth while to explore the situation further. Experiments are continuing (MacDonald *et al.*) below 1°K on the measurement of thermoelectric power as part of the search for a possible suitable material. There is the further possibility that metal may yet be obtained of *sufficiently high* purity so that even at these low temperatures the conduction is *not* limited by impurity or defect scattering. In that case the Lorenz number, L, may be much lower than the limiting value, and indeed L falls with T^2 at low temperatures so long as the scattering is due only to thermal vibrations (cf. Wilson, loc. cit., pp. 290–1, and Berman and MacDonald (1951, 1952) for some experimental results on sodium and copper).

---

† Actually S is negative for gold at these low temperatures; this means simply that the direction of J must be reversed (cf. eqn. (4)) to provide cooling.

‡ Ignoring the 'phonon-drag' or Gurevich (1945, 1946) effect; in general this should be unimportant below 1°K.

We return therefore to the analysis of the problem. If appreciable cooling *can* be achieved then the Thomson effect can assist in the cooling when μ is of the same sign as S, and we recall that $\mu = T\,dS/dT$. Some expressions including the Thomson effect are given in Appendix I, but we shall not consider them further here. It remains to analyse the *rate* of refrigeration. We consider now that our thermoelectric conductor of specific heat per unit volume, C, has attached to the end ($x=0$) a substance of total specific heat G, and at time $t=0$ the current is switched on. We now have to solve:

$$\kappa\frac{\partial^2 T}{\partial x^2} - C\frac{\partial T}{\partial t} = -\mathscr{J}^2/\sigma \qquad . \quad . \quad . \quad . \quad . \quad . \quad (6)$$

subject to

$$-\kappa A\left(\frac{\partial T}{\partial x}\right)_{x=0} + G\left(\frac{\partial T}{\partial t}\right)_{x=0} = -\mathscr{J}T_0 S_0. \qquad . \quad . \quad . \quad (7)$$

and $\qquad T(x) = T_l \quad$ for all x at $t=0$,

$\qquad T(l) = T_l \quad$ for all t.

We shall treat κ, C, σ, G and T_0 and S_0 in (7) as constants (a valid approximation for moderate cooling). In Appendix II we outline the solution of eqn. (6) which then yields

$$T(x,t) = T_l - M\left\{1-\frac{x}{l}\right\} + N\left\{1-\left(\frac{x}{l}\right)^2\right\}$$
$$+\sum_{n=0}^{\infty} B_n \exp(-K\beta_n{}^2 t)\left(\cos\beta_n\frac{x}{l} - \frac{\beta_n}{\Lambda}\sin\beta_n\frac{x}{l}\right) \qquad . \quad . \quad . \quad (8)$$

where $M = JT_0S_0/\kappa$; $N = J^2/2\kappa\sigma \quad (J = \mathscr{J}l)$,

$K = \kappa/Cl^2$,

$\Lambda = ClA/G$,

β_n are the (positive) roots of the equation $\beta_n \tan\beta_n = \Lambda$,

$$B_n = \frac{2}{[1+(\beta_n{}^2/\Lambda^2)+(1/\Lambda)]}\left\{\frac{M}{\beta_n{}^2} - 2N\left(\frac{\sin\beta_n}{\beta_n{}^3} - \frac{1-\cos\beta_n}{\beta_n{}^2\Lambda}\right)\right\}.$$

Let us consider two limiting cases:

(*a*) *Negligible additional heat-capacity*: $\Lambda \to \infty$

Equation (8) then reduces to

$$T(x,t) = T_l - M\left\{\left(1-\frac{x}{l}\right) - \frac{8}{\pi^2}\sum_{n=0}^{\infty}\frac{1}{(2n+1)^2}\exp\left[\frac{-(2n+1)^2 t}{t_1}\right]\times\cos(2n+1)\frac{\pi x}{2l}\right\} + N\left\{\left(1-\left(\frac{x}{l}\right)^2\right) - \frac{32}{\pi^3}\sum_{n=0}^{\infty}\frac{(-1)^n}{(2n+1)^3}\times\exp\left[\frac{-(2n+1)^2 t}{t_1}\right]\cos(2n+1)\frac{\pi x}{2l}\right\} \qquad (9)$$

(writing $t_1 = 4Cl^2/\pi^2\kappa$).

For $t \gg t_1$, we have

$$T(x) \simeq T_l - M\left(1-\frac{x}{l}\right) + N\left(1-\left(\frac{x}{l}\right)^2\right) \quad . \; . \; . \quad (10)$$

and $T(0) \equiv T_0 = T_l - (JT_0S_0/\kappa) + (J^2/2\kappa\sigma)$ (cf. eqn. (3) with $H=0$).

$T(x, t)$ from eqn. (9) is plotted in figs. 2 and 3, setting $J = \sigma S_0 T_0$ which gives the maximum final cooling (cf. eqn. (4)).

Fig. 2

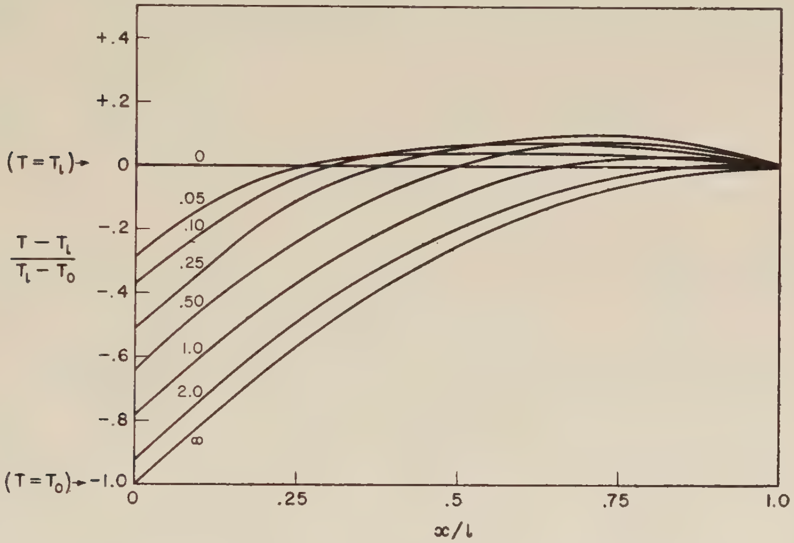

Theoretical curves for cooling of bar with negligible additional heat capacity. The indices on the curves refer to values of the parameter t_1.

If we ignore the early part of the cooling process ($t \ll t_1$) then we need only retain the first term in the series of eqn. (9) and the maximum *rate* of refrigeration for the 'unloaded' bar is then given by

$$J = \frac{\pi}{4}\sigma S_0 T_0 \quad . \; . \; . \; . \; . \; . \; . \; . \; . \quad (11)$$

which is thus rather close to the value required to give maximum final refrigeration.

Fig. 3

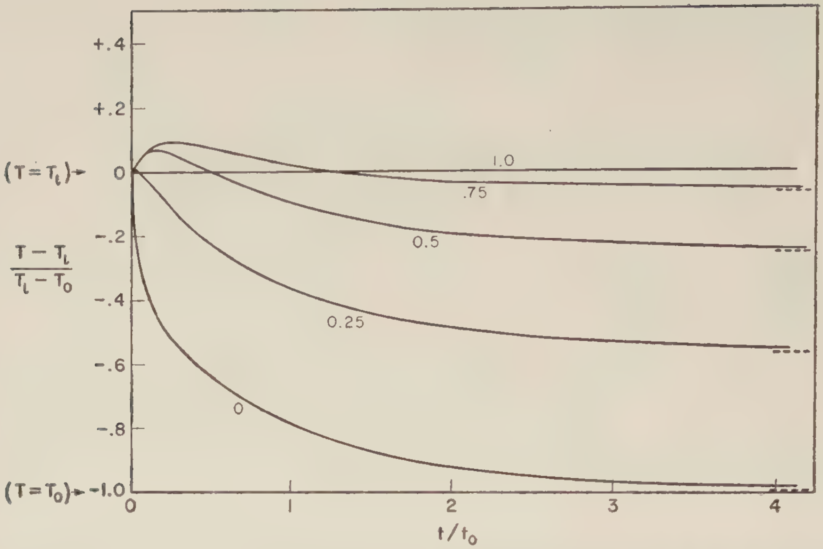

Theoretical curves for cooling of bar with negligible additional heat capacity. The indices on the curves refer to the values of the parameter x/l.

Fig. 4

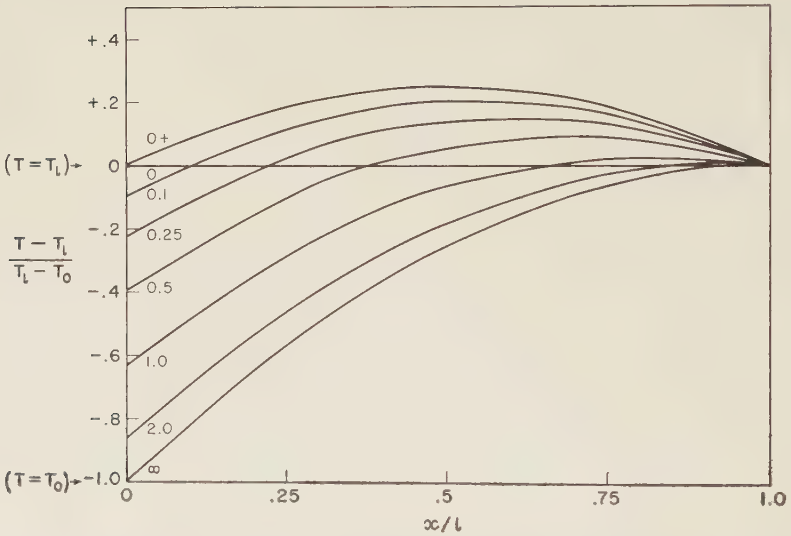

Theoretical curves for cooling of bar with large additional capacity at cold end. The indices on the curves refer to values of the parameter t_2. The curve labelled 0+ refers to the situation after the initial adjustment of the bar itself to the Joule heating ($t \gg t_1$, but $t \ll t_2$).

(*b*) *Large additional heat-capacity*: $\Lambda \to 0$

Equation (8) now reduces to

$$T(x,t) = T_l - M\left(1-\frac{x}{l}\right).\left[1-\exp\left(-t/t_2\right)\right] + N\left\{\left(1-\frac{x}{l}\right)^2 - \left(1-\frac{x}{l}\right)\right.$$
$$\left. \times \exp\left(-t/t_2\right) - \frac{8}{\pi^3}\sum_{n=0}^{\infty}\frac{1}{(2n+1)^3}\exp\left[\frac{-4(2n+1)^2 t}{t_1}\right]\sin\left(2n+1\right)\frac{\pi x}{l}\right\} \quad . \quad . \quad . \quad (12)$$

where

$$t_2 = \frac{lG}{\kappa A} \quad (\text{and } t_2 = t_1/4\Lambda).$$

The terms in the infinite series correspond to the initial thermal adjustment of the bar itself to the Joule heating; this process is relatively a very rapid one since $t_1/t_2 = 4\Lambda$ and $\Lambda \to 0$. Thereafter the system approaches the final state with a simple relaxation time, t_2, and the optimum *rate* of refrigeration is given by $J = \sigma T_0 S_0$, the *same* value necessary to achieve maximum cooling. In fig. 4, $T(x,t)$ is plotted for this case. We may note that for a given thermal load capacity (G), t_2 can in principle be made as short as we please by making l/A sufficiently small. If we have a thermal element with $\kappa \simeq 4$ joules/cm deg sec; $C \simeq 10^{-3}$ joules/mol deg (typical of pure gold at 1°K) and take $l = 10$ cm, then $t_1 \simeq 10^{-2}$ sec; if further $A = 10^{-2}$ cm^2 (the cross sectional area considered previously), then a body of total heat capacity about 1 joule/deg (i.e. $G \simeq 1/4$ cal/deg, which is quite large in low temperature work) could be cooled in about 4 min.

§ 3. EXPERIMENTAL INVESTIGATIONS

We have mentioned in § 2 that the present theory of electron transport predicts absolute thermoelectric powers of the order of 10^{-8} v/deg for metals at temperatures around 1°K. As, however, we have found very much larger values for some metals (e.g. about $-0{\cdot}5\,\mu$v/deg for Cu, $-0{\cdot}6\,\mu$v/deg for Ag; $-5{\cdot}5\,\mu$v/deg for Au; and about $-1{\cdot}1\,\mu$v/deg for Pt) it is clear that the magnitude of thermoelectric power cannot as yet be predicted theoretically with any certainty at the lowest temperatures (save that $S = 0$ at $T = 0$°K). We have therefore measured the thermoelectric power, electrical resistivity and thermal conductivity of several compounds as well as pure metals at low temperatures in order to see whether they might not show larger absolute thermoelectric powers than the pure metals referred to above. The materials selected were Bi_2Te_3, which we believe to contain intrinsic holes in the valence band (cf. Mooser and Pearson 1958) and the semi-metallic compounds Bi_2Se_3 and InTe which contain a relatively small number of free charge carriers. Such materials are useful for thermoelectric cooling in the room temperature region and they were chosen for this investigation because their resistivities would not be large at the lowest temperature.

The measurements, which were made by methods standard in this laboratory (cf. White and Woods 1955, Christian *et al.* 1958), are shown in figs. 5 to 8 and the electrical data on the compounds are given in Appendix III.

Fig. 5

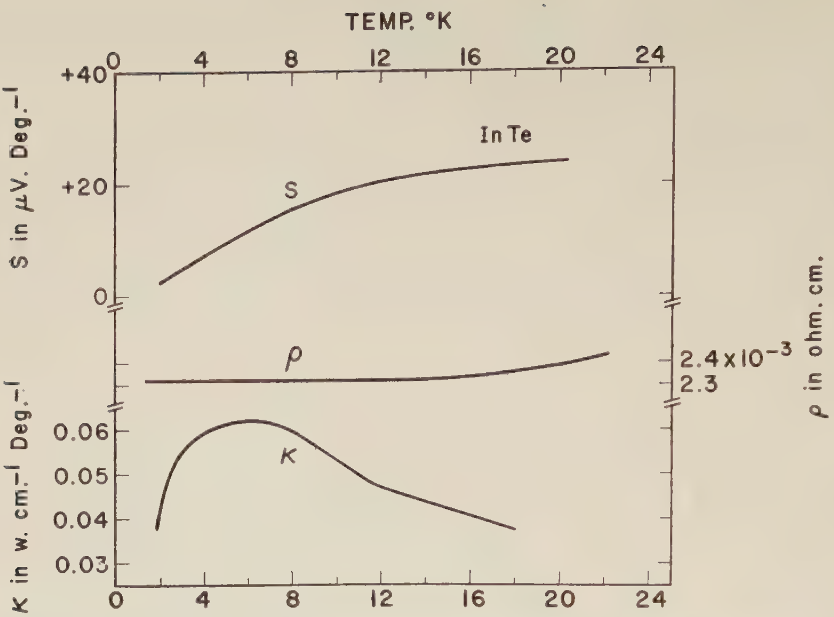

Electronic transport data for the compound p-type InTe. (S: absolute thermoelectric power; ρ ($=1/\sigma$): electrical resistivity; κ: thermal conductivity).

Fig. 6

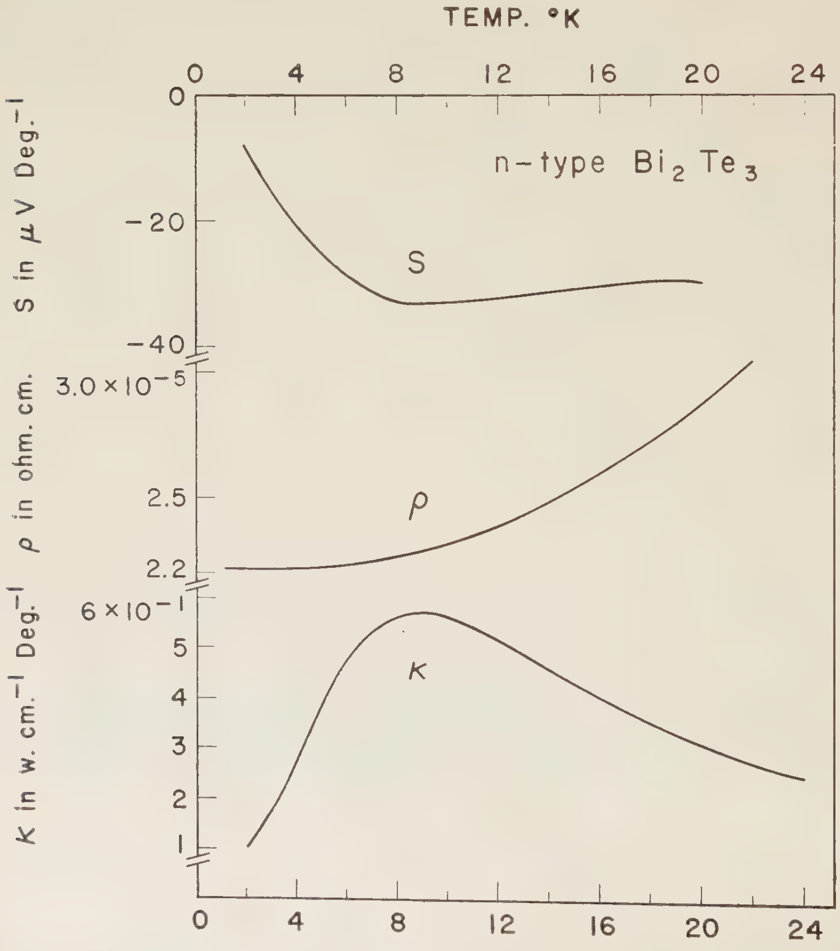

Electronic transport data for the compound n-type Bi_2Te_3.

Fig. 7

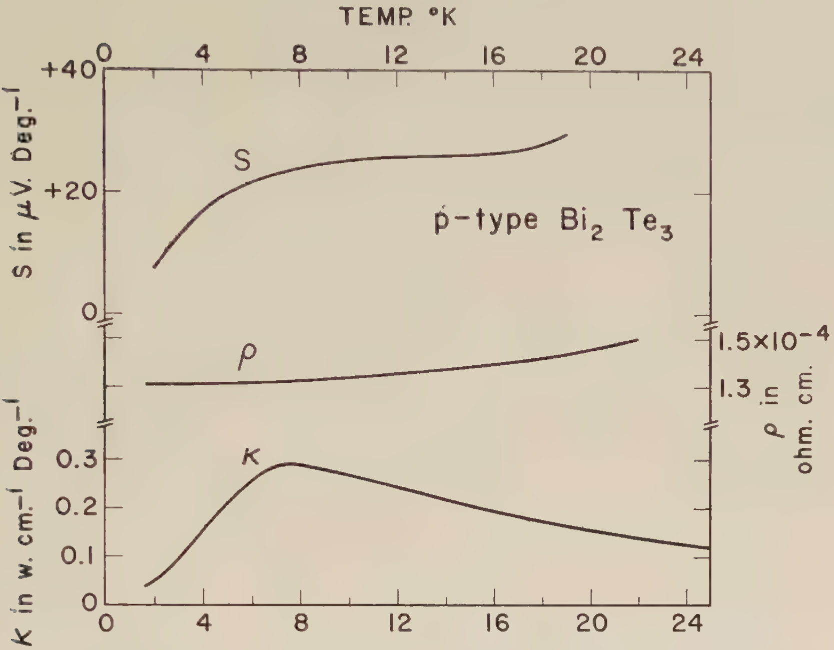

Electronic transport data for the compound p-type Bi_2Te_3.

Fig. 8

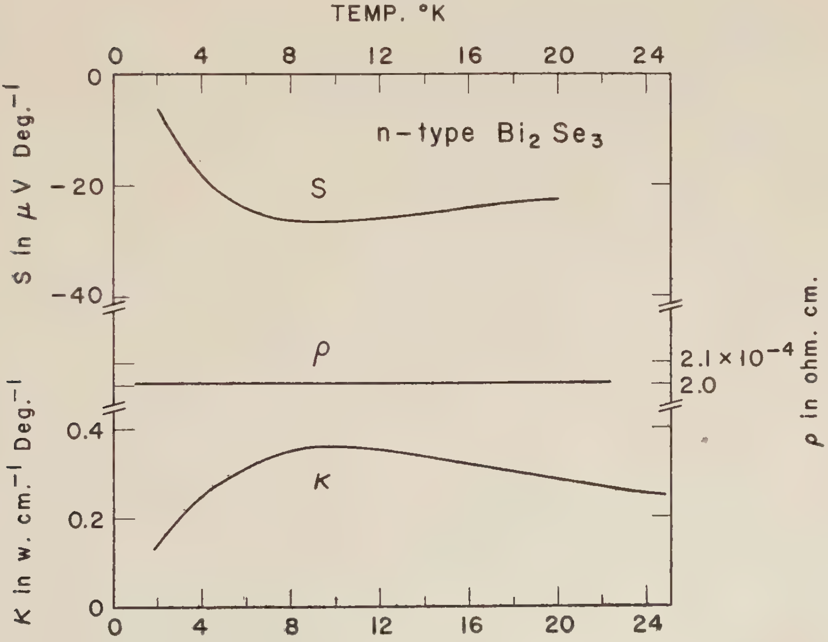

Electronic transport data for the compound n-type Bi_2Se_3.

It can be seen that these substances have thermoelectric powers at 1°K which are of the order of a microvolt per degree. In this respect they are already inferior to pure gold at the lowest temperatures. In addition the Lorenz number is very much higher for the compounds rendering the comparison still more unfavourable. Comparable data for pure gold are shown in fig. 9. In fig. 10 data for the parameter S^2/L (cf. eqn. (5)) are collected for all the compounds and for gold; the data show clearly the superiority of gold in this field.

Fig. 9

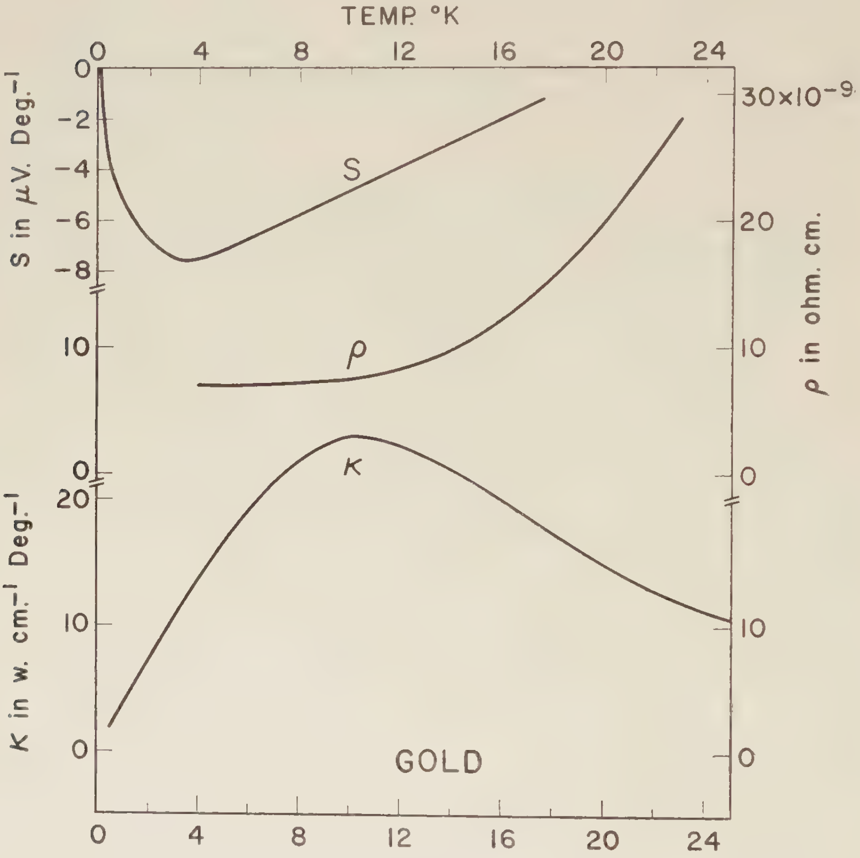

Electronic transport data for high purity gold.

We have found that the absolute thermoelectric power of gold increases with purity at low temperatures, in so far as a sample having a value of $R_{4\cdot 2^\circ\mathrm{K}}/R_{295^\circ\mathrm{K}} \simeq 64 \times 10^{-3}$ had a value of $S \simeq -2\cdot 7\ \mu\mathrm{v/deg}$ at 1°K, while a sample with $R_{4\cdot 2^\circ\mathrm{K}}/R_{295^\circ\mathrm{K}} \simeq 3\cdot 2 \times 10^{-3}$ showed $S \simeq -5\cdot 5\ \mu\mathrm{v/deg}$ at 1°K. It therefore would appear that at present the only hope of finding a material suitable for thermoelectric cooling at these low temperatures lies in the direction of a great improvement in the purity of a metal such as gold. This might be expected to lead to a significant increase in thermoelectric power and if a *sufficiently pure metal were to be obtained*, so that the conductivity was limited at the low temperatures required by thermal processes rather than by impurity or defect scattering, the Lorenz parameter, $\kappa/\sigma T$, could then be much lower than its limiting value of about $2{\cdot}5 \times 10^{-8}$ (volts/deg)^2.

Fig. 10

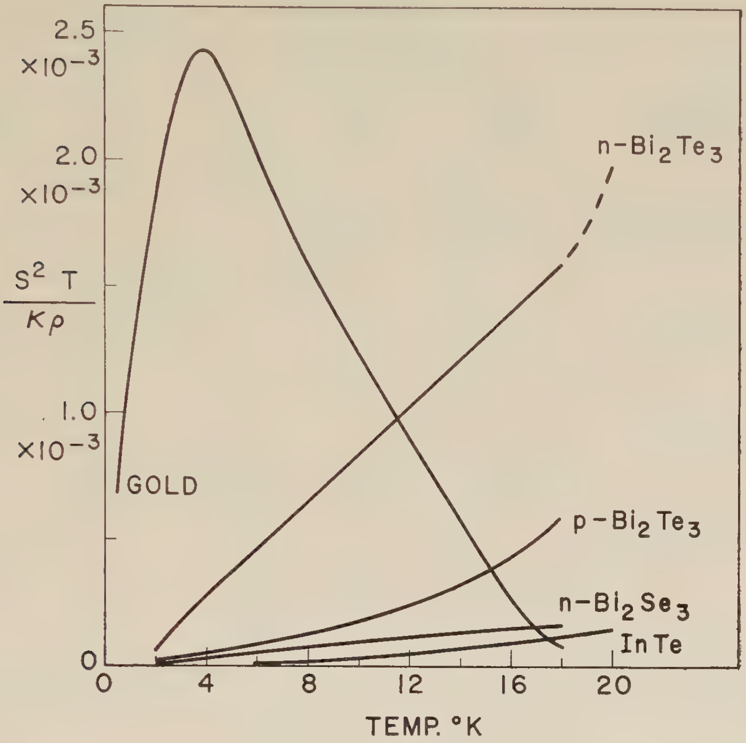

The parameter $S^2T/\kappa\rho$ for various substances.

The Lorenz number is often considered as a useful parameter in discussions of electron transport properties of conductors. In metals it is essentially constant at high temperatures and also at sufficiently low temperatures where impurity scattering is dominant. (In both these regions a common mean free path may be defined for electrical and thermal conductivity.) However, it is not a dimensionless parameter, having the dimensions (volt/deg)^2, and it only involves two of the transport parameters (κ, σ). It seems possible that the dimensionless parameter, $S^2\sigma T/\kappa$, suggested by this work and which involves all three of the transport coefficients, might also prove useful. In a metal this number would be expected to vary as T^2 at sufficiently low and high temperatures, while at low temperatures if the scattering is dominated by *thermal* processes, conventional theory would predict a *constant* value ($\kappa \propto T^{-2}$, $\sigma \propto T^{-5}$, $S \propto T$).

ACKNOWLEDGMENTS

We are grateful to Messrs. F. W. Richardson and J. Broome for liquefying the helium required for this investigation and to Miss Joan Spong for assistance in numerical computation and in some of the experiments.

APPENDIX I

We have
$$\kappa \frac{\partial^2 T}{\partial x^2} = \mu \mathscr{J} \frac{\partial T}{\partial x} - \frac{\mathscr{J}^2}{\sigma}$$

together with
$$\left(\frac{\partial T}{\partial x}\right)_0 = \mathscr{J} \frac{T_0 S_0}{\kappa} - \frac{\dot{Q}}{A\kappa}$$

$$T(l) = T_l \, (\text{constant}).$$

The solution for T_0 is, assuming μ, σ, κ constant,

$$T_0 = T_l - \frac{J}{\mu\sigma} + \frac{1}{\mu}\left\{T_0 S_0 - \frac{\kappa}{\mu\sigma} - \frac{H}{J}\right\} \cdot \left[1 - \exp\left(\frac{\mu J}{\kappa}\right)\right],$$

where $H = \dot{Q} l / A$.

If μ is 'small'
$$\left(\frac{\mu S_0}{L_0} \ll 1 ; \; \frac{\mu^2 \sigma H}{2} \ll 1\right)$$

we find maximum cooling for

$$J \simeq \sigma S_0 T_0 \left(1 + \frac{\mu S_0}{2L_0} - \frac{\mu H}{2\kappa S_0 T_0}\right) \qquad (13)$$

and with this value

$$\frac{\Delta T}{T_0} \simeq \frac{S_0^{\,2}}{2L_0}\left\{1 + \frac{2\mu S_0}{3L_0} - \frac{2H}{\sigma S_0^{\,2} T_0^{\,2}}\right\}. \qquad (14)$$

If we choose l/A so that the heat flux is negligible ($H \ll \sigma T_0^{\,2} S_0^{\,2}/\kappa$) then the optimum conditions may be derived exactly (still assuming μ, σ, κ constant). The optimum current is given by

$$J = -\frac{\kappa}{\mu} \ln\left(1 - \frac{\mu\sigma S_0 T_0}{\kappa}\right) \qquad (15)$$

and the corresponding cooling is

$$\frac{\Delta T}{T_0} = -\frac{S_0}{\mu} \cdot \left\{\frac{\kappa}{\mu\sigma S_0 T_0} \ln\left(1 - \frac{\mu\sigma S_0 T_0}{\kappa}\right) + 1\right\}. \qquad (16)$$

APPENDIX II

We have to solve
$$\kappa \frac{\partial^2 T}{\partial x^2} - C \frac{\partial T}{\partial t} = -\frac{\mathscr{J}^2}{\sigma}$$

subject to

$$T(x, 0) = T_l \quad (t = 0),$$
$$T(l) = T_l \quad (t \geqslant 0),$$
$$\kappa \left(\frac{\partial T}{\partial x}\right) - \frac{G}{A}\left(\frac{\partial T}{\partial t}\right) = \mathscr{J} T_0 S_0 \quad (x = 0).$$

We let

$$T(x,t)=T_l-M\left(1-\frac{x}{l}\right)+N\left(1-\left(\frac{x}{l}\right)^2\right)+v(x,t),$$

where

$$M=\frac{JT_0S_0}{\kappa}, \quad \text{and } J=\mathscr{J}l,$$

$$N=J^2/2\sigma\kappa.$$

We have then to solve

$$\kappa\frac{\partial^2 v}{\partial x^2}-C\frac{\partial v}{\partial t}=0 \qquad \text{. . . . . (17)}$$

subject to

$$v(x,0)=M\left(1-\frac{x}{l}\right)-N\left(1-\left(\frac{x}{l}\right)^2\right), \qquad \text{. . . . . (18)}$$

$$v(l)=0 \quad (t\geqslant 0), \qquad \text{. . . . . (19)}$$

$$\kappa\frac{\partial v}{\partial x}-\frac{G}{A}\frac{\partial v}{\partial t}=0 \quad (x=0). \qquad \text{. . . . . (20)}$$

Equation (17) is satisfied, together with (19) and (20), if we set

$$v=\sum_{n=0}^{\infty}B_n\exp(-K\beta_n{}^2t)\left\{\cos\beta_n\frac{x}{l}-\frac{\beta_n}{\Lambda}\sin\beta_n\frac{x}{l}\right\}$$

where β_n are the (positive) roots of the equation $\beta_n\tan\beta_n=\Lambda$;

$$\Lambda=ClA/G, \quad \text{and } K=\kappa/Cl^2.$$

Equation (18) is satisfied if we can expand $v(x,0)$ as the series

$$v(x,0)=\sum_{n=0}^{\infty}B_nX_n$$

valid in the range $0\leqslant x\leqslant l$, where

$$X_n=\cos\beta_n\frac{x}{l}-\sin\beta_n\frac{x}{l}.$$

The functions X_n are *not* orthogonal (cf. Carslaw and Jaeger 1947, p. 93 *et seq.*, for a similar problem, where however the elements *are* orthogonal), but we find

$$\int_0^l X_mX_n\,dx=-\frac{l}{\Lambda} \quad (m=n),$$

$$\int_0^l X_n{}^2\,dx=\frac{l}{2}\left\{1+\frac{\beta_n{}^2}{2}-\frac{1}{\Lambda}\right\}.$$

Then generally

$$B_n=\frac{2}{l[1+(\beta_n{}^2/\Lambda)+(1/\Lambda)]}\left\{\int_0^l\left(v(x,0)\cos\beta_n\frac{x}{l}-\frac{\beta_n}{\Lambda}\sin\beta_n\frac{x}{l}\right)dx+\frac{l}{\Lambda}v(0,0)\right\}.$$

In this specific problem

$$v(x,0)=M\left(1-\frac{x}{l}\right)-N\left(1-\left(\frac{x}{l}\right)^2\right)$$

and B_n reduces to

$$B_n = \frac{2}{[1+(\beta_n^2/\Lambda^2)+(1/\Lambda)]}\left\{\frac{M}{\beta_n^2} - 2N\left(\frac{\sin\beta_n}{\beta_n^3} + \frac{\cos\beta_n - 1}{\beta_n^2\Lambda}\right)\right\},$$

the result given in the text.

APPENDIX III

Room Temperature Data on the Bi_2Te_3, Bi_2Se_3 *and* InTe *Samples Examined*

Bi_2Te_3 p-type

Conductivity $\sigma = 6{\cdot}7 \times 10^2\ \Omega^{-1}\,\mathrm{cm}^{-1}$.
Hall coefficient $R = +5{\cdot}6 \times 10^{-1}\ \mathrm{cm}^3/\mathrm{coulomb}$.
Hole concentration $p = 1{\cdot}1 \times 10^{19}\ \mathrm{cm}^{-3}$.
Hole mobility $\mu_p = R\sigma = 375\ \mathrm{cm}^2/\mathrm{volt\ sec}$.

Bi_2Te_3 n-type

Conductivity $\sigma = 9{\cdot}2 \times 10^2\ \Omega^{-1}\,\mathrm{cm}^{-1}$.
Hall coefficient $R = -5{\cdot}3 \times 10^{-1}\ \mathrm{cm}^3/\mathrm{coulomb}$.
Electron concentration $n = 1{\cdot}2 \times 10^{19}\ \mathrm{cm}^{-3}$.
Electron mobility $\mu_n = 488\ \mathrm{cm}^2/\mathrm{volt\ sec}$.

Bi_2Se_3 n-type

Conductivity $\sigma = 2{\cdot}4 \times 10^3\ \Omega^{-1}\,\mathrm{cm}^{-1}$.
Hall coefficient $R = -3{\cdot}25 \times 10^{-1}\ \mathrm{cm}^3/\mathrm{coulomb}$.
Electron concentration $n = 1{\cdot}9 \times 10^{19}\ \mathrm{cm}^{-3}$.
Electron mobility $\mu_n = 780\ \mathrm{cm}^2/\mathrm{volt\ sec}$.

InTe p-type

Conductivity $\sigma = 2{\cdot}0 \times 10^2\ \Omega^{-1}\,\mathrm{cm}^{-1}$.
Hall coefficient $R = +1{\cdot}0 \times 10^{-1}\ \mathrm{cm}^3/\mathrm{coulomb}$.
Hole concentration $p = 6{\cdot}25 \times 10^{19}\ \mathrm{cm}^{-3}$.
Electron mobility $\mu_p = 20\ \mathrm{cm}^2/\mathrm{volt\ sec}$.

REFERENCES

BERMAN, R., and MACDONALD, D. K. C., 1951, *Proc. roy. Soc.* A, **209,** 368; 1952, *Ibid.*, **211,** 122.

CARSLAW, H. S., and JAEGER, J. C., 1947, *Conduction of Heat in Solids* (Oxford: Clarendon Press).

CHRISTIAN, J. W., JAN, J.-P., PEARSON, W. B., and TEMPLETON, I. M., 1958, *Proc. roy. Soc.* A, **245,** 213.

GUREVICH, L., 1945, *J. Phys., Moscow*, **9,** 477; 1946, *Ibid.*, **10,** 67.

JOFFÉ, A. F., 1957, *Semiconductor Thermoelements and Thermoelectric Cooling* (London: Infosearch). Orig. pub. in 1956 by Pub. House, U.S.S.R. Acad. Sci., Moscow–Leningrad.

MACDONALD, D. K. C., PEARSON, W. B., and TEMPLETON, I. M., 1958, *Phil. Mag.*, **3,** 657.

MOOSER, E., and PEARSON, W. B., 1958, *J. Chem. Phys. Solids*, **7,** 65.

MOTT, N. F., and JONES, H., 1936, *Theory of Properties of Metals and Alloys* (Oxford: Clarendon Press).

WHITE, G. K., and WOODS, S. B., 1955, *Canad. J. Phys.*, **33,** 58.

WILSON, A. H., 1953, *Theory of Metals*, 2nd. edn (Cambridge: University Press).

Surface Growths and Whiskers on an Aluminium–Magnesium Alloy†

By P. J. E. Forsyth, P. G. Partridge and D. A. Ryder
Ministry of Supply, Royal Aircraft Establishment, Farnborough, Hants.

[Received August 27, 1958; and in revised form December 9, 1958]

As part of a general study of the surface deterioration occurring on aluminium–magnesium alloys during heat treatment, polished specimens were treated at various temperatures, *in vacuo* and in various atmospheres, and subsequently microscopically examined. The surface on which the observations were made was usually electrolytically polished prior to any heat treatment, to remove approximately 0·025 mm from the original. A few observations were also made on mechanically polished specimens.

Most of the observations were made on specimens cut from aluminium 7% magnesium extruded strip, although a few were cut from strip which had been cold-rolled from the above extrusion.

If electrolytically polished material is heat treated in vacuum (1–2 μHg) at any temperature between the eutectic temperature (450°c) and the solidus temperature for the alloy (520°c), small surface growths occur. The rate of growth is dependent on temperature; pronounced growth may occur in 22 hours at 460°c, whereas at 445°c, that is just below the eutectic temperature for the aluminium–magnesium system, no growths could be observed after 100 hours. These growths lie along grain boundaries, and have a marked crystalline form of hexagonal or rectangular prisms shown in fig. 1 (Pl. 57).

It would seem that they grow only where grain boundaries meet the surface and others which are found within grains have been formed while grain boundaries were migrating. Migrating grain boundaries leave residual, thermally etched grooves, and it can be seen from fig. 2 (Pl. 57) that growths occurred at several stages during migration. Sometimes these boundary growths are not regular prisms, but seem to be composed of two crystals fused together, each growing with the orientation of its parent grain. These growths may extend in a vermicular form along grain boundaries the sides of the prisms losing their clearly defined crystalline form, but the top faces remaining plane. At temperatures very close to the solidus marked, growth along one axis occurs to form whiskers having a geometric section, the platform at the end still remaining as a crystalline facet. A whisker of this type is shown in fig. 3 (Pl. 58), and fig. 4 (Pl. 58) shows the end facet. These crystalline forms may be generated from the normal crystalline growth by tapering down to the final section or may be parallel over their full length, emerging as new growths from the parent metal surface itself. X-ray powder photographs of growths of geometric form have shown their composition to be aluminium containing approximately 3·5 at. % magnesium. No growth spirals have been observed either on the faces of the small crystals or on the end platforms of the whiskers, although irregular terraces are often observed on the former.

---

† Communicated by the Authors.

Above the solidus temperature, that is 520°C for this alloy, a very rapid and profuse whisker growth occurs over the whole specimen surface. These whisker growths are illustrated in figs. 5 and 6 (Pl. 59), and x-ray reflection photographs have shown that they are polycrystals of pure aluminium. It can be seen that they are of a fluted form and often branch and divide. They may be several hundred microns in length. Ribbon-like growths were also observed under these conditions. The form of these various surface growths is summarized in fig. 7.

All of the growths observed appear to be associated with grain boundaries emerging at the free surface of the material. It is known that as a general rule the concentration of solute in alloys is higher in the grain boundaries than in the grains, and that boundary diffusion rates are many times greater than the bulk diffusion rate (McLean 1957). Loss of magnesium by volatilization occurs generally over the whole surface, but because of a greater concentration at boundaries it will occur more rapidly there. It is suggested that as the eutectic temperature is exceeded the boundaries approach the molten condition, and material of eutectic composition rapidly diffuses along them to the free surface. Evaporation of magnesium occurs and the mobility of the remaining surface ions results in geometric crystal facets forming. In this condition a residual magnesium content of 3·5 at. % is maintained. The whiskers formed just above the solidus are pure aluminium, because of the loss of magnesium due to its greatly increased vapour pressure at these temperatures. These whiskers seem to be formed by a process of exudation of liquid metal of an indeterminate composition, the magnesium of which is rapidly lost by volatilization. This reduction in magnesium content causes an increase in freezing temperature and the exuded material solidifies, further exudation occurs below this material which in turn freezes, and the whisker grows by a process analogous to continuous casting. It was noticed that this growth from the liquid was aided by gravity, and more profuse growths occurred on the underside of specimens. The surface regions of the specimen having lost magnesium will remain solid at a temperature at which the inside material is beginning to liquate. This material together with the oxide skin will present a stiff outer coating.

The change in volume occurring as liquid is formed acting against the restriction of this surrounding region provides the driving force for this exudation. It is to be expected that the exudation will occur through crevices and imperfections in the oxide skin.

The extrusion mechanism for the solid state growth is more difficult to define, but it may be partly accounted for by the rapid diffusion of magnesium atoms to the metal surface, where they are lost by evaporation. This would result in a continuously maintained vacancy concentration along the boundary near the specimen surface. Such a concentration would tend to diffuse back down the grain boundaries with a resulting exchange of aluminium atoms. Sections cut through growths and the specimen itself show that in all cases diffusion is occurring through a small perforation in the surface film, this is shown in fig. 7. These perforations must initially lie along the grain boundary trace on the surface, and the fact that double crystals can grow together results in grain boundaries appearing in the growths. It appears that surface growth terminates when the grain boundary moves from its original position due to the removal of the boundary which was acting as a diffusion pipe.

Fig. 7

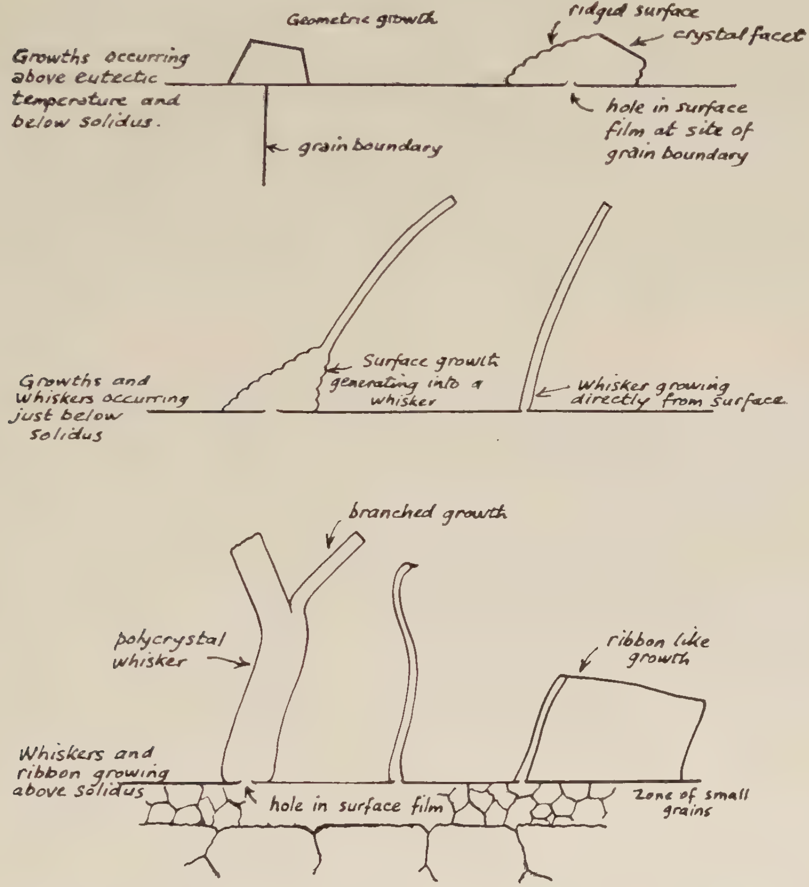
Geometric growth
ridged surface
crystal facet
Growths occurring above eutectic temperature and below solidus.
grain boundary
hole in surface film at site of grain boundary
Surface growth generating into a whisker
Growths and whiskers occurring just below solidus
whisker growing directly from surface
branched growth
polycrystal whisker
ribbon like growth
Whiskers and ribbon growing above solidus
hole in surface film
Zone of small grains

Various forms of surface growth on aluminium 7% magnesium.

It is generally considered that whisker growth by any of the numerous mechanisms proposed in the literature, requires a dislocation or dislocations as growth sites. Franks (1958) has recently discussed the requirements for whisker growth from the solid state. He considers that whisker growth may be regarded as an extrusion process over a region so restricted that only a small number of dislocations is involved, these dislocations act together to extrude a perfectly ordered lattice. In all of the growths we have observed the section of the growth is considerably larger than the diffusion pipe through the oxide, and it is not feasible that the growth could occur by the simple formation of closed loops of dislocations from an Eshelby source as Franks has suggested. It is however obvious that considerable surface migration must have occurred to produce the sharply defined crystalline facets we observe, and it may be that this has caused the lateral spread of the crystallites.

Whisker growths observed in these experiments are so similar in appearance to others described in the literature on the subject that it is difficult to imagine that their mechanism of formation can be very different. If dislocations play a part in these whisker growths they must be grain boundary dislocations as the growth is associated exclusively with grain boundaries.

ACKNOWLEDGMENTS

This paper is published by the permission of the Chief Scientist, Ministry of Supply. Crown copyright reserved. Reproduced by permission of the Controller, H.M. Stationery Office. The authors are indebted to Mr. D. Clark for the x-ray analyses.

REFERENCES

FRANKS, J., 1958, *Acta Met.*, **6**, 103.
McLEAN, D., 1957, *Grain Boundaries in Metals* (Oxford : Clarendon Press).

X-ray Line Broadening in Plastically Deformed Calcite†

By M. S. Paterson
Department of Geophysics, The Australian National University,
Canberra, Australia

[Received August 26, 1958]

Abstract

The broadening of several x-ray powder lines of calcite as a result of plastic deformation under a high confining pressure has been studied in Solenhofen limestone. The dependence of the broadening on the Bragg angle, the apparent influence of elastic anisotropy and the results of Fourier analysis of the lines suggest that the broadening is due mainly to internal strains. The stored energy associated with the internal strains is estimated to be an appreciable fraction, possibly one half or more, of the energy (about 10 cal g^{-1}) expended during deformation. The amount of broadening and the estimated stored energy are relatively large in comparison to the values for most deformed metals. There is no evidence for the presence of stacking faults.

§ 1. Introduction

During the past thirty years there have been many studies of the broadening of the x-ray powder lines in metals as a result of plastic deformation. The usual aim has been to determine the nature of the lattice imperfections giving rise to the broadening and there has been much discussion of whether the decrease of crystallite size or the introduction of internal stresses is the more important factor (Barrett 1952). Recent work has shown that stacking faults can also be important in some cases (Warren and Warekois 1953, and many more recent papers by various authors). However, there seems to have been no work done on x-ray line broadening resulting from plastic deformation of non-metallic crystalline substances, with the exception of the work of Rosenthal and Kaufman (1952) on marble.

Using a photometric technique, Rosenthal and Kaufman measured the breadth of the (651) calcite line‡ after plastic deformation and then after grinding the deformed specimen to successively finer powders. Measurements were also made on virgin marble after grinding it to the same grain sizes. They argued that, since marble is brittle at atmospheric pressure, grinding will release any internal stresses without further plastic deformation, thus enabling one to test whether the line broadening is due to small crystallite size or to internal strains. They concluded that the broadening is mainly due to internal strains.

---

† Communicated by the Author.

‡ These are trigonal indices based on the x-ray unit cell; the corresponding Miller-Bravais indices based on the x-ray unit cell are $(1\ 4\ \bar{5}\ 12)$.

In the present experiments, a Geiger-counter diffractometer has been used for measurements on several calcite reflections from a plastically deformed limestone. In analysing the results, an attempt is made to gain further information about the nature of lattice imperfections resulting from plastic deformation in calcite and to estimate the stored energy.

§ 2. PREPARATION OF SPECIMENS

Solenhofen limestone was chosen as specimen material for the following reasons:

(1) It is fairly pure calcite (96%) and is free from dolomite.

(2) The grain size is small (of the order of 10 microns) so that uniform powder lines are obtained without rotating the specimen.

(3) It is a compact material from which specimens suitable for deformation are readily obtained. For this reason it is preferable to artificially prepared polycrystalline calcite.

(4) Its stress-strain behaviour is well known (Birch 1950).

Before deformation the specimens were cylinders 1 cm in diameter and 2 cm in length, prepared with diamond cutting equipment. The deformation was done in a high-pressure apparatus at about 8000 atmospheres confining pressure, sufficient additional axial load being applied to the specimens to produce the required permanent strain (calcite is ductile under these conditions). Finally the specimen was cut in half longitudinally, and the face exposed was carefully ground flat on abrasive papers, finishing with 600-grade paper. A freshly cut face on virgin material was also ground flat in the same way and this was used as the sample of undeformed material. Since calcite is brittle at atmospheric pressure (except for a limited capacity for twinning under favourable circumstances), it was assumed that the cutting and grinding procedure does not appreciably affect the line breadths†.

Several specimens were used in preliminary work, giving approximately the same line broadening after a given deformation. Some measurements were also made on other calcite rocks. A coarse-grained, pure, white marble (Wombeyan marble, Paterson 1958), when deformed 20% at 8000 kg cm^{-2}, gave a line-broadening about two-thirds that for Solenhofen limestone. A finer-grained, less pure, marble gave a similar result.

All results given in this paper were obtained from one specimen of Solenhofen limestone which had been compressed 15% plastically at a confining pressure of about 8000 kg $\mathrm{cm^{-2}}$. The measured difference between the axial stress and the confining pressure when this plastic strain was reached was about 12 000 kg $\mathrm{cm^{-2}}$ (based on final cross sectional area). This figure is not corrected for the friction on the piston in the high pressure apparatus. The friction is not known; it is likely to contribute at least 10% so that the true principal stress difference was probably about 10 000 kg $\mathrm{cm^{-2}}$.

---

† The assumption that the surface preparation of the specimens did not affect the line breadths was later tested by measuring the breadth of the $(10\bar{1}4)$ line from the undeformed specimen after etching it with dilute HCl. The breadth was found to be slightly decreased (by about 8%), showing that the grinding did cause some deformation of the surface layers. This effect will be compensated for, at least in part, by the similar preparation of deformed and undeformed specimens and will not give rise to significant error. It was also observed that etched and unetched specimens of the undeformed limestone gave almost the same integrated intensity in the (1014) line, suggesting that the undeformed material gives negligible extinction.

§ 3. X-RAY LINES STUDIED AND MEASURING PROCEDURE

A Norelco 'counting rate computer' was used with a Philips PW1010 stabilized x-ray set and Philips Geiger-counter diffractometer and circuit panel in order to step-scan and record the lines automatically. Except where stated, the following experimental conditions were used:

Copper K_α radiation, with nickel filter.
Take-off angle from x-ray target: approximately 2°.
Incident beam divergence: 1°.
Receiving slit: 0·1 mm (equivalent to 0·03° 2θ).
(0·05 mm for $10\bar{1}4$ line.)
Step-scanning interval: 0·01° 2θ in the x-ray line.
0·05° 2θ in the background.

The total count at each angular interval varied from 25 600 or 12 800 near the peak of the line to 3200 or 1600 in the background. The overall stability of the apparatus was found to be within ± 1% over 24 hours or more. The total scanning time for one line was usually between 12 and 24 hours.

Table 1 lists the x-ray lines studied and fig. 1 shows the relative orientations of the corresponding lattice planes. These lines were chosen because their intensity is sufficient for accurate measurement in reasonable time and their spacing is the most favourable for the intensity distribution to fall to background level between the lines.

Table 1. X-ray Lines Studied

X-ray line (Miller-Bravais X-ray indices)	Relative intensity (ASTM card)	Bragg angle (degrees θ)	sin θ	cos θ	cot θ
$10\bar{1}4$	100	14·71	0·254	0·967	3·81
$11\bar{2}0$	14	18·00	0·309	0·951	3·08
$11\bar{2}3$	18	19·72	0·337	0·941	2·79
$20\bar{2}2$	18	21·59	0·368	0·930	2·53

The measured intensities were corrected for losses due to the dead-time of the Geiger-counter (Klug and Alexander 1954), assuming the dead-time of 200 microseconds quoted by the manufacturers. The corrections never exceeded a few per cent. The background intensity was interpolated between measurements made on both sides of a line, assuming linear variation with angle; in most cases, the background intensity was almost equal on both sides of the line. The intensity distribution of the line was then obtained by subtracting the background from the corrected measured intensity values. The intensity distributions obtained in this way for the (11$\bar{2}$0) line are plotted in fig. 2.

Fig. 1

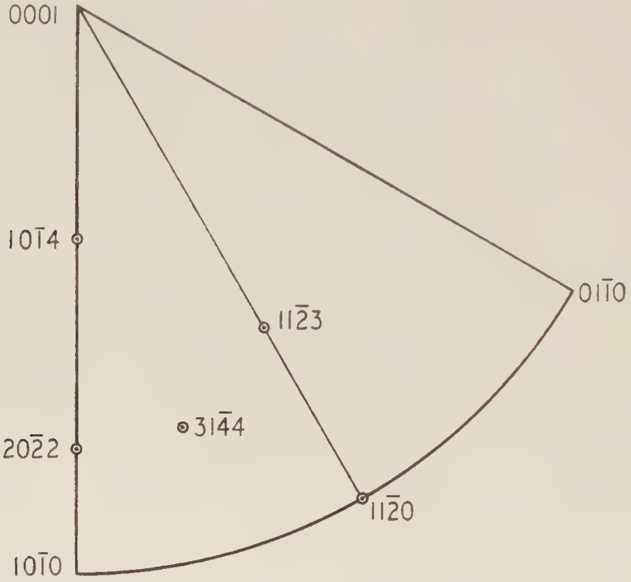

Fig. 2

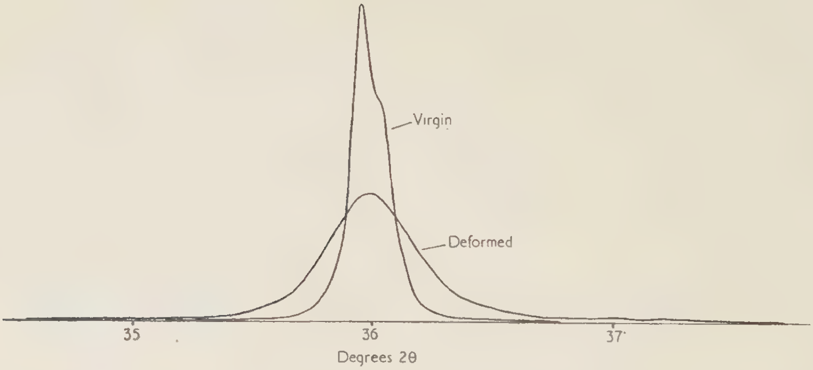

Stokes' (1948) Fourier method of correcting for the instrumental broadening was used. It has the advantage of giving the Fourier components of the lines directly. The line profile from the undeformed specimen was taken as the instrumental broadening, so that the derived true broadening can be attributed to the effects of plastic deformation. The relatively large instrumental broadening is unavoidable at such low Bragg angles but the accuracy of the measurements should be sufficient to give reliable values for the derived true broadening.

Lipson–Beevers 3° strips were used for the Fourier calculations. For optimum use of the strips, the 3° interval was taken to correspond to 0·05° 2θ on the X-ray line. This is equivalent to using an artificial lattice spacing of about 15 Å.

§ 4. Results

If the Stokes' correction procedure is carried through completely, the intensity distribution of the true line broadening resulting from plastic deformation is obtained. Figure 3 shows the result for the measurements on the (1120) line given in fig. 2. The broken curves in fig. 3 are plots of the Gauss and Cauchy functions, $(1/\beta)\exp(-\pi x^2/\beta^2)$ and $\beta/(\beta^2+\pi^2x^2)$, having the same integral breadth β as the intensity distribution derived from the measurements. It is seen that the true profile falls between these extremes. This conclusion also applies to the other lines studied.

Fig. 3

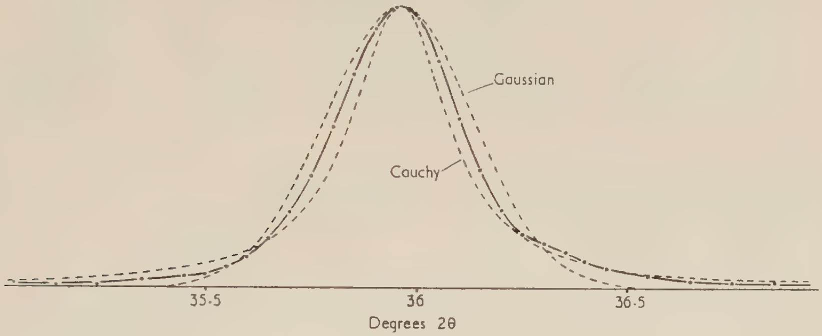

For the sake of further discussion, the method of Warren and Averbach (1950, 1955) is used for presenting the experimental results. If x is the angular displacement from a chosen zero, such as the peak of the X-ray reflection, the intensity distribution of the true line broadening can be written

$$f(x)=\frac{A_0}{2}+\sum_1^\infty (A_n\cos nx+B_n\sin nx).$$

If the broadening function is approximately symmetrical about the zero of x, the Fourier sine coefficients B_n will be small and the main character of the broadening will be represented by a plot of the cosine coefficients A_n versus n.

The values of A_n and B_n for the four X-ray lines of table 1, corrected for instrumental broadening, are given in figs. 4 (a) and 4 (b). The zero of x was chosen in each case at very nearly the peak of the line from virgin material and the same 2θ value was used as zero of x for the deformed material. It is seen that the coefficients B_n are fairly small compared with the A_n, so that a discussion of the broadening mainly in terms of the coefficient A_n is justified.

Fig. 4

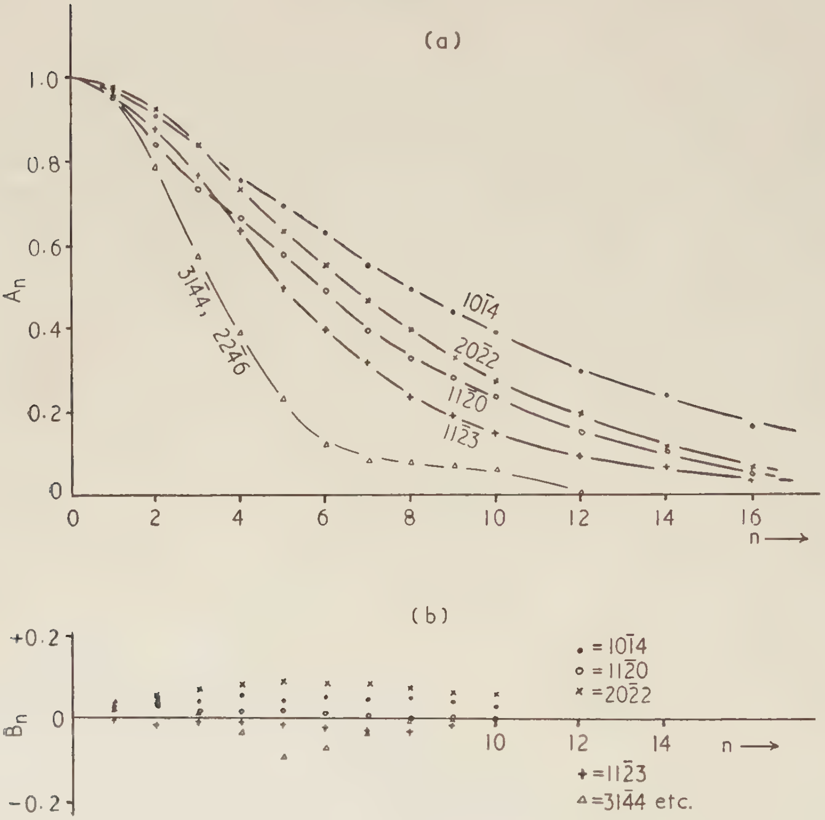

A series of measurements was also made on the (10$\bar{1}$4), (1123) and (2022) lines using molybdenum K_α radiation. Although in principle these give no new information, the results are plotted in figs. 5 (*a*) and 5 (*b*) for comparison with the results in figs. 4 (*a*) and 4 (*b*). They suggest that features such as the cross-over of the A_n versus n curves for (10$\bar{1}$4) and (20$\bar{2}$2) and the signs of the B_n terms are significant and not just the result of errors of measurement. When correction is made for the difference in Bragg angle, the molybdenum radiation results agree well with those for copper radiation.

The small B_n terms are probably due partly to shifts of the lines and partly to slight asymmetry. If a symmetrical line were displaced by an amount X (in units of x) to a higher Bragg angle, we should have

$$\tan nX = \frac{B_n}{A_n},$$

that is, a positive value of B_n would indicate a line shift to a higher Bragg angle. The observed B_n values can be largely accounted for by line shifts of approximately 0·01° 2θ to higher angles for $(10\bar{1}4)$ and $(11\bar{2}0)$, 0·01° 2θ to a lower angle for $(11\bar{2}3)$ and 0·02° 2θ to a higher angle for $(20\bar{2}2)$. There is, in addition, slight asymmetry in some of the lines, especially $(11\bar{2}3)$, but it is not certain whether this is outside the limits of experimental error.

Fig. 5

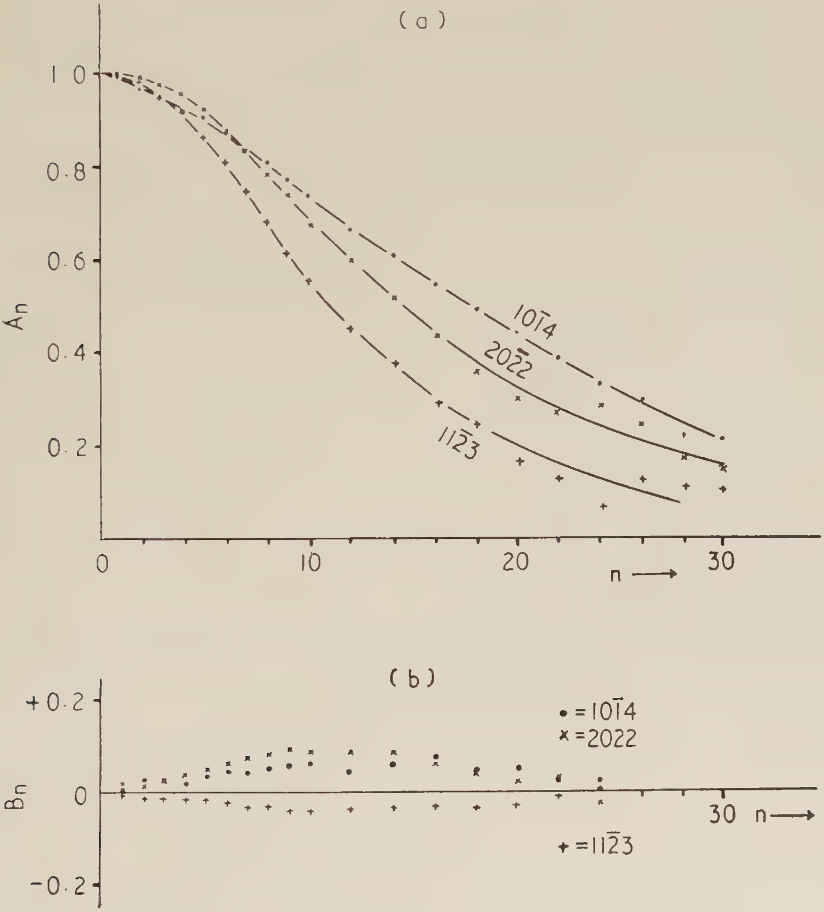

Since there was no check on the stability of the equipment over the whole series of measurements, no critical observations on intensities can be made. The integrated intensity does not appear to change by more than about 10% as a result of plastic deformation. This suggests that there is no little influence of extinction.

The apparent background intensity (that is, the minimum intensity between the lines) was not significantly changed as a result of deformation in the case of (1014) and (1120) lines. It increased by about 5% for the (1123) and (2022) lines. It is therefore possible that some of the extreme tails of these lines have become masked by the adjacent lines. However, no large error is indicated; these changes in background only amount to about $\frac{1}{2}$% of the peak height for the undeformed specimen.

§ 5. ANALYSIS OF RESULTS

X-ray line broadening may be due to several causes. In the case of plastically deformed materials, small particle size, internal strain and stacking faults are generally considered the most likely causes and the first step in analysing the observations is to attempt to decide which of these factors are important. Unfortunately, it is not possible to do this uniquely with the experimental information available but in this section it will be shown that an explanation of the broadening in terms of internal strains appears to fit the observations best.

In principle it should be possible to distinguish particle size broadening from internal strain broadening by analysis of the A_n versus n curve since its initial slope is a measure of the particle size (Warren and Averbach 1950). If stacking faults are present, they will also influence the initial slope, which may then be interpreted in terms of an 'apparent particle size' (Paterson 1952). However, in practice the errors in the measurement of the tails of the lines strongly influence the values of A_n near $n=0$ and values of apparent particle size deduced from the initial slope of the A_n curve are of doubtful reliability (Easterbrook and Wilson 1952). Inspection of the curves in fig. 4 (*a*) suggests that the average apparent particle size is not less than roughly 1000 Å.

We shall therefore resort to the earlier tests for particle size or internal strain broadening which use the integral breadths of the x-ray lines, quantities which are more reliably known. These tests are based on very simple models which may be considered as extreme cases (van Arkel 1925, Stokes *et al.* 1943, Smith and Stickley 1943).

The integral breadths of the lines can be obtained from the corrected line profiles (cf. fig. 3) or directly from the Fourier coefficients by the use of the formula:

$$\beta = \left(\frac{A_0}{2}\right) \Big/ \left(\frac{A_0}{2} + \sum_1^\infty (A_n \cos nX + B_n \sin nX)\right)$$

where X is the line shift discussed above. The values of the integral breadths, expressed in units of 2θ, are given in table 2.

If the line broadening is a simple small-size effect, the average particle size D should be given by $D = K\lambda/(\beta \cos\theta)$ where K is a constant of the order of unity and λ is the x-ray wavelength (James 1948). The value of K depends on the particle shape and the indices of the reflecting plane but in the absence of information on the particle shape we shall assume $K = 1$. The average particle sizes calculated from $\lambda/(\beta \cos\theta)$ are given in table 2. The variation from reflection to reflection could probably be explained in terms of a suitable particle shape, but the absolute values are much smaller than is consistent with the initial slopes of the A_n versus n curves (see above), in so far as these are reliable. That is, the smallest particle size consistent with the initial slope of the A_n versus n curve is still too large to explain most of the observed broadening.

Table 2. Integral Breadths and Equivalent Particle Sizes and Internal Strains

X-ray line	Integral breadth β (2θ) (radians)	Particle size $\lambda/(\beta \cos \theta)$ (Å)	Internal strain (integral breadth ξ)	Internal stress (integral breadth ξ/E_{hkil}) (dyne cm^{-2})
$10\bar{1}4$	0·0053	300	0·0100	94×10^{-8}
$11\bar{2}0$	0·0076	210	0·0117	104×10^{-8}
$11\bar{2}3$	0·0084	195	0·0117	92×10^{-8}
$20\bar{2}2$	0·0064	260	0·0081	104×10^{-8}
	Mean deviation:	16%	13%	5%

If the line broadening were due to internal strains which vary slowly enough through the crystals so that there is correlation of the phases of scattering from regions sufficiently large to eliminate small-size broadening, then the x-ray line profile should correspond to the distribution function of internal strains. If ξ is the integral breadth of this distribution function of internal strains, the line broadening will be $\beta(2\theta) = 2\xi \tan\theta$ if the internal strain is independent of crystallographic direction and $\beta(2\theta) = 2\xi \tan\theta/E_{hkil}$ if the internal stress is independent of crystallographic direction†; E_{hkil} is the Young's modulus in the direction normal to the reflecting plane. In the first case, the integral breadth ξ of the internal strain distribution deduced from the line broadening should be the same for all lines; in the second case, the quantity ξ/E_{hkil} should be the same for all lines. Both quantities are given in table 2, with the assumption that the line broadening is due entirely to internal strain. The values of

---

† The exact relation here will depend on the internal stress model (Blackman 1946) but this expression is the one usually assumed as a simple approximation for the effect of elastic anisotropy on line broadening (van Arkel 1925, Stokes *et al.* 1943, Smith and Stickley 1943).

E_{hkil} (table 3) were calculated from the elastic constants for calcite given by Hearmon (1946). It is seen that, while the model of isotropic internal strains does not fit the observations very well, the internal strain model fits quite well when suitable allowance is made for elastic anisotropy.

Table 3. Young's Modulus for Calcite (units of 10^{11} dyne cm^{-2})

$hkil$	$10\bar{1}4$	$11\bar{2}0$	$11\bar{2}3$	$10\bar{1}1$	$31\bar{4}4$
E_{hkil}	9·40	8·85	7·88	12·84	11·53

A more satisfactory way of distinguishing between the models of broadening is to measure different orders of reflections from the same crystallographic plane. However, the overlap of the broadened lines at the higher Bragg angles makes this procedure impracticable for calcite.

Fig. 6

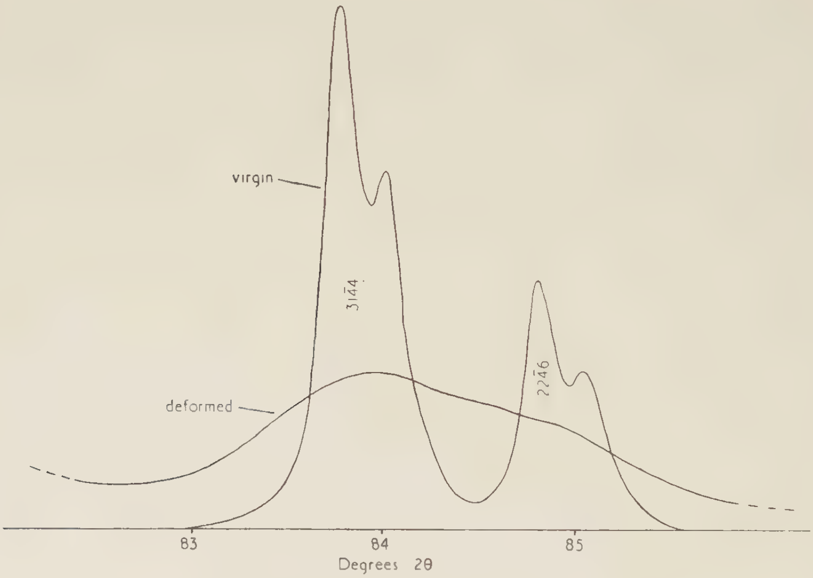

The best resolved higher order reflection from the planes studied above is (2246), but even this reflection becomes indistinguishably merged with the adjacent (3144) reflection after deformation (fig. 6) and a direct comparison with the first order ($11\bar{2}3$) reflection is not possible. However, it is interesting to consider the average broadening of the (2246) and ($31\bar{4}4$) reflections.

If the two lines of fig. 6 are treated as one in Stokes' correction for instrumental broadening, using the same 2θ value as zero for deformed and undeformed specimens, an average broadening function for the two lines will be obtained, the Fourier components of which are also plotted in fig. 4. The integral breadth β, calculated from the A_n coefficients, is 0·0118 radians 2θ (the neglect of line shifts may make this figure slightly too high). This corresponds to an apparent average particle size of 90 Å or to an internal strain breadth, ξ, of 0·0130. Comparison with the figures in table 2 again shows that the internal strain model is favoured rather than the particle size model, even when the high value of $E_{31\bar{4}4}$ is considered.

Summarizing, the following grounds may be given for preferring to attribute the line broadening mainly to internal strain rather than to small particle size :

(1) The initial slope of the A_n versus n curves (if reliable) indicate a particle size too large to explain the observed integral breadths.

(2) The variation of integral breadth with Bragg angle favours an internal strain model, especially if elastic anisotropy of the crystals is considered.

(3) Rosenthal and Kaufman's experiment (see § 1) suggests the presence of considerable internal strains.

However, some line broadening from small particle size cannot be excluded. It seems unlikely that stacking faults are important unless their nature is such as to give no appreciable line shifts (cf. body-centred cubic materials, Guentert and Warren 1958) and to give a small initial slope of the A_n versus n curves for a large integral breadth (which is unlikely).

§ 6. INTERNAL STRAINS

In this section an attempt will be made to calculate the r.m.s. value of the internal strains in deformed Solenhofen limestone on the assumption that the x-ray line broadening is due entirely to internal strains.

Warren and Averbach (1950) have shown that, for broadening due to internal strains,

$$A_n(l) = \int_0^\infty p_n(Z_n) \cos 2\pi l Z_n \, dZ_n. \quad . \quad . \quad . \quad . \quad (1)$$

Here $Z_n a_3$ is the relative displacement of two unit cells separated by a distance na_3 in the direction normal to the reflecting planes, the spacing of which is a_3, and l is the order of reflection. $p_n(Z_n)$ is the family of distribution functions of the Z_n, there being one distribution function for each value of n. In the absence of measurements on many orders of reflections from one plane, giving $A_n(l)$ as a function of l, the eqns. (1) cannot be solved for $p_n(Z_n)$ without making special assumptions about the form of $p_n(Z_n)$.

An attempt may be made to place limits on the r.m.s. internal strain by making the following alternative assumptions, in which it is implied that the form of $p_n(Z_n)$ is independent of n:

(1) $p_n(Z_n)$ of Gaussian form, assumed by Warren and Averbach (1950).

(2) $p_n(Z_n)$ of Cauchy form up to $|Z_n|/n=0{\cdot}2$ and zero for larger values of $|Z_n|$ (that is, cut off at the limit of Hooke's law in order to avoid an infinitely large value of the r.m.s. strain)—considered by Williamson and Smallman (1954).

In each case the r.m.s. value of Z_n can be obtained as a function of n by solving the eqns. (1) (Warren and Averbach 1950, Williamson and Smallman 1954). The results for the x-ray lines of table 2 are given in fig. 7, in which the actual r.m.s. displacements $\bar{Z}_n a_3$ are plotted against the distances na_3.

The initial slope of the $\bar{Z}_n a_3$ versus na_3 curve is a measure of the r.m.s. local strain in the specimen, but values deduced from the results in fig. 7 will be of doubtful accuracy because of the influence of tail errors. With this reservation, one may take 0·03 as an approximate value of the r.m.s. local internal strain which falls within the limits set by these two extreme cases.

Fig. 7

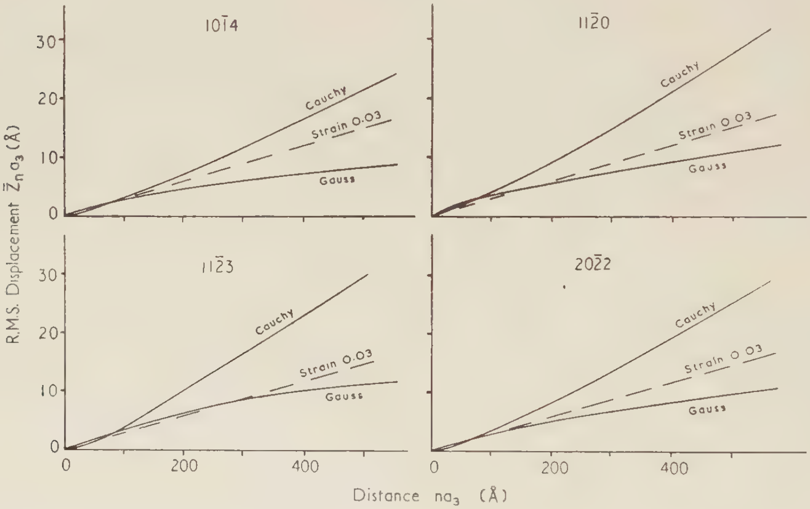

The shape of the $\bar{Z}_n a_3$ versus na_3 curve seems to depend rather sensitively on the form of the distribution functions $p_n(Z_n)$ and it is therefore not possible to deduce the average distance over which the strains are uniform, as was done by Warren and Averbach (1950). Williamson and Smallman (1954) have already pointed out this difficulty.

If it is assumed that in regions large enough to give no small-size broadening the r.m.s. value of the internal strain is independent of the distance over which the displacement is measured (this corresponds to $p_n(Z_n)=p_1(Z_n/n)$ or a linear plot of $\bar{Z}_n a_3$ versus na_3), the line profile itself will represent the form of the distribution function for internal strains (Stokes and Wilson 1944). Under this assumption, the r.m.s. internal strain can be calculated numerically from the measured line profiles, giving the values 0·0060, 0·0085, 0·0058 and 0·0043 for the lines $(10\bar{1}4)$, $(11\bar{2}0)$, $(11\bar{2}3)$ and $(20\bar{2}2)$ respectively, or an average value of 0·006. On the other hand, many workers have also assumed a particular form for the line profile and then calculated the r.m.s. internal strain from its integral breadth (Haworth 1937, Brindley and Ridley 1938, 1939, Williamson and Smallman 1954, Michell and Haig 1957). If this procedure is applied to the present results, the average r.m.s. internal strain is 0·004 for a Gaussian distribution and 0·02 for a Cauchy distribution, cut off at strain 0·2 (Williamson and Smallman 1954, Michell and Haig 1957).

The various estimates for the r.m.s. internal strain, assuming the line broadening to be entirely due to internal strain, are given in table 4. The value 0·006 is a lower limit since the assumption of small strain gradients is unlikely to be valid. The value 0·03 is probably an approximate upper limit, considerably dependent on tail errors.

Table 4. R.M.S. Internal Strains and Stored Energy
(assuming all broadening due to internal strains)

Method of estimating internal strain	Strain distribution function assumed	R.M.S. internal strain $(\overline{e^2})^{1/2}$	Stored energy (cal gm^{-1})
Initial slope of $\bar{Z}_n a_3$ vs. na_3 curve	Between Gaussian and cut-off Cauchy	0·03	12
Line profile, assuming small strain gradients	Observed line profile	0·006	0·5
	Cut-off Cauchy	0·02	5
	Gaussian	0·004	0·2
Total work done in plastic deformation of specimen: 9			

§ 7. Stored Energy

The stored energies corresponding to the r.m.s. internal strains, $(\overline{e^2})^{1/2}$, have been calculated using Stibitz's (1936) formula, $3E\overline{e^2}/2(1+2\nu^2)$, and are given in table 4. The value of E and ν were taken to be 10^{12} dyne cm^{-2} and $\frac{1}{3}$, respectively. This value of E is an average of the single crystal values and is about twice that usually quoted for polycrystalline material.

Thus if one assumes that the x-ray line broadening is entirely due to internal strains, the stored energy in the specimens is at least 0·5 cal g^{-1} and probably as high as 12 cal g^{-1}. The higher figure is to be preferred because of the better assumptions underlying it, although it is more sensitive to tail errors. It is also supported by a comparison with the results of Michell and Haig (1957) on highly deformed nickel; they found that the stored energy measured calorimetrically was about twice that calculated from the x-ray line broadening using the same procedure as was used to obtain the value of 5 cal g^{-1} in table 4 (except for a small allowance for small size broadening).

However, by calculation from the stress–strain curve, with an approximate correction for friction in the apparatus (see § 2), the total work done on the specimen during plastic deformation was approximately 9 cal g^{-1}. Within experimental error, this is equal to the value of the stored energy derived above.

So far no account has been taken of the possibility that a minor proportion of the broadening is a small-size effect. This would probably reduce the estimated value of the stored energy. If the broadening were entirely a small-size effect and one assumes 100 erg cm^{-2} as the order of the interfacial energy of the x-ray domains†, the stored energy would be of the order of 1 cal g^{-1}. This figure is probably an upper limit and 0·1 cal g^{-1} may be a better estimate. Thus, to a first approximation, that part of the line broadening which corresponds to a small size effect may be neglected in calculating the stored energy, thereby reducing the estimated value of the stored energy. If only about 70% of the line-broadening were due to internal strains (as is suggested by the initial slopes of the A_n versus n curves) the estimated value of the stored energy would be about one-half that obtained when the broadening is attributed entirely to internal strains.

The conclusion from the present work is therefore that an appreciable percentage (at least 10% and possibly one-half or more) of the energy expended in plastic deformation is stored in the calcite after 15% plastic strain. At first sight this suggests a relatively greater stored energy in deformed calcite than in deformed metals. Thus Clarebrough, Hargreaves and West (1955) found the fraction of energy stored in copper to be 2 to 6% after small plastic strains and 1 to 2% after large plastic strains. However, their minimum plastic strain was 40% and they found that the fraction of energy stored increases rapidly as the strain is decreased at small strains.

§ 8. Discussion

In comparison with the x-ray line broadening resulting from plastic deformation of metals, the broadening in calcite is relatively large. For example, the value of β for the $(20\bar{2}2)$ reflection of calcite is about twice that found by Michell and Haig (1957) for the (111) reflection of nickel filings at the same Bragg angle, in spite of the deformation of the calcite being slight compared with that of the nickel filings. However, this can be attributed, at least in part, to the high yield stress of calcite if the internal strain hypothesis is valid. Previous workers (Megaw and Stokes 1945, Warren and Averbach 1950, Paterson 1954) have noticed that the average absolute or r.m.s. internal strains calculated from the line broadening are similar in magnitude to the macroscopic yield strain. In calcite, the final yield stress of 10 000 kg cm^{-2} and Young's modulus of 10^6 kg cm^{-2} correspond to a strain of 0·01, which is rather less than the r.m.s. local internal strain obtained from the A_n versus n plot but is of the same order.

---

† There seems to be no information on interfacial or surface energies for calcite, so estimates have been made by the following reasoning. Comparison with other substances (see Herring 1953, Jacobs and Tompkins 1955, McLean 1957) suggests an order of magnitude of 1000 erg cm^{-2} for the surface energy of calcite. Further, it is known that in metals (McLean 1957) the grain-boundary energy is about one-third of the free surface energy and the energy of a coherent twin interface or simple low-angle boundary is often of the order of 10% of the grain boundary energy. The boundaries of the x-ray domains are likely to be mostly of a very low energy type, so that, by analogy with metals, their average interfacial energy is not likely to exceed 100 erg cm^{-2} in order of magnitude, and 10 erg cm^{-2} may be nearer the true value.

An anomalously large x-ray line broadening might have been expected from effects associated with incipient phase change, such as stacking faults, since the calcite phase of $CaCO_3$ is probably unstable under the pressure and temperature conditions applying during the deformation (Jamieson 1953, MacDonald 1956). Such effects have been observed in metals (for example, Hess and Barrett 1952). However, the initial slope of the A_n versus n plot does not suggest any appreciable amount of faulting.

REFERENCES

Arkel, A. E. van, 1925, *Physica*, **5,** 208.

Barrett, C. S., 1952, *Structures of Metals*, 2nd Ed., Chap. XVII (New York: McGraw-Hill Book Co. Inc.).

Birch, F. (Ed), 1950, *Handbook of Physical Constants* (Geological Society of America, Special Papers No. 36).

Blackman, N. M., 1946, *Phys. Rev.*, **70,** 698.

Brindley, G. W., and Ridley, P., 1938, *Proc. phys. Soc. Lond.*, **50,** 501; 1939, *Ibid.*, **51,** 432.

Clarebrough, L. M., Hargreaves, M. E., and West, G. W., 1955, *Proc. roy. Soc.* A, **232,** 252.

Easterbrook, J. N., and Wilson, A. J. C., 1952, *Proc. phys. Soc. Lond.* B, **65,** 67.

Guentert, O. J., and Warren, B. E., 1958, *J. appl. Phys.*, **29,** 40.

Haworth, F. E., 1937, *Phys. Rev.*, **52,** 613.

Hearmon, R. F. S., 1946, *Rev. mod. Phys.*, **18,** 409.

Herring, C., 1953, *Structures and Properties of Solid Surfaces*, Ed. R. Gomer and C. S. Smith, Chap. 1 (Chicago: University Press).

Hess, J. B., and Barrett, C. S., 1952, *Trans. Amer. Inst. min. (metall.) Engrs*, **194,** 645.

Jacobs, P. W. M., and Tompkins, F. C., 1955, *Chemistry of the Solid State*, Ed. W. E. Garner, Chap. 4. (London: Butterworths).

James, R. W., 1948, *The Optical Principles of the Diffraction of X-rays* (London: Bell), p. 528.

Jamieson, J. C., 1953, *J. chem. Phys.*, **21,** 1385.

Klug, H. P., and Alexander, L. E., 1954, *X-ray Diffraction Procedures* (New York: Wiley), p. 281.

MacDonald, G. J. F., 1956, *Amer. min.*, **41,** 744.

McLean, D., 1957, *Grain Boundaries in Metals*, Chap. III (Oxford : Clarendon Press).
Megaw, H. D., and Stokes, A. R., 1945, *J. Inst. Met.*, **71,** 279.
Michell, D., and Haig, F. D., 1957, *Phil. Mag.*, **2,** 15.
Paterson, M. S., 1952, *J. appl. Phys.*, **23,** 499 and 805 ; 1954, *Acta met.*, **2,** 823 ; 1958, *Bull. geol. Soc. Amer.*, **69,** 465.
Rosenthal, D., and Kaufman, M., 1952, *J. appl. Phys.*, **23,** 600.
Smith, C. S., and Stickly, E. E., 1943, *Phys. Rev.*, **64,** 191.
Stibitz, G. R., 1936, *Phys. Rev.*, **49,** 862.
Stokes, A. R., 1948, *Proc. phys. Soc. Lond.*, **61,** 382.
Stokes, A. R., Pascoe, K. J., and Lipson, H., 1943, *Nature, Lond.*, **151,** 137.
Stokes, A. R., and Wilson, A. J. C., 1944, *Proc. phys. Soc. Lond.*, **56,** 174.
Warren, B. E., 1955, *Acta cryst.* **8,** 483.
Warren, B. E., and Averbach, B. L., 1950, *J. appl. Phys.*, **21,** 595.
Warren, B. E., and Warekois, E. P., 1953, *J. appl. Phys.*, **24,** 951.
Williamson, G. K., and Smallman, R. E., 1954, *Acta cryst.*, **7,** 574.

The Detection of Dislocations by Low Temperature Heat Conductivity Measurements†

By Jenifer N. Lomer‡ and H. M. Rosenberg
The Clarendon Laboratory, Oxford

[Received November 1, 1958]

Abstract

The lattice heat conductivity of a specimen after straining is reduced by the dislocations produced by the deformation. A theory by Klemens enables the dislocation density to be calculated from the decrease in the lattice conductivity at liquid helium temperatures. In the present experiments copper–zinc single and polycrystals (7, 15 and 30% Zn) have been deformed by various amounts and the increase in the dislocation density has been determined by heat conductivity measurements. The results are shown to be in qualitative agreement with current theories of work hardening. In stage I of the stress/strain curve there is only a slight increase in dislocation density, but there is a rapid increase in stage II. Whereas in both these stages the dislocation density is independent of the zinc content, the onset of stage III is strongly dependent on it. During stage III there is very little increase in dislocation density. In stage I the dislocation density is proportional to the stress, whereas in stage II it is proportional to $(\text{stress})^2$. Transmission electron microscope experiments on some of the specimens show that the Klemens theory overestimates the dislocation density by a factor of about 6. Comparison of electrical resistivity data with the lattice thermal conductivity results gives further evidence for suggesting that the electrical resistivity is affected by stacking faults rather than by dislocations. Experiments on specimens taken at various stages during a fatigue test show that the dislocation density increases during the first two hundred fatigue cycles, but thereafter it remains constant.

§ 1. Introduction

The measurement of dislocation densities in a cold-worked metal is by no means simple, and no satisfactory general method has yet been developed. The density can be estimated from x-ray line broadening experiments, but this usually requires specimens in the form of filings and the x-ray micro-beam technique is not usually satisfactory for large deformations. The electron microscope can be used to detect dislocations but this necessitates specimens in the form of thin foils. Etch pits can also be used but it is very difficult and tedious to get the correct technique for etching a particular substance. In addition, for high dislocation densities it is difficult to resolve the individual etch pits. Indirect estimates of the dislocation densities may also be made from changes in the stored energy, density and electrical resistivity. All these methods are dependent on theoretical estimates for the effect of a single dislocation, and assume no interaction between the dislocations.

---

† Communicated by the Authors.
‡ Now at the Department of Physics, Reading University.

The present paper describes experiments on α-brass specimens, in which the multiplication of dislocations during deformation has been detected by measuring the change in the lattice heat conductivity at liquid helium temperatures. It is believed that this method gives a relative accuracy which is not surpassed by other techniques. The criticism that the absolute values depend on the theoretical value for the effect of a single dislocation, and therefore is not accurately known, applies to this method also, but an idea of the absolute accuracy was obtained by counting the dislocations directly from electron microscope pictures of thin foils prepared from specimens whose heat conductivity had previously been measured. Some experiments were also carried out on specimens at various stages during a fatigue test, to see how the dislocations multiply as the number of fatigue cycles is increased.

§ 2. THEORY

The thermal conductivity of a metal may be divided into two components, the electronic conductivity K_e and the lattice conductivity K_g. When a metal is strained, the lattice defects introduced cause scattering of the phonons and electrons, and hence the conductivity is reduced. In particular, the lattice conductivity is very sensitive to both the type and concentration of the defects, and the reduction in the helium range has been ascribed to dislocations. Measurements of the change in K_g at low temperatures therefore provide a method of determining dislocation densities.

Unfortunately in a pure metal most of the heat is transported by the electrons, rather than by the lattice vibrations (e.g. at 4°K in pure copper K_e is about 100 times greater than K_g) and it is difficult to measure K_g at all. One way of overcoming this difficulty is to use a superconductor at a temperature sufficiently below the superconducting transition temperature for all the heat to be carried by the lattice vibrations (Olsen and Renton 1952). Experiments have been made on the detection of damage on such specimens by measurements of the change in thermal conductivity (Mendelssohn and Montgomery 1956, Rowell 1958.) However, such investigations are limited to experiments on niobium and lead, unless one resorts to measurements below 1°K. An alternative method is to cause a reduction in K_e by the addition of impurities, until it is comparable with K_g, which is not much affected. This is because at low temperatures the dominant lattice vibrations are those of long wavelength which are not scattered by the impurity atoms. The scattering of the electrons by the impurity atoms on the other hand is the same at all temperatures and hence K_e is reduced even in the helium range. Hence in an alloy a large proportion of the heat transport will be by the lattice waves, and changes in K_g can be measured.

In order to separate K_g from the total heat conductivity K, we must consider the form of both K_e and K_g. No justification is given here for the temperature dependence of the various terms, the reader is referred to the review article by Klemens (1956 a) for details.

At low temperatures, for an alloy, K_e is limited by the scattering of electrons by the impurity atoms and is given by the relation:

$$K_e = AT \quad . \quad . \quad . \quad . \quad . \quad . \quad . \quad . \quad . \quad (1)$$

where the constant A is related to the residual resistance R_o by the relation:

$$A = L/R_o \quad . \quad . \quad . \quad . \quad . \quad . \quad . \quad . \quad . \quad (2)$$

where L is the Lorenz number.

Fig. 1

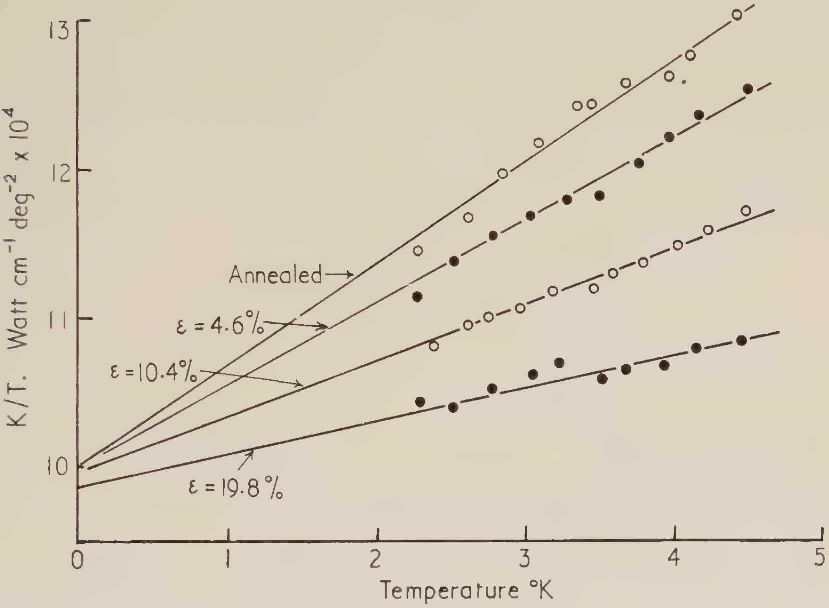

Typical curves of K/T against T for a specimen (Cu–Zn 15%) after various amounts of strain showing the decrease in slope due to the extra dislocation scattering.

The lattice heat conduction in the helium range in an annealed specimen is limited by the scattering of the lattice vibrations by the conduction electrons and by any dislocations which are present. Both these mechanisms give a conductivity of the form:

$$K_g = BT^2. \quad . \quad . \quad . \quad . \quad . \quad . \quad . \quad . \quad . \quad (3)$$

As the specimen is strained, dislocations are introduced, and the effective value of B will decrease. From the change in B, the number of dislocations which have been introduced can be calculated.

The scattering of phonons by dislocations has been calculated by Klemens (1955) and the appropriate thermal resistance W_D, is given by:

$$W_D T^2 = \frac{h^2 v}{70 k^3} \cdot N b^2$$

where b is the magnitude of the Burgers vector, N the number of dislocations per sq. cm, v the phonon velocity, h and k the Planck and Boltzmann constants, respectively. In a more general treatment of the problem, Klemens (1958) finds that the numerical constant 70 is reduced by a factor of 16, and the relation becomes:

$$W_D T^2 = \frac{h^2 v}{4{\cdot}5 k^3} \cdot N b^2.$$

Combining (1) and (3) we see that the total conductivity K, is

$$K = K_e + K_g = AT + BT^2. \qquad \text{. . . . . . (4)}$$

Thus a plot of K/T against T should give a straight line with a slope of B and an intercept on the K/T axis of A. This value of A can be checked using (2) if the residual electrical resistance is measured. A representative series of plots of K/T against T are shown in fig. 1 and it will be seen that good straight lines are obtained. In practice, the residual electrical resistivity was actually used as a definite point on the K/T axis.

§ 3. THE SPECIMENS

The alloys which were chosen for this work were a series of α-brasses containing 7, 15 and 30% zinc. Preliminary experiments showed that with 5% zinc about half of the total thermal conductivity was lattice conduction and hence for the alloys used in the present work, K_g (or the constant B in (3)) could be obtained quite accurately.

The specimens were made from Johnson Matthey spectrographically standardized metals. These were melted and shaken together in quartz tubes *in vacuo*. On cooling, the slugs of metal were swaged down to rods of 2·5 mm diameter. Some sections of the rod were used to make single crystals using the Bridgeman technique. These, together with the polycrystalline specimens, were homogenized just below the melting point in evacuated quartz tubes for about 40 hours. The single crystals were etched with a saturated solution of ferric chloride in hydrochloric acid, and their orientation was determined with an optical goniometer.

The overall length of each specimen was 4 cm. Two 24 S.W.G. copper wires were hard-soldered on to them about 2 cm apart to act as contacts both for the thermometers and for the electrical leads used in the determination of the residual resistance.

The specimens used in connection with the electron microscope examination were made from 0·025 cm brass strip, 1·5 cm wide and 4 cm long. Copper contacts were hard-soldered on as before.

For the fatigue experiments the specimens were 1·5 mm diameter wires which over a central section of about 1 cm had been turned down to 1 mm diameter. Copper contacts were again hard-soldered at either end of this narrow section, and the specimen was fatigued in compression/tension.

§ 4. THE EXPERIMENTS

Thermal conductivity measurements were taken in the range 2 to 5°K in an apparatus and manner very similar to that previously described (Rosenberg 1955). One end of the specimen was attached to the high-pressure chamber of a Simon expansion helium liquefier and the other end was heated electrically. The temperature gradient along the specimen was measured by two helium gas thermometers attached to the specimen contacts. In view of the fact that we were interested in measuring the small changes in conductivity produced by deformation, it was necessary to measure K as accurately as possible and so the heat input to the specimen was always arranged to be large enough for the temperature difference along the specimen to be measured to better then 1%. Although eqn. (4) was found to hold up to about 10°K, sufficient accuracy could be attained from measurements in the liquid helium range.

In all the alloys used the residual electrical resistance R_o was attained by 20°K. It was measured by immersing the specimen in a dewar of liquid hydrogen, passing a current through it and measuring the potential across the copper contacts with a galvanometer amplifier (MacDonald 1947, 1956). The room temperature resistivity, R_T, was also measured and this, together with R_o, was used to calculate the change in form factor after deformation, as is shown below.

Both the electrical and thermal conductivity of the annealed specimen were measured and then it was extended by about 1% at room temperature in a Hounsfield Tensometer. R_T and R_o were re-measured and a further thermal conductivity determination was made. These measurements were repeated after further deformation until the specimen broke. In some cases one-half of the broken specimen was drawn down through dies until the diameter had been reduced to about 0·75 mm, and further measurements were taken at various stages during the process.

From the conductivity measurements made after each deformation, plots of K/T against T were drawn and the value of B in eqn. (3) was determined. Whilst the form factor, F, of the annealed specimen had to be determined by direct measurement, the changes in F, due to the deformation and the value of the strain, ϵ, were calculated from R_T and R_o. Assuming Mattheissen's rule to hold, it can be shown quite easily that:

$$\frac{F_S}{F_A}=\frac{(R_T-R_o)_S}{(R_T-R_o)_A}$$

and

$$\epsilon=1-\sqrt{(F_S/F_A)}$$

where the subscripts A and S refer to the annealed and strained states respectively. This method was considered to be more accurate than direct measurement of the strain because the cross section of the specimen sometimes became uneven after deformation.

§ 5. The Results

The main results are shown in figs. 2 and 3, in which the dislocation density is plotted against the strain. It will be seen that for small to moderate deformations (fig. 2) all the experimental results fall onto two curves. The lower curve is for single crystal specimens oriented so that they would deform in single slip. The upper curve is for polycrystals

Fig. 2

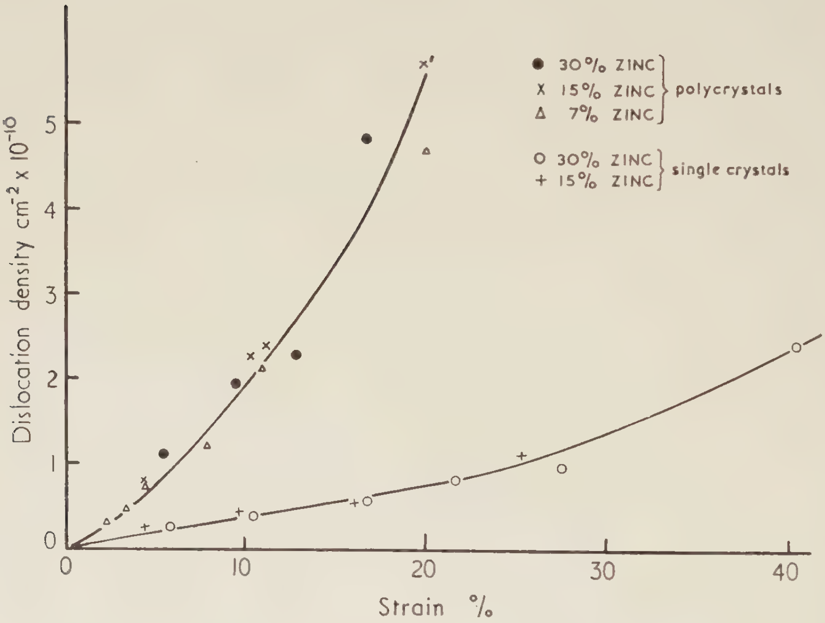

The dependence of the dislocation density on the strain for small and moderate strains. The lower curve was obtained for single crystals which deformed in single slip. It should be noted that there is little difference in behaviour between specimens of different zinc content.

which have deformed by multiple slip. It will be noted that the curves are the same, independent of the zinc content. For single slip, the dislocation density is proportional to $(\text{strain})^m$ where m is approximately 0·75. For multiple slip, m is about 1·2. For any given extension there are about five times more dislocations produced in multiple slip than in single slip.

Fig. 3

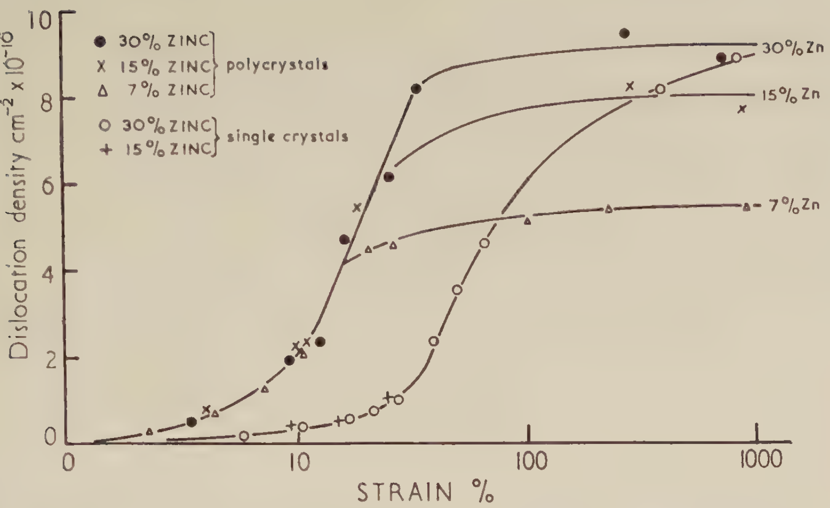

The dependence of the dislocation density on the strain for large strains. It should be noted that the dislocation density at which the curves flatten off is dependent on the zinc content.

Fig. 4

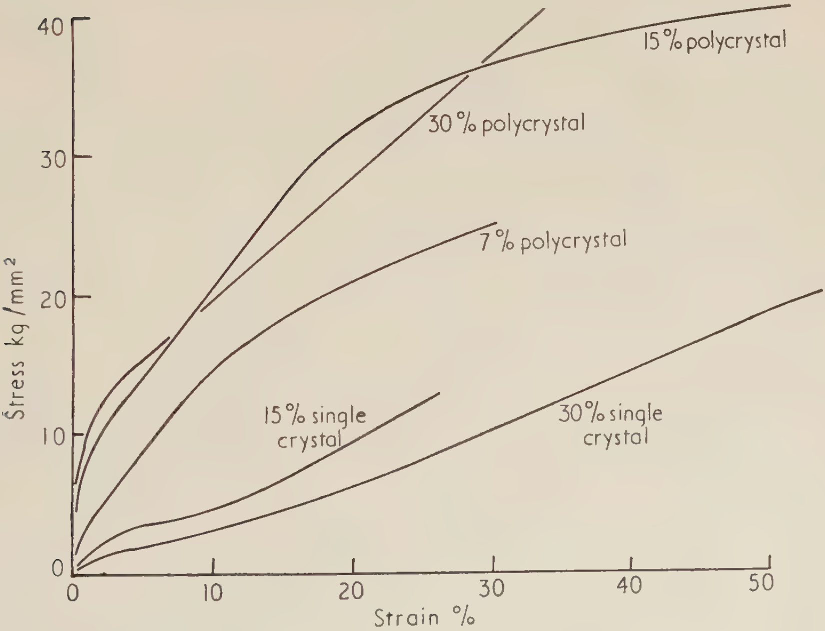

The stress/strain curves for the specimens used in this research.

For larger extensions, the number of dislocations tends to a constant value (fig. 3) and this ultimate value is dependent on the zinc content: the higher the proportion of zinc, the higher the ultimate dislocation density. The stress/strain curves for the specimens are shown in fig. 4.

A log–log plot of the dislocation density against the stress is shown in fig. 5. It will be noted that in this type of plot the points from specimens of different zinc content do not fall on a single curve. The graphs show that N is proportional to (stress)^p, where p is approximately unity for single slip and is equal to 2 for multiple slip.

Fig. 5

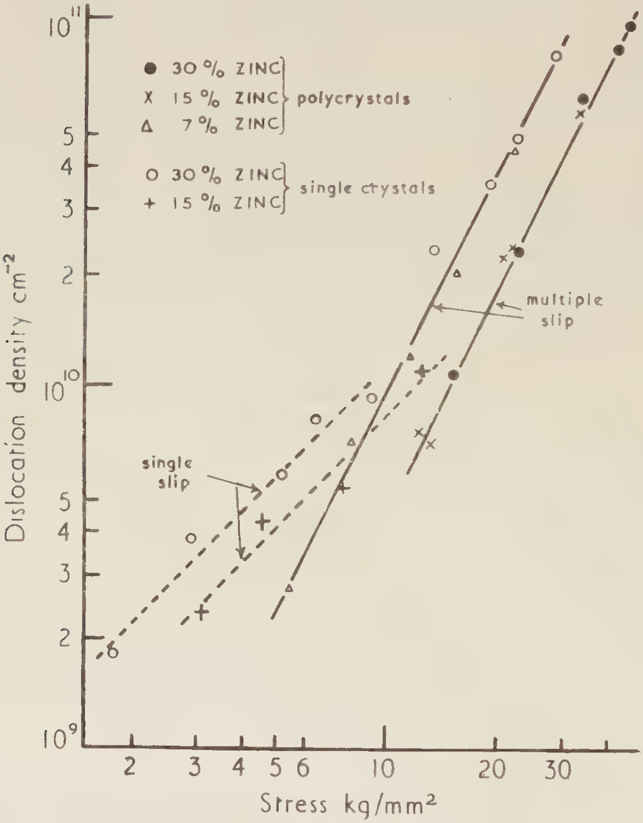

The dependence of the dislocation density on the yield stress. For single slip (dashed lines) the dislocation density is approximately proportional to the stress, whereas for multiple slip it is proportional to (stress)^2.

Whilst the theory of Klemens gave a basis on which to calculate the dislocation density, there was considerable doubt as to whether it was quantitatively correct. In order to check this, it was necessary to measure the dislocation density of a strained specimen both by the heat conductivity and by an independent method. The only independent method which seemed to be satisfactory was that developed by Hirsch *et al.* (1956) in which thin foils are examined by transmission in the electron microscope. When this is done the dislocations show up as dark lines on the screen and their density can be measured directly. Two 30% zinc specimens were made in the form of thin strip and their conductivities were measured after annealing. They were then deformed by 16·5% and 9·3% and were re-measured. The dislocation densities were calculated in the usual way from the decrease in conductivity. The specimens were then electro-polished until portions of them were about 1000 Å thick and these were examined in the electron microscope. From the resulting pictures the dislocation densities of the two specimens were calculated. The values obtained by this method are of course not necessarily those relating to the specimen as a whole because only a limited number of pictures and counts can be taken and each picture only covers a very small portion of the specimen. Nevertheless, the counts should give a fair idea of the number of dislocations present even if they are not strictly representative of the entire specimen. The ratio of the dislocation densities for the two specimens was 1 : 2·4 from heat conduction measurements and 1 : 1·6 from the electron microscope counts. In view of the small number of pictures taken this must be considered quite satisfactory agreement. It was found that the heat conduction measurements gave a value of the dislocation densities which was about six times greater than that obtained by direct counts. Hence, whilst the dislocation densities from the heat conduction experiments have been calculated using Klemens' theory, the numerical values have all been reduced by a factor of six.

§ 6. DISCUSSION

6.1. *The Absolute Magnitude of the Dislocation Density*

The fact that the dislocation density, N as calculated from Klemens' theory is greater than that determined from the electron microscope examination is confirmed by other experiments in which N from the heat conduction data was compared with determinations by other independent methods. Sproull *et al.* (1958) measured the change in the heat conductivity of compressed lithium fluoride crystals and determined N by etch pit counts. They found that the heat conductivity gave a value of N which was about 70 times the etch pit value. Kemp *et al.* (1958) report that the values of N from stored energy and density changes are less than those from heat conductivity measurements by factors of 5·5 and 2 respectively. In the light of these experiments and our results from the electron microscope investigation (in which the dislocations can be counted directly) it seems fairly definite that heat conductivity measurements overestimate the value of N by a factor of about 6.

It has been suggested (Klemens 1956 a) that one reason why N might be overestimated by heat conduction measurements is that if the dislocations occurred in pile-ups of n dislocations each, then the phonon scattering would be increased by a factor of n, due to the overlap of the strain fields. This does not seem to be very likely, because our measurements were taken when there was no external stress in the specimens and hence the pile-ups might relax. Thus individual dislocations would not be as close together as they were during the actual deformation. In addition, close pile-ups are not seen in the electron microscope pictures.

6.2. *Comparison with the Theory of Work-hardening*

The present experiments and earlier work (in which the dislocation density, as calculated by heat conductivity changes, was shown to vary in the same way as did the yield stress (Lomer and Rosenberg 1957)), show that heat conduction experiments do give a method of detecting the relative changes of dislocation density with some degree of accuracy. In addition to this, the electron microscope measurements enable us to have a fair idea of the absolute values involved. We should therefore like to give a short discussion on the interpretation of the data presented in figs. 2 and 3 in the light of present-day ideas of the deformation and work-hardening of metals.

Fig. 6

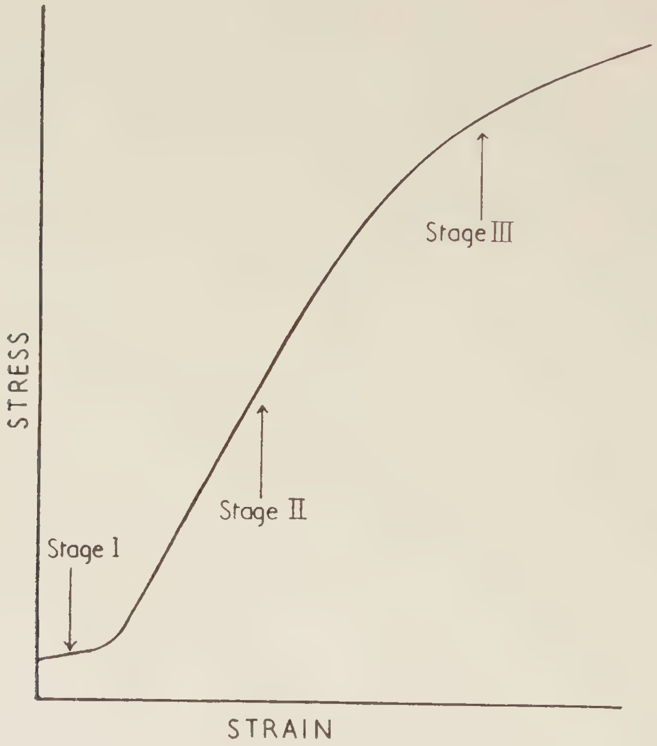

A typical stress/strain curve for a single crystal, showing the three stages of deformation.

A typical stress–strain curve of a metal is shown in fig. 6. It can be divided into three main sections which are usually called stages I, II and III. Stage I is the region of easy glide, in which very little hardening takes place. It occurs in single crystals which are so oriented that only one glide system operates. Stage II is the region of rapid work-hardening where the stress/strain curve is linear. Stage III begins where this curve bends over to a parabolic form. The interpretation of the various stages is now reasonably well understood and the various mechanisms have been reviewed in detail by Seeger (1957 a). During stage I slip occurs on only one set of planes. There are few obstacles and so each dislocation can travel an appreciable distance before it is stopped. Hence, for a given strain, relatively few dislocations will have to be formed. Towards the end of stage I some slip and hence dislocation multiplication occurs on other planes, and some of these dislocations will combine with those on the first glide plane to form Cottrell–Lomer sessile dislocations (Lomer 1951). These act as obstacles to the dislocations in the primary plane which form pile-ups behind the sessile dislocations. As deformation proceeds more obstacles are formed and the number of pile-ups increases. Thus the distances through which the dislocations move are continuously reduced and hence more dislocations have to be formed to enable deformation to proceed. This is the region known as stage II and Seeger *et al.* (1957) have shown that a scheme such as that just described leads to a linear stress/strain curve. In polycrystals where, due to the constraints on the crystallites, single slip (i.e. stage I) cannot occur, the stress/strain curve would be expected to start off in stage II. This has been confirmed by Feltham and Meakin (1957) in experiments on polycrystalline copper. In alloys of the α-brass series, where the zinc atoms fit quite well into the crystal lattice, and hence are unlikely to act as barriers to dislocation movement, there would seem to be no reason for the multiplication of dislocations in stage II to be dependent on the zinc content.

In stage III, the parabolic section of the stress/strain curve, deformation proceeds by cross slip of screw dislocations at the head of the pile-ups onto planes which are free of obstacles. For this to occur, these dislocations, which are usually extended dislocations, must have sufficient stress applied to them so that the two partials are united to form a proper dislocation again. The stress which is required will depend on the separation of the partials (i.e. on the stacking fault energy). The lower the stacking fault energy, the greater the separation of the partials and hence the higher the stress required to reform a proper dislocation. Now the stacking fault energy decreases very considerably as zinc is added to copper (Warren and Warekois 1955, Smallman and Westmacott 1957). This means the higher the zinc content, the greater will be the stress required for cross slip to occur ; i.e. as the amount of zinc is increased, stage III will set in at a higher stress. Once we are in stage III, slip can again occur on planes which are free of obstacles and hence in order to continue the extension little or no increase in the number of dislocations is necessary.

The experimental results shown in figs. 2 and 3 follow the behaviour predicted by the mechanisms of work hardening which have been described in the preceding paragraphs. The lower curve in fig. 2 which is for stage I in single crystals shows that very little dislocation multiplication is necessary to enable extension to proceed. The upper curve which corresponds to the linear region of the stress/strain curves, of several polycrystals, shows that the dislocations are multiplying very considerably throughout the deformation. It will also be noted that for any given extension the dislocation density is independent of the zinc concentration, within the experimental error, which is also in accord with the conclusions drawn in the preceding section.

As the deformation proceeds, we enter stage III. This is shown in fig. 3. This is the region where cross slip can occur onto neighbouring planes and little further dislocation multiplication should arise. This is precisely what is observed. The actual point at which stage III begins depends on the zinc concentration, the higher the zinc content the greater is the extension before stage III is able to begin. Due to the form of the stress/strain curves this implies that stage III begins at a higher stress for specimens containing more zinc. This is also in agreement with the theoretical predictions.

The fact that the dislocation density in stage III tends to a constant value does not mean that it is impossible to introduce more dislocations into a specimen. This can be done with other types of deformation. For example, Clareborough *et al.* (1957) have shown by stored energy measurements that N for copper compressed by 70% is $1{\cdot}3\times10^{11}$ cm^{-2}, and Kemp *et al.* (1958) report similar work on Cu—30% Zn deformed in torsion in which N was 4×10^{11} cm^{-2}. Smallman and Westmacott (1957) quote values of 3×10^{11} and 1×10^{12} cm^{-2} for filings of copper and copper-27% zinc respectively. The fact that more dislocations can apparently be introduced by compression and torsion suggests that in these methods of deformation, cross slip might be inhibited and that the type of work hardening corresponding to that observed in stage III of a tensile experiment might not occur.

In spite of the good qualitative agreement between our results and the theory of work hardening which has been described, there is at the moment no adequate theory which gives the actual numbers of dislocations which might be expected after given deformations in the various stages. Van Bueren (1955) proposed a theory of cold work in which the over-riding work-hardening process is the formation of vacancies by the non-conservation movement of jogs in screw dislocations. This is not the same mechanism as that considered above. From his theory, however, it is possible to calculate the ratio of the number of dislocations formed in multiple and single slip after a given extension. This it is felt will depend on the geometry of the slip planes rather than on the precise method of work hardening. From van Bueren's theory the ratio of dislocations in multiple and single slip comes out to be 4 for a strain of 0·1. This compares quite well with the ratio of 5 from our experiments. It is interesting to note that for single slip van Bueren's theory gives the dislocation density as proportional to $(\text{strain})^{3/4}$ which is the same dependence as found in our experiments. For multiple slip, however, he predicts a strict proportionality to the strain, whereas we found a $(\text{strain})^{1/2}$ dependence. For the 30% zinc single crystal in stage II N is also proportional to a power of the strain slightly larger than unity, where in this case the strain is the total strain minus the strain produced in stage I. It should be noted that Clareborough *et al.* (1957) found that N is approximately proportional to the strain in their compressed specimens.

Figure 5 shows that in stage I the dislocation density, N, is proportional to the applied stress. This is the dependence one would expect if the dislocations were held up at a fixed number of barriers and the distance each dislocation moved was independent of the stress. In stage II N is proportional to $(\text{stress})^2$. This is in agreement with the theory developed by Seeger *et al.* (1957) and similar results have been determined from electrical resistivity measurements by Blewitt *et al.* (1955).

6.3. *The Effect of Dislocations on the Electrical Resistivity: Stacking Faults*

Several theories have been proposed which estimate the effect of the scattering of electrons by dislocations and the consequent increase in the electrical resistivity. Hunter and Nabarro (1953) neglected the core of the dislocation and calculated the effect of the scattering by the strain field, but Harrison (1958) has shown that the scattering by the core is probably more important than that of the strain field. Nevertheless, whatever value is taken for the resistivity per unit length of dislocation line, the dislocation densities of cold-worked metals come out to be much higher than other experiments suggest. To account for the large increases in resistivity Broom (1952) and later Klemens (1956 b), Seeger (1956) and Ziman (1958) suggested that if the dislocations dissociate into partials, the regions of stacking fault between the partials will contribute much more to the resistivity than do the actual dislocations themselves. Alloys which have a high stacking fault probability show much larger resistivity changes on deformation than do those with a low stacking fault probability. (E.g. compare the work of Smallman and Westmacott (1957) with the electrical resistance measurements of Crampton *et al.* (1941).) The present experiments provide more evidence for the high resistivity of stacking faults.

Figure 7 shows the variation of the ratio N_E/N_T with zinc content, where N_E and N_T are the dislocation densities as determined by electrical resistivity and lattice thermal conductivity respectively, at the same point on the stress/strain curve. For this plot the value given by Harrison (1958) of 5×10^{-14} ohm per cm of dislocation has been used to calculate N_E. It will be noted that this ratio is not constant as it would be if there was merely an error in the estimate of the scattering cross section of a dislocation for either N_E or N_T. At 30% zinc the ratio increases very markedly. This is the concentration where the stacking fault probability becomes high and this is shown by the increase in N_E as compared with N_T. N_T will not be affected because the wavelength of the phonons at low temperatures is too long for them to be scattered by stacking faults. It will be noted that for zero zinc content $N_E/N_T = 12$ which suggests that 11/12 of the resistivity might be ascribed to stacking faults. Seeger (1957 b) considers that 39/40 of the resistivity is due to stacking faults In view of the uncertainties in the estimates of the dislocation densities this would not appear to be a very serious disagreement. Our results also show that N_E/N_T for 30% zinc is about 10 times greater than the extrapolated value of the ratio for zero content. This compares quite well with the increase by a factor of 8 in the stacking fault probability between pure copper and

Fig. 7

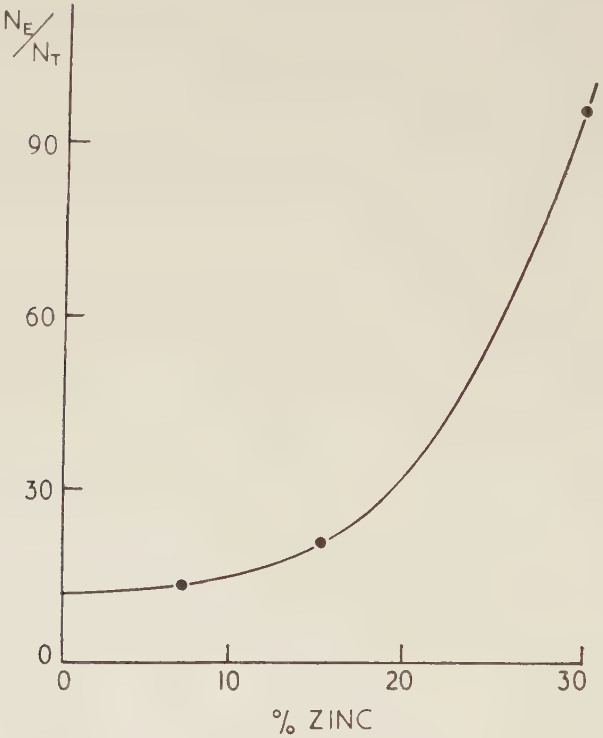

The ratio of the dislocation density, as calculated from electrical resistivity measurements, to that calculated from thermal conductivity experiments, plotted against the zinc content. It is suggested that the sharp rise in the ratio at higher zinc concentrations is due to the fact that the electrical resistivity is affected by stacking faults rather than by the dislocations.

copper–30% zinc as found by Smallman and Westmacott (1957). Similar agreement between the relative increase in the electrical resistivity on deformation and the stacking fault probability has been obtained by Christian and Spreadborough (1956).

6.4. *The Increase in Dislocation Density during Fatigue*

As a metal is fatigued a progressive hardening of the specimen occurs during the first 10^3 cycles of the test. There is considerable evidence (Broom and Ham 1957, McCammon and Rosenberg 1956) that this hardening is of a different nature from that produced during ordinary tensile deformation. The fatigue hardening is accompanied by an increase in the electrical resistivity during a similar period (possibly up to 10^4 cycles). This increase in resistivity is between five and ten times greater than that which occurs if the specimen is deformed in tension to the same stress level. The effect is very similar whether the fatigue and tensile deformations are made at 20°K or at room temperature. At one time it was thought that the extra electrical resistivity observed in fatigued specimens was due to the presence of point defects. If, however, the deformations are carried out at 20°K and the specimens are warmed up to room temperature very similar proportions of resistivity anneal out for both types of deformation, i.e. the large extra resistivity in the fatigued specimen remains and it does not anneal out even by 200°C. This makes it

Fig. 8

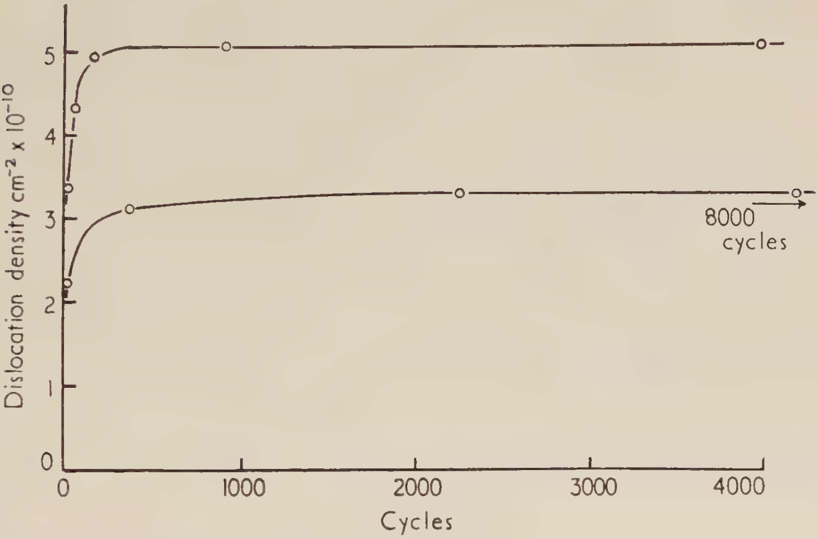

The change in the dislocation density as copper–zinc specimens are fatigued. It will be noted that the dislocations multiply during the first few hundred cycles but thereafter their number remains constant. The two curves refer to two different fatigue loadings.

highly unlikely that it can be due to point defects. One other possibility was that the extra resistivity in the fatigued specimens might be due to dislocations.

For this reason heat conduction experiments were made at intervals during a room temperature fatigue test on two specimens which were fatigued at different loadings. The build-up of the dislocations during the tests is shown in fig. 8. Two main points should be noted. The dislocation density builds up rapidly during the first 100 cycles and by about 200 cycles it has reached a saturation value. This saturation value is very similar to that which is obtained if the specimen is deformed in tension to the same stress level. Thus the increase in resistivity cannot be ascribed to extra dislocations. It is possible that the extra electrical resistivity might be due to regions of stacking faults which are formed during fatigue (MacCrone 1958).

SUMMARY

The experiments show that the measurement of the low temperature lattice heat conductivity can be a useful tool in detecting relative changes in dislocation density after deformation, particularly since it is not affected by the presence of stacking faults. Whilst it seems that the theory as it stands at present underestimates the scattering cross section of a dislocation for phonons, a good idea of the absolute values involved can be obtained by scaling down the calculated results by a factor of about 6. The experiments confirm the main hypotheses put forward to explain the three stages of a stress/strain curve. They also show that stacking faults contribute much more to changes in the electrical resistivity than do dislocations themselves. Experiments on fatigued specimens show that the build-up of dislocations during fatigue occurs during the first two hundred cycles and they cannot contribute materially to the extra electrical resistivity observed in fatigued specimens.

ACKNOWLEDGMENTS

We are most grateful to Dr. P. B. Hirsch and Mr. P. Partridge who carried out the electron microscope examination for us. We should also like to thank Dr. T. Broom and Dr. J. D. Campbell for help and advice in preparing and deforming the specimens, and Dr. D. Hull, Dr. P. G. Klemens, Dr. W. M. Lomer, Mr. R. K. MacCrone, Dr. A. Seeger and Dr. H. G. van Bueren for most useful consultation.

REFERENCES

BLEWITT, T. H., COLTMAN, R. R., and REDMAN, J. K., 1955, *Rep. on Conf. on Defects in Solids* (London : Physical Society), p. 369.
BROOM, T., 1952, *Proc. phys. Soc. Lond.* B, **65,** 871.
BROOM, T., and HAM, R. K., 1957, *Proc. roy. Soc.* A, **242,** 166.
CHRISTIAN, J. W., and SPREADBOROUGH, J., 1956, *Phil. Mag.*, **1,** 1069.

CLAREBOROUGH, L. M., HARGREAVES, M. E., and WEST, G. W., 1957, *Acta Met.*, **5,** 738.

CRAMPTON, D. K., BURGHOFF, H. L., and STACY, J. T., 1941, *Trans. Amer. Inst. min.* (*metal.*) *Engrs*, **143,** 228.

FELTHAM, P., and MEAKIN, J. D., 1957, *Phil. Mag.*, **2,** 105, 1237.

HARRISON, W. A., 1958, *J. Phys. Chem. Solids*, **5,** 44.

HIRSCH, P. B., HORNE, R. W., and WHELAN, M. J., 1956, *Phil. Mag.*, **1,** 677.

HUNTER, S. C., and NABARRO, F. R. N., 1953, *Proc. roy. Soc.* A, **220,** 542.

KEMP, W. R. G., KLEMENS, P. G., and TAINSH, R. J., 1958, *Proc. Kamerlingh Onnes Conf., Physica*, **24,** 170.

KLEMENS, P. G., 1955, *Proc. phys. Soc. Lond.* A, **68,** 1113 ; 1956 a, *Handbuch der Physik*, **14** (Berlin : Springer-Verlag) ; 1956 b, *Canad. J. Phys.*, **34,** 1212 ; 1958, *Prog. in Solid State Physics*, **7,** 1.

LOMER, J. N., and ROSENBERG, H. M., 1957, *Proc. 5th Int. Conf. on Low Temp. Phys. and Chem.*, (Madison, Wis.), p. 394.

LOMER, W. M., 1951, *Phil. Mag.*, **42,** 1327.

MACCRONE, R. K., 1958, private communication.

MACDONALD, D. K. C., 1947, *J. sci. Instrum.*, **24,** 232 ; 1956, *Handbuch der Physik*, **14** (Berlin : Springer-Verlag).

MCCAMMON, R. D., and ROSENBERG, H. M., 1956, *Phil. Mag.*, **1,** 964.

MENDELSSOHN, K., and MONTGOMERY, H., 1956, *Phil. Mag.*, **1,** 718.

OLSEN, J. L., and RENTON, C. A., 1952, *Phil. Mag.*, **43,** 946.

ROSENBERG, H. M., 1955, *Phil. Trans.* A, **247,** 441.

ROWELL, P., 1958, *D.Phil. Thesis, Oxford University.*

SEEGER, A., 1956, *Canad. J. Phys.*, **34,** 1219 ; 1957 a, *Dislocations and Mechanical Properties of Crystals* (John Wiley), p. 243 ; 1957 b, *Ibid.*, p. 347.

SEEGER, A., DIEHL, J., MADER, S., and REBSTOCK, H., 1957, *Phil. Mag.*, **2,** 323.

SMALLMAN, R. E., and WESTMACOTT, K. H., 1957, *Phil. Mag.*, **2,** 669.

SPROULL, R. L., MOSS, M., and WEINSTOCK, H., 1958, *Bull. Amer. phys. Soc.*, **3,** 126. 127.

VAN BUEREN, H. G., 1955, *Acta Met.*, **3,** 519.

WARREN, B. E., and WAREKOIS, E. P., 1955, *Acta Met.*, **3,** 473.

ZIMAN, J. M., 1958, *Nuovo Cim.*, **7,** Suppl. No. 2, 353.

Nuclear Magnetic Resonance in Silver-Cadmium†

By L. E. Drain
Metallurgy Division, A.E.R.E., Harwell

[Received October 28, 1958]

Abstract

Nuclear magnetic resonance shifts and line widths have been measured in alloys of silver and cadmium at 300°K in a field of 4200 gauss. The resonances of ^{109}Ag and ^{107}Ag nuclei were observed in the α and β phases and those of ^{113}Cd and ^{111}Cd nuclei in all the room temperature phases. In primary solutions of cadmium in silver, the Knight shifts of all the resonances decrease linearly as the cadmium content increases, the total variation being about 14% of their values at the centre of the phase range. It is shown that in a disordered alloy a contribution to nuclear magnetic resonance line width can arise from the variations of the shifts of nuclei with their immediate surroundings. The results suggest that in α silver–cadmium alloys, the influence of the cadmium atoms on the shift of silver nuclei is confined to nearest and next nearest neighbours. Line widths in the β phase suggest an ordered structure. The relation of nuclear magnetic resonance shifts to the density of states at the Fermi surface is discussed and a calculation of the variation of this quantity with composition made from the Knight shift results. The result is compared with other experimental and theoretical evidence.

§1. Introduction

Since Knight's (1949) discovery of the shift of nuclear magnetic resonance frequencies in metals compared with non-metals, measurements have been made on a considerable number of pure metals and on some alloys. The shift is due to the fact that the conduction electrons are polarized by a magnetic field, H, and so give rise to a subsidiary field, ΔH, which enhances the applied field at the nuclei. The frequency of magnetic resonance is thus higher for a nucleus in a metal than in an insulator in the same external field.

Townes *et al.* (1950) have derived an expression for the shift which may be written

$$\frac{\Delta\nu}{\nu}=\frac{\Delta H}{H}=\frac{8\pi}{3}\chi_p\overline{|\psi(0)|^2}=\frac{8\pi}{3}\mu^2N(\xi)\overline{|\psi(0)|^2} \quad . \quad . \quad (1)$$

where ν and $\nu+\Delta\nu$ are the frequencies of resonance in the non-metal and metal respectively. χ_p is the Pauli spin paramagnetic susceptibility of the electrons per gram atom and $\psi(0)$ is the value at the nucleus of the wave function for an electron of the Fermi energy, ξ. The average of the square modulus of this quantity is taken over the Fermi surface. The wave functions are assumed to be normalized over a gram atom of material‡.

---

† Communicated by the Author.

‡ In pure metals it is convenient to normalize over an atomic volume but in alloys this is not as useful, since the wave functions are not the same for each atom.

Neglecting the effect of electron exchange and correlation, χ_p may be written as $\mu^2 N(\xi)$ where μ is the Bohr magneton and $N(\xi)$ is the density of states (per gram atom) at the Fermi surface.

The behaviour of $N(\xi)$ on alloying is of great interest in the theory of metals. When the addition of an alloying element to a metal changes the average number of conduction electrons per atom, the number of electrons in the conduction band varies with composition. If it is assumed that the form of the conduction band is not significantly changed by alloying, the variation of $N(\xi)$ with composition is directly related to the form of the band. Nuclear magnetic resonance provides a method of investigating changes in $N(\xi)$ for the Knight shift is directly related to this quantity by eqn. (1). However, the interpretation of changes in the shift is complicated by our lack of knowledge about the behaviour of the factor $\overline{|\psi(0)|^2}$.

The choice of alloys on which measurements can be made over an extensive composition range is limited to those whose components have isotopes with nuclear spin $\frac{1}{2}$. With higher spins there is the possibility of the interaction of nuclear electric quadrupole moments with crystalline electric fields. This interaction occurs when the surroundings of the nuclei do not have cubic symmetry and can produce a broadening of the magnetic resonance so large that the resonance becomes unobservable in all except moderately dilute alloys. Thus Bloembergen and Rowland (1953) found that at ordinary temperatures, the ^{63}Cu magnetic resonance from brass became unobservable for zinc contents in excess of 20%.

Table 1. Magnetic Isotopes of Silver and Cadmium

Nucleus	Spin	Magnetic moment nuclear magnetons	Natural abundance	Resonance frequency in field of 4200 gauss
^{107}Ag	$\frac{1}{2}$	−0·1130	51·35%	723 Kc/s
^{109}Ag	$\frac{1}{2}$	−0·1299	48·65%	833 Kc/s
^{111}Cd	$\frac{1}{2}$	−0·5922	12·86%	3·80 Mc/s
^{113}Cd	$\frac{1}{2}$	−0·6195	12·34%	3·97 Mc/s

From the alloys free of this difficulty, the silver–cadmium system was chosen for examination because of the comparatively large amount of physical information available on alloys of this type, particularly on the structurally analogous copper–zinc system. The nuclear moments of the magnetic isotopes of silver and cadmium are given in table 1. They are small and the observation of the resonances, especially those of silver, is rather difficult.

§ 2. Experimental Method

The crossed coil system originated by Bloch *et al.* (1946) was used for detecting the nuclear magnetic resonance. The control of the coupling between the coils was done electrically by means of a subsidiary balancing circuit previously described (Drain 1955). By suitable adjustment of the controls, either absorption or dispersion signals could be recorded.

The magnetic field of approximately 4200 gauss was provided by a permanent magnet previously described (Drain 1955). At the position of maximum homogeneity the variation of the magnetic field over the volume of a specimen, 0·7 cm^3, was about 0·5 gauss. The field of the magnet had a temperature coefficient of about −0·5 gauss/°c To avoid corrections for temperature the magnet was enclosed in a thermostatically controlled oven whose temperature was kept constant to ±0·1°c at about 30°c. The balancing circuit was also enclosed in the oven and the stability of balance was thereby considerably improved.

The field could be varied over a range of approximately ±50 gauss by means of coils wound around the pole pieces of the magnet. A slight hysteresis of about 1% of the range of variation of the field was found; to avoid errors from this source care was taken to cycle the field in a consistent way during a series of measurements. About 10 cycles were made before a series was started and measurements were always taken with increasing magnetic field.

The radio frequency oscillator was variable in frequency and employed the modified Colpitts circuit described by Gouriet (1950). The frequency was generally stable to about 2 parts in 10^5 over periods of $\frac{1}{4}$ or $\frac{1}{2}$ hr and was frequently checked by comparison with a 100 Kc/s quartz crystal oscillator.

To achieve adequate sensitivity, the A.F. modulation method of operation was used (Bloembergen *et al.* 1948). The main field was modulated at 39 c/s by means of a second pair of coils on the magnet. The A.F. signal after detection was selected by a tuned amplifier and mixed with the original frequency. The d.c. output proportional to the derivative of the resonance curve was fed to a recording milliammeter. The effective pass-band of this system of detection is governed by the time constant of the d.c. output circuit. To get adequate sensitivity a time constant of 1 min was used in most of these experiments. This necessitated a slow passage through resonance in order not to distort the shape of the line. Usually about an hour was required for one curve. If the time constant is small compared with the time taken to sweep through the width of the line, the line is to a first approximation displaced in time by the time constant. Where necessary a correction was made for this.

To determine the position of the centre of a recorded resonance derivative curve in the presence of considerable noise, the method adopted was to trace the curve and rotate the tracing through 180°. The position of best fit of the tracing and the original was judged visually and thus the centre of symmetry of the curve located. Resonance curves were repeated several times and the error in obtaining the line centre estimated from the differences between the individual results. To check the magnetic field at the specimen the position of the resonance from a reference sample was measured two or three times during a series of measurements. For the cadmium resonances, saturated sodium hydroxide solution was a convenient reference since the ^{23}Na resonance was strong enough to be displayed on an oscillograph. For the silver resonances no suitable strong resonance was available that could be tuned in on the same receiving coil and pure silver was used as the reference point.

To reduce the effect of any errors in the field calibration the frequencies used were selected so that the resonances occurred at very nearly the same field strength for each specimen. If ν_A and ν_B are frequencies used for the resonances from the metal and non-metal respectively and H_A and H_B are the corresponding fields, the Knight shift is given by the expression

$$\frac{\Delta\nu}{\nu} = \frac{\Delta H}{H} = \frac{\nu_A - \nu_B}{\nu_B} - \frac{\nu_A}{\nu_B}\left(\frac{H_A - H_B}{H_A}\right). \qquad (2)$$

If the second term is small, errors in the field calibration do not contribute very much to the result.

The alloys were made by melting weighed quantities of the elements in an argon atmosphere in sealed silica tubes. Johnson and Matthey fine silver and spectrographically pure cadmium were used. An analysis of the silver showed that it was at least 99·98% pure. High purity is probably not an important consideration, however, as Knight shifts appear to be insensitive to impurities (Knight 1956) and quadrupole effects are absent for this system.

The first alloys made (Nos. 1–5) were air-cooled from the molten state. Later, to achieve greater uniformity in composition, the method adopted was to quench from the melt in water followed by several weeks annealing just below the melting point.

To achieve the penetration of the metal by the radio-frequency field finely divided material was used. The alloy ingots were ground on an 'Aloxite' cutting-off wheel using a metallographic polishing machine with paraffin as a lubricant. The grindings were collected, dried and sieved. The material that would pass through a 300 mesh (52 μ) sieve was selected. The skin depth for pure silver at 800 Kc/s is 70 μ so that distortion of the resonance from the skin effect should be negligible (Chapman *et al.* 1957). To avoid contamination by ferromagnetic impurities the grinding wheels were soaked before use for a day in moderately concentrated hydrochloric acid.

For alloys containing more than about 25% cadmium, the powders could be used directly as ground, the oxide coating apparently providing sufficient insulation between the particles. For alloys rich in silver, however, the oxide coating was insufficient and the insulation was obtained by washing the powder for a minute in a $\frac{1}{2}$ M sodium sulphide solution slightly acidified with sulphuric acid. A coating of shellac was then applied by means of a dilute solution of shellac in methylated spirit.

Since no quadrupole interactions can be involved in this system, the resonance is expected to be insensitive to crystal defects. It was therefore considered unnecessary to anneal the powders after grinding. A trial on one alloy (24% Cd) showed that the positions and shapes of the resonances were unaffected by annealing at 310°C for one hour.

Chemical analysis of the alloys was made of samples of both powders and ingots. Both silver and cadmium were estimated. The values in table 2 are considered to be correct to 1% of the minor constituent or 0·2% of the total whichever is the greater.

The phases present in the alloys are given in column 2 of table 2. Where doubt existed as to the phases present, the alloy was examined metallographically or by x-ray diffraction. The crystal structures of the phases observed in the alloys investigated were as follows:

α, face-centred cubic; β, body-centred cubic; γ, complex cubic; ϵ and η, close packed hexagonal.

§ 3. DISCUSSION OF RESULTS

The positions of the ^{111}Cd and ^{113}Cd resonances were measured for alloys containing from 5% to 95% cadmium. The ^{109}Ag and ^{107}Ag resonances were measured in the α and β phases only. For alloys containing less than 50% silver, the silver resonances were too weak for observation. In table 2 the magnetic resonance shifts relative to non-metallic reference compounds are given. The reference compound for silver was a 6 M $AgNO_3$ solution with 0·8 M $Mn(NO_3)_2$ added and for cadmium, a saturated (approximately 5 M) $CdCl_2$ solution. The positions of the cadmium resonances were measured for varying amounts of $MnCl_2$ catalyst from 0 to 0·05 M and also for a 2 M $CdCl_2$ solution. No differences were found within experimental error. From the measurements on these cadmium solutions the following ratio of gyromagnetic ratios could be deduced:

$$\frac{\gamma\,^{113}\mathrm{Cd}}{\gamma\,^{23}\mathrm{Na}} = 0{\cdot}83857 \pm 0{\cdot}00004 \quad \frac{\gamma\,^{111}\mathrm{Cd}}{\gamma\,^{23}\mathrm{Na}} = 0{\cdot}80165 \pm 0{\cdot}00004$$

in agreement with the results of Proctor and Yu (1949).

To obtain adequate resonance signals from the reference solutions, the dispersion mode of the magnetic resonance was recorded. For the metallic samples the absorption mode was always used. The line widths given in table 2 refer to the separations of the maxima and minima of the derivative absorption curves. Corrections have been made for magnetic field inhomogeneity and modulation amplitude.

The value of the Knight shift for pure silver, 0·524 ± 0·004% is in good agreement with that given by Sogo and Jeffries (1954) and close to that of Brun *et al.* (1954).

For cadmium, the shift 0·412 ± 0·005% agrees with the mean (isotropic) shift found by Rowland (1956) and is close to those determined by Knight (1956) and Masuda (1957). Owing to the somewhat low value of our field, the asymmetry of the cadmium resonances due to the anisotropic shift is not very pronounced but an approximate value of 0·05% for the anisotropy was derived from the line shape. This agrees with Rowland's (1956) and Masuda's (1957) measurements.

Since changes in the position of a resonance with alloy composition are of more interest than accurate values of the Knight shift, the errors given in table 2 are those for determining the position of the resonance in the alloy only and do not include those involved in the determination of the resonance position in the non-metallic reference. When more than five measurements of a resonance position were made, the r.m.s. deviation from the mean is given; when fewer measurements were available the error listed (0·005%) is the maximum deviation from the mean value in similar measurements when a large number of determinations were made unless the poor quality of the resonance curves indicated that the error may have been greater. Then an estimate is given. The root mean square deviations in the determination of the resonance positions in the non-metallic references was 0·003% for ^{111}Cd, ^{113}Cd and ^{109}Ag and 0·005% for ^{107}Ag.

Fig. 1

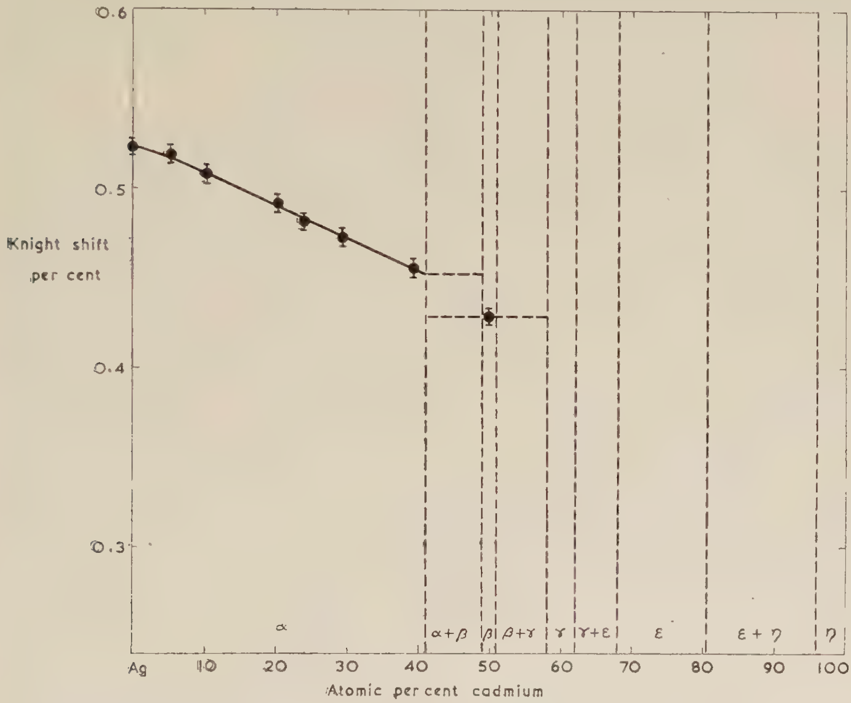

The variation of Knight shift with composition for ^{109}Ag and ^{107}Ag nuclei in silver–cadmium alloys.

In all cases the values of the shifts of the two cadmium resonances and of the two silver resonances agree between themselves to within experimental error. The means of the experimental values are plotted against composition in figs. 1 and 2. In the case of two-phase alloys the magnetic resonance was usually split into a doublet, since in general the magnetic resonance shift is different in the two phases. In the case of mixed $\epsilon+\eta$ phases, however, the difference in shift was too small for the two resonances to be resolved.

Perhaps the most interesting result is the fall in the Knight shift of both the silver and cadmium resonances in the α phase as the concentration of cadmium is increased, whereas in the analogous copper–zinc system the observations of Bloembergen and Rowland do not indicate a significant variation of the ^{63}Cu resonance frequency in the α phase (Bloembergen, N., private communication). This need not indicate any fundamental difference between the electronic structures of the two alloy systems but could be a result of nuclear electric quadrupole interactions which modify the resonance in the copper–zinc system. Bloembergen and Rowland (1953) have shown that owing to these interactions, the ^{63}Cu resonance is not observed from nuclei that are nearest or next nearest neighbours of a zinc atom. Quadrupole interactions are absent in the silver–cadmium system and the observed signal intensities in fact show that all the ^{109}Ag and ^{107}Ag nuclei in the alloys contribute to their respective resonances.

Fig. 2

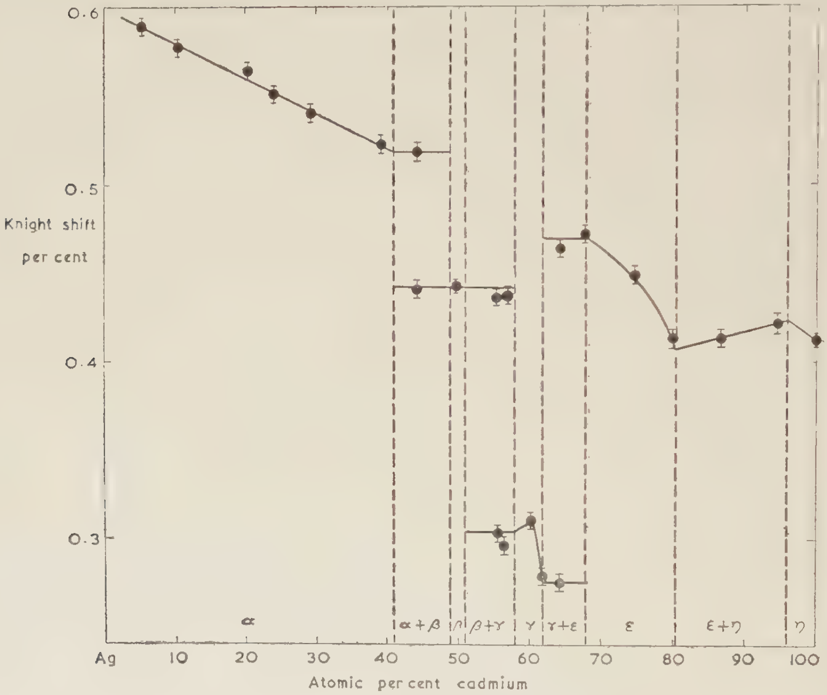

The variation of Knight shift with Composition for ^{113}Cd and ^{111}Cd nuclei in silver–cadmium alloys.

To explain the apparent difference in the behaviour of the Knight shift in the two systems and to account for the line width results to be discussed in the next section, it is necessary to consider the effect of local surroundings on the resonance shift of a nucleus. The postulate will be made that the Knight shift of a nucleus in an alloy depends not only on the type of atom and on the composition of the alloy but also on the nature of its immediate surroundings. In the copper–zinc system the magnetic resonance is only seen from those copper nuclei that are not close to a zinc atom. These have surroundings that are essentially the same as in pure copper and thus no great change in Knight shift should be expected. In the silver–cadmium system, of course, the observed silver resonance lines are representative of all the silver nuclei. It is suggested that if it were possible to eliminate the effect of quadrupole broadening in the brasses so that the resonance from all the nuclei were observed, the behaviour of the nuclear resonance shift would be similar to that in the silver–cadmium alloy.

Since more physical measurements are available for the Cu–Zn system than for the Ag–Cd system, information about the former system will be used in the discussion of the latter if necessary, the assumption being made that the two systems are exactly analogous (except, of course, for nuclear properties).

§4. THE INTERPRETATION OF LINE WIDTHS

The increase in nuclear resonance line width as cadmium is added to silver in the α phase (table 2) may be partly explained by the increase in spin–spin interactions due to the larger magnetic moment of the cadmium nuclei. Consideration should be given, however, to another source of broadening that arises from the effect discussed in the last section that all the silver atoms may not show the same shift. We could, for example, make the assumption that the difference of the shift of the resonance from a silver nucleus in the alloy from that in pure silver is proportional to the number of nearest neighbours which are cadmium and is independent of more distant neighbours. Assuming that the alloy is disordered, the line broadening effect may then be readily calculated. An asymmetry of the magnetic resonance curve could be produced by this effect, particularly at low solute concentrations, but at the compositions studied here and with the resolution available no detectable asymmetry could be expected. Experimentally there was no evidence of unsymmetrical resonances in any of the α-phase alloys.

Since macroscopic composition inhomogeneities can also produce line broadening, the quantitative discussion will concern only the results for the alloy containing 24 at. % cadmium. For this alloy special care was taken to avoid these inhomogeneities by quenching the molten alloy in water to prevent the large-scale movement of the ingredients. In the quenched specimen a small-scale variation in composition of about 5% was found over regions of about 0·03 mm. This was removed by annealing for 5 weeks at 700°C.

To compare the line broadening with theoretical estimates, the mean square line width is required, but since the signal/noise ratio was poor,

Table 2. Nuclear Magnetic Resonance Shifts and Line Widths in Silver–Cadmium Alloys at 303°K. $H = 4200$ gauss

Composition at % Cd	Phases present	Alloy Ref. No.	Magnetic resonance shifts ($\times 10^{-5}$)				Line widths (gauss)		
			^{113}Cd	^{111}Cd	^{109}Ag	^{107}Ag	^{113}Cd	^{111}Cd	^{109}Ag
0	α	—	—	—	524 ± 2	520 ± 3	—	—	0·70 ± 0·2
5·2	α	12	590 ± 5	588 ± 5	519 ± 5	519 ± 5	n.m.	n.m.	1·30 ± 0·3
10·4	α	7	576 ± 5	578 ± 5	507 ± 5	510 ± 5	1·20 ± 0·3	n.m.	1·20 ± 0·3
20·2	α	5	565 ± 5	562 ± 5	492 ± 5	492 ± 5	2·20 ± 0·2	2·10 ± 0·2	1·90 ± 0·2
23·9 M	α	16	551 ± 3	550 ± 5	482 ± 3	483 ± 5	2·00 ± 0·2	2·10 ± 0·2	1·90 ± 0·2
29·2	α	1	540 ± 5	541 ± 5	474 ± 5	472 ± 5	2·20 ± 0·2	2·10 ± 0·2	2·20 ± 0·2
39·1 X	α	10	523 ± 5	524 ± 5	455 ± 5	458 ± 5	2·30 ± 0·2	2·00 ± 0·2	1·90 ± 0·2
44·1 XM	α	4	514 ± 5	522 ± 5	n.o.	n.o.	2·60 ± 0·4	2·30 ± 0·3	n.o.
	β		441 ± 5	440 ± 5	n.o.	n.o.	1·70 ± 0·4	1·60 ± 0·4	n.o.
49·7 X	β	18	445 ± 1	440 ± 2	429 ± 2	n.o.	0·90 ± 0·2	1·00 ± 0·2	1·35 ± 0·2
56·0	β	21	438 ± 2	435 ± 3	n.o.	n.o.	1·20 ± 0·2	1·15 ± 0·2	n.o.
	γ		307 ± 2	298 ± 3	n.o.	n.o.	2·40 ± 0·2	2·20 ± 0·2	n.o.
56·1 X	β	6	438 ± 5	437 ± 5	n.o.	n.o.	1·00 ± 0·2	1·00 ± 0·2	n.o.
	γ		295 ± 5	300 ± 8	n.o.	n.o.	2·20 ± 0·2	2·30 ± 0·2	n.o.
60·2	γ	17	312 ± 2	309 ± 2	n.o.	n.o.	2·10 ± 0·2	2·20 ± 0·2	n.o.
61·6 XM	γ*	8	278 ± 5	281 ± 5	n.o.	n.o.	2·30 ± 0·2	2·40 ± 0·2	n.o.
64·1 M	γ	13	277 ± 5	275 ± 5	n.o.	n.o.	2·40 ± 0·3	2·50 ± 0·3	n.o.
	ϵ		462 ± 5	466 ± 5	n.o.	n.o.	n.m.	n.m.	n.o.
67·6 X	ϵ	9	474 ± 5	470 ± 5	n.o.	n.o.	1·80 ± 0·2	1·70 ± 0·2	n.o.
74·7	ϵ	20	449 ± 2	449 ± 2	n.o.	n.o.	1·70 ± 0·2	1·80 ± 0·2	n.o.
80·0 M	ϵ	15	413 ± 5	412 ± 5	n.o.	n.o.	1·90 ± 0·2	2·00 ± 0·2	n.o.
86·7	$\epsilon + \eta$	19	415 ± 5	410 ± 5	n.o.	n.o.	2·30 ± 0·2	2·30 ± 0·2	n.o.
94·6 X	$\epsilon + \eta$	11	422 ± 5	422 ± 5	n.o.	n.o.	2·10 ± 0·2	2·20 ± 0·2	n.o.
100·0	η	—	412 ± 2	411 ± 3	—	—	2·04 ± 0·1	1·96 ± 0·1	—

X: X-ray analysis made.
M: Metallographic analysis made.
*: There was a small amount of another phase present.
n.o.: Resonance not observed.
n.m.: Signal too poor for measurement of line width.

this could not be obtained directly owing to the large errors which would be introduced by uncertainties in the tails of the resonance curves. Since the curves were found to be approximately gaussian in shape, the gaussian curve approximating most closely to an observed curve was taken as the true curve and the mean square width deduced from this. Corrections were made for field inhomogeneity and A.F. modulation. The experimental values and estimates of several contributions to the line width are given in table 3. The contribution from the indirect spin–spin exchange effect was estimated by assuming that the interaction between two silver nuclei has the value estimated by Ruderman and Kittel (1954) for pure silver and that for other pairs of nuclei, the interaction was increased in proportion to the magnetic moments involved. The residual width is compared with that calculated on the assumption that the magnetic resonance shift for a nucleus is governed only by the relative numbers of silver and cadmium atoms that are nearest neighbours. While the comparison shows that this assumption cannot be entirely true, the presence of a considerable broadening effect does indicate that the influence of an impurity atom on Knight Shift is confined largely to near neighbours. The observed line width could be explained either by assuming that only about 70% of the variation of the shift is due to nearest neighbours, the rest being a long-range effect, or by assuming that there are about 24 neighbours which are equally effective in changing the shift.

Table 3. The Mean Square Width of Magnetic Resonances in a Silver–Cadmium Alloy containing 24 at. % cadmium. $H=4200$ gauss

	^{109}Ag resonance	^{113}Cd resonance
Experimental values	0·74 ± 0·1	0·85 ± 0·1 gauss^2
Contributions from		
(i) Dipolar interactions	0·02	0·02
(ii) Indirect spin–spin interactions	0·30	0·24
(iii) Remainder	0·42 ± 0·1	0·58 ± 0·1
Broadening due to dependence of shift on situation of nucleus assuming		
(*a*) that it is dependent on nearest neighbours only	0·84	1·04
(*b*) that 70% of variation is due to nearest neighbours	0·42	0·52
(*c*) that there are 24 neighbours equally effective	0·42	0·52

Another possible contribution to the line width that may also be important arises from the fact that in a disordered alloy the surroundings of an atom deviate from cubic symmetry. This gives the possibility of broadening through the anisotropy of the Knight shift. In order to resolve the effects of the various contributions to the line width, measurements of the variation of line width with magnetic field are desirable.

If the effect of impurity is confined largely to nearest neighbours, a variation of nuclear magnetic resonance line width and shift could be produced by ordering the atoms of the lattice. Since heat treatment at temperatures of the order of 190°C has been found to increase ordering in the α-phase of the copper–zinc system (Rosenblatt *et al.* 1955) the effect was tried of annealing the alloy specimen containing 24 at.% cadmium for 2 months at a temperature decreasing gradually from 170°C to 110°C. No change in the position of either the ^{109}Ag or the ^{113}Cd resonance could be detected. The resonances became slightly narrower, the new line widths both being $1{\cdot}7 \pm 0{\cdot}2$ gauss, but this observed decrease is on the limits of experimental error. The absence of a significant effect may be due to the possibility that the treatment given did not in fact produce appreciable ordering and does not necessarily invalidate the conclusion that the effect of solute atoms on the shift of the solvent is largely confined to near neighbours.

In the β phase, both the silver and cadmium resonances are much narrower than in the major part of the α phase. The width is about that expected from indirect spin–spin exchange interactions and there appears to be no term from the variation of shift between nuclei of the same type. Thus all nuclei appear to be in equivalent positions and an ordered structure is indicated. Information about ordering may also in principle be obtained from the magnitude of the broadening due to spin–spin interactions. If the main source of broadening is from the indirect exchange effect, the width of the ^{109}Ag resonance (expressed in gauss) is expected to be greater than that of the ^{113}Cd resonance, because interactions with the magnetic cadmium nuclei give the major contribution to the line widths of both resonances. The silver resonances are broadened by both magnetic cadmium isotopes, whereas, owing to the properties of the exchange interaction, the cadmium resonances are broadened only by the unlike cadmium nuclei.

Assuming that the interaction between two spins varies as the inverse cube of their distance apart, the ratios of widths expected are 1·69 and 1·28 for the ordered and disordered body-centred cubic structures respectively. The experimental value ($1{\cdot}5 \pm 0{\cdot}3$) is not sufficiently accurate to verify the structure but it is not inconsistent with the ordered structure indicated above. The cadmium resonances in the γ phase are again broad and it is probable that variations of shift with the surroundings of a nucleus and anisotropic shift contribute to the width as in the α phase.

§ 5. MAGNETIC RESONANCE SHIFTS AND THE DENSITY OF STATES

From eqn. (1) we see that the metallic shift depends on both $N(\xi)$ and $\overline{|\psi(0)|^2}$. It is important to determine how $N(\xi)$ varies with composition to compare the behaviour with that deduced by other methods. Changes in shift do not necessarily reflect directly corresponding changes in $N(\xi)$, because variations of the term $\overline{|\psi(0)|^2}$ must be taken into account.

The wave functions will be considered as extending throughout the alloy but having different shapes and amplitudes at different atoms. It is found from experiment that the ratio of the Knight shifts of the silver and cadmium nuclei is independent of composition in the α phase. Hence, by eqn. (1), it follows that on the average the ratio of the wave functions at the nuclei of the silver and cadmium atoms is constant. This result suggests that the following postulates may be valid; (i) that on the average the ratio of the probabilities of the silver and cadmium atoms having a conduction electron of the Fermi energy within their respective atomic volumes is constant; (ii) that the shapes of the wave functions around the silver and cadmium atoms are independent of alloy composition. The amplitudes of the wave functions must vary with composition to preserve their normalization over a gram atom of the alloy.

In order that a calculation of the density of states at the Fermi surface can be made, it is suggested that the shapes of the electronic wave functions in the atomic volumes of A and B atoms in an alloy of A and B metals are taken to be the same as in the respective pure metals. When atomic volumes are changed by alloying, the assumption will be made that the ratio

$$\alpha = \frac{\overline{|\psi(0, A_i)|^2}}{\int_{A_i} \overline{|\psi|^2}\, dv} \qquad \ldots\ldots\ldots \quad (3)$$

is the same in the alloy as in the pure metal where $\psi(0, A_i)$ is the wave function for an electron at the Fermi surface evaluated at the nucleus of the atom A_i and the integration extends over the volume of the A atom. An alternative assumption which may be suggested is that the ratio of $\overline{|\psi(0, A_i)|^2}$ to the mean value of $\overline{|\psi|^2}$ in the atomic volume of A_i is constant. The first assumption seems to be more realistic since if the atomic volumes become large so that the atoms are effectively free, α remains finite whereas the ratio assumed constant in the alternative assumption tends to infinity. α and the corresponding quantity β for the B atoms may be deduced from Knight shift measurements on the pure metals combined with a knowledge of the density of states in the pure metals from measurements of electronic specific heat.

The assumption made here is somewhat different from that proposed by Knight (1956). He suggested that in a dilute alloy, the ratio of the value of $|\psi(0)|^2$ at a solute nucleus in the alloy to its value at a solute nucleus in a free atom is the same as the corresponding ratio for the solvent, the wave functions being normalized over one atom. This assumption is not easy to test since a knowledge of the atomic hyperfine structure constant for cadmium is required. This constant is not known with accuracy and uncertain corrections may have to be applied in a divalent metal. From Knight's argument, one may deduce the general result that the ratio of the shifts for two given nuclei should be the same for any alloy in which the nuclei are present, but for systems so far investigated (cf. Knight (1956)), the ratio is only constant to within a factor of about 1·7. The discrepancies are probably due to the fact that Knight's treatment does not allow for the possibility of having different numbers of conduction electrons associated with the solute and solvent. This possibility is an important feature of the present treatment and would seem to be physically necessary.

The Knight shift for an atom A_i in the alloy is given by

$$\left[\frac{\Delta H}{H}\right]_{A_i}=\frac{8\pi}{3}\,\mu^2N(\xi)\overline{|\psi(0,A_i)|^2}. \quad . \quad . \quad . \quad . \qquad (4)$$

The measured Knight shift is the mean for all A atoms in the alloy

$$\left[\frac{\Delta H}{H}\right]_{A}=\frac{8\pi}{3}\,\mu^2N(\xi)\overline{|\psi(0,\bar{A})|^2} \quad . \quad . \quad . \quad . \quad . \qquad (5)$$

where $\overline{|\psi(0,\bar{A})|^2}$ is the mean value of $\overline{|\psi(0,A_i)|^2}$ over all the A atoms.

Since the wave function for the alloy is normalized over a gram atom, we have

$$\sum_i \int_{A_i}\overline{|\psi|^2}\,dv+\sum_j \int_{B_j}\overline{|\psi|^2}\,dv=1 \quad . \quad . \quad . \quad . \quad . \quad . \quad . \qquad (6)$$

where the summations extend over all atoms in a gram atom. Using eqn. (3),

$$\begin{aligned}1&=\frac{1}{\alpha}\sum_i\overline{|\psi(0,A_i)|^2}+\frac{1}{\beta}\sum_j\overline{|\psi(0,B_j)|^2}\\&=\frac{1}{\alpha}(1-c)N_0\overline{|\psi(0,\bar{A})|^2}+\frac{1}{\beta}cN_0\overline{|\psi(0,\bar{B})|^2} \quad . \quad . \quad . \qquad (7)\end{aligned}$$

where c is the atomic fraction of B atoms in the alloy and N_0 Avagadro's number.

If

$$\left[\frac{\Delta H}{H}\right]_{AA} \text{ and } \left[\frac{\Delta H}{H}\right]_{BB}$$

are the Knight shifts in the pure metals, we thus obtain

$$N(\xi)=(1-c)N_A(\xi)\left[\frac{\Delta H}{H}\right]_A\bigg/\left[\frac{\Delta H}{H}\right]_{AA}+cN_B(\xi)\left[\frac{\Delta H}{H}\right]_B\bigg/\left[\frac{\Delta H}{H}\right]_{BB}, \quad . \quad . \quad . \quad . \qquad (8)$$

$N(\xi)$ refers to the alloy and N_A (ξ) and N_B (ξ) to the pure metals.

Substituting values for the silver–cadmium system the variation of $N(\xi)$ with composition was calculated. The result is given in fig. 3 (*a*). For the densities of states in the pure metals, the following values derived from electronic specific heat measurements were used; silver, 0·26 electrons/atom ev (Corak *et al.* 1955), cadmium, 0·28 electrons/atom ev (Samoilov 1952, Smith and Wolcott 1956). The results obtained from the alternative assumption are also given in fig. 3 (*a*). These results must be regarded with considerable reservation but errors introduced may to some extent compensate one another, for while the wave functions around the silver atoms are likely to assume a greater 'p' character when cadmium is added, those around the cadmium atoms are probably more 's' than has been assumed.

According to the above calculation, the ratio of the average electron density around the cadmium atoms to that around the silver atoms is 1·56 for all the α phase alloys and is 1·41 in the β phase. The fact that these ratios are not 2 does not necessarily indicate a transfer of electrons from cadmium to silver, since the calculation refers to electrons at the Fermi surface only. Electrons near the bottom of the conduction band may have quite a different distribution.

Fig. 3

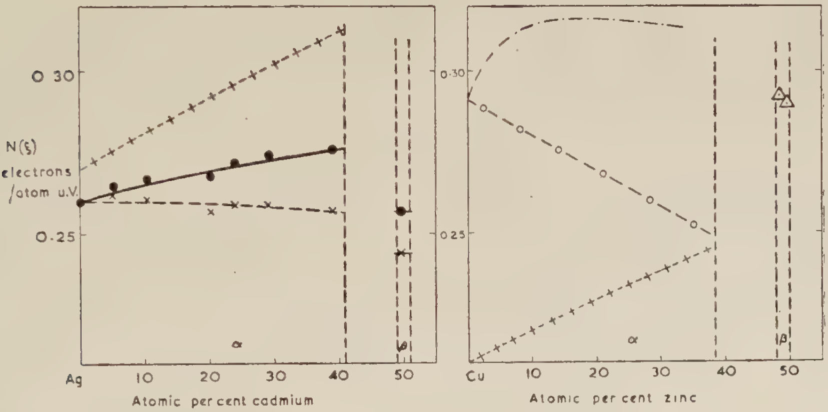

(a) (b)

The variation of the density of states at the Fermi surface with composition for

(*a*) Ag–Cd alloys; (*b*) Cu–Zn alloys.
● Calculated from nuclear magnetic resonance shifts.
X Calculated with the alternative assumption.

Values from specific heat results: —·— Rayne (1957); △ Smith (unpublished): —o—o— form of variation suggested by Henry and Rogers (1956); — + — + values from free electron hypothesis assuming $(1+c)$ electrons per atom.

A calculation of the distribution of conduction electrons may be made from the screening potential of Mott (1936). Assuming that the volumes associated with the silver and cadmium atoms are the same, the ratio of the numbers of conduction electrons associated with the cadmium and silver atoms has the value 1·74. If the electron transfer is calculated by the method of Varley (1954), the ratio is found to be approximately 1·3.

It may be remarked, however, that the detailed application of Varley's theory does not lead to the correct result concerning the variation of Knight shift with composition.

The most direct method of measuring $N(\xi)$ is by means of specific heats at low temperatures. The specific heat term linear with temperature is attributed to the conduction electrons. No measurements are available for the silver-cadmium system but in the analogous copper–zinc system Rayne (1957) finds that the electron specific heat increases as zinc is added to copper. His results are shown in fig. 3 (*b*). While this general behaviour is not inconsistent with our results, the rapid rise in the electron specific heat for compositions from 0 to 10% Zn is difficult to reconcile, as it is not reflected in any correspondingly rapid change in Knight shift.

To explain the behaviour of magnetic susceptibility in alloys of copper, Henry and Rogers (1956) have assumed, following a calculation of Jones (1937), that the density of states falls as the electron/atom ratio increases. The assumed rate of fall is too high to fit in with a reasonable interpretation of the results of this paper. Childs and Penfold (1957) consider that the assumption of a falling density of states curve is not essential to the explanation of the magnetic susceptibility results. They have also measured the susceptibility of an α-phase silver-cadmium alloy. It appears that the variation with composition is very similar to that in the copper–zinc system.

It has been proposed (Mott and Jones 1936) that the main effect of alloying an element with another of different valency is to change the number of electrons in the conduction band. The form of the band is assumed to be substantially unchanged. In particular, the addition of cadmium to silver or zinc to copper raised the Fermi level in relation to the conduction band. With the assumption of free electrons, $N(\xi)$ is proportional to $n^{1/3}$ where n is the number of conduction electrons. For copper and silver a maximum value of $N(E)$ is expected approximately when the energy surfaces just touch the boundaries of the first Brillouin zone. Detailed calculations of the band structures of copper and silver have been made (Howarth 1955) and it appears probable that in the pure metals, the point to which the conduction band is filled is well below the maximum. The results of x-ray emission spectra (Cauchois 1953) confirm that there is a maximum in $N(E)$ above the Fermi level. Thus $N(\xi)$ should increase as the electron/atom ratio is raised.

From measurements of the anomalous skin effect, Pippard (1957) deduced the form of the Fermi surface in copper. He finds that the Fermi surface just touches the boundary of the first Brillouin zone. This suggests that $N(\xi)$ may be close to a maximum value in pure copper.

The effect of zone structure on the electronic properties is shown to a marked degree in the γ-phase alloys. The small value of the cadmium Knight shift shows that $N(\xi)$ is considerably smaller than in the other phases. This is consistent with the suggestion that a Brillouin zone is almost full (Jones 1934). Although there is a rapid change in shift with composition in the γ range, the behaviour does not reflect the large variation of bulk magnetic susceptibility (Smith 1935). This is doubtless because the shift is dependent only on spin paramagnetism whereas the diamagnetism of the γ phase is attributed to the translational motion of the small fraction of the electrons that overlap into the next zone (Jones 1934). Unfortunately, the present results are not complete or accurate enough to determine the exact form of the variation of shift with composition in the γ phase. In particular, it is not possible to determine with certainty whether the maximum suggested by the results is in fact real.

Recent measurements of P. L. Smith (unpublished) of the electron specific heat of γ phase copper–zinc alloys also show that the density of states at the Fermi surface is less in the γ phase than in the α or β phases, but the rapid fall of the electronic specific heat coefficient from 0·55 to 0·21 millijoules/mole/deg^2 across the phase does not seem to be in agreement with the nuclear magnetic resonance results.

§ 6. CONCLUSIONS

Whilst the results of this paper can be interpreted in terms of the band theory of metals, quantitative information about the density of states at the Fermi surface cannot be obtained from nuclear magnetic resonance shifts without making simplifying assumptions about the electronic wave functions. If reliable measurements of the density of states could be made by other methods, nuclear resonance shifts would lead to information about the wave functions. In particular, the approximations suggested in this paper could be tested.

Since variations of magnetic resonance shift of nuclei in different situations in an alloy are shown by a broadening of the observed resonance line, the range of influence of an impurity atom in a metal can be found. In the silver–cadmium system, the effect of an impurity atom on the Knight shift has been found to extend at least to its nearest and next nearest neighbours. Measurements of line width with a higher and variable field would enable more definite conclusions to be reached. Such measurements may also be useful in the study of ordering effects in alloys. Silver alloys are particularly suitable for this type of investigation since the small magnetic moments of the silver nuclei result in a small line width due to spin–spin interactions.

Of particular interest would be accurate measurements of shifts for very low concentrations of solute. For dilute alloys, Friedel (1955) has suggested that the nuclear resonance shift of the solvent is unaffected by the solute. From the measurements reported here, there appears to be a significant variation of shift for the most dilute alloys but the possibility of the curve of shift against composition having zero slope for very small solute concentrations cannot be entirely excluded.

Recently, Blandin *et al.* (1959) have emphasized that there exist comparatively long-range changes of electronic density around an impurity atom in a metal. These were not considered in Friedel's (1955) original calculations and can result in a decreased density of conduction electrons in some regions close to an impurity. For solutions of cadmium in silver, the nearest neighbour atoms of a cadmium atom are in such a region and thus a mechanism is provided for the observed decrease in the Knight shift of the nuclei of these neighbours.

ACKNOWLEDGMENTS

The author wishes to acknowledge the assistance of many members of the Metallurgy Division, A.E.R.E. Thanks are due particularly to Mr. A. D. Le Claire and Mr. J. Butterworth for theoretical discussions and for help with the design of apparatus, to Mr. C. Austing for the chemical analyses, to Miss J. Murray and Mr. E. Sykes for metallographic analyses and advice, to Mr. Law for x-ray measurements and to Mr. C. Thomas and Mr. A. Rowe for help in the preparation of the alloys. The author also wishes to thank the Electronics Division, A.E.R.E., particularly Mr. C. N. Davey and Mr. A. R. Coward who constructed much of the equipment. In addition the author is indebted to Dr. H. M. Finniston, Dr. M. Lomer, Dr. V. Heine, Dr. T. J. Rowland and Dr. J. Varley for valuable comments on the manuscript and to Professor J. Friedel for the communication of his calculations before publication.

REFERENCES

BLANDIN, A., DANIEL, E., and FRIEDEL, J., 1959, *Phil. Mag.* (in the press).
BLOCH, F., HANSEN, W. W., and PACKARD, M. E., 1946, *Phys. Rev.*, **70,** 474.
BLOEMBERGEN, N., PURCELL, E. M., and POUND, R. V., 1948, *Phys. Rev.*, **73,** 679
BLOEMBERGEN, N., and ROWLAND, T. J., 1953, *Acta Met.*, **1,** 731.
BRUN, E., OESER, J., STAUB, H. H., and TELSHAW, C. G., 1954, *Phys. Rev.*, **93,** 172.
CAUCHOIS, Y., 1953, *Phil. Mag.*, **44,** 173.
CHAPMAN, A. C., RHODES, P., and SEYMOUR, E. F. W., 1957, *Proc. phys. Soc. Lond.* B, **52,** 345.
CHILDS, B. G., and PENFOLD, J., 1957, *Phil. Mag.*, **2,** 389.
CORAK, W. S., GARFUNKEL, M. P., SATTERTHWAITE, C. B., and WEXLER, A., 1955, *Phys. Rev.*, **98,** 1699.
DRAIN, L. E., 1955, *Disc. Faraday Soc.*, **19,** 200.
FRIEDEL, J., 1955, *J. Phys. Radium*, **16,** 444.
GOURIET, G. G., 1950, *Wireless Eng.*, **27,** 105.
HENRY, W. G., and ROGERS, J. L., 1956, *Phil. Mag.*, **1,** 237.
HOWARTH, D. J., 1955, *Phys. Rev.*, **99,** 469.
JONES, H., 1934, *Proc. roy. Soc.* A, **144,** 225; 1937, *Proc. phys. Soc. Lond.*, **49,** 250.
KNIGHT, W. D., 1949, *Phys. Rev.*, **76,** 1259; 1956, *Solid State Physics*, Vol. 2 (New York: Academic Press Inc.), p. 93.
MASUDA, Y., 1957, *J. phys. Soc. Japan*, **12,** 523.
MOTT, N. F., 1936, *Proc. Camb. phil. Soc.*, **32,** 281.
MOTT, N. F., and JONES, H., 1936, *Theory of the Properties of Metals and Alloys* (Oxford: University Press), p. 171.
PIPPARD, A. B., 1957, *Phil. Trans. roy. Soc.*, **250,** 325.

PROCTOR, W. G., and YU, F. C., 1949, *Phys. Rev.*, **76,** 1728.
RAYNE, J. A., 1957, *Phys. Rev.*, **108,** 22,
ROSENBLATT, D. B., SMOLUCHOWSKI, R., and DIENES, G. J., 1955, *J. appl. Phys.*, **26,** 1044.
ROWLAND, T. J., 1956, *Phys. Rev.*, **103,** 1670.
RUDERMAN, M. A., and KITTEL, C., 1954, *Phys. Rev.*, **96,** 99.
SAMOILOV, B. N., 1952, *Dokl. Ak. Nauk, S.S.S.R.*, **86,** 281.
SOGO, P. B., and JEFFRIES, C. D., 1954, *Phys. Rev.*, **93,** 174.
SMITH, C. S., 1935, *Physics*, **6,** 47.
SMITH, P. L., and WOLCOTT, N. M., 1956, *Phil. Mag.*, **1,** 854.
TOWNES, C. H., HERRING, C., and KNIGHT, W. D., 1950, *Phys. Rev.*, **77,** 852.
VARLEY, J. H. O., 1954, *Phil. Mag.*, **45,** 887.

A Possible Determination of the Activation Energy for Self-Diffusion in Aluminium†

By T. FEDERIGHI
Istituto Sperimentale dei Metalli Leggeri, C.P. 129, Novara, Italy

[Received October 28, 1958]

ABSTRACT

A more detailed study of the so-called stage II of the annealing out of the quenched-in resistivity in 99·995% aluminium (whose existence was established in a preceding paper) has been carried out. The process is found to be a single activated one, the activation energy being $Q=1{\cdot}33\pm0{\cdot}05$ ev; the analytical shape of the isothermal curves is given by $f=1-(t/\tau)^m$ where $m\sim0{\cdot}55$ and $\tau=2{\cdot}6\ 10^{-8}\exp(Q/kt)$ sec. Several considerations leave little doubt that Q is to be identified with the activation energy for self-diffusion in aluminium, although the nature of the defects and the mechanism of annealing out are yet not clearly understood.

§ 1. INTRODUCTION

THE determination of the self-diffusion coefficients in metals is usually carried out by the employment of radioactive isotopes. Unfortunately in the case of aluminium, for which an isotope with a sufficiently long life was not practically available until recently (see for instance Rightmire *et al.* 1957) it has not been possible till now to determine the value of these important coefficients.

Now some recent results of Panseri and Federighi (1958) on the isochronal annealing of quenched-in vacancies in aluminium suggest a new possible way for the determination of the activation energy for self-diffusion in the particular case of this metal. During the annealing process after quenching from high temperature it has been found that an appreciable fraction of quenched-in resistivity (namely the so-called stage II) is annealed out at relatively high temperature (~150°c). A rough estimation of the activation energy of the process gives the value $1{\cdot}3\pm0{\cdot}2$ ev which is about that expected for self-diffusion in aluminium (Nowick 1951): for this and other reasons discussed in the previous paper, this stage of recovery can be related to the dispersion, by normal self-diffusion, of clusters of vacancies of some unspecified shape and originated in the first stage of the process. If one accepts the given interpretation, a more precise determination of the activation energy of stage II of the recovery of the quenched-in resistivity should then give, at the same time, a more precise value for the activation energy for self-diffusion in aluminium. The results of a research carried out to this purpose are reported in this paper.

---

† Communicated by the Author.

It must be emphasized that the interpretation of stage II in terms of clusters of vacancies can yet leave some reasonable doubts, especially keeping in mind the recent observations of Hirsch *et al.* (1958) of dislocation loops in quenched aluminium (and not of clusters of vacancies). However, the actual experimental results have appeared interesting enough to be considered as a contribution to the clarification of the features of the process.

§ 2. Experimental Part

The research has been carried out by means of electrical resistance measurements on Al 99·995% wire samples similar to those described in the above-quoted paper. However, as a substantial difference, actual measurements have been carried out in a stirred oil bath at 20°c (instead of -195°) as the defects are annealing out at higher temperatures (~ 150°c). The precision of measurements was more than one per cent of the total variation of resistivity during the second stage which amounted to about 3 mμ ohm cm (quenching from 600°c).

To deduce the activation energy of the process the selected procedure has been to determine the isothermal annealing curves of stage II at several temperatures. For each isothermal curve the procedure has been as follows. The sample was initially quenched from 600°c into brine at 2°c and then immediately dipped into an oil bath at 80°c for three minutes; this time was sufficient to anneal out completely the first stage in which the formation of clusters takes place. Hence, after the determination of the initial electrical resistance R_i at 20°c, the sample was annealed in an oil bath for increasing times at the chosen temperature, and each time the value of its electrical resistance at 20°c was determined. After a sufficiently long time of annealing the sample was annealed for half an hour at 240°c and then the final value R_f (at 20°c) of the sample was determined; it was known that 240°c was a sufficiently high temperature to anneal out all the quenched-in resistivity.

Results have been reported in normalized form, namely the fraction $f=(R_i-R_t)/(R_i-R_f)$ has been used; in this expression R_t is the value of the resistance after an annealing time t.

§ 3. Results

3.1. *The Activation Energy*

Isothermal curves obtained on a sample quenched several times from 600°c and annealed each time at a different temperature (selected without a particular order) in the range 130 to 170°c are shown in fig. 1 where the fraction f is plotted with the logarithm of time.

It immediately appears that all the excess of resistivity can be annealed out at each temperature, if sufficient time is left for the process. To determine the activation energy one can suppose, as usual, that the time t to observe a fraction of recovery is proportional to exp (Q/kT) where Q is the activation energy. In fig. 2 the experimental values of time to obtain a selected fraction f of recovery and deduced from the results of fig. 1 are plotted on logarithmic scale with $1/T$ (for the meaning of τ see hereafter); as these experimental points lie with noticeable precision on straight lines the value of Q can be deduced to be $Q = 1{\cdot}33 \pm 0{\cdot}05$ ev without any appreciable dependence upon f.

These results, namely the total annealing out at each temperature, the alignment of points in fig. 2 and the constancy of Q at all values of f, are the essential conditions to be satisfied (as in effect they are) if a clear physical meaning is to be attributed to the experimental value of Q.

Fig. 1

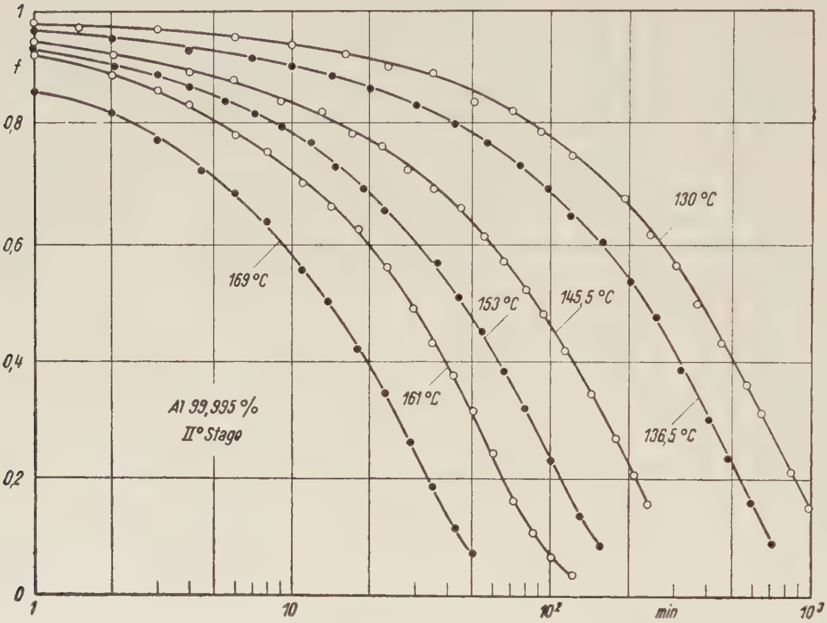

Isothermal curves obtained for a sample quenched several times from 600°c and annealed each time at a different temperature.

Similar results, not reported here, have been obtained also for another sample.

3.2. *Shape of the Annealing Isotherms*

The experimental isothermal curves can be fitted with very high precision, for value of f between 1 and 0·1 (namely for about 90% of the annealing process), by the law:

$$f = 1 - (t/\tau)^m \quad . \quad . \quad . \quad . \quad . \quad . \quad . \quad . \quad . \quad (1)$$

where m and τ are two constants. This is the only law which has been found to fit satisfactorily with experimental points.

The preceding law (1) can be tested by plotting $1-f$ with time on logarithmic scales, as a straight line should then be obtained. Figure 3 shows this for experimental points of fig. 1; small deviations from a straight line (apart from the final part of the curves) are observed only for low value of $1-f$ where experimental errors are relatively larger.

From fig. 3 the values of m and τ can be easily deduced for each curve; they are reported in the table. As an example of the fitting of experimental points by the law (1), in fig. 4 experimental points of the isothermal curve at 161°C are reported, together the law (1) computed using the values of m and τ of the table; the agreement appears to be very good.

Fig. 2

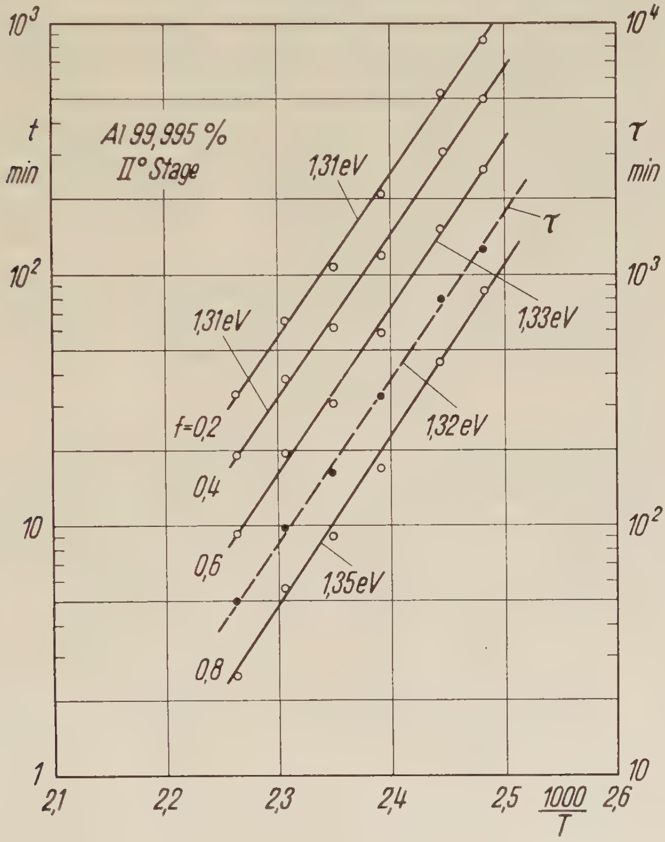

Determination of the activation energy from the data of fig. 1 (for the meaning of τ see § 3.2).

As shown in the table the resulting value of m is slightly larger than 0·5 (~ 0·55) and no systematic dependence upon the annealing temperature appears to exist. On the other hand, τ is very dependent upon the annealing temperature and, as shown again in fig. 2, it can be described by the law:

$$\tau=\tau_0 \exp(Q/kT) \qquad (2)$$

Fig. 3

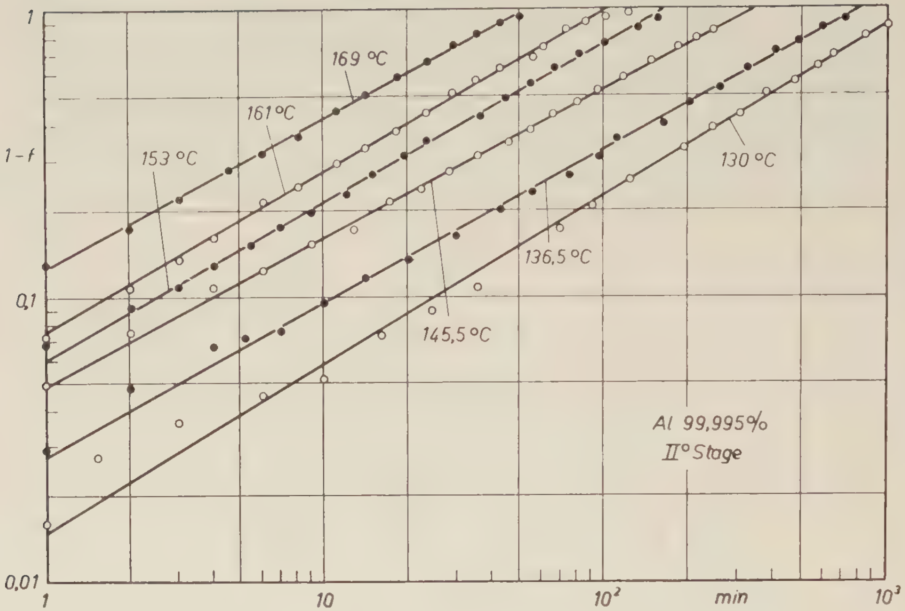

Testing of analytical shape of isothermal curves of fig. 1.

Fig. 4

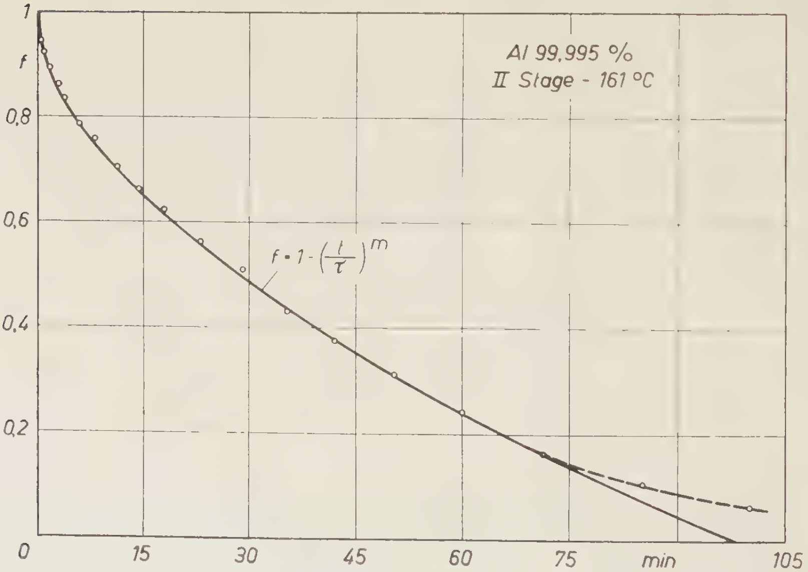

Fitting of experimental points of isothermal curve at 161°c by the analytical law $f = 1-(t/\tau)^m$.

where $\tau_0 \simeq 2{\cdot}6 \times 10^{-8}$ sec, and $Q \simeq 1{\cdot}32$ ev is again the activation energy of the process.

From the preceding law (1) it can be immediately deduced that f is the solution of the equation:

$$\dot{f} = \frac{-m}{\tau}(1-f)^{(m-1)/m}$$

where τ is given by (2). If one identifies the value of m with 0·5 then the preceding equation can be simplified in:

$$\dot{f} = -1/2\tau(1-f).$$

Values of m and τ for the Isothermal Curves of Fig. 1

°C	m	τ (min)
130	0·59	1270
136·5	0·54	800
145·5	0·52	340
153	0·55	160
161	0·56	100
169	0·53	51

§ 4. DISCUSSION

4.1. *The Value of Q*

It is now necessary to discuss briefly if the obtained activation energy can be really identified with the activation energy for self-diffusion in aluminium. First of all it is necessary to remember that in the preceding quoted paper, evidences were reported showing that the second stage is not due to a fraction of vacancies trapped near impurity atoms or to the precipitation of impurities or finally, to the annealing out of dislocations introduced by plastic deformation during the quenching operations. Therefore the hypothesis that the second stage is related to the dispersion by self-diffusion of clusters of vacancies of some unspecified form is not in contradiction with experience (however for other alternatives, see the next sub-section).

Now some considerations will show that the experimental value of Q is about that expected for the activation self-diffusion energy. First of all it can be noted that it is in agreement with the lower range of a theoretical estimate of Nowick (1951) who reported $Q = 1{\cdot}43 \pm 0{\cdot}09$ ev. From the experimental point of view there are very few data; Seymour (1953) tried to determine Q by means of nuclear magnetic resonance measurements; however, for some unknown reasons his result ($Q = 0{\cdot}91$ ev) was too low to be considered the true self-diffusion activation energy. But a new attempt to determine the value of Q from nuclear magnetic resonance measurements has been carried out recently by Spokas (1957), obtaining $Q = 1{\cdot}4 \pm 0{\cdot}1$ ev; therefore the actual value is also in agreement with the lower range of Spokas' result. Finally it is well known that Q should be given also by the sum of E_f and E_m, namely the formation and migration energies of vacancies. Now E_f is reported as $0{\cdot}76 \pm 0{\cdot}04$ ev by Bradshaw and Pearson (1957) and Panseri and Federighi (1958), and E_m is reported as $0{\cdot}58 \pm 0{\cdot}03$ ev again by these last authors; therefore one obtains $Q = 1{\cdot}34 \pm 0{\cdot}07$ ev which is quite in agreement with the experimental result. Also DeSorbo and Turnbull (1958) are publishing some new results for E_f ($0{\cdot}79 \pm 0{\cdot}04$ ev) and for E_m ($0{\cdot}52 \pm 0{\cdot}04$ ev) and from these results one obtains $Q = 1{\cdot}31 \pm 0{\cdot}08$ ev which is again in agreement with the actual result.

4.2. *Dislocation Loops or Clusters of Vacancies?*

In the preceding sub-section evidence has been presented to suggest the identity of the experimental value of Q with the true activation energy for self-diffusion in aluminium. However, there are other questions which can leave some doubts; these are related to our lack of knowledge on the exact nature of the defects producing stage II and on the exact mechanism by which they are annealed out.

Let us suppose for instance that the actual defects are really true clusters of some unspecified shape; if they anneal out by evaporation of single vacancies then the activation energy can be given by $Q = E_f + E_m$; however, if they are sufficiently small they could move slowly as a whole toward dislocations, as in common strain ageing phenomenon, and in this case there is *a priori* no evidence that the migration energy of these defects should coincide with the self-diffusion energy. Some evidence for a strain ageing phenomenon can perhaps be given by the analytical shape of the isothermal curves (see § 4.3).

The question is also complicated by the fact that vacancies could in effect condense in more complex aggregates than simple clusters, as in stacking fault or in dislocation loops; the activation energy for the annealing process would then depend upon the mechanism of annealing (Friedel 1956, Chap. V). In effect Hirsch *et al.* have shown quite recently that many dislocation loops originated from the condensation of vacancies are observable by electron transmission microscopy in quenched aluminium. Now if the temperature of the sample inside the microscope is less than 130°c (as it should be reasonable to suppose) one has then two possibilities:

(1) To identify the dislocation loops with the defects that produce the second stage in the annealing out of resistivity (namely with our clusters of unspecified shape) or

(2) to suppose that in the meantime a large fraction of vacancies has condensed into loops, another large fraction has condensed into small clusters not observable by the electron microscope; in this last case stage II should probably be due to the annealing out of these clusters, while no appreciable effect should be referred to dislocation loops on resistivity.

It is suggested that this question would probably be resolved by electron transmission microscopy by observing if dislocation loops in quenched–annealed aluminium are annealed out in the same way as stage II of resistivity.

In conclusion the question is still unresolved, and until the exact mechanism of the annealing process of the stage II defect is known and the shape of the curves of fig. 1 understood some doubts will exist about the identification of Q with the self-diffusion energy.

Therefore the determination of Q by the usual employment of a radioactive isotope should be very interesting not only for a mere determination of the value of Q itself, but also for its possible bearing on the interpretation of the actual results.

4.3. *On the Analytical Shape of the Isothermal Curves*

A clear understanding of the nature of the defects of the second stage and of the mechanism of annealing out should explain at the same time the analytical shape given by (1) for the isothermal curves. Here it will be shown that the exponent $m=0{\cdot}5$, which is about the experimental value, can be formally justified by a simple strain ageing process toward dislocations of particles of infinite compressibility as a cluster of vacancies.

In this case the force of a dislocation on the defects can be expressed (Friedel 1956, Chap. XIII) as a function of the distance R by $F \sim W\,.\,\mathbf{b}^2/R^3$ where W is the interaction energy and $\mathbf{b}$ the Burgers vector; the drift velocity the defects acquire is $v=DF/kT$ where D is the diffusion coefficient of the defects; at time t all the defects inside a circle of radius

$$R=vt=DW\mathbf{b}^2t/R^3kT$$

have reached dislocations. This is an equation in R, which solved gives

$$R(t)=(DW\mathbf{b}^2t/kT)^{1/4}.$$

The concentration of defects which have reached dislocations is $c=\pi R^2\rho c_0$ where ρ is the density of dislocation and c_0 the initial concentration of the defects. Therefore the fraction f is given by

$$f=1-c/c_0=1-(\pi^2\rho^2DW\mathbf{b}^2t/kT)^{1/2}. \quad . \quad . \quad . \quad . \quad . \quad (3)$$

As D should be given by $D=D_0\exp(-Q/kT)$ where Q is the experimentally observed value, one obtains from (1) and (3):

$$\tau_0=kT/\pi^2\,.\,\rho^2\,.\,D_0W\mathbf{b}^2.$$

Assuming $T=430°\text{K}$, $\rho=10^8\,\text{cm}^{-2}$, $\tau_0=2{\cdot}6\times10^{-8}\,\text{sec}$, and W a fraction of electron volts, the value of D_0 is of the order of $10^5\,\text{cm}^2/\text{sec}$.

Although this value is relatively very high, this interpretation seems to support the view that stage II could be due to some complex aggregate of vacancies moving toward dislocations. It may be however that the same analytical shape can also be obtained by other mechanisms, for instance by evaporation of vacancies from clusters or dislocation loops and then movement towards dislocations (other than loops).

§ 5. CONCLUSION

The stage II in the annealing out of the quenched-in resistivity in 99·995% aluminium results in a single activated process; the activation energy is $Q = 1{\cdot}33 \pm 0{\cdot}05$ ev and the analytical shape of the isothermal curves is given by $f = 1-(t/\tau)^m$ where $m \sim 0{\cdot}55$ and $\tau = \tau_0 \exp(Q/kT)$ with $\tau_0 = 2{\cdot}6 \times 10^{-8}$ sec.

The value of Q is about that expected for the activation energy for self-diffusion in aluminium, and is in good agreement with some recent results obtained by magnetic resonance measurements and with the sum of the formation and migration energies of vacancies in aluminium. These considerations support the view that Q is the true activation energy for self-diffusion in aluminium.

However, the actual lack of knowledge of the exact nature of the defects which are annealing out in stage II and of the mechanism of annealing, leave yet some reasonable doubts on the accuracy of interpretation.

ACKNOWLEDGMENTS

The author is grateful to Professor C. Panseri, Director of I.S.M.L. for encouragement and to his colleague Dr. L. Passari for criticism and comments.

Note added in proof.—An account of Spokas experiments, quoted in the paper, has been recently given by C. P. Slichter (1958, *Suppl. Nuovo Cimento*, **9,** 104).

REFERENCES

BRADSHAW, F. J., and PEARSON, S., 1957, *Phil. Mag.*, **2,** 570.
DESORBO, W., and TURNBULL, D., 1958, *Acta Met.* (to be published).
FRIEDEL, J., 1956, *Les Dislocations* (Paris: Gauthier-Villars).
HIRSCH, P. B., SILCOX, J., SMALLMAN, R. E., and WESTMACOTT, K. H., 1958, *Phil. Mag.*, **3,** 897.
NOWICK, A. S., 1951, *J. appl. Phys.*, **22,** 1182.
PANSERI, C., and FEDERIGHI, T., 1958, *Phil. Mag.*, **3,** 1233.
RIGHTMIRE, R. A., KOHMAN, T. P., and ALLEN, A. J., 1957, *Int. J. appl. Rad. Iso.*, **2,** 274.
SEYMOUR, E. F. W., 1953, *Proc. phys. Soc. Lond.* A, **66,** 85.
SPOKAS, J., 1957, *Thesis*, University of Illinois; quoted by DeSorbo and Turnbull.

Helical Dislocations in Quenched Aluminium-4% Copper Alloys†

By G. Thomas
Department of Metallurgy, Cambridge University

and M. J. Whelan
Crystallographic Laboratory, Cavendish Laboratory, Cambridge, England

[Received January 28, 1959]

Abstract

Experiments by transmission electron microscopy on thin foils of polycrystalline Al-4% Cu alloys, quenched from various temperatures have revealed helical dislocation lines which are thought to be produced by condensation of vacancies on dislocations of predominantly screw character. The axes of the helices are parallel to the Burgers vector, i.e. parallel to [110] directions. In material quenched from 500°c and 540°c the helical dislocations vary in radius and pitch from about 250 Å to more than 1500 Å. Material quenched from 440°c contains irregular helices with pitch several hundred angstroms and much smaller radius. Preliminary estimates suggest that the vacancy concentration required to produce the observed climb is $\sim 3\times10^{-5}$ (500° and 540°c quenches) and $\sim 2\times10^{-6}$ (440°c quench). The helices appear to interact with each other and with other dislocations to produce intertwined helices and rows of loops. Observations of connected helices of opposite hand and of the lengths of helical dislocations suggest that loops from sources of slip active during quenching may be very elongated with long screw components. Dislocation loops are also observed. Some appear to be formed by interaction of helices, others from collapsed vacancy discs. The latter occur in some areas in bands parallel to the traces of {111} planes and are thought to be associated with slip bands. Elsewhere very few collapsed vacancy discs are observed. The observations suggest that nucleation of loops in the quenched alloy may be a difficult process, and that some vacancies may remain quenched in. The observations are also discussed in relation to precipitation effects.

§ 1. Introduction

Recently much interest has centred round the behaviour of point defects (vacancies, interstitials) in metals and alloys (for review see Seitz 1952, Cottrell 1957, Broom and Ham 1957). Several methods of introducing an excess of point defects exist, for example, by radiation damage, by cold work, or by quenching from high temperatures. The latter provides a rapid and convenient way of obtaining a concentration of vacancies of about 1 in 10^5 to 1 in 10^4 at large supersaturations. Several proposals have been made as to the mechanisms by which these vacancies 'anneal out', such as the formation of cavities along dislocations (Coulomb and Friedel 1957), the condensation of vacancies into collapsed discs to form loops of dislocation line (Kuhlmann-Wilsdorf 1958, Kimura *et al.* 1958 a, b, c, Maddin *et al.* 1958, Kuhlmann–Wilsdorf *et al.* 1958), and the condensation of vacancies on dislocations causing climb (Seitz 1952, Cottrell 1957).

---

† Communicated by the Authors.

Direct electron microscope evidence in favour of the second mechanism (collapsed vacancy discs) has been obtained by Hirsch *et al.* (1958 b), who observed small dislocation loops with the expected properties in quenched aluminium. Loops have also been observed in quenched aluminium and nickel by Wilsdorf (reported by Kuhlmann–Wilsdorf *et al.* 1958). More recently Hirsch and Silcox (1958), and Smallman and his co-workers (unpublished) have observed similar loops in quenched copper, while Silcox and Hirsch (1959) have observed defects related to collapsed discs of stacking fault in quenched gold. Thus it appears that this mechanism accounts satisfactorily for the disappearance of vacancies and for the quench hardening effects observed in these metals. However, the conclusions of Hirsch *et al.* (1958 b) about the third mechanism (climb) were not so detailed. In aluminium a few very irregular dislocations were observed which were attributed to climb of dislocations left in the metal after annealing, but generally their specimens contained very few dislocations other than loops.

Microscopic evidence for climb of dislocations in fluorite crystals has been obtained using decoration techniques (Bontinck and Amelinckx 1957, Amelinckx *et al.* 1957. Bontinck 1957). These workers have observed helical dislocations of diameter 10 μ or more produced by climb after heating fluorite crystals to 1100°c, and have described their properties and modes of formation in some detail. The axes of the helices were close to [110] as expected for the climb of screw dislocations, and very often the pitch of a helix was roughly equal to its radius. Such a dislocation can glide only on the helicoidal surface (or prismatic cylinder) containing the dislocation line and the Burgers vector. Similar effects have recently been observed in germanium crystals by decoration (Dash 1958) and by etching (Tweet 1958), while Barber *et al.* (1957) and Jones and Mitchell (1958) have decorated helical dislocations in alkali halide and silver halide crystals. In the last case however (silver halide) the dislocations appear to be produced by prismatic glide only, climb being unimportant. On the theoretical side Weertman (1957) has considered the problem of climb of a dislocation of arbitrary orientation, and has shown that the equilibrium form of a dislocation pinned at two points and subjected to a chemical stress by a supersaturation of vacancies is always a helix. Pure screw dislocations under a sufficiently large chemical stress are in unstable equilibrium and are expected to give rise to helices with the largest number of turns.

During the course of some electron microscope experiments designed to study precipitation effects, the present authors examined thin foils of quenched Al-4% Cu alloy. Contrast effects have been observed which are interpreted in terms of helical dislocations and closed loops. The helical dislocations appear to be produced by climb, while the loops appear to form both by condensation of vacancies into collapsed discs and by interactions of helical dislocations. The purpose of the present paper is to describe some of these effects and to discuss their significance†.

§ 2. Experimental Technique

Foils of Al-3·7 wt. % Cu alloy of total impurity < 0·003% and 0·005 in. thick were prepared from thicker sheet by several stages of cold rolling with intermediate anneals. The foils were then solution heat treated for 10 hours at 540°c. Some of the foils were quenched directly from 540°c into iced brine, others from 500°c, while a further batch was allowed to age for 3 hours at 440°c before quenching. Thin foils suitable for transmission electron microscopy were prepared by electro-polishing in a phosphoric-chromic acid bath (Nicholson *et al.* 1958).

The specimens were examined in the Siemens Elmiskop 1 electron microscope operating at 100 kv at instrumental magnifications of × 20 000 and × 40 000. The specimens were mounted in the stereo-holder so that the foils could be tilted through a few degrees in order to obtain optimum dislocation contrast, and in a few cases to determine Burgers vectors of helical dislocations. Selected area diffraction patterns were also taken to establish crystallographic orientations.

§ 3. Results

3.1. *General Arrangement*

The figures (Pls. 60–66) are typical transmission electron micrographs observed from the thin foils. They show contrast effects in the form of zig-zag lines (fig. 1, Pl. 60), coiled-up lines (fig. 2, Pl. 61, figs. 3 and 4, Pl. 62, figs. 5, 6 and 7, Pl. 63), and closed loops arranged either randomly or in rows (fig. 2, and fig. 18, Pl. 65, figs. 19 and 20, Pl. 66). All these contrast effects can be interpreted in terms of helical dislocations viewed at various angles and in terms of dislocation loops. Orientation measurements by selected area diffraction have shown that to within experimental error the helices always run parallel to the projections of the [110] directions on the foil surface. Since this has been observed for several different orientations it follows that the axes of the helices are parallel to [110]. On many of the micrographs the orientations are indicated by prominent crystallographic directions in the foil surface.

Contrast experiments have been performed by tilting the specimen to determine the Burgers vectors of the helical dislocations. The contrast in certain helices is observed to vanish when the reciprocal lattice vector of the Bragg reflection producing the contrast is perpendicular to the axes of the helices (full details will be described elsewhere). The kinematical theory of diffraction contrast from dislocations (Hirsch *et al.* 1958 a) shows that dislocations become invisible when their Burgers vectors are perpendicular to the reciprocal lattice vector. This observation therefore proves conclusively that the Burgers vectors of the helical dislocations are along their axes, as expected for dislocations with predominantly screw character which have climbed.

---

† R. E. Smallman (private communication) has recently observed similar helical dislocations in Al–Ag alloys.

The helical dislocations vary in radius and pitch, and very often the pitch is about equal to the radius in agreement with the observations of Amelinckx *et al.* (1957) on fluorite crystals (see for example figs. 1, 5 and 6). Figure 1 (*a*), (*b*) and (*c*) shows helices of about 250 Å radius and pitch which except at isolated points remain remarkably uniform along their lengths. In fig. 3 the helices have slightly smaller radii, while the helix at A in fig. 5 has a radius of about 1500 Å or greater. All these specimens were quenched from the same temperature 540°c. Figures 5 and 6 also show that the helices can be of different size in the same area (e.g. compare fig. 5 at A and B), and may have variable pitch and radius (fig. 6 at A.) The first effect may be due to a difference in Burgers vector of the dislocations. Weertman (1957) has shown that if the force acting on a dislocation due to an internal stress is taken into account, as well as the chemical stress, the equilibrium form will depend on the Burgers vector. The orientation in fig. 5 is such that dislocations A and B could be helices of the same hand whose axes are at right angles, i.e. the helices could have perpendicular Burgers vectors.

The vacancy concentration required to produce the observed climb has been estimated approximately by counting the number of turns of dislocation line in helices and loops on several micrographs. The thickness of the foil is known from the projected lengths of helices running through the foil at an angle, so that the number of turns N per unit volume can be worked out. The vacancy concentration is $\sim \pi R^2 bN$ where R is the average helix (or loop) radius and $\mathbf{b}$ is the Burgers vector. For example, in fig. 1 (*a*), where the foil thickness is $\sim 0{\cdot}6\,\mu$, N is $\sim 5\times10^{13}$ and $R \sim 250$ Å, corresponding to a vacancy concentration of $\sim 3\times10^{-5}$. In fig. 6, where the helices are larger N is $\sim 5\times10^{12}$ and $R\sim 1000$ Å, so that the vacancy concentration works out to $\sim 4{\cdot}5\times10^{-5}$, i.e. of the same order of magnitude as in fig. 1 (*a*). No significant difference in vacancy concentration between material quenched from 500°c and 540°c could be detected. In fact micrographs of specimens quenched from these temperatures are very similar, the spread in helix size in any one specimen being larger than any differences due to quenching temperature. The average value of the vacancy concentration for both these quenching temperatures was about 3×10^{-5}, although individual values ranged from about 10^{-5} to 5×10^{-5}. In specimens quenched from 440°c (below the solid solution temperature) there is a noticeable difference in the amount of climb which has taken place. Figure 7 shows a typical area in material quenched from 440°c; the helices are irregular, the average radius being ~ 70 Å and the pitch ~ 300–400 Å or more. This may be due to the fact that vacancies remain in solution after quenching (see § 4). The vacancy concentration required to produce the climb in typical specimens quenched from 440°c works out to $\sim 2 \times 10^{-6}$. However, even in these specimens some helices of larger diameter have occasionally been observed.

One of the interesting features of the observations is the absence of large numbers of dislocation loops such as those studied by Hirsch *et al.* (1958 b) in quenched aluminium. Except in the neighbourhood of some helical dislocations and certain bands (see § 3.3), small loops ($\sim$200 A diameter) never occur in large numbers. For example, in figs. 3 and 4 no evidence of loops in regions away from the helical dislocations is visible. When isolated loops occur they tend to be few in number and large in diameter (e.g. figs. 11, 18 and 20). All these observations suggest that the vacancies have difficulty in nucleating loops in this material and that they prefer to migrate to dislocations as suggested by Thomas (1959). This is in marked contrast to the behaviour of vacancies in quenched aluminium.

3.2. *Geometry of the Helices*

3.2.1. *Helices viewed side on.*

A helical dislocation when viewed perpendicular to its axis will (if regular) appear as a sine wave. This is very nearly the case in fig. 1 (*a*), (*b*) and (*c*). The normal to the foil surface in this area is close to [101] and the helices run almost parallel to the plane of the foil in the $[\bar{1}01]$ direction. The original dislocations before climb may have been either in the (111) or $(1\bar{1}1)$ planes. This micrograph illustrates the very long lengths of the screw dislocations which have become helical; the dislocation A in fig. 1 (*a*) runs for about $4\frac{1}{2}\,\mu$ before it leaves the foil at the top and bottom surfaces. This finite length is due to the fact that the surface of the foil is not quite parallel to (101). Dislocations B and C on these micrographs appear to be longer (about $7\,\mu$ for B); this is undoubtedly due to the fact that these dislocations do not lie entirely along the same $[\bar{1}01]$ line. For example, dislocation C in fig. 1 (*b*) and (*c*) appears to consist of several helical segments in parallel $[\bar{1}01]$ directions connected by short lengths of dislocation line so that the mean direction of this dislocation is not quite parallel to $[\bar{1}01]$. Assuming that before climb this dislocation was either in the (111) or $(1\bar{1}1)$ plane, the short segments turn out to lie at roughly 45° to the axes of the helices, i.e. at 45° to the Burgers vector. They therefore appear to be mixed dislocations of roughly equal edge and screw content. The climb of a mixed dislocation has been considered by Amelinckx *et al.* (1957); they argue that a mixed dislocation will tend to climb from both ends (assumed fixed) in the manner shown schematically in fig. 8 (taken from Amelinckx *et al.* 1957). The final result is a short length of mixed dislocation connecting two similar helical dislocations with displaced axes. Apart from the fact that little variation of radius and pitch along the helices is observed, the arrangement at C in fig. 1 (*b*) and (*c*) is qualitatively similar to that depicted in fig. 8. It is concluded that this dislocation was not entirely in the screw orientation when climb commenced. However, the helix at C in fig. 1

shows several displaced helical segments with connecting links and does not appear to be pinned at two points as shown in fig. 8. This suggests that the winding-up of the original dislocation into a helix has occurred simultaneously at several points along its length, i.e. that the turns are not necessarily generated from two fixed points as in fig. 8. The uniformity in pitch and radius of the helices in fig. 1 also suggests that the climb process occurs fairly uniformly along the length of a screw dislocation.

Fig. 8

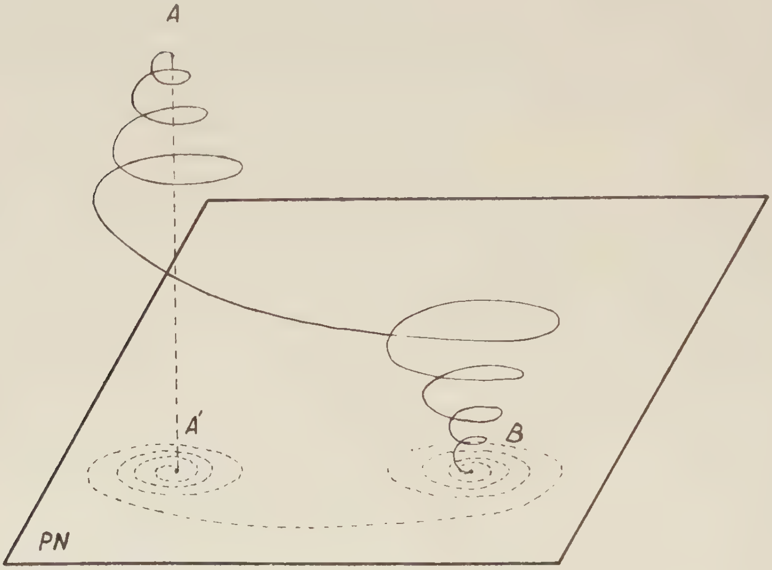

(Taken from Amelinckx *et al.* 1957.) Climb of a mixed dislocation pinned at A and B. The Burgers vector is normal to the plane PN. The ends of the dislocations at A and B spiral in opposite directions introducing new turns. The dislocation can glide on the helicoidal surface containing the dislocation line and the Burgers vector.

Figure 1 (*a*) at D and fig. 1 (*b*) at E and F illustrate a rather interesting effect. It appears that when a helix leaves the surface of the foil at a shallow angle only part of each successive turn enters the surface; this gives rise to short segments of line which decreases in length towards the end of the helix. This is to be expected only if the zig-zag lines in this case are of projections of helices and not of any other configuration. This effect is also visible in many other cases, e.g. fig. 6 at A.

3.2.2. *Helices viewed at an angle*

When a regular helix is viewed at an angle to its axis other than 90° the projected shape develops cusps, and as the angle of tilt is increased these cusps turn into loops. This sequence of effects is illustrated in fig. 9 (*a*) and (*b*) where (*a*) represents the case of a right-handed helix and (*b*) the case of a left-handed helix. Helices of opposite hand are produced by climb of dislocations with opposite Burgers vectors. Many of the effects observed on the micrographs can be interpreted in terms of these ideas, although in some cases not without ambiguity. Figure 2 (*a*) at A and fig. 2 (*b*) at A show examples of projected helices with cusps of opposite sense. The normal to the foil in this area is near [101], and the original screw dislocation would have been in the (111) plane either in the [011] or [110] directions.

Fig. 9

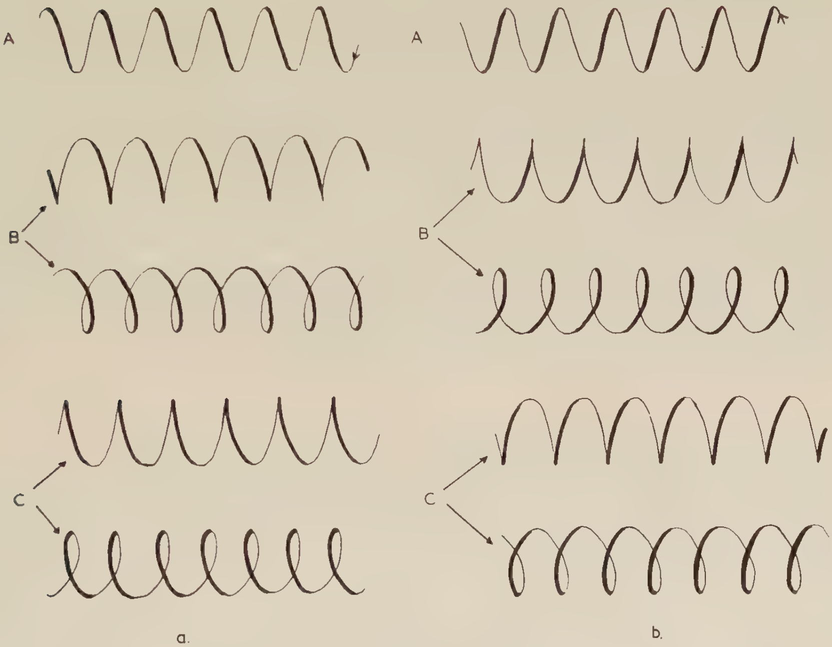

Projected images of helical dislocations. A: viewed perpendicular to axis of helix, B: viewed at positive angles, C: viewed at negative angles. (*a*) Represents the case of a right-handed helix, (*b*) represents the case of a left-handed helix.

Thus the axes of the helices emerge from the foil at an angle of 30°. Since there are two possible axes ([011] and [110]) inclined at ± 30° to the foil surface, it is not possible to decide in this case whether fig. 2 (*a*) at A represents two parallel helices with opposite Burgers vectors (for example, case B in fig. 9 (*a*) and (*b*)), or two helices of the same hand inclined at positive and negative angles to the line of sight (for example, fig. 9 (*a*), cases B and C).

Although in this case the orientation is such that the interpretation is ambiguous, some of the helices in fig. 2 (*b*) do have parallel and opposite

Burgers vectors. For example, the connected intertwined helices seen at A and B in fig. 2 (*b*) can only be formed from helices with common axes (see below). Figure 1 (*a*) and similar areas in fig. 1 (*b*) and (*c*) also illustrate the effect of inclination of the axis of the helix rather well. The inclined helix at G in fig. 1 (*a*) runs parallel to either the [011] or [110] directions, which are again inclined at ± 30° to the foil surface. The cusp-like appearance of this dislocation is to be compared with the zig-zag appearance of the dislocations A and B on the same micrograph.

In other areas where the orientation is less symmetrical, no overlapping of certain projected [110] directions occurs. In these cases it is possible to distinguish between helices of opposite Burgers vector if they appear parallel and wind in opposite senses. Figure 4 at A and B shows an example of this. The normal to the foil in this area is close to [103] so that the helices must lie along [011]; the original screws were probably in (111). This micrograph also shows an interesting effect at C; the long straight dislocations are probably of edge orientation near the (111) plane. These are seen to have interacted with the helices at several places and appear to be held up by them. The dislocation D has apparently annihilated with the helix B giving rise to the features near C; this suggests that D is an edge dislocation with opposite Burgers vector to B. D however does not appear to have interacted with helix A in agreement with the conclusion that A and B have opposite Burgers vectors. A similar dislocation can be seen to have annihilated with one half of an isolated loop at E.

3.2.3. *Helices lying close to slip planes*

Groups of helices are often observed whose axial directions appear to lie close to a common {111} slip plane. Figure 3 shows a typical example. The normal to the foil is close to [101], and the axes of the helices lie either in $[0\bar{1}1]$ or $[\bar{1}\bar{1}0]$. If the original screws were in an inclined slip plane (either (111) or $(1\bar{1}1)$). then the trace of such a plane should be parallel to $[\bar{1}01]$ in this orientation. In fact all the helices in fig. 3 appear to be distributed about a mean plane which makes a trace about 5° away from this direction. This slight discrepancy can be explained if the normal to the foil is not quite parallel to [101]. It is thought that the helices in fig. 3 were originally screw dislocations generated by some source (or sources) made active by quenching strains. The screw dislocations may cross-slip slightly out of their slip planes and this may account for the rather irregular distribution of helices in fig. 3. However, this interpretation is uncertain because of the ambiguous effects discussed above associated with this orientation. It is not known for example whether the helices of opposite sense visible in fig. 3 are parallel helices of opposite hand, or non-parallel helices of the same hand.

Many of the helices visible on the micrographs may have been generated in the same way from screws gliding on {111} slip planes, e.g. figs. 4 and 20.

3.2.4. *Intertwined helices and connected helices of opposite hand*

Many examples have been observed of pairs of helices of opposite hand connected together at their ends. Two types are commonly observed: (1) those in which the helices are intertwined and (2) those in which the helices are well separated and connected by a length of mixed dislocation. Figures 2 (*b*), 10, 11, and 16 show examples of both types.

Fig. 12

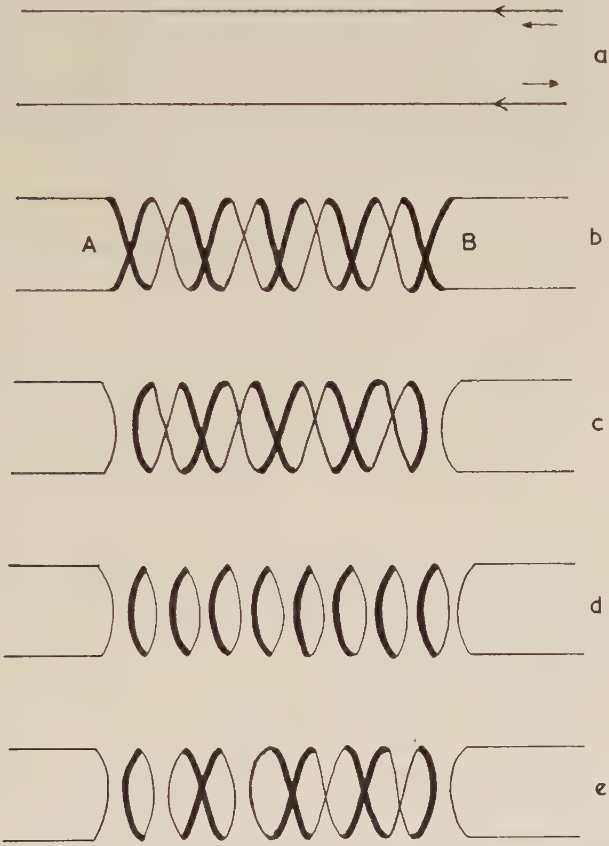

Schematic representation of formation and interaction of helices of opposite hand (following Bontinck 1957). (*a*) Two screw dislocations with opposite Burgers vectors. (*b*) Intertwined helices of opposite hand produced by climb of screw dislocations in (*a*). (*c*) Closed system of intertwined helices formed by annihilation at A and B. (*d*) and (*e*) systems of loops, Lissajous-like figures and closed intertwined helices.

Figure 2 (*b*) at A and B, fig. 10 at A and fig. 11 show intertwined helices. These are thought to be produced by the mechanism suggested by Bontinck (1957) to explain similar dislocation configurations in fluorite crystals. Two screw dislocations of opposite Burgers vectors lying close together (fig. 12 (*a*)) climb into helices of opposite hand (fig. 12 (*b*)). Eventually the helices may attract each other and annihilate at the intersection points. If this happens at points such as A and B in fig. 12 (*b*) a closed system of intertwined helices of opposite hand is produced (fig. 12 (*c*)). If the helices intersect at every turn a system of closed loops arranged along a line results (fig. 12 (*d*)), while if intersections occur at several points at random a system of loops, Lissajous-like figures, and intertwined helices may be produced. Many of the features visible on the micrographs can be explained in this way; for example fig. 2 (*b*) shows intertwined helices at A, B and C, Lissajous figures at D and E, and closed loops at F and G. Rows of closed loops are also visible in fig. 2 (*a*) at C and in fig. 18.

It is interesting to consider a possible mechanism which can give rise to the two closely spaced screw dislocations required in the above explanation. Bontinck (1957) envisages a hairpin-shaped dislocation, both arms of which are nearly in the screw orientation. Such a dislocation might possibly result from the action of a stress on a closed loop formed from a collapsed disc of vacancies. Consider in fig. 13 a closed loop AB formed in this way. The loop can glide on the prismatic cylinder containing the dislocation line and the Burgers vector and such movement has in fact been observed by Hirsch *et al.* (1958 b) for loops in quenched aluminium. The edge segments A and B of the loop will, under a suitable stress, glide in opposite directions to A′ and B′ and will remain connected by long lengths of dislocation line of very nearly screw orientation. These dislocations will then be able to climb into helices of opposite sign in the manner suggested by Bontinck. The intertwined helices, such as at A and B in fig. 2 (*b*) and at A in fig. 10, may therefore arise from a single collapsed disc of vacancies. Figures 14 and 15 also support this hypothesis. At A these micrographs show elongated loops which may have been produced by glide of prismatic loops. Many of these elongated loops appear to run approximately parallel to the [110] directions as expected by theory.

Fig. 13

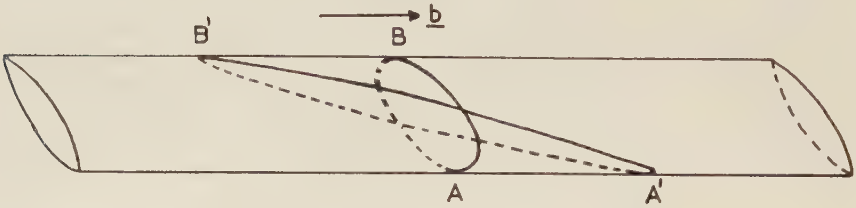

Prismatic glide of a closed loop of dislocation line formed by condensation of vacancies. Under a suitable uniform stress the edge segments at A and B can glide to A′ and B′. The long lengths of connecting dislocation are nearly in the screw orientation and can climb into helices of opposite hand (see fig. 14 (Pl. 64) and fig. 15 (Pl. 65)).

An example of the second type of connected helix is shown in fig. 16. In this micrograph the helices of opposite hand are separated by a distance large compared with their radii. This seems to suggest that they may have been formed from a dislocation loop of large dimensions such as might be produced by a source of slip active during quenching. In fact many of the directions of such helices and their connecting lines seem to lie close to {111} planes. Figure 16 shows an area where the normal to the foil is close to [112]; the two parallel helices run in the [101] direction and were probably formed from a large dislocation loop lying in the (111) plane, the screw parts of which have climbed into helices. If this explanation is correct, and taking into account fig. 1 (*a*), (*b*) and (*c*) which shows that the screw components are very long, a loop from a source in this quenched material should be very elongated as shown schematically in fig. 17. The edge components of the loop have moved much farther than the screw components. This observation is in agreement with the conclusion of Wilsdorf and Kuhlmann-Wilsdorf (1955), who arrived at the same idea from replica studies using a precipitation technique to decorate the dislocations in Al-2% Cu alloy. Thus many of the helices of opposite sense visible on other micrographs may have been connected with each other, although it is only in favourable cases such as fig. 16 that the connecting dislocation is included in the thin section of the foil. The screw components of the dislocation loops therefore appear to be less mobile than the edge components. This is presumably due to the fact that the screw components are rapidly converted into helices by climb and become immobile in the slip plane. In contrast to this the edge components can glide conservatively in the slip plane while climbing.

Fig. 17

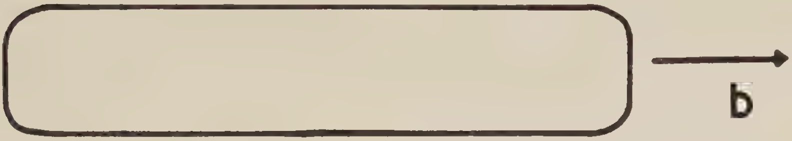

Schematic diagram of the shape of a dislocation loop lying in (111) and glissile in this plane, inferred from many micrographs. The screw components are much longer than the edge components.

3.3. *Dislocation Loops*

Although in most areas vacancies appear to condense on screw dislocations to form helices, nevertheless closed loops of dislocation line have been observed in some regions. A distinction can be drawn between two types of loop which are commonly observed, i.e. loops arranged in rows and loops arranged randomly.

Examples of the first type are observed frequently, e.g. fig. 2 (*a*) at C, fig. 2 (*b*) at F and G, and fig. 18 at A and B. The dislocation loops appear from projection to be arranged in rows with a common [110] axial direction. In fig. 2 (*a*) at C the axis of the loops emerges from the foil surface at an angle of 30°, while in fig. 18 rows of loops parallel to [101] at A and to $[0\bar{1}1]$ at B are visible. It is not known with certainty how these configurations are formed, but similar effects have been observed by Bontinck and Amelinckx (1957) and Bontinck (1957) in fluorite crystals, and their explanation mentioned in § 3.2.4 involving interaction of helices of opposite hand would account satisfactorily for the observed features. In support of this, fig. 18 shows that the loops at A and B have about the same diameter as neighbouring helices, suggesting that they have been formed from similar helices. Another possible mechanism giving rise to rows of loops (also suggested by Bontinck and Amelinckx) is the interaction of helical dislocations with screws of opposite sign. The basis of this mechanism is similar to the first but since one of the dislocations is not helical the spacing of the loops is doubled. The screws in this case must be generated after most of the residual screws have climbed into helices. Some evidence in support of this view is available; fig. 2 (*a*) at D and E shows long straight dislocation lines which seem to have interacted with helices like screws of opposite Burgers vector.

An example of the second type of distribution of loops (bands of loops) is seen in fig. 19. These regions show loops of the type observed by Hirsch *et al.* (1958 b) in quenched aluminium, but whereas in the latter case loops were observed to be uniformly distributed in the interior of grains, the distribution of loops in the quenched alloy is not uniform. In fact most regions show very few loops (see for example figs. 1 to 6). When small loops are observed in large numbers they appear to occur in bands (fig. 19) or near regions containing helical dislocations (fig. 15). The absence of large numbers of loops in most areas is in marked contrast to aluminium quenched under similar conditions and implies that the nucleation of loops may be a difficult process in the quenched alloy. Figure 19 shows an area where three bands of loops are visible at A, B and C. The normal to the foil in this area is close to [105], so that these bands run parallel to the traces of $(1\bar{1}1)$ slip planes which cut through the foil at an angle close to 45° in this orientation. The width of these bands can therefore be explained if collapsed discs of vacancies have formed on or close to the $(1\bar{1}1)$ plane. In this area 10 bands (all running parallel) were counted in a distance of about 13 μ. The average spacing between bands was about 1 μ, and the loop size about 300 Å or greater. The loops appear to be arranged randomly rather than in rows as in the previous case, and show no tendency to have hexagonal shapes. The projected shapes of the loops in fig. 19 are elongated and different loops appear to be elongated in different directions. This is probably due to the fact that the loops lie on inclined planes. Assuming that the loops are roughly circular in shape and that they lie in planes perpendicular to the [110] directions, this elongation in different directions suggests that the loops may have different Burgers vectors. For example some of the loops in fig. 19 may have [011] Burgers vectors, i.e. parallel to the axis of the helix at A; others may have [110] Burgers vectors. The explanation of these bands is not completely understood, but it is felt that they are almost certainly connected with the passage of dislocations along {111} planes, i.e. with slip bands. A possible explanation is that a gliding screw dislocation may collect vacancies during the quench which condense to form a single turn. The screw dislocation may then be pulled away leaving behind a closed loop. This explanation is consistent with the above suggestion that the loops have both [011] and [110] Burgers vectors since both these directions are possible Burgers vectors of dislocations gliding in $(1\bar{1}1)$. Such loops might act as nuclei for further vacancy condensation and might nucleate new loops in neighbouring regions. The details of this mechanism are however not clear at present. It is also important to note that there is very little evidence for the presence of dislocation lines other than loops in the bands of fig. 19. This is taken to mean that in this area the loops are nucleated by something left behind by the gliding dislocations. Other areas have been observed containing complex arrangements of helical dislocations and also many small loops (e.g. fig. 15 and fig. 20 at A). These may be regions of slip bands containing gliding dislocations which have become helical. All these micrographs suggest that there is a strong tendency for collapsed discs of vacancies to nucleate in the slip bands.

Some loops have been observed in the interior of grains away from slip bands and helical dislocations. Figure 20 shows a typical example; at B the loops are few in number and as large as $0{\cdot}4\,\mu$ in diameter. It is very striking to compare the dimensions of the loops near B in fig. 20 and those near the helical dislocations at A on the same micrograph. All these observations seem to point towards an increased difficulty of nucleating loops in the alloy as compared with quenched aluminium. In the interior of grains away from slip bands few centres of nucleation (if any) are formed. The loops are therefore large and few in number. Appreciable nucleation of loops appears to occur only in the neighbourhood of slip bands.

§ 4. DISCUSSION

The observations have shown that helical dislocations are produced by climb of screw dislocations in quenched Al-4% Cu alloys, and that their properties are as predicted by previous workers (Bontinck and Amelinckx 1957, Bontinck 1957, Amelinckx *et al.* 1957). The only difference between these new observations and those of the latter workers on fluorite crystals appears to be in the scale of the arrangement. The geometry of the helices and their modes of interaction with each other and with other dislocations to produce intertwined helices and loops all confirm the dislocation theory in detail. The dislocation rings emitted by sources during quenching seem to be very elongated with long screw components; this elongation is probably due to the fact that the screws climb rapidly into helices and become stuck. It also appears that vacancies can condense into dislocation loops (other than those formed by interaction of helices), and that the nucleation of small loops occurs relatively easily near certain bands, which are tentatively identified as slip bands, and appears to be difficult in most other regions.

As regards the vacancy concentration required to produce the observed climb in specimens quenched from 540°C, the average value obtained ($\sim 3 \times 10^{-5}$) appears to be somewhat lower than in aluminium quenched from the same temperature ($\sim 10^{-4}$, Silcox, private communication), and lower than the value for the equilibrium concentration of vacancies at 540°C in pure aluminium ($\sim 1{\cdot}5 \times 10^{-4}$) determined by Bradshaw and Pearson (1957) from resistivity measurements. The value obtained for specimens quenched from 440°C ($\sim 2 \times 10^{-6}$) is considerably lower than the equilibrium concentration at 440°C calculated from the formula of Bradshaw and Pearson for pure aluminium ($\sim 3{\cdot}5 \times 10^{-5}$). Assuming that the vacancy concentration is the same in Al-4% Cu and Al at the same temperature, this seems to suggest that not all of the vacancies in equilibrium at high temperatures are able to migrate to dislocations after quenching, particularly after quenching from the lower temperature 440°C, and that a considerable fraction of them may still be in solution. Although our estimates of vacancy concentration required to produce the observed climb are only preliminary and rather approximate, it is felt that if in error they would represent an overestimate of true concentration. Thus some of the vacancies may possibly remain 'quenched-in'. This observation is in general agreement with the interpretation of electrical resistivity measurements of Panseri *et al.* (1958) on Al–Mg alloys of various compositions quenched from 550°C. These authors found that a concentration of magnesium as low as 0·13 at. % was sufficient to suppress almost completely the annealing out at room temperature of the 'quenched-in' resistivity due to vacancies which occurs in pure aluminium (Wintenberger 1957), and they suggest that this is strong evidence for most of the vacancies remaining in solution, possibly associated with solute atoms. Similar effects may be expected to occur in aluminium copper alloys, and 'quenched-in' vacancies are presumably responsible for the observed kinetics of zone formation in the alloys as suggested by Federighi (1958) and DeSorbo *et al.* (1958).

If a large fraction of vacancies remains in solution, this raises the interesting question of when the helices are formed during the quench. Weertman's theory (1957) applies only to helices in equilibrium with a supersaturation of vacancies, and the conditions occurring during quenching are probably far from equilibrium conditions. It is possible that the observed helices may represent an approach towards equilibrium for some supersaturation conditions existing at a relatively high temperature during the quench, where vacancies are sufficiently mobile, and that these helices are 'frozen-in' at the lower temperatures. The pitch and radius of a helical dislocation would therefore be expected to depend not only on quenching temperature but also on quenching rate. Thus the poorly defined helices of small radius (fig. 7) observed in material quenched from 440°c may possibly be produced by quenching conditions in which the alloy does not remain at a high enough temperature for a sufficiently long time for appreciable climb of the dislocations to occur. The majority of the vacancies in this case are probably still in solution. It is interesting to note that Bradshaw and Pearson (1957) estimate a transition temperature of 470°c for aluminium above which not all the vacancies can be retained during the quench. Vacancies lost during the quench may be responsible for most of the climb observed in the alloy. Association with solute atoms probably prevents these 'lost' vacancies from nucleating loops homogeneously during the quench so that climb of dislocations is favoured preferentially. However, these remarks are rather speculative at present, and further experiments on the dependence of pitch and radius of the helices on quenching temperature are in progress.

One of the features of the observations which is not understood at present is the origin of the large number of screw dislocations in the quenched alloys. It is not known for example whether most of these dislocations are produced by quenching strains, or whether they have remained in the metal even after annealing at 540°c. Some preliminary observations on furnace cooled specimens have shown an appreciable dislocation density suggesting that not all the dislocations are produced by quenching strains. There is also a marked difference in dislocation arrangement between quenched Al-4% Cu alloy, which shows mainly helices, and quenched aluminium (Hirsch *et al*. 1958 b), which shows mainly loops. This is probably due to a higher residual dislocation density in the alloy and to the increased difficulty in nucleating loops as compared with pure aluminium. Evidence on the dependence of quenching effects on the concentration of copper in alloys of various compositions might also be useful in this context.

It is also interesting to consider the results in relation to certain precipitation phenomena. It is well known from the results of several workers (Fink and Smith 1938, Gayler 1940, Castaing and Guinier 1949, Castaing 1949) that precipitation of the θ' phase in Al-4% Cu alloys occurs preferentially at grain boundaries and slip bands, and at dislocations (Thomas and Nutting 1955, Wilsdorf and Kuhlmann-Wilsdorf 1955). The stress field around a dislocation of mainly edge character can be partially relaxed by segregation of smaller copper atoms to regions of compression. The higher concentration of solute atoms in the neighbourhood of edge dislocations would therefore be expected to produce preferential precipitation in these regions. The behaviour near a screw dislocation is not so clear since no dilatation occurs to the first order. However, as the observations have shown, screw dislocations in quenched material are rapidly converted into helices in which the segments of dislocation line have mainly edge character. Thus it seems very likely that precipitation would occur preferentially on these helices, and this may be the explanation of some of the precipitate patterns which have been observed (Thomas and Nutting 1955, Wilsdorf and Kuhlmann-Wilsdorf 1955). The results also show that precipitation in slip bands is to be expected since as we have seen these bands contain helical dislocations and (or) closed loops of mainly edge character.

Moreover, Seitz (1952) has suggested that the movement of copper atoms to precipitates during ageing is aided by formation of vacancy-copper atom pairs; this same mechanism has been invoked by Thomas (1959) to explain preferential precipitation at dislocations and the locking of dislocations in certain Al–Mg–Zn alloys. Thus the vacancies responsible for climb should also be effective in transporting copper atoms to the dislocations and in providing nuclei for further precipitation. Locking by segregation of copper atoms may also account for the very stable character of the helices; no movement of helical dislocations has ever been observed in the microscope. This certainly is an attractive hypothesis and requires further investigation. Experiments are now in progress to observe precipitation at dislocations directly in the thin foils.

ACKNOWLEDGMENTS

The authors are indebted to Professor N. F. Mott, F.R.S., Professor A. H. Cottrell, F.R.S., and Dr. W. H. Taylor for their interest and encouragement, to them and to Dr. P. B. Hirsch and Dr. J. Nutting for much valuable advice. Thanks are also due to several of our colleagues, to Professor F. C. Frank, F.R.S., and to Dr. J. W. Mitchell, F.R.S., for useful discussions. Acknowledgments for financial support are due to an I.C.I. Fellowship (G. T.) and to a D.S.I.R. Research Fellowship (M. J. W.).

REFERENCES

AMELINCKX, S., BONTINCK, W., DEKEYSER, W., and SEITZ, F., 1957, *Phil. Mag.*, **2,** 355.

BARBER, D. J., HARVEY, K. B., and MITCHELL, J. W., 1957, *Phil. Mag.*, **2,** 704.

BONTINCK, W., 1957, *Phil. Mag.*, **2,** 561.

BONTINCK, W., and AMELINCKX, S., 1957, *Phil. Mag.*, **2,** 94.

BRADSHAW, F. J., and PEARSON, S., 1957, *Phil. Mag.*, **2,** 570.

BROOM, T., and HAM, R. K., 1957, *Institute of Metals Monograph and Report Series* No. 23, p. 41.

CASTAING, R., 1949, *Compt. rend.*, **228,** 1341.

CASTAING, R., and GUINIER, A., 1949, *Compt. rend.*, **228,** 2033.

COTTRELL, A. H., 1957, *Institute of Metals Monograph and Report Series* No. 23, p. 1.

COULOMB, P., and FRIEDEL, J., 1957, *Report of Lake Placid Conference on Dislocations and Mechanical Properties of Crystals* (New York : Wiley and Sons), p. 555.

DASH, W. C., 1958, *Report of Cooperstown Conference on Growth and Perfection of Crystals* (New York : Wiley and Sons), p. 361.

DESORBO, W., TREAFTIS, H. N., and TURNBULL, D., 1958, *Acta Met.*, **6,** 401.

FEDERIGHI, T., 1958, *Acta Met.*, **6,** 379.

FINK, W. L., and SMITH, D. W., 1938, *Trans. Amer. Inst. min. (metall.) Engrs*, **128,** 223.

GAYLER, M. L. V., 1940, *J. Inst. Met.*, **66,** 72.

HIRSCH, P. B., and SILCOX, J., 1958, *Report of the Cooperstown Conference on Growth and Perfection of Crystals* (New York : Wiley and Sons), p. 262.

HIRSCH, P. B., HOWIE, A., and WHELAN, M. J., 1958 a, *Report of Fourth International Conference on Electron Microscopy, Berlin* (in the press).

HIRSCH, P. B., SILCOX, J., SMALLMAN, R. E., and WESTMACOTT, K. H., 1958 b, *Phil. Mag.*, **3,** 897.

JONES, D. A., and MITCHELL, J. W., 1958, *Phil. Mag.*, **3,** 1.

KIMURA, H., MADDIN, R., and KUHLMANN-WILSDORF, D., 1958 a, *Acta. Met.* (in the press); 1958 b, *J. Metals*, **10,** 93; 1958 c, *Bull. Amer. phys. Soc.*, **3,** 122.

KUHLMANN-WILSDORF, D., 1958, *Phil. Mag.*, **3,** 125.

KUHLMANN-WILSDORF, D., MADDIN, R., and KIMURA, H., 1958, *Z. Metallk.*, **49,** 584.

MADDIN, R., KIMURA, H., and KUHLMANN-WILSDORF, D., 1958, *Bull. Amer. phys. Soc.*, **3,** 125.

NICHOLSON, R. B., THOMAS, G., and NUTTING, J., 1958, *Brit. J. appl. Phys.*, **9,** 23.

PANSERI, C., GATTO, F., and FEDERIGHI, T., 1958, *Acta. Met.*, **6,** 198.

SEITZ, F., 1952, *Advanc. Phys.*, **1,** 43.

SILCOX, J., and HIRSCH, P. B., 1959, *Phil. Mag.*, **4,** 72.

THOMAS, G., 1959, *Phil. Mag.* (in the press).

THOMAS, G., and NUTTING, J., 1955, *Institute of Metals Monograph and Report Series* No. 18, p. 57.

TWEET, A. G., 1958, *J. appl. Phys.*, **29,** 1520.

WEERTMAN, W., 1957, *Phys. Rev.*, 107, 1259.

WILSDORF, H., and KUHLMANN-WILSDORF, D., 1955, *Report of the Conference on Defects in Crystalline Solids* (London : Physical Society), p. 175.

WINTENBERGER, M., 1957, *Rev. Métall.*, **54,** 942.

CORRESPONDENCE

Some New Yield Phenomena in Molybdenum

By A. A. Johnson and D. E. Peacock
Physical Metallurgy Department, Imperial College, London, S.W.7

[Received December 2, 1958]

Yield points in molybdenum have been observed by many workers (e.g. Johnson 1959) but so far no studies of strain ageing have been reported. The work described in this letter was undertaken as a preliminary survey of strain ageing in this metal and has revealed two yield phenomena, unconnected with strain ageing, not previously reported for a polycrystalline metal.

A one-quarter inch diameter rod of molybdenum was prepared from an arc-cast ingot by rolling and swaging, with suitable intermediate annealing treatments. The final swaging operation gave a reduction in area of about 90%. The main interstitial impurities were carbon ($\sim 0{\cdot}008\%$), nitrogen ($\sim 0{\cdot}003\%$) and oxygen ($< 0{\cdot}001\%$). The rod was machined into twenty tensile test pieces of gauge length 0·75 in. and diameter 0·1 in. which were recrystallized by annealing in an argon atmosphere at about 1250°c for one hour. The final average grain diameter as determined by the linear intercept method on a transverse section was 0·03 mm. The tensile tests were carried out on a Hounsfield tensometer modified to give a constant strain rate of $0{\cdot}88 \times 10^{-4}\,\mathrm{sec}^{-1}$. The specimens were prestrained to just beyond the Lüders strain region, removed from the tensometer, annealed for one hour at temperatures from 20° to 750°c and then retested. Annealing treatments up to 200°c were carried out in a silicone oil bath maintained to within ±0·1°c of its nominal temperature; above this temperature an argon atmosphere furnace was used that could only be controlled to within ±5°c.

Figure 1 (*a*) shows a typical load-elongation curve obtained during the prestraining treatment and fig. 1 (*b*) that obtained on retesting the same specimen after resting it for one hour at room temperature. Two points should be noted. First, that there is a drop in stress in the middle of the Lüders strain region and, secondly, that there is a step in the curve on retesting. The Lüders strain anomaly was observed in every specimen although its position and shape varied. The step observed on retesting was insensitive to annealing temperature and a further experiment in which the rest period was restricted to about 20 sec at room temperature gave a similar result. A yield point reappeared after annealing at 570°c and above and the yield drop increased in magnitude with the annealing

Fig. 1

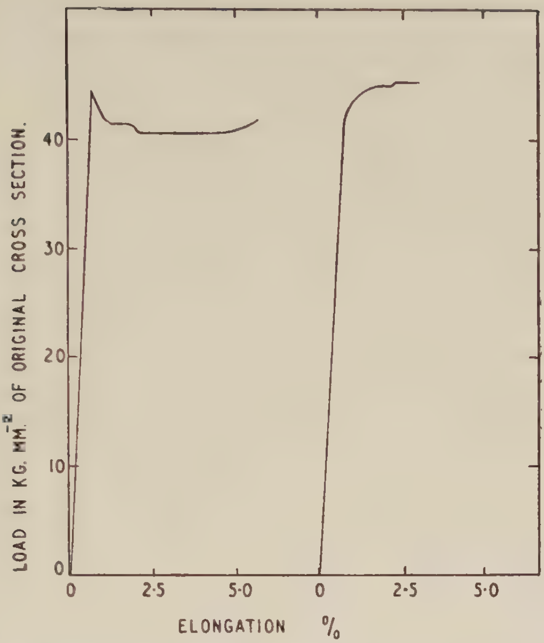

(*a*) A typical load–elongation curve obtained whilst prestraining a recrystallized tensile specimen at room temperature.

(*b*) A load–elongation curve for the same specimen obtained by retesting after removing the stress and resting for one hour at room temperature.

Fig. 2

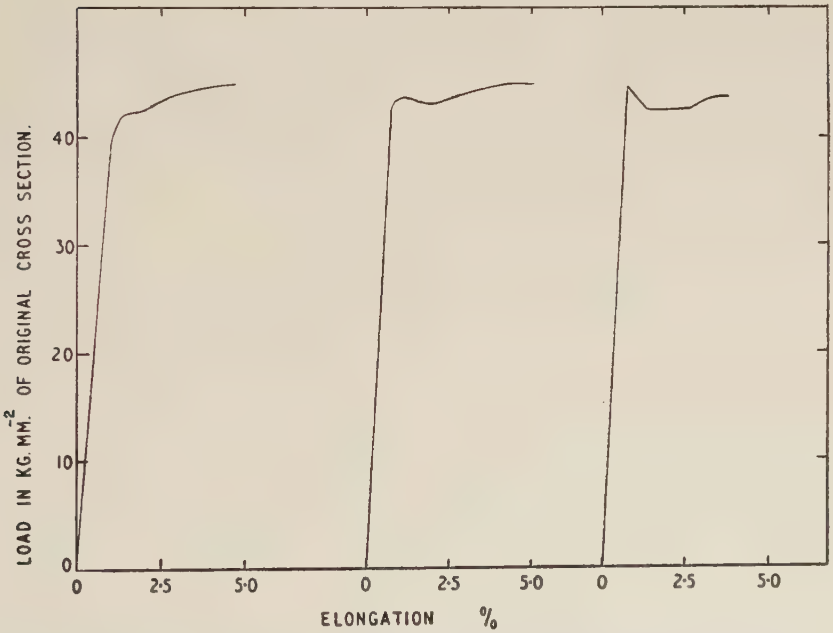

Load–elongation curves for three specimens retested after prestraining and annealing at (*a*) 535°, (*b*) 570° and (*c*) 640°c.

temperature. The fall in stress during the Lüders elongation did not return at any temperature up to 750°c but was observed in specimens which had been recrystallized by annealing at 1250°c for one hour. Load–elongation curves for three specimens retested after prestraining and annealing at 535°, 570° and 640°c are shown in fig. 2.

In order to explain the fall in stress observed in the Lüders strain region, we suggest that during the first part of the Lüders elongation dislocation pile-ups occur at sub-grain boundaries and the strain is propagated from one sub-grain to the next and where necessary across grain boundaries. This is followed by the collapse of the sub-grain boundaries and a further propagation of strain through the specimen as larger pile-ups are produced in the longer lengths of slip plane made available. It might be expected that an increase in stress would be observed before the collapse of the sub-grain boundaries and in fact a small increase was observed in several cases. Alternatively the effect could be explained by supposing that during the Lüders elongation a second Lüders band starts from the opposite end of the specimen causing the stress required to maintain the same strain rate to fall. At the moment we cannot offer a satisfactory explanation for the stepped load–elongation curves, neither can we attribute the return of the yield point to any specific impurity. It seems unlikely that the step is the result of an ageing process and it presumably arises from the locking of dislocations by some intersection mechanism on unloading. It is interesting to note that, because molybdenum has a body-centred cubic structure, this locking must be due to something other than the Cottrell–Lomer barriers which Makin (1958) invokes to explain unloading effects in copper single crystals.

ACKNOWLEDGMENTS

The writers are indebted to Mr. D. O. Pickman of A.R.D.E., Woolwich, for supplying and fabricating the molybdenum and arranging for its analysis and to Professor J. G. Ball for his continual interest and encouragement. The work was performed whilst one of us (A.A.J.) held a London University I.C.I. Research Fellowship and the other (D.E.P.) a D.S.I.R. Research Studentship.

REFERENCES

JOHNSON, A. A., 1959, *Phil. Mag.*, **4,** 194.
MAKIN, M. J., 1958, *Phil. Mag.*, **3,** 287.

The Direct Observation of Metallic Surfaces in the Electron Microscope

By K. THOMAS and K. F. HALE
Communication from the National Physical Laboratory,
Teddington, Middlesex

[Received December 4, 1958]

IN the usual method of thinning metallic test-pieces by electrolytic polishing for investigation of their structure by transmission in the electron microscope (Tomlinson 1958), the specimen is coated with varnish leaving a 'window' on both sides of the foil. For the present work this has been modified by leaving a window on one side only, so that on polishing one surface is preserved. The varnish is then dissolved away.

The surface detail which is retained aids the interpretation of dislocation arrays in deformed material. In stainless steel extended 2%, rows of dislocations similar to those found in rolled material (Whelan, Hirsch and Horne 1957) may now often be seen associated with a permanently visible trace (fig. 1, Pl. 67). The traces may be shown by electron diffraction to correspond to the intersection of a (111) slip plane with the surface of the specimen. They appear at one end only of the dislocations, that is, on one surface. Thus they show where slip planes intersect the preserved surface. The slip traces visible in fig. 1 help to determine that this is a case of slip in two (111) planes, the planes being roughly parallel and perpendicular to the surface. It may be noted that not all traces show associated dislocations, for example fig. 2 (Pl. 67), where a (111) plane is approximately parallel to the surface.

Surface effects may be of particular importance in the case of fatigue, and a comparative investigation is being made of tensile and fatigue specimens. In aluminium coarse slip traces may be observed, in for example a specimen fatigued for 5×10^5 cycles (approximately half the fatigue life) at 135 ± 120 Kg/cm^2. However, of the dislocations observed in these foils, none have yet been found associated with the slip traces. This may be because of the mobility of dislocations in aluminium, and further metals are being studied.

Figure 3 (Pl. 68) illustrates another application of the technique, showing crystallographic growths on the surface of a 0·0025 cm foil of heavily rolled spectroscopically pure aluminium annealed *in vacuo* ($\sim 10^{-4}$ mm) for six hours. There is a tendency for the shape to be hexagonal (initially triangular) on a (111) surface, and square on a (100) surface. The fringes observable within some of the growth outlines (fig. 4, Pl. 68) are presumably moiré patterns (Bassett *et al.* 1958) due to misorientation between the substrate and growth lattices, and give an indication of the imperfections present (probably in the substrate). Here the fringes are parallel to the ⟨112⟩ intersection of (110) planes with the near (111) surface. Dislocations are visible for example along the direction of the arrows. These growths may be similar to the larger crystallographic platelets observed optically by Forsyth *et al.* (1958) on the surface of Al–Mg alloys annealed *in vacuo*, and are being further investigated. The possible effects of vacuum annealing on the fatigue properties of test-pieces must clearly be considered.

This technique could be applied to many investigations. Structural changes with distance from the surface could be studied by reducing one surface of test-pieces by varying amounts, and then completing the thinning from the opposite side.

ACKNOWLEDGMENT

The work described above has been carried out as part of the General Research Programme of the National Physical Laboratory, and this paper is published by permission of the Director of the Laboratory.

REFERENCES

BASSETT, G. A., MENTER, J. W., and PASHLEY, D. W., 1958, *Proc. roy. Soc.* A, **246**, 345.

FORSYTH, P. J. E., PARTRIDGE, P. G., and RYDER, D. A., 1959, *Phil. Mag.*, **4**, 447.

TOMLINSON, H. M., 1958, *Phil. Mag.*, **3**, 867.

WHELAN, M. J., HIRSCH, P. B., and HORNE, R. W., 1957, *Proc. roy. Soc.* A, **240**, 524.

REVIEWS OF BOOKS

Elementary Statistical Physics. By C. Kittel. (New York: John Wiley & Sons, Inc.) [Pp. 228.] 64*s.*

A few years ago Professor Kittel wrote a textbook on solid state physics which has been a great success and has served to define a syllabus of what every physicist ought to know in that particular branch of the subject. His new textbook shows the same ambitious scope in introducing fresh topics to students; he discusses, for example, the Wiener–Khintchine theorem, the Onsager reciprocal relations, the Boltzmann transport equation, and the Kramers–Kronig relations. It may be stretching a point to label these 'statistical physics', let alone 'elementary statistical physics', but they are undoubtedly interesting and significant topics. At the same time he aims to expound the basic principles of statistical mechanics, using the Gibbs method, up to a level sufficiently advanced for most non-specialists. His discussion of some of these principles—of the concept of phase space and Liouville's theorem, for example, or of indistinguishability in quantum mechanics and the range of application of Fermi–Dirac and Bose–Einstein statistics—could be criticized; on the other hand the way in which he introduces entropy at a very early stage and identifies it subsequently with the thermodynamic parameter is elegant and convincing. Altogether the book could be of considerable value if used in the manner that its author probably intended, i.e. to supplement a rather detailed course of lectures or for later reference by a research student wanting to clear his mind about particular points. It is hardly suitable, however, for an undergraduate who knows little of the subject beforehand, because there is not enough argument in words to accompany the neat mathematical development. Moreover, the 45 sections that compose the book are often inadequately linked, so that it is difficult to read consecutively, particularly towards the end.

T. E. F.

Kinetic Theory of Gases. By R. D. Present. (New York: McGraw-Hill Book Co., Inc.) [Pp. 280.] 60*s.*

This is a substantial textbook, intended for the final year of an honours course in physics. It concerns kinetic theory only, no space being devoted to statistical mechanics. This restriction may be regretted, since so many of the interesting topics in kinetic theory, such as the Maxwell Distribution Law or Brownian Motion, can be analysed so much more powerfully by statistical methods. It is clear, however, that the author is primarily interested in transport theory and he goes into this branch of the subject in considerable detail, criticizing the traditional mean free path method and developing an alternative approach based on considerations of momentum transfer. The book contains some interesting material, but it is a trifle heavy-handed in style. Kinetic theory arguments can usually be presented in very simple terms, if all that is aimed at is a vivid understanding of the physical principles involved, and numerical exactitude is not required. Otherwise they can be discussed rigorously, which requires laborious and tedious mathematics. Professor Present is inclined to strike an unhappy mean between these two extremes.

T. E. F.

Statistical Physics. By L. D. Landau and E. M. Lifshitz, translated by E. Peierls and R. F. Peierls. (London: Pergamon Press, 1958.) [Pp. 484.] 80*s.*

It is difficult to praise too highly this second volume of the Landau and Lifshitz treatise, which should be on the shelves of every theoretical physicist, and constantly read, both for the wide range of problems and methods which it contains and for the insight it shows into apparently old and worn-out subjects. The translation is perfect, and the format of good quality. There is only one serious defect, which greatly lessens its use as a book of reference: the index is quite inadequate. For example, to find " Onsager relations " one must not look there, or at, say, " Irreversible Processes, Thermodynamics of "; one must guess from " Kinetic coefficients " that this is the subject of § 119. Again, neither " Dispersion relation " nor " Kramers–Kronig relation " is indexed, but only " Susceptibility, generalized ". Also, surely, in a book of this size and standing, we might have something better for the reference to the literature than, say (R. E. Peierls, 1934 and L. Landau, 1937) without chapter, verse, journal, volume, or page. It is almost true that Landau and Lifshitz have said better all that was in the original papers, but the reader should learn to discover that for himself. J. M. Z.

A History of Technology. Volume V. *The Late Nineteenth Century c.* 1850–*c.* 1900. Edited by C. Singer, E. J. Holmyard, A. R. Hall, and T. I. Williams. (Oxford: Clarendon Press, 1958.) [Pp. 888.] 168*s*.

This beautifully produced volume completes the series which is doing so much to stimulate enquiry into the way our material civilization arose. Although we now take for granted many of the inventions which are here described, it is a period still within living memory. It also has its lesson, for there is a clear picture of Britain, the industrial giant of 1850, living on its fat, and falling behind Germany and the United States in technical progress. The failure of the governing élite to appreciate the need for a new scale and style of education, to match the new processes and machines which managers had to instal and workmen to use, has its echoes today.

The problem of presentation is greatest in this volume, for many developments, especially in the older industries, were very technical, and not easily explained in a short essay. Nevertheless, the standard is exceptionally high. The weaknesses, here and there, are not lack of accuracy or clarity but tendencies towards antiquarianism, the urge to describe superficially each separate invention or new model, as if it were an item in a museum collection, instead of concentrating on the problems which the inventors had to face, and the basic solutions which they found. Now that the facts have been established, historians of science must proceed to theories and explanations if they are to make their discipline a part of general knowledge.

One naturally wonders how much ' pure ' science had to do with the progress of the applied arts. The chemical and electrical industries obviously cannot be separated from ' Natural Philosophy '. Civil engineering, also, owed much to theoretical studies by the most distinguished mathematicians of the day (although we note, on p. 492 a familiar situation " Maxwell's treatment [of the loaded chain and arch] was difficult, and probably few engineers read the *Philosophical Magazine* in which it was printed "). One suspects also that the design of prime movers was more influenced by the new science of thermodynamics than is allowed in the text. On the other hand it was to be another half century before many industries—ceramics, glass, rubber, photography, textiles—were to be amenable to the same deliberate planning from sound general theories as was then possible in the production of heavy chemicals and dye stuffs on the construction of railway systems. What then passed for science was very often merely more care in the controls of material and conditions of manufacture, and some empirical experiments in the cookery book manner to find the optimum recipe. J. M. Z.

Statistical Theory of Irreversible Processes. By R. EISENSCHITZ. (Oxford, 1958.) [Pp. 83.] 8*s*. 6*d*.

THE aim of this little book is sound: to give a united account of the theories of dissipative processes in gases, liquids, and solids. Unfortunately, the condensation of a highly mathematical subject into such a small volume is not easy, and has not really succeeded. Whilst the derivation of the formulae for classical gases is fairly complete, and there are useful comments on the status of the theory of viscosity and thermal conductivity in liquids, the sections on quantum statistics are too brief and superficial to be helpful either to beginners or to experts. There are also numerical misprints in the mathematical formulae, and the documentation is inadequate. It would have been better if the author had concentrated on a clear and accurate survey of one topic, or else had written a much larger book. J. M. Z.

Solid State Physics.—Advances in Research and Application, Volume 7. By FREDERICK SEITZ and DAVID TURNBULL. (New York: Academic Press Inc.) [Pp. 525.] Price 96*s*.

THE seventh volume of this invaluable series contains notably a long and exhaustive review by Calloway of the electron band theory in solids and articles by Klemens on lattice thermal conductivity and by Huntington on the elastic constant of crystals. The editors are to be congratulated on the thorough coverage which they continue to give of the subject. N. F. M.

Growth and Perfection of Crystals. Edited by R. H. DOREMUS, B. W. ROBERTS and DAVID TURNBULL. (New York: John Wiley & Sons, Inc., 1959.) [Pp. xviii + 609.] £5.

THIS book, edited by Doremus and other scientists on the staff of the General Electric Laboratories of Schenectady, New York, contains the papers given at a conference in Cooperstown, New York, in August, 1958. The speed of publication is remarkable, and the organizers are warmly to be congratulated on this, as on the quality of the production. The main headings are: Growth of whiskers, properties of whiskers, growth of crystals of the solvent phase, growth of crystals of the solute phase, crystallization of polymus. N. F. M.

Fourier Transforms and X-ray Diffraction. By H. LIPSON and C. A. TAYLOR. (London: G. Bell and Son, 1958.) [Pp. 76.] 18*s*. 6*d*.

THIS book has been written to provide an introduction to Fourier-transform theory that will serve as a basis for those who wish to apply the theory to x-ray diffraction. In the introductory chapter the authors show in a simple way the particular applicability of the Fourier-transform to the problem of the diffraction of x-rays by crystals. A few short chapters are then devoted to developing the more relevant details of the theory of Fourier-transforms; no effort has been made to achieve complete mathematical rigidity, and as a result the text should readily be understood by the average third-year student of Physics. The last part of the book is given over to consideration of some practical applications of the Fourier-transform to problems of x-ray diffraction, and in the appendices the results of calculations made on a hypothetical structure are shown in a large number of diagrams, which illustrate many of the points made in the text.

In addition to providing a very readable introduction for those studying problems of x-ray diffraction for the first time, this book may also serve as a reminder of the essential simplicity of the Fourier-transforms to those who are more familiar with the subject. P. J. B.

BOOK NOTICES

The following reprints have appeared as Dover books:

The Theory of the Properties of Metals and Alloys. By N. F. MOTT, and H. JONES.

Theoretical Mechanics: An Introduction to Mathematical Physics. By J. S. AMES, and F. D. MURNAGHAN.

Statics and the Dynamics of a Particle. By W. D. MACMILLAN.

Vector Analysis with an Introduction to Tensor Analysis. By A. P. WILLS.

Introduction to Bessel Functions. By F. BOWMAN.

The Fundamental Principles of Quantum Mechanics with Elementary Applications. By E. C. KEMBLE.

An Introduction to Fourier Methods and the Laplace Transformation. By P. FRANKLIN.

Quantum Electrodynamics. By J. SCHWINGER.

[*The Editors do not hold themselves responsible for the views expressed by their correspondents.*]

Fig. 1

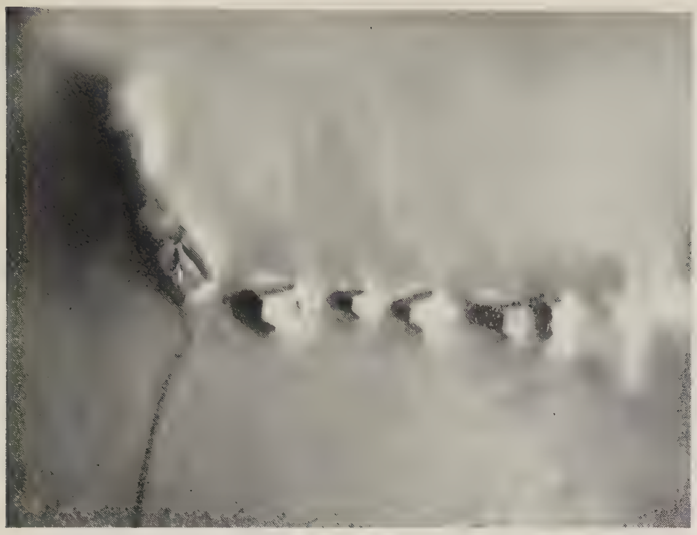

Crystallites formed above the eutectic temperature (×500).

Fig. 2

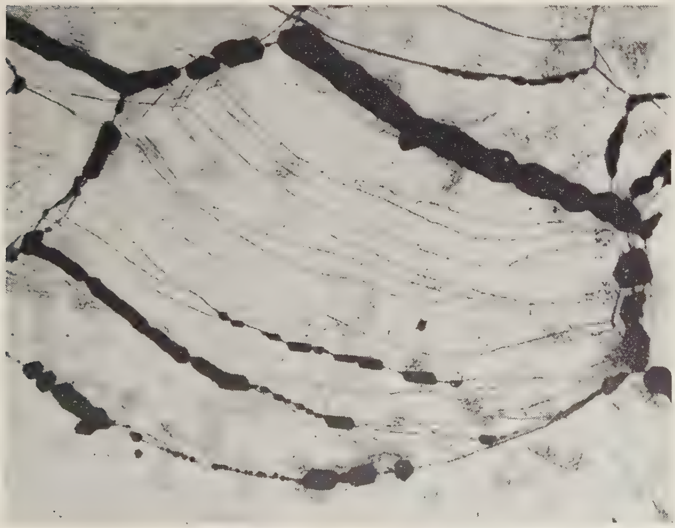

Boundary migration and crystallites (×100).

Fig. 3

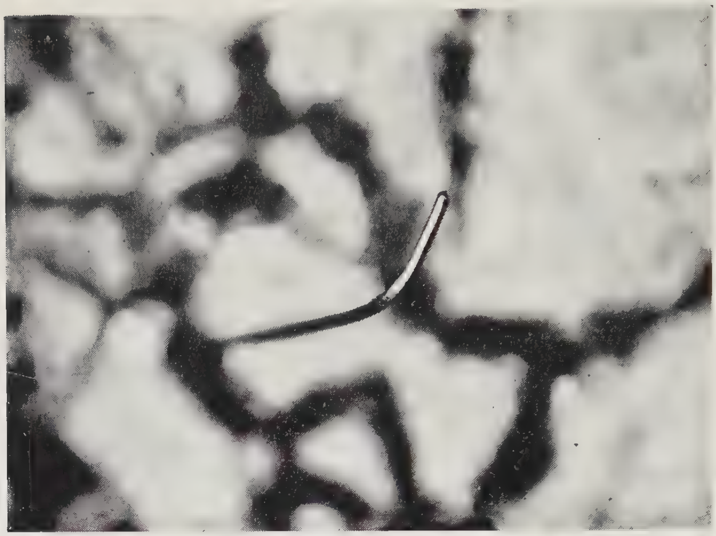

Whisker growths occurring just below the solidus temperature (×100).

Fig. 4

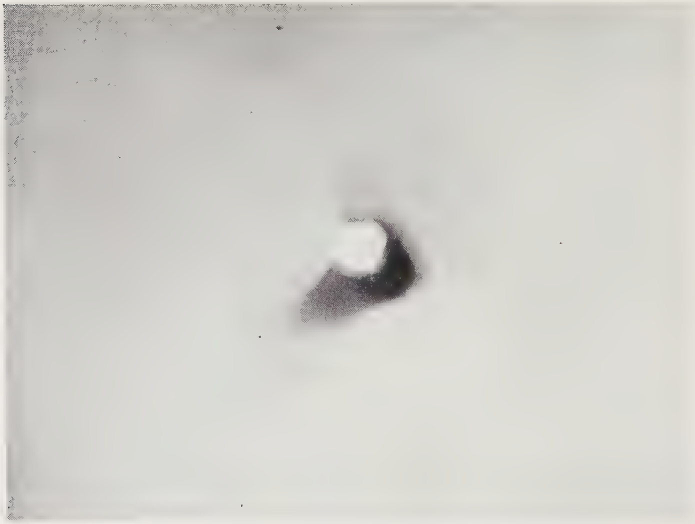

Crystal facet on tip of whisker formed just below the solidus temperature (×2500).

Fig. 5

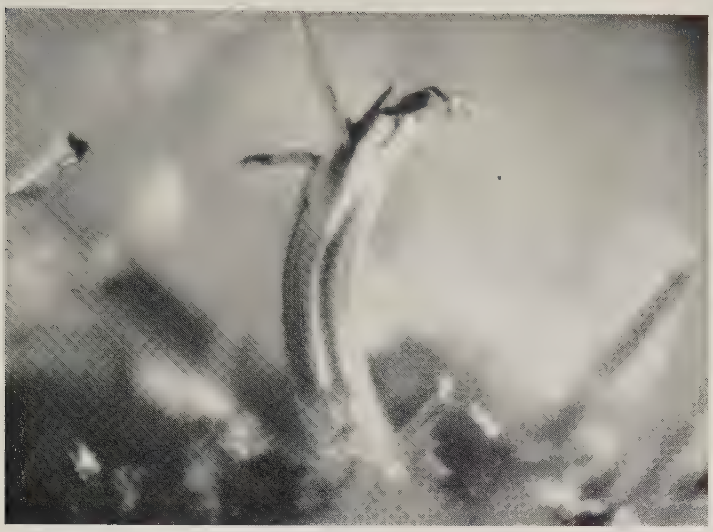

Branched whisker grown above solidus temperature (×50).

Fig. 6

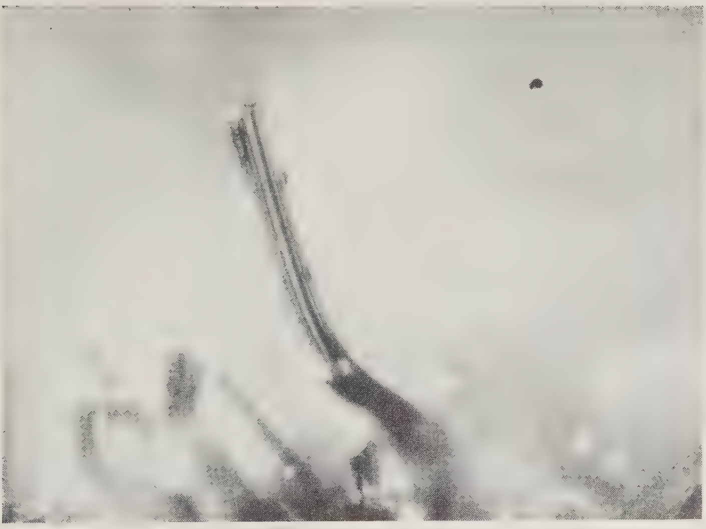

Whisker grown above solidus temperature showing fluted construction (×50).

Fig. 1

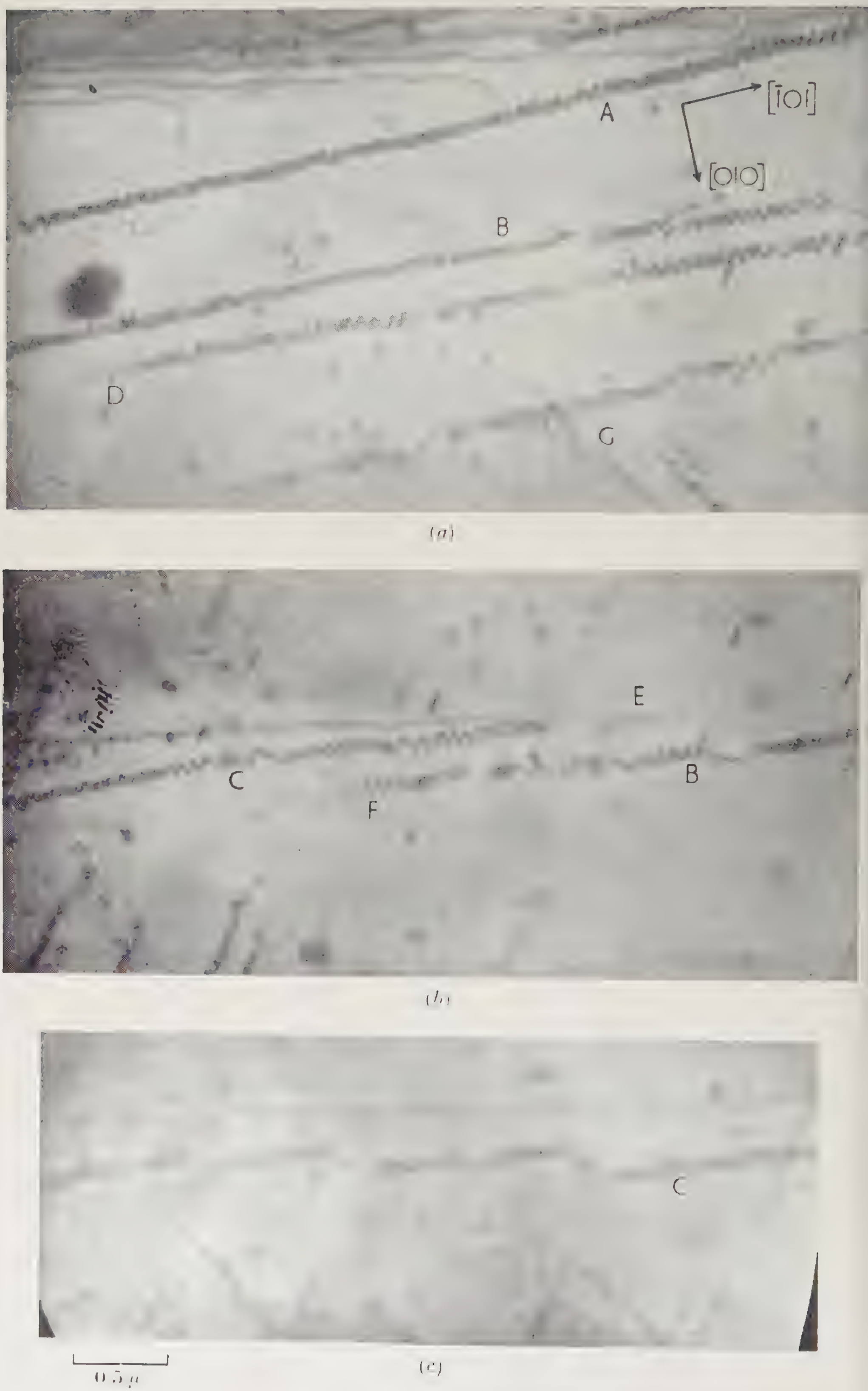

(a)

(b)

(c)

Fig. 2

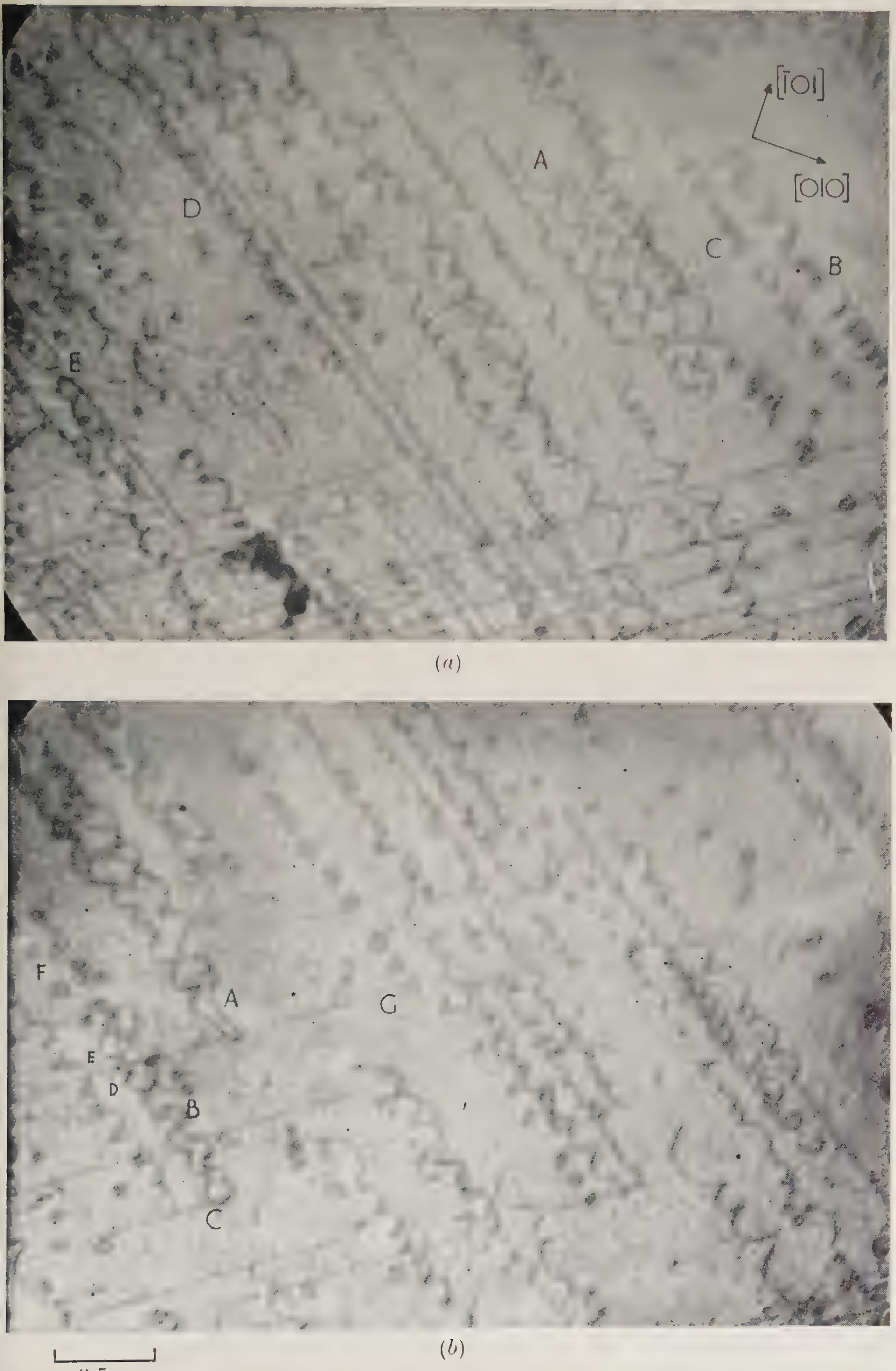

(a)

(b)

Fig. 3

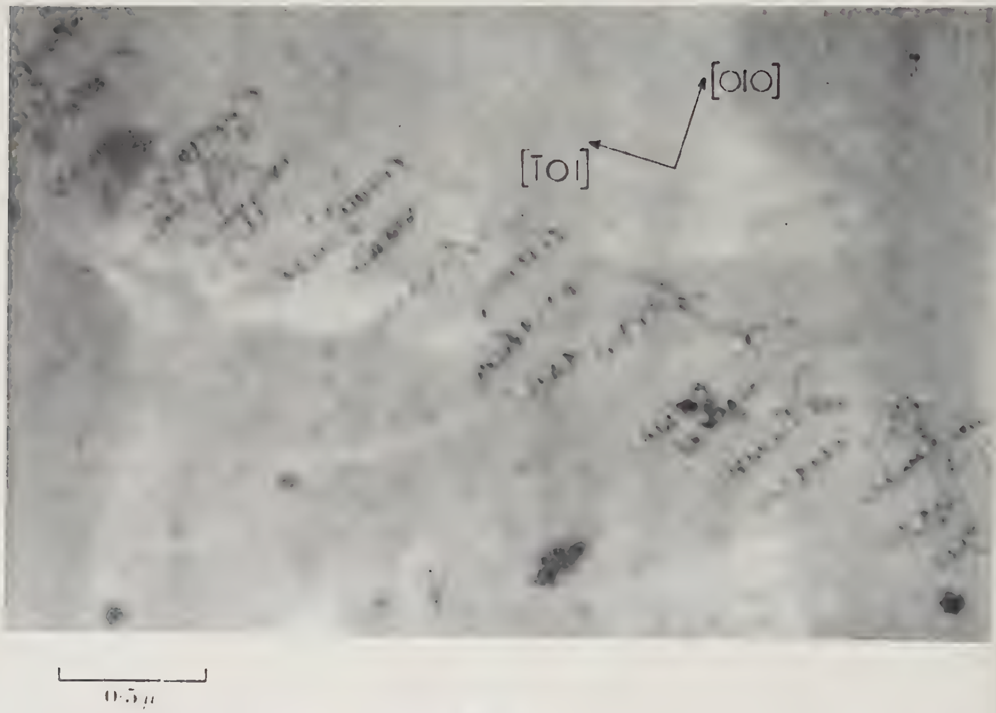

Fig. 4

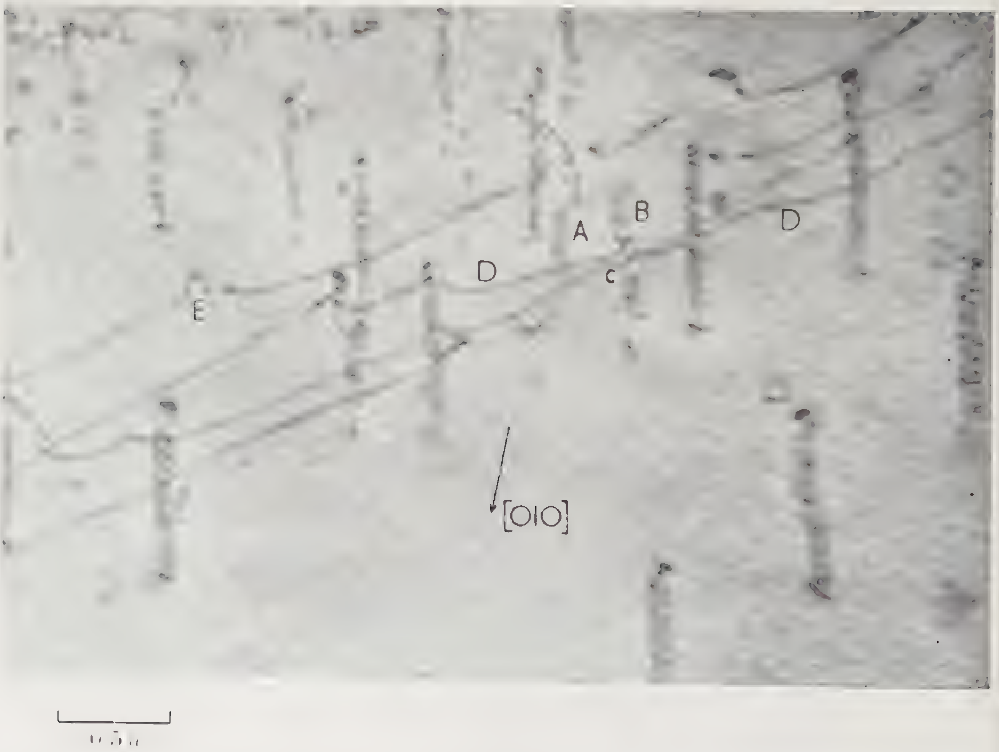

Fig. 5

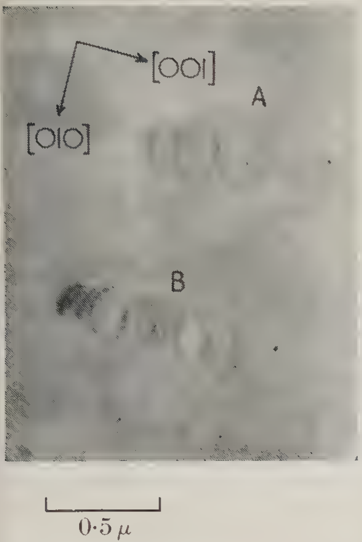

Fig. 6

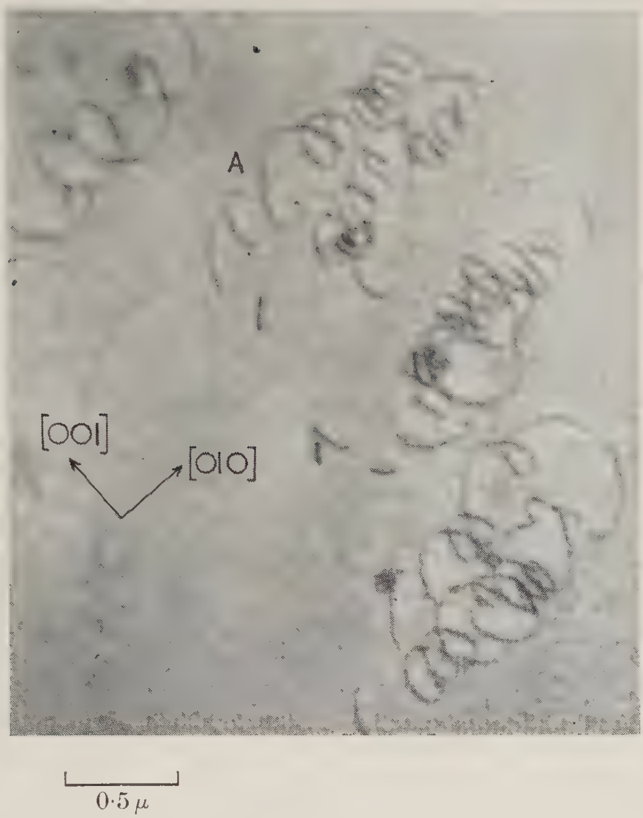

Fig. 7

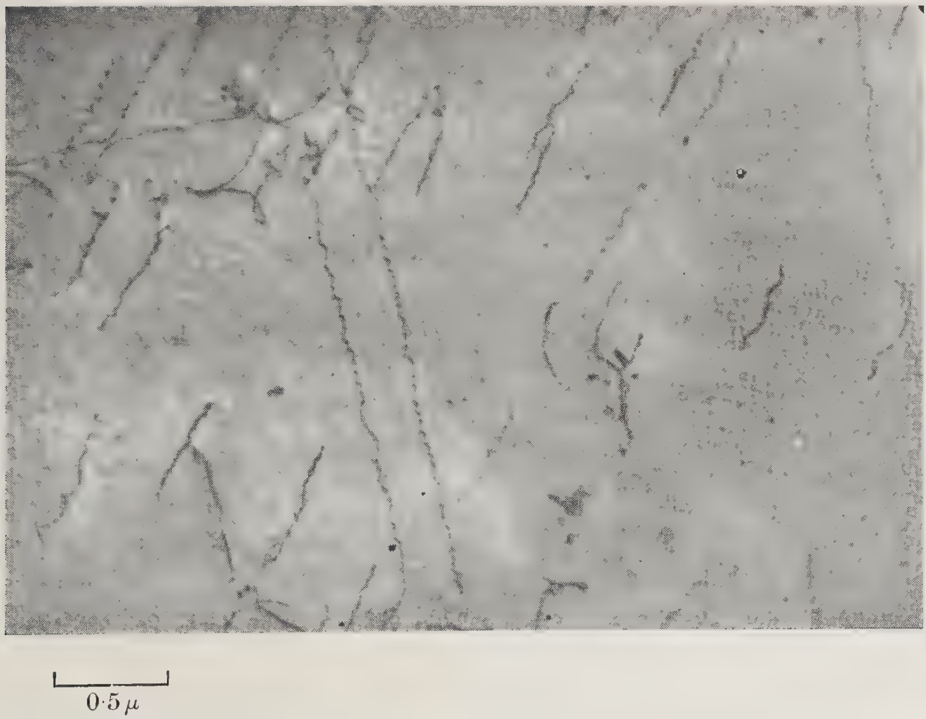

Fig. 10

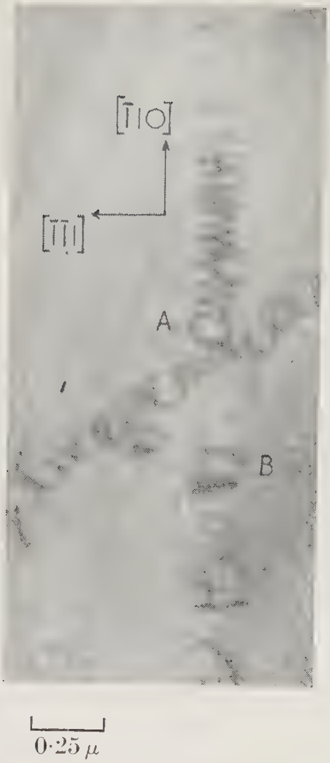

Fig. 11

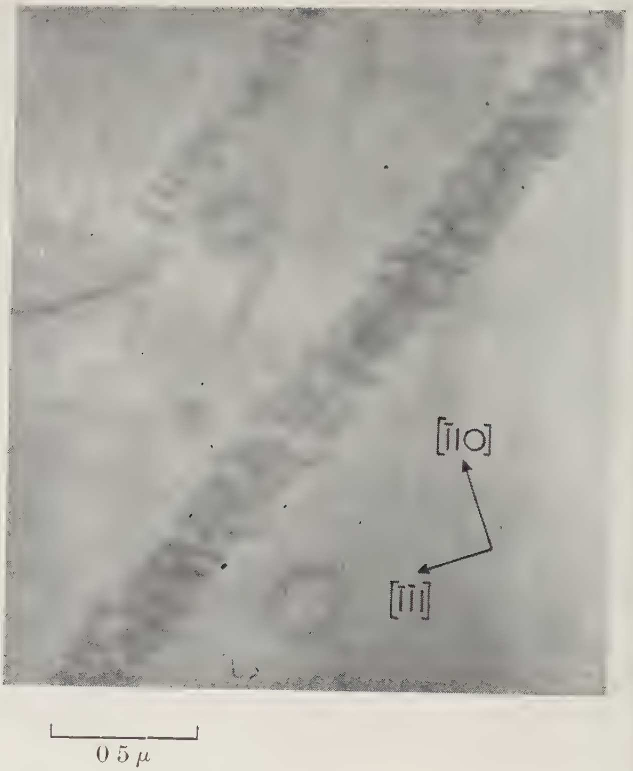

Fig. 14

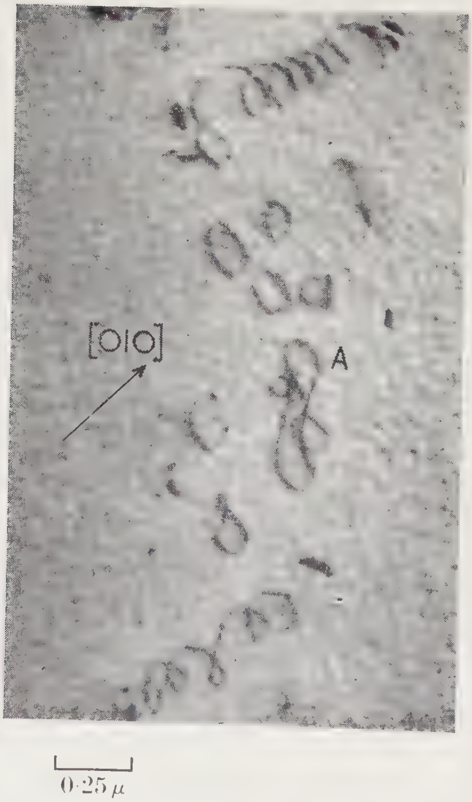

Fig. 16

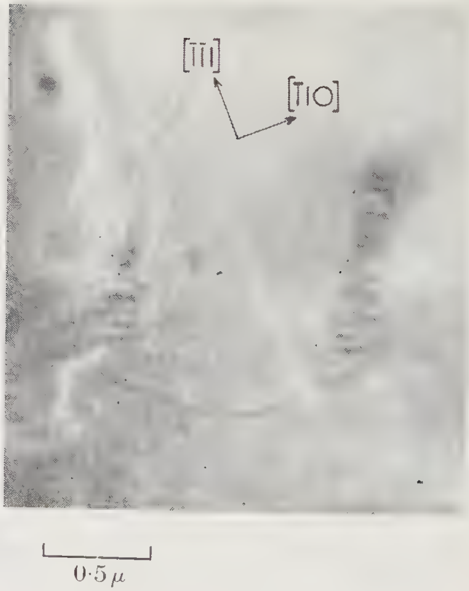

Fig. 15

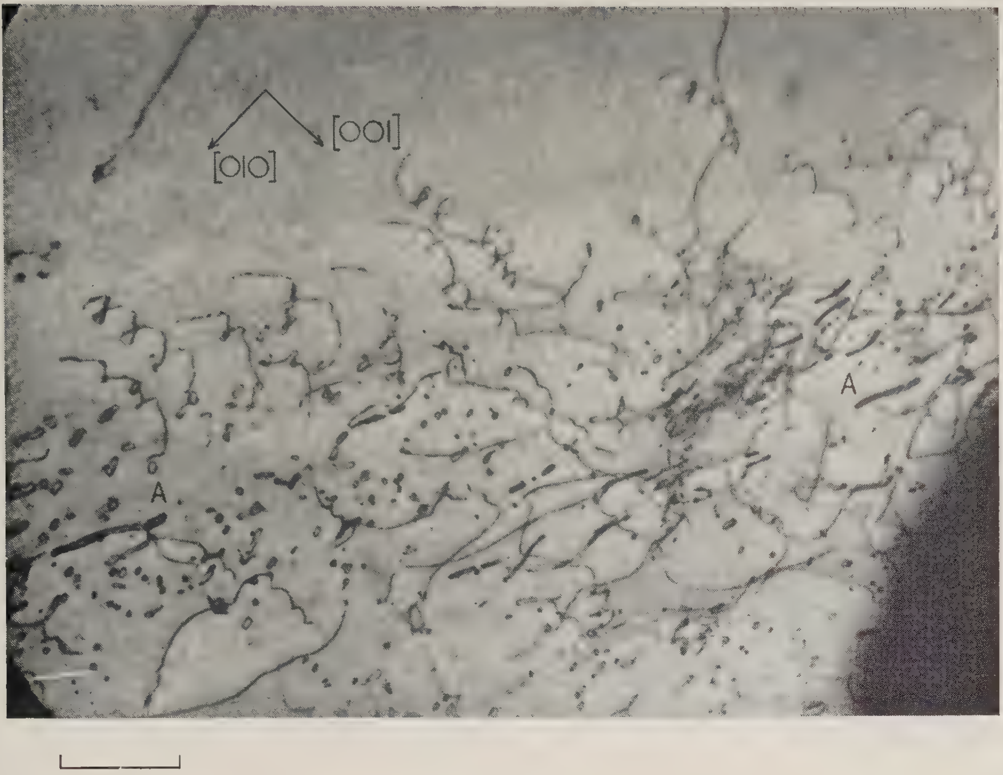

Fig. 18

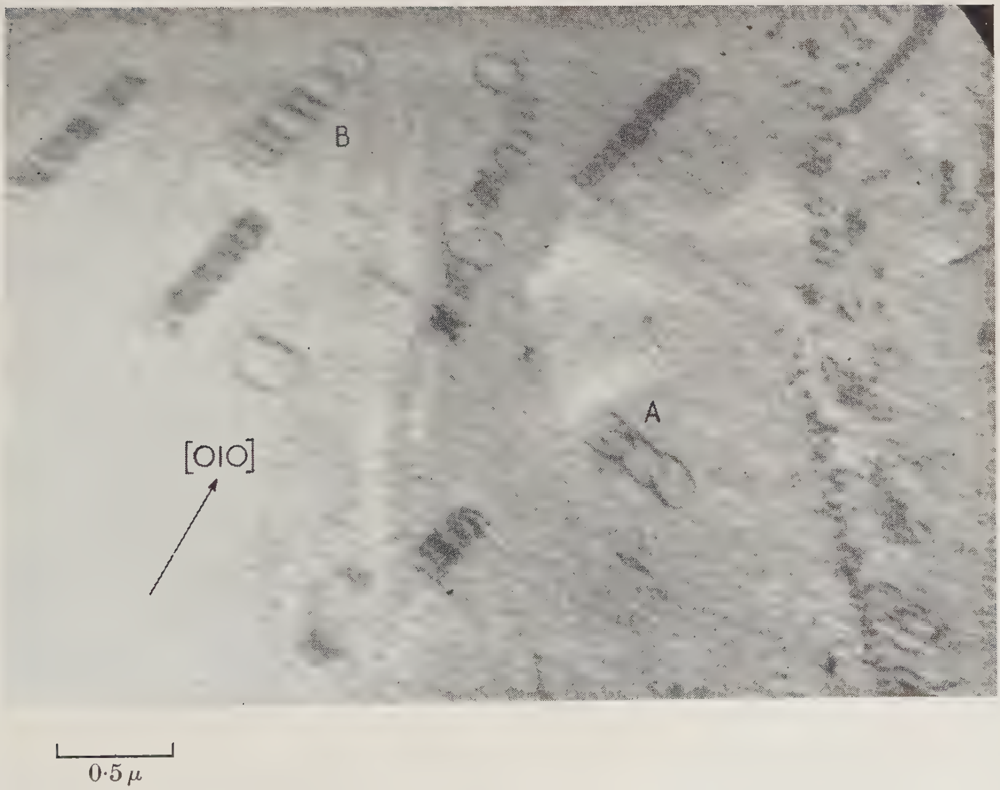

Fig. 19

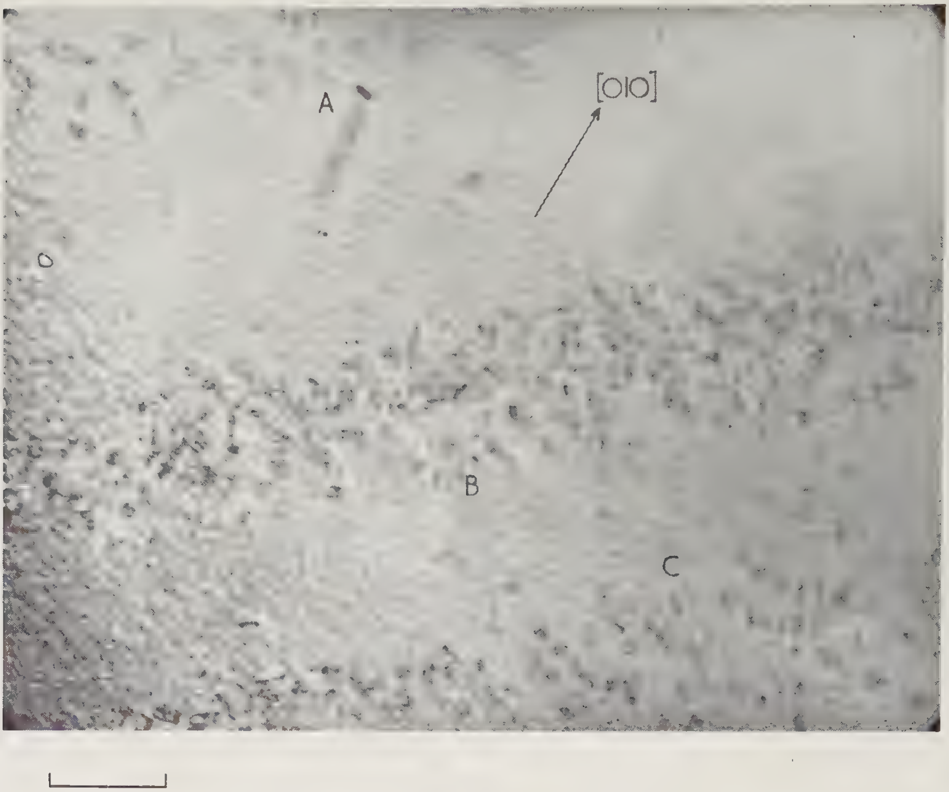

Fig. 20

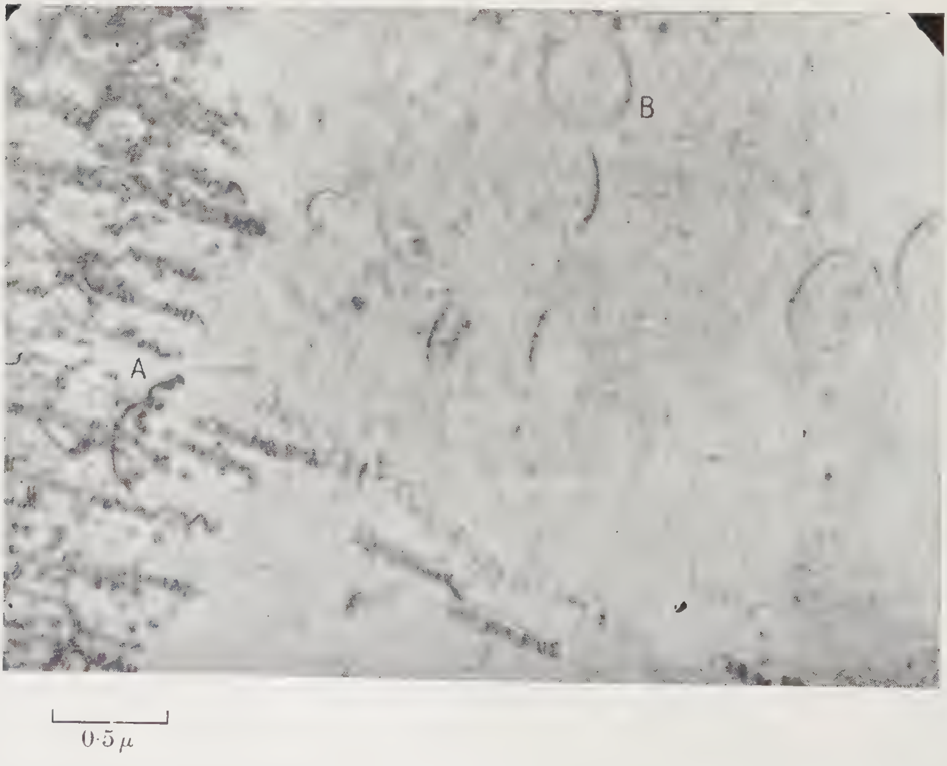

CAPTIONS TO PLATES

Fig. 1. Helical dislocations viewed side on in Al-4% Cu quenched from 540°c. The helices run parallel to $[\bar{1}01]$. Figure 1 (*a*) at the left joins fig. 1 (*b*) at the right; similarly for fig. 1 (*b*) and (*c*). C: helical segments joined by straight segments. D, E, and F: short lines produced by successive turns of helices intercepted by the foil surface. G: helix lying in an inclined [110] direction. Mag. × 30 000.

Fig. 2. Al-4% Cu quenched from 540°c. (*a*) A, B: inclined helices with cusps of opposite sense. C: rows of loops. D, E : helices which have interacted with screws of opposite Burgers vector. (*b*) A, B: intertwined helices. D, E: Lissajous-type figures. F, G: rows of loops. Mag. × 30 000.

Fig. 3. Helices lying close to slip planes. Note the helices of opposite sense. Note also the absence of loops in regions away from the helices. Quenched from 540°c. Mag. × 40 000.

Fig. 4. Al-4% Cu quenched from 540°c. The normal to foil is close to [103]; the helices run parallel to [011]. A, B: helices of opposite hand without ambiguity. D: probable edge dislocation. C: annihilation. E: interaction with a loop. Mag. × 30 000.

Fig. 5. A, B: helices of different radius and pitch. The helix A has a radius of ~1500 Å. A and B may be two helices with perpendicular Burgers vectors. Quenched from 540°c. Mag. × 30 000.

Fig. 6. Region showing large helices. A: parts of loops from subsequent turns of the helix. Quenched from 540°c. Mag. × 30 000.

Fig. 7. Poorly developed helices typical of material quenched from 440°c. The pitch of the helices appears to be about 300–400 Å or greater. Note the small average radius of the helices. Mag. × 30 000.

Fig. 10. A: intertwined helices running parallel to $[\bar{1}01]$. Loops such as at B may result from interactions of the helices (see fig. 12). Quenched from 540°c. Mag. × 40 000.

Fig. 11. Intertwined helices of opposite hand running parallel to $[0\bar{1}1]$. Quenched from 540°c. Mag. × 40 000.

Fig. 14. Region showing loops and helices running parallel to $[0\bar{1}1]$. The normal to the foil is close to [103]. The elongated loop at A may be formed by prismatic glide of a loop in the [011] direction (see fig. 13). Quenched from 540°c. Mag. × 40 000.

Fig. 15. Complex arrangement of helices and loops. Some of the loops appear to be less than 100 Å in diameter. Note the elongated loops, e.g. at A. Quenched from 540°c. Mag. × 30 000.

Fig. 16. Connected helices of opposite hand. The normal to the foil is close to [112]; helices run parallel to $[\bar{1}01]$. Quenched from 500°c. Mag. × 30 000.

Fig. 18. Region showing rows of loops and helices. The normal to the foil is close to [105]. Rows of loops at A and B probably run parallel to [101] and $[0\bar{1}1]$. Quenched from 500°c. Mag. × 30 000.

Fig. 19. A, B and C: bands of irregularly arranged loops parallel to the traces of $(1\bar{1}1)$ planes. The width of the bands is about equal to the projected width of the $(1\bar{1}1)$ slip planes. The bands may be due to collapsed discs of vacancies forming on or close to slip planes active during quenching. Normal to the foil is close to [105]. Quenched from 500°c. Mag. × 30 000.

Fig. 20. Region containing helices and loops of small diameter near A. Note the very large loops near B. Quenched from 500°c. Mag. × 30 000.

Fig. 1

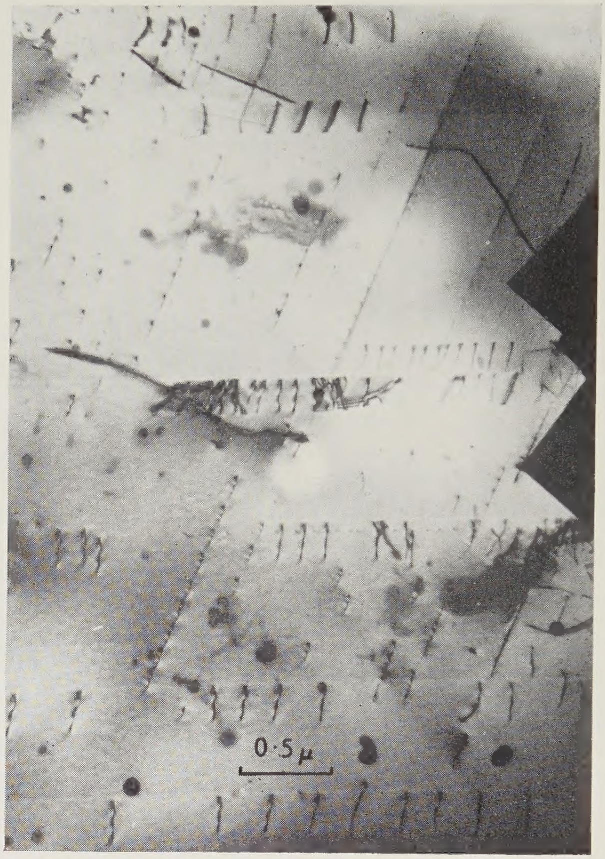

Slip traces showing associated dislocations, in stainless steel.

Fig. 2

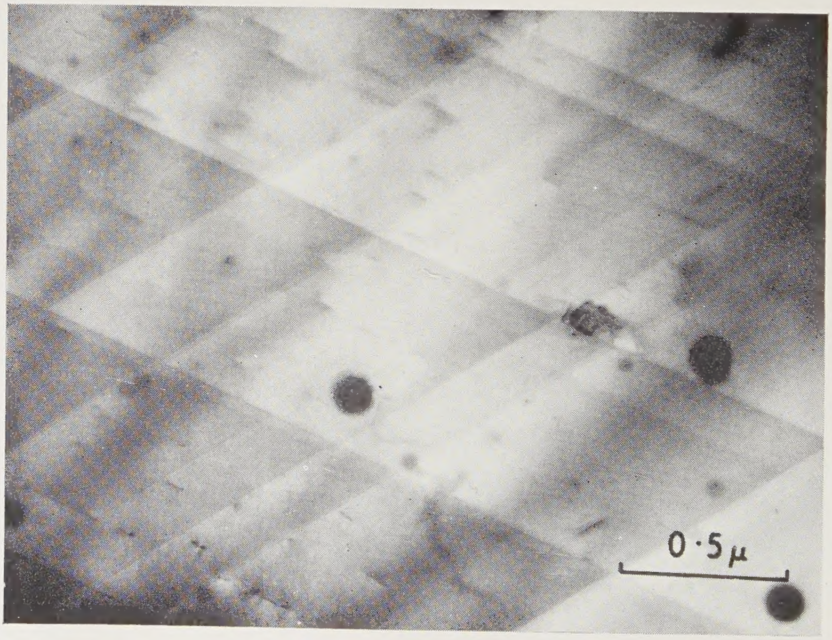

Slip traces not showing associated dislocations, in stainless steel.

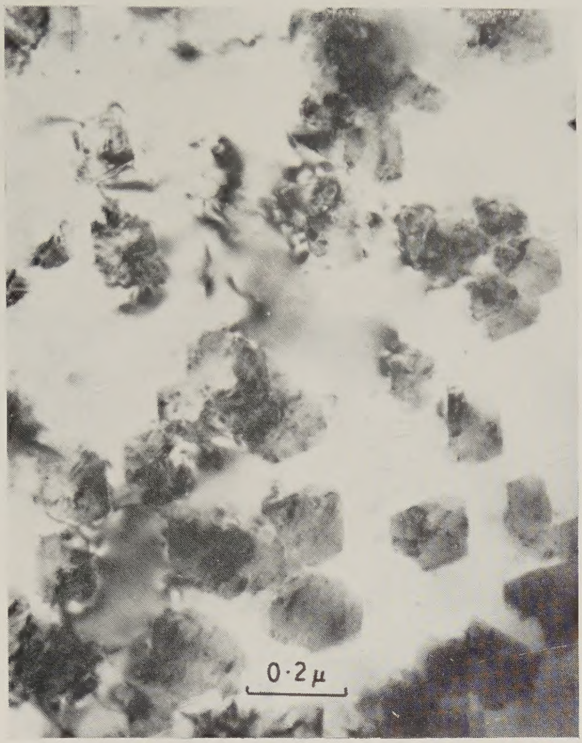

Fig. 3

Crystallographic growths on vacuum annealed aluminium.

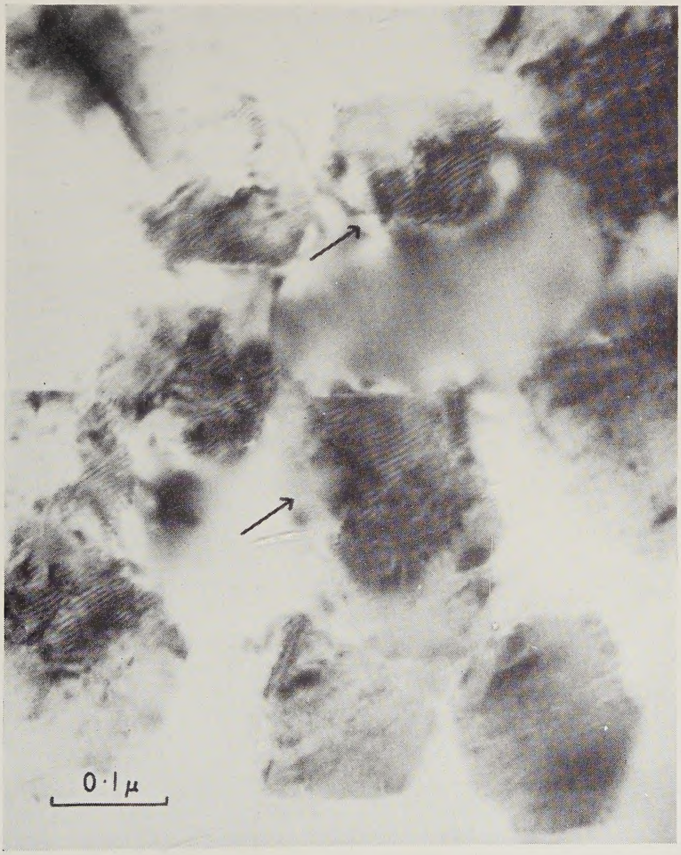

Fig. 4

Moiré patterns within growth outlines.